Lignin-based flocculant and dispersant for wastewater treatment

A Thesis Presented to the

Faculty of Graduate Studies of

Lakehead University

by

Agha Hasan

Submitted in partial fulfillment of requirements

for the degree of Doctor of Philosophy in Biotechnology

April 2018

Dedications

To my late mother who has been my constant source of inspiration.

To my wife and children for all of their support, patience and encouragement.

ACKNOWLEDGMENTS

First of all I offer my sincere gratitude to my supervisor, Dr. Pedram Fatehi for his excellent and continued guidance throughout the course of my research at Lakehead University. His support and training played a crucial part in my academic experience and ability to complete this research project.

I would like to extend my sincere thanks to my committee members, Dr. Baoqiang Liao and Dr. Sudip Rakshit for their valuable input in preparing this thesis.

I also wish to extent my sincere thanks to Mr. Michael Sorokopud, Dr. Guoseheng Wu, Mr. Martin Griffith and Mr. Greg Krepka, LUIL department, Lakehead University.

A special thank you to Dr. Mohan Konduri, Dr. Yiqian Zhang, Dr. Fangong Kong, Dr. Jacquelyn Price, Germaine Cave, Dr. Weijue Gao, Armin Kazzaz, and Leila Nazemnejad for their continuous encouragement and great support. I would also like to thank all other group members for their support and kindness inside and outside of the lab. They leave me endless pleasant memories in my lab experience and there are too many of them to list here.

I would also like to thank my wife and children for their overwhelming support and sacrifices.

The financial assistance from FPInnovations, OGS and NSERC, Canada are also much appreciated.

ABSTRACT

The wastewaters produced from different industries contain fine and charged suspended particles and other impurities. Today, the removal of these colloidal particles from the wastewater has become a serious challenge for industry. Flocculation of the fine particles using polymers followed by settling is a popular technique in industry. Synthetic flocculants have been used in wastewater treatment systems, which are not biodegradable and eco-friendly. Therefore, natural based flocculants have been attracting wide interest of researchers because they are of biodegradable and are environmentally friendly.

In this study, kraft lignin derived from black liquor of kraft pulping process, was copolymerized with acrylamide (AM) and (2-methacryloyloxyethyl) trimethyl ammonium chloride (DMC) in an aqueous solution in the presence of as an initiator potassium persulfate ($K_2S_2O_8$) to produce a water-soluble lignin-based copolymer. The influence of the reaction conditions on the charge density and solubility of resultant lignin copolymers were investigated. The resultant lignin copolymer was characterized by Fourier transform infrared (FTIR) spectrophotometry, nuclear magnetic resonance (HNMR), thermogravimetric analyzer (TGA), molecular weight and elemental analyses.

The applications of the resultant copolymer as a flocculant in kaolin and bentonite suspensions were systematically assessed. The flocculation studies allowed for correlating the polymer characteristics, namely the charge density and molecular weight, with its adsorption affinity as well as the zeta potential and relative turbidity of kaolin and bentonite suspensions. This study showed that a highly charged cationic lignin adsorbed more than low charged ones, and an increase in the molecular weight of cationic lignin enhanced its adsorption. Thus, cationic flocculants with higher molecular weights and charge densities were more effective in reducing the turbidity of clay suspensions.

One of the important findings of this work was that both polymer bridging and charge neutralization mechanisms facilitated the destabilizing of the colloidal particles to form flocs. An improved reflocculation ability of cationic polymers was observed as the molecular weight and charge density of the polymers increased. The flocculation studies also confirmed that the

flocculation efficiency of these cationic lignin polymers depended on the adsorbed amount of polymer on kaolin and bentonite particles, but not on the unadsorbed amount present in the suspensions.

In this study, the flocs size and structure of cationic lignin in kaolin suspension was determined by a focused beam reflectance measurement (FBRM) and the results were correlated with flocs properties obtained by small-angle laser light scattering technology (SALLS). The results showed that the flocs produced were larger and more porous as the polymer's charge density and molecular weight increased. Also, the flocs strength decreased as the flocs size increased. A strong correlation between the size of flocs and sedimentation behavior of kaolin suspension was established by a vertical scan analyzer. The results demonstrated that the maximum rate of settling increased with the increase in floc size.

The effect of solution pH and salt concentration on the dispersant performance of anionic kraft lignin in kaolin suspensions was also studied. The adsorbed anionic kraft lignin on kaolin particles induced electrostatic repulsion between the particles at a more basic pH and thereby improved the dispersibility of suspensions. The results showed that the adsorption of lignin polymers decreased with pH increase, but increased with ionic strength increase.

In this study, the mechanism of self-assembly of kraft lignin-based polymers in aqueous solutions was investigated using dynamic light scattering (DLS) and the results were correlated with conformation and viscoelastic properties of the adsorbed polymer layers on particles via Quartz crystal microbalance with dissipation (QCM-D) analysis. The results showed that a higher molecular weight lignin polymer was adsorbed in a greater quantity, and that more mass interacted as the molecular weight increased.

The results in this work provided insights into the fundamental understanding of the flocculation, dispersion and self-assembly behavior of kraft lignin-based polymers in various systems. These results can help establish the criteria for selecting and developing kraft lignin based flocculants or dispersants for altered applications. The results of this thesis contributed to knowledge on the chemical modification and characterization of lignin products and to the fundamentals associated with the performance analysis of flocculation and dispersion systems.

Table of Contents

List of Figures

List of Tables

List of abbreviations

AM	Acrylamide
ANOVA	Analysis of variance
BET	Brunauer-Emmett Teller
CLD	Chord length distribution
DADMAC	Diallyldimethyl ammonium chloride
DDJ	Dynamic drainage Jar
D_f	Fractal dimension
DLS	Dynamic light scattering
DLVO	Derjaguin-Landau-Vervey-Overbeek
DMC	(2-methacryloyloxyethyl) trimethyl ammonium chloride
DSI	Destabilization index
EDX	Energy-dispersive X-ray spectroscopy
FBRM	Focused beam reflectance measurement
FI	Flocculation index
FTIR	Fourier transform infrared spectrophotometry
GPC	Gel permeation chromatography
Hy	Hydrodynamic diameter
KL	Kraft lignin
KAD	Kraft lignin-AM-DMC
KLD	Kraft lignin-DMC
KAM	Kraft lignin-AM
M_N	Number-average molecular weight
M_W	Weight-average molecular weight
NIR	Near Infrared Reflectance
NMR	Nuclear magnetic resonance
PDA	Photometric dispersion analysis
PDI	Polydispersity index
$K_2S_2O_8$	Potassium persulfate
PVSK	Potassium polyvinylsulfate

QCM-D	Quartz crystal microbalance with dissipation
RCF	Relative centrifugal force
RGD	Rayleigh-Gans-Debye
SALLS	Small-angle laser light scattering technology
SEM	Scanning electron microscopy
STEP	Space- and Time-resolved Extinction Profiles
TGA	Thermogravimetric analyzer
XRD	X-ray diffractometer

Chapter 1: Introduction

1.1 Overview

The growing resource crisis and environmental pollutions remain serious concerns in the world (Robinson and Chong, 2014). Heavy metal ions, aromatic compounds and dyes are often found in the wastewater as a result of industrial discharges. They are the common contaminants of wastewater and many of them are known to be toxic and/or carcinogenic (Razali and Ariffin, 2015a; Wang et al., 2016). The complex structure, poor biodegradability and toxicity of these pollutants provide great challenges for their remediations. The separation of dissolved and suspended particles from various wastewater effluents has become a matter of interests, and significant efforts have been put into the development of efficient and cost-effective treatment methods.

Currently, some of the wastewater treatment methods, for example, adsorption, oxidation, membrane filtration, are not remarkably effective when dealing with significant stable harmful pollutants in effluents. In contrast, flocculation process is recognized as one of the most widely used methods for treating wastewater effluents because it is proved as an efficient and economic process (Nasser and James, 2006; Liimatainen et al., 2011).

Previously, inorganic and organic flocculants have been used in treating municipal, papermaking, and mining effluents (Ye et al, 2003; Ahmad et al., 2005; Yu et al., 2010). These flocculants could be cationic, neutral, and anionic. Inorganic flocculants, such as alum, ferric chloride, were not very attractive to use because of their large volume requirement, pH sensitivity, and inefficiency in treating some wastewater effluents (Wang et al., 2016). On the other hand, a wide range of flocculants have been developed to improve the flocculation process in wastewater treatment including synthetic and natural organic flocculants.

In recent years, many synthetic organic flocculants such as acrylamide, diallyldimethyl ammonium chloride (DADMAC) and polyacrylic acid have gained widespread use in several industrial applications. Although these water soluble synthetic polymers find wide applications as flocculants, their usage is debatable because of the potential public health hazard they introduce to wastewater (Ye et al., 2003; Bratby et al., 2006).

To address these issues of synthetic flocculants, new environmentally friendly and effective flocculants should be generated. Natural organic flocculants are toxin free, eco-friendly, and effective at low dosage (Singh et al., 2000; Wang et al., 2013). For many years, biopolymer-based flocculants, such as guar gum, chitosan, starch and cellulose, have been researched for their potential use in industry (Singh et al., 2000; Wang et al., 2013; Ben et al., 2011, Zou et al., 2011; Razali et al., 2015b). However, the use of these polymers for other applications in food and fermentation processes, pharmaceutical, cosmetics, agricultural and papermaking industries limited their availability for use as flocculants (Pelton, 1986; Wang et al., 2011).

In this context, kraft lignin appears to be a promising candidate for flocculant productions. However, kraft lignin has a limited solubility due to its phenylpropane-based structure (Sableviciene et al., 2005; Zakzeski et al., 2010). In addition, kraft lignin does not have sufficient functionality to be used as flocculants for wastewater effluents. To enhance the flocculation affinity of kraft lignin, cationic groups, such as the quaternary ammonium, can be introduced to kraft lignin, via polymerization techniques to produce inexpensive, nontoxic, and biodegradable cationic polymers to be used as suitable flocculants for wastewater systems (Ahvazi, et al., 2011).

To control and optimize the flocculation process, it is important to understand the flocculation mechanism. However, details underlying the mechanism for removal of impurities or contaminants from wastewater with natural flocculants are not fully understood. Several flocculation mechanisms, such as charge neutralization, bridging and electrostatic patch, have been proposed to explain the destabilization of colloidal suspensions by polymers and the mechanism of flocs formation (Razali et al., 2011). These mechanisms are crucially dependent on the adsorption of flocculants on particles suspended in wastewater. If there is an affinity between polymer segments and a particle surface, the adsorption of polymers may occur. Adsorption of polymers onto the particles' surface may occur via electrostatic interaction or hydrogen bonding (Gregory, 1990; Szyguła et al., 2009; Petzold et al., 2003). The extent of adsorption and configuration of the adsorbed polymers not only depends on the polymer characteristics (e.g., molecular weight, charge density) but also on the properties of the colloidal systems (Gregory, 1990). For example, the pH of colloidal suspensions containing clay influences both the net surface charge density of clay particles, polymer functional groups and

adsorption mechanism of polymers on clay surfaces. Similarly, the adsorption of polymers on the surfaces of clay particles is strongly dependent on ionic strength of the colloidal systems (Chen, 1998). These factors have a great influence on the efficiency of flocculants used in the systems. However, other factors, such as particle size, particle density, and liquid density, also exert considerable influence on the tendency of fine particles to disperse, flocculate and settle. These factors have potential influence on the formation of flocs and the structural properties of the flocs produced during the dispersion and flocculation process. Since the behavior of kraft lignin-based polymers as flocculants and dispersants have not been understood, their interactions with components of colloidal systems have not been evaluated.

The main goal of this dissertation was to develop a method to synthesize kraft lignin-based flocculants or dispersants, which would be renewable, biodegradable, and non-toxic with performance comparable to the commercial ones. In this chapter **(chapter 1)**, a brief summary of the subsequent chapters in this thesis is provided. Furthermore, the objectives of this research work are also presented.

Chapter 2 provides a brief introduction to the flocculation process described in literature related to the current studies. Literature review is structured into sections discussing the background information related to the nature of flocculant (e.g., composition, charge density, molecular weight, etc.) and the properties of flocculants used in wastewater treatment systems. The second section discusses various methods used in literature and in this study to evaluate the properties of lignin based polymers as well as flocculant and dispersion analyses.

Chapter 3 discusses the copolymerization of lignin, acrylamide (AM) and (2-methacryloyloxyethyl) trimethyl ammonium chloride (DMC) to produce kraft lignin-AM-DMC (KAD) copolymers. The obtained results in this chapter can be used to optimize the reaction conditions in order to attain the targeted properties. Also, lignin copolymers were characterized to confirm their properties. Charge density and solubility parameters of the copolymers were determined. The production of homopolymers of PDMC and PAM were also illustrated. Furthermore, the activation energies of copolymer and homopolymers were assessed.

Chapter 4 deals with the use of orthogonal experimental design for determining the optimum conditions to produce kraft lignin-based copolymers. The grafted samples were prepared via

copolymerization, in which the factors studied were the reaction temperature, reaction time, pH, initiator concentration, and monomer concentrations. The potential impact of these factors on the charge density and lignin solubility of produced copolymer were evaluated using the orthogonal design method. The variance trend was discrepant for the two responses (charge density and solubility). Statistical analysis of the model was performed with the statistical assessment for analysis of variance (ANOVA). The regression analysis of the results of the orthogonal experiments was performed and validated.

Chapter 5 provides discussion on the use of lignin copolymers with two different molecular weights, but with a similar charge density, as flocculants for simulated kaolin and bentonite suspensions. The adsorption, zeta potential and relative turbidity analysis were then assessed. The influence of pH on the copolymer adsorption and turbidity removal of kaolin and bentonite suspension was evaluated.

Chapter 6 illustrates the behavior of two lignin copolymers, with the same molecular weights but different charge densities, as flocculants for kaolin and bentonite suspensions. The adsorption, zeta potential and flocculation analyses were performed to determine the effectiveness of the copolymers. The impact of the copolymers in changing the particle size distributions of kaolin and bentonite particles was identified. The flocculation and reflocculation of the particles were studied in order to reveal the flocculation mechanism.

Chapter 7 discusses the polymerization of kraft lignin and 2-[(methacryloyloxy) ethyl] trimethylammonium chloride (DMC) to produce cationic kraft lignin–DMC polymer. The flocculation behavior of suspension systems containing cationic polymers with different molecular weights and charge densities was studied to obtain the information about flocculation kinetics and flocs characteristics. In this chapter, focused beam reflectance measurement (FBRM), vertical scan analyzer and photometric dispersion analysis (PDA) were used to study the floc structure, size and their settling behavior. The fractal dimension of the flocs was measured by a small-angle light scattering technology (SALLS) and used for characterizing the compaction of flocs. Furthermore, correlations were developed between the adsorption of cationic polymers on the kaolin particles and the zeta potential of the kaolin suspensions.

Chapter 8 describes the polymerization of kraft lignin and acrylamide to produce kraft lignin-acrylamide dispersants with different molecular weights and charge densities for kaolin suspensions. The adsorption, zeta potential and turbidity analyses were then performed on kaolin suspension at varied pH. The impact of various physiochemical properties, such as ionic strength, particle size and suspension pH, on the adsorption capacity of the polymers were then evaluated. The surface tension and contact angle studies of modified and unmodified lignin were performed at different pHs. The impact of shear rate on the stability of kaolin dispersion was evaluated.

Chapter 9 describes the self-assembly of kraft lignin-acrylamide polymers. The effect of molecular weight of the polymers on aggregation at different salt concentrations in aqueous solutions was investigated. Particle aggregation was studied using a vertical scan analyzer and dynamic light scattering (DLS) techniques. Quartz crystal microbalance with dissipation (QCM-D) measurement was utilized to study the viscoelastic and self- assembly behavior of the polymers.

Chapter 10 states the overall conclusions and recommendations for future work.

1.2 Objectives

The objectives of this study are to:

1. synthesize and characterize kraft lignin-AM-DMC copolymers via free radical polymerization in aqueous solutions;
2. determine the main reaction factors that impact the production and properties of kraft lignin-AM-DMC copolymers;
3. assess how the molecular weight of kraft lignin-AM-DMC influence the flocculation of kaolin and bentonite suspensions;
4. investigate how the charge density of kraft lignin-AM-DMC impact the flocculation of kaolin and bentonite suspension;
5. synthesize and characterize kraft lignin-DMC as flocculant for kaolin and bentonite suspensions;
6. synthesize and characterize kraft lignin-AM as a dispersant for kaolin suspensions; and
7. investigate the self-assembly behavior of kraft lignin-AM polymer in aqueous solution.

1.3 References

Ahmad, A.L., Ismail, S., Bhatia, S. 2005. Optimization of coagulation–flocculation process for palm oil mill effluent using response surface methodology. Environ. Sci. Technol., 39, 2828–2834.

Ahvazi, B., Wojciechowicz, O., Ton.-That, T.M., Hawari, J. 2011. Preparation of lignopolyols from wheat straw soda lignin. Agriculture Food Chem., 59, 10505-10516.

Ben, W., Yulian, Z., Chunbao, M., 2011. Preparation of Cationic Chitosan-Polyacrylamide Flocculant and Its Properties in Wastewater Treatment. Journal Ocean University China (Oceanic and Coastal Sea Research) 10, 42-46.

Bratby, J., 2006. Coagulants, in Coagulation and Flocculation in Water and Wastewater Treatment, 2nd ed., IWA Publishing, London, 50-68.

Chen, W.J. 1998. Effects of surface charge and shear during orthokinetic flocculation on the adsorption and sedimentation of kaolin suspensions in polyelectrolyte solutions. Sep. Purif. Technol., 33(4), 569- 590.

Gregory, J., Lee, S. 1990. The effect of charge density and molecular mass of cationic polymers on flocculation kinetics in aqueous solution. Journal Water SRT—Aqua, 39, 265–274.

Liimatainen, H., Sirvio, J., Sundman, O., Visanko, M., Ninimaki, J., Hormi, O. 2011. Flocculation performance of a cationic biopolymer derived from a cellulosic source in mild aqueous solution/ Bioresour. Technol., 102, 9626–9632.

Nasser, M.S., James, A.E. 2006. The effect of polyacrylamide charge density and molecular weight on the flocculation and sedimentation behaviour of kaolinite suspensions. Sep. Purif. Technol., 52, 241–252.

Pelton, R.H., 1986. Electrolyte effects in the adsorption and desorption of a cationic polyacrylamide on cellulose fibers. J. Colloid Interface Sci., 111 (2), 475–485.

Petzold, G., Mende, M., Lunkwitz, K., Schwarz, S., Buchhammer, H.M. 2003. Higher efficiency in the flocculation of clay suspensions by using combinations of oppositely charged polyelectrolytes. Colloids Surf. A Physicochem. Eng. Asp., 218 (1–3), 47–57.

Razali, M.A.A., Ariffin, A. 2015a. Polymeric flocculant based on cassava starch grafted polydiallyldimethylammonium chloride: Flocculation behavior and mechanism. Appl. Surf. Sci., 351, 89–94.

Razali, M.A.A., Ismail, H., Ariffin, A. 2015b. Graft copolymerization of polyDADMAC to cassava starch: Evaluation of process variables via central composite design. Ind. Crops. Prod., 65, 535–545.

Razali, M.A.A., Ahmad, Z., Ahmad, M.S.B., Ariffin, A. 2011. Treatment of pulp and paper mill wastewater with various molecular weight of polyDADMAC induced flocculation. J. Chem. Eng., 166, 529–535.

Robinson, M.F., Chong, A. 2014. Review on application of flocculants in wastewater treatment. Pro. Safety and Env. Protec., 92 (6), 489–508.

Sableviciene, D., Klimaviciute, R., Bendoraitiene, J., Zemaitaitis, A., 2005. Flocculation properties of high-substituted cationic starches. Colloids Surf. A Physicochem. Eng. Asp., 259 (1–3), 23–30.

Singh, R.P., Karmakar, G.P., Rath, S.K., Karmakar, N.C., Pandey, S.R., Tripathy, T., Panda, J., Kanan, K., Jain, S.K., Lan, N.T. 2000. Biodegradable drag reducing agents and flocculants based on polysaccharides: materials and applications. Polym. Eng. Sci., 40, 46–60.

Szyguła, A., Guibal, E., Palacín, M.A., Ruiz, M., Sastre, A.M. 2009. Removal of an anionic dye (Acid Blue 92) by coagulation–flocculation using chitosan. J. Environ. Manag., 90, 2979–2986.

Wang, J. P., Y. Z. Chen, Y.Z., Wang, Y., Yuan, S.J., Sheng, G.P., Yu. H. Q. 2012. A novel efficient cationic flocculant prepared through grafting two monomers onto chitosan induced by Gamma radiation. RSC Adv., 2, 494–500.

Wang, J. P., Chen, Y.Z., Wang, Y., Yuan, H. Q., Yu. H.Q. 2011. Optimization of the coagulation-flocculation process for pulp mill wastewater treatment using a combination of uniform design and response surface methodology. Water Res., 45, 5633-5640.

Wang, S., Konduri, M.K.R., Hou., Q., Fatehi, P. 2016. Cationic xylan-METAC copolymer as a flocculant for clay suspensions/ RSC Advance 6, 40258-40269.

Ye, Q., Zhang, Z., Ge, X. 2003. Highly Efficient Flocculant Synthesized through the Dispersion Copolymerization of Water Soluble Monomers Induced by γ-Ray Irradiation: Synthesis and Polymerization Kinetics. Appl. Polym. Sci., 89, 2108 –2115.

Yu, W., Gregory, J., Campos, L. 2010. The effect of additional coagulant on the re-growth of alum–kaolin flocs. Sep. Purif. Technol., 74, 305–309.

Zakzeski, J., Bruijnincx, P. C. A., Jongerius, A. L., Weckhuysen, B. M. 2010. The Catalytic Valorization of Lignin for the Production of Renewable. Chemical Rev., 110, 3552–3599.

Zou, J., Zhu, H., Wang, F., Sui, H., Fan, J. 2011. Preparation of a new inorganic–organic composite flocculant used in solid–liquid separation for waste drilling fluid. J. Chem. Eng., 171, 350–356.

Chapter 2: Literature review

2.1 Introduction

This literature review is to provide a fundamental knowledge related to kaolin and bentonite particles, polymers' properties, and impact of solution properties on the stability of clay particles. In addition, physicochemical properties of clay, clay particle interaction, type of polymer clay interaction and adsorption of polymers on clay surfaces under various reaction conditions are addressed in this chapter. Systematic studies conducted in the literature on the modification of natural polymers using different methods in treating wastewater are also presented. The modification of kraft lignin to produce cationic flocculants using different methods employed in the literature are also discussed.

A pool of advanced techniques, such as gel permeation chromatography (GPC), nuclear magnetic resonance (NMR) spectroscopy, Brunauer-Emmett-Teller (BET) surface area analyzer, zeta potential analyzer, scanning electron microscopy (SEM), thermo gravimetric analyzer, particle charge detector, photometric dispersion analyzer, X-ray diffractometer (XRD), particle size analyzer, static light scattering analyzer (TURBISCAN), focused beam reflectance measurement (FBRM), Quartz crystal microbalance with dissipation (QCM-D), dynamic light scattering (DLS) and LUMiSizer are utilized in this work to meet the objectives, and their fundamentals are discussed.

2.2 Background

2.2.1 Colloidal suspensions

In colloidal systems, the moving particles can collide with each other due to Brownian motion. Colloids, due to the effect of surface properties such as surface charge, can exist as stable dispersions. They are, therefore, more sensitive to surface phenomena than to gravitational forces. Colloidal particles can form suspensions, which are highly stable over time. Such suspensions include solid, liquid or gas, gels, aerosols, emulsions, and foams. The stability of a colloid suspension depends on the equilibrium between two types of opposing forces; Van der Waals' and an electrostatic interaction force. In aqueous media, hydrophobic colloidal particles are generally negatively charged (for example, clay-water systems), where they form stable suspensions because their surface charge is the same and they repel each other. The surface of

the electrically charged particle is at a different potential from the solvent medium. The potential difference between the shear plane and the solution is called the zeta potential. When this potential difference reduces to zero or close to zero, the particles tend to agglomerate under the influence of the Van der Waals' forces and the colloidal suspension becomes destabilized. This phenomenon of colloidal systems is proposed and developed by DLVO (Derjaguin-Landau-Vervey-Overbeek) theory. To remove the colloidal materials from suspension, altering the surface properties of the particles to make the fine particles to settle rapidly are considered. Kaolin is the main clay mineral present in many industrial processes, such as the mining, mineral, painting, ceramics, pharmaceutical and dye industries. Bentonite has great potential to be utilized in most industrial applications due to its large surface areas and swelling property to form viscous water suspensions for stabilizing emulsions, bonding and plasticizing. For this reason, it is important to gain an understanding of the interactions between the colloidal particles to endure better colloidal stability.

2.2.2 Properties of kaolin

Kaolin is a white and soft powder mainly composed of fine-grained plate-like particles. Kaolin as found in nature usually contains varying amounts of other minerals, such as muscovite, quartz, feldspar, and anatase. The primary industrial application of kaolin is in papermaking as a coating and paper filler. Due to the white color, fine particle size and plate-like structure, kaolin is suitable as the pigment for paint, ceramic raw material, functional filler, extender, cosmetic, food additive, and adhesives.

Table 2.1. Chemical and mineral compositions of kaolin (Konduri and Fatehi, 2017)

Chemical compositions				**Mineral compositions**	
Element	**wt.%**	**Calculated oxides**	**wt.%**	**Mineral**	**wt.%**
O	49.88			kaolinite	34
Al	21.54	Al_2O_3	40.71	Dickite	29
Si	25.94	SiO_2	55.49	Narcite	28

Ti	0.65	TiO_2	1.09	Tridymite	4
Fe	0.51	FeO_2	0.66	Hematite	2
Cu	0.60	CuO	0.75	Magnetite	2
Mn	0.33	MnO	0.61		
P	0.18	P_2O_5	0.42		
Na	0.21	Na_2O_8	0.28		

The chemical compositions of the kaolin samples are shown in Table 2.1. The clay consists overwhelmingly of SiO_2 and Al_2O_3, which are the main components of the mineral kaolinite (Atesok et al., 1998; Chen et al., 2007). Kaoline has a 1:1 hydrated aluminosilicate structure ($Al_2Si_2O_5$ $(OH)_4$) with chemical compositions (39.8% alumina, 46.3% silica, 13.9% water) consisting of stacked pairs of tetrahedral silica sheets and octahedral alumina sheets. Each pair of sheets is bound together through common oxygen atoms, and successive pairs are held together by hydrogen bonding between silica–oxygen and aluminum-hydroxyl groups. Hence, the resulting crystal contains a silica face of SiO_2 tetrahedral, an alumina face carrying AlOH groups, and edges that carry both SiOH and AlOH sites. The surfaces of kaolin are believed to carry a constant negative charge due to the isomorphous substitution of Si^{4+} by Al^{3+} in silica layer, whereas the positive charge on the alumina face and on the edges is due to the protonation/ deprotonation of exposed hydroxyl groups (White, 1987). The model structure of kaolin is shown in Figure 2.1 (Tombac and Szekeres, 2006). Kaolin crystal has a molecular weight of 258,071 g/mol, and its diameter is reported in the range of 0.2–10 μm, with thickness of 0.7 nm, and density of 2.6 g/cm^3 (Atesok et al., 1998; Chen et al., 2007).

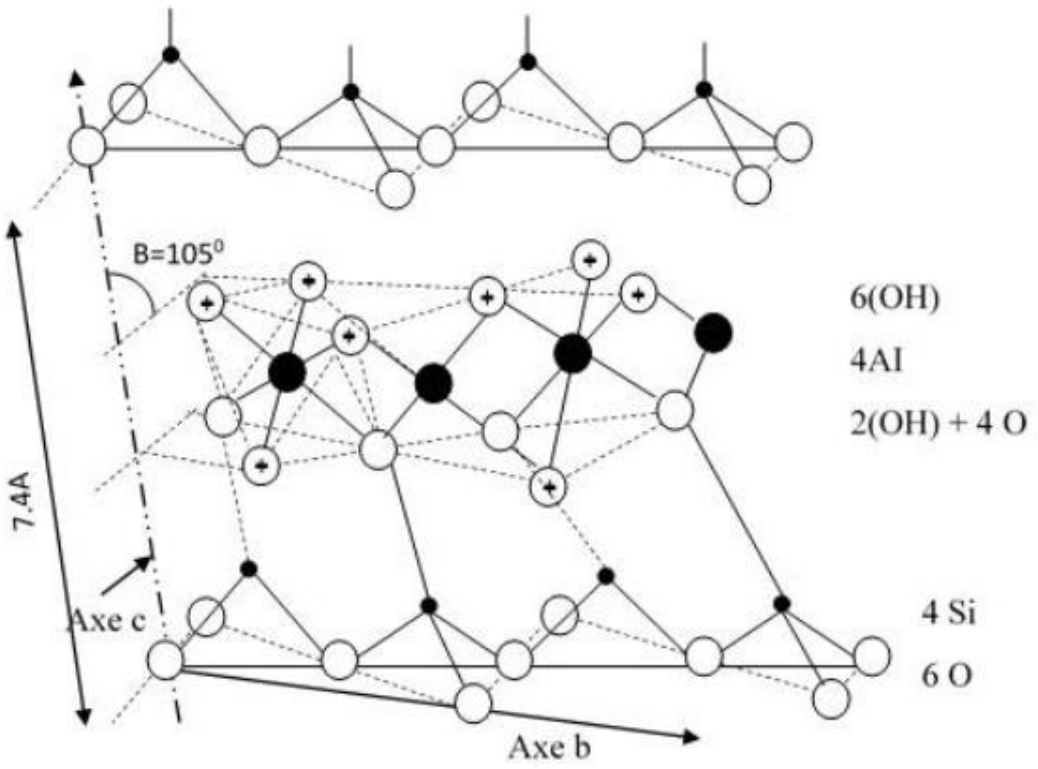

Figure 2.1. Model structure of kaolin (Tombac and Szekeres, 2006)

2.2.3 Properties of bentonite

Bentonite is an important commercial mineral mainly composed of smectite group of clay minerals. It has a wide application in drilling mud, drilling gel, the metal casting industry, detergents, fungicides, sprays, cleansers, polishes, ceramic, paper, cosmetics and medicines. Bentonite clay is primarily composed of montmorillonite 2:1 hydrous aluminosilicate mineral with an overall negative charge. Bentonite has a large surface area, high cation exchange capacity, chemical and mechanical stability and a layered structure that predisposes it as a good adsorbent (Ravi et al., 2013; Karnland et al., 2006).

The main constituent of bentonite is montmorillonite, composed of units made up of two silica tetrahedral sheets with a central alumina octahedral sheet (Figure 2.2). Each platelet consists of three sandwich-arranged layers: a central octahedral alumina (Al_2O_3) layer and two tetrahedral silica (SiO_2) layers. The silicon ion and the aluminum ion often undergo isomorphous substitutions by low valence metals, such as magnesium and iron. In turn, these substitutions

lead to a charge imbalance, compensated by exchangeable cations with water molecules bound together by ion-dipole forces. These ions, with no more place inside the structure, migrate to the external silica layers and are the main causes of hydration in the crystal lattice (Karnland et al., 2006).

Bentonite clay consists of 65-75 % montmorillonite, 10-14 % quartz, 5-9 % feldspars, 2-4 % mica, 3-5 % carbonates and chlorite, and 1-3 % heavy metals. The chemical composition of bentonite is 61-65 % SiO_2, 22-25 % Al_2O_3 , 1-7 % Fe_2O_3, 1-2 % MgO, 0-0.6 % CaO, 0-1% Na_2O, and 0-3% K_2O (Pusch and Karnland, 1983). Previously, bentonite surface's charge density (-9.0 μg/g) and particle size (5.8 μm) were reported to be greater than kaolin's surface area (-6.3 μg/.g) and particle size (5.8 μm) (Wang et al., 2016). The high negative charge density of bentonite indicates the presence of a greater number of oxide anions in montmorillonite structure (Schmidt and Lagaly, 1999).

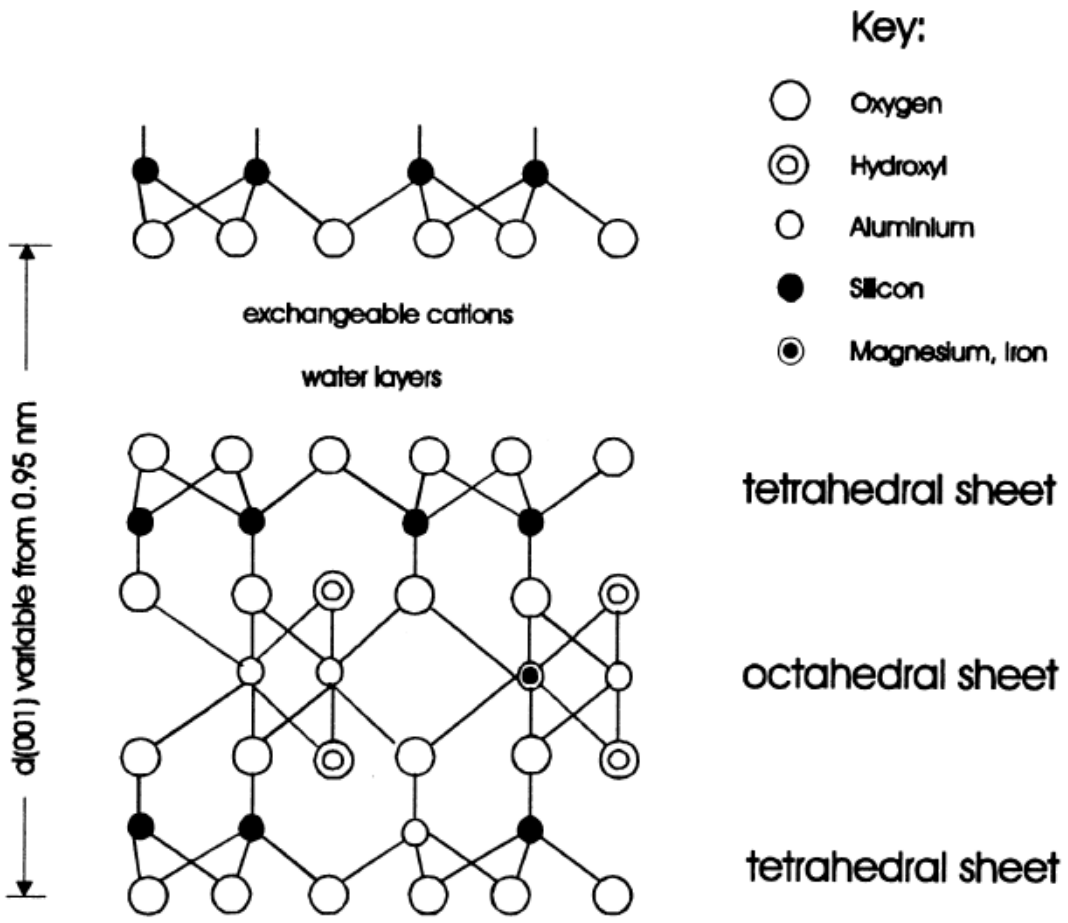

Figure 2.2. Schematic illustration of montmorillonite mineral layers and water molecules (Hofmann et al., 1933).

2.2.4 Colloidal properties of clay suspensions

The interaction of cationic polymers with clays in an aqueous medium is of fundamental importance in controlling the colloidal stability in a variety of applications, such as soil stabilization, paper, nanocomposite manufacturing, the mining industry, wastewater treatment, and mud preparations for drilling oil wall (Shirazi et al., 2003; Chibowski et al., 2009). As discussed above, kaolin and bentonite have a complicated surface chemistry because of the heterogeneity of the charged edges and faces. However, the addition of polymers alters the surface properties of the colloids via electrostatic interaction (Solberg and Wagberg, 2003; Chena et al., 2007) to promote destabilization. Flocculation of the fine negatively charged particles using cationic polymers followed by sedimentation is a crucial phenomenon in determining the efficiency of industrial separation processes (Wang et al., 2016).

2.2.5 Flocculant or dispersant for mineral suspensions

Polymeric materials used as flocculants are mostly water-soluble, and play a crucial role in water treatment process. With respect to charge, polymers can be characterized by their ionic nature, which can be anionic, cationic and nonionic. Acrylamide is a water-soluble polymer and can be produced in its anionic form (Mabire et al., 1984; Audebert, 1988; Fang et al., 2010; Wang and Wang et al., 2011). In addition, polymers that are produced using 2-(methacryloyloxy) ethyl] trimethyl ammonium chloride (DMC) cationic monomer contain quaternary ammonium groups that distribute positive charges along the macromolecular backbone (Pal et al., 2006). Cationic functional groups can strongly interact with suspended, negatively charged particles and hence are useful in many applications, including wastewater treatment. The modification of natural polysaccharides by copolymerizing the DMC with or without acrylamide has been widely applied in the treatment of negatively charged particles in various industrial effluents (Table 2.2). In this regard, lignin based flocculants can be produced and used as flocculants. Interaction of modified polymer with clay particles leads to flocculation through polymer bridging, polymer patching, and charge neutralization or combination of these mechanisms (Yu et al., 2006; Wang et al., 2009; Ghimici et al., 2010; Li et al., 2011). These flocculation mechanisms depend on key parameters, such as the charge density and molecular weight of polymers, which greatly influence the adsorption and conformation of the polymers on particle surface (Gill and Herrington, 1987; Zhu et al., 2009; Wong et al., 2006). Therefore, the interaction of lignin-based flocculants with clay suspension should be studied to understand the mechanisms of flocculation.

Table 2.2. Represents various flocculant and their applications

Cationic flocculant	**Type of wastewater**	**References**
Xylan-g-METAC	Kaolin and bentonite clay suspensions	Wang et al., 2016
Xylan-g-METAC	Azo dye	Wang et al., 2015
Chitosan-g-DMC	Pulp mill wastewater	Wang et al., 2009
Chitosan-g-AM-DMC	Waste water treatment plant	Wang et al., 2011
Chitosan-g-PAM-DMC	Pulp mill wastewater	Wang et al., 2012
Carboxymethyl chitosan-PDMC	Dye contaminated suspension	Yang et al., 2014

Starch-AM-DMC	Waste drilling fluid	Zou et al., 2011
Starch-AM-DMC	Pulp mill effluent	Wang et al., 2011
Starch-g-DMC	Kaolin suspension	Wang et al., 2013
Sludge Lignin-g-DMC	Humic acid (HA) solution	Li et al., 2015
Xanthan-PAM	Mine waste water	Ghorai et al., 2013
Amylopectin-PAM	Kaolin suspension	Rath and Singh, 1997
Amylose-g-PAM	Mine wastewater	Karmakar and Singh,1998
Chitosan-g-PAM	Natural water	Zhang et al., 2010
Sludge Lignin-g-PAM	Dye wastewater	Fang et al., 2010
Sludge Lignin -g- PAM	Pulp and papermaking sludge	Rong et al., 2013
Starch-g-PAM	Silica suspension/Wastewater	Fanta et al., 1972; Mishra et al., 2013
Cellulose-g- PAM	Kaolin suspension	Okieimen, 2003; Machida et al., 1971
Chitosan-g-PAM	Kaolin suspension	Wang et al., 2013, Wang et al., 2008; Yuan et al., 2010

The large variety of chemical being used as dispersants includes inorganic or low molecular weight organic salts and polymers (Farrokhpay et al., 2006). The polymeric dispersants may be nonionic, anionic, cationic or amphoteric (Zhou et al., 2007, Hsu et al., 2016). Anionic polymers are the most efficient dispersants because they increase the surface charges of particles, and therefore keep the clay particles separated, dispersed, or stabilized (Gan et al., 2013). The main purpose of adding a dispersant is to minimize the particle-particle interaction by enhancing electrostatic or steric repulsion. Electrostatic stabilization induces electrostatic repulsive forces and is effective in keeping the clay particles dispersed in aqueous media (Zhou et al., 2007). Physicochemical factors, such as dispersant dosage, surface tension of the dispersants at solid/liquid interface, and the nature of the functional groups in the dispersants, play key roles in imparting the dispersion strength to a dispersant (Farrokhpay et al., 2006).

The effectiveness of polymeric dispersants is correlated with adsorption characteristics of the dispersant on the particles. These polymeric dispersants can adsorb to the clay particles' surface via hydrogen bonding, hydrophobic interaction, and affect the stability of clay particles (Farrokhpay et al., 2006). The adsorption of dispersants at solid/liquid interface depends on the many factors, such as surface characteristics of the particles, polymer charge density, polymer molecular weight and compositions of the dispersion medium. The effectiveness of a dispersant may also vary with the pH and ionic strength of the dispersion medium (Zhou et al., 2007). Therefore, it is essential to study the adsorption of polymeric dispersants on clay under varied process conditions. Dispersants have a wide range of applications in industry (Table 2.3). However, the current industrially used dispersants are oil-based, which are environmentally hazardous. On the other hand, polymers such as cellulose, starch, and guar gum are modified and used as dispersants for clay suspensions (Pawlik et al., 2003). However, a wide range of industrial usage of these polymers limited their availability as dispersants. To overcome the shortfall of these bio-based polymers, karft lignin-based dispersants can potentially be produced and serve for this purpose.

Table 2.3. Examples of various dispersants and their applications

Dispersant	**Application**	**References**
Calcium lignosulfonate	Cement	Ouyang et al., 2006
Alkali lignin	Coal–water slurry	Zhou et al., 2007
Sulfonated lignin	Dye	Qin et al., 2015
Sugar cane baggase-lignosulfonates	Pesticide formulations	Li and Ge, 2011
Lignosulfonates	Coal water slurry	Qin et al., 2016
Carboxymethylated lignin	Graphite suspension	Gan et al., 2013
Partially hydrolyzed polyacrylamide	Oil sand ores	Li et al., 2008
Humic acid	Coal–water slurries	Pawlik, 2005
Sodium polymethacrylate	Iron oxide (Hematite)	Nsib, 2006

Polyacrylamide	Paint	Farrokhpay et al., 2006
Acrylamide copolymers	Ceramic slurries ($BaTiO_3$)	Hsu et al., 2016
Styrene-acrylic acid	Coal water mixture	Yoshihara, 1999
Sodium polyacrylate	Kaolin	Xiumei et al., 2017

2.2.6 Lignin

Lignin is one of the three major polymeric components found in the cell walls of higher order plants. Along with the other two major components, cellulose and hemicellulose, lignin forms a highly efficient composite system that is synthesized entirely from carbon, oxygen, hydrogen, and energy from the sun. Lignin's role in this composite is to act as a matrix material that binds the plant polysaccharide microfibrils and fibers, thereby imparting the strength and rigidity to the plant stem necessary for vertical growth (Kirk, 1971; Vanholme et al., 2010; Baurhoo et al., 2008; Saake and Lehnen, 2012). Lignin also performs other biological functions; helping protect plants from biological attack and assisting in water transport by sealing plant cell walls against water leaks. Although the total lignin content varies widely from plant to plant, it is estimated that a total of 30% of the organic carbon in plant biomass worldwide is contained in lignin (Mansfield et al., 1999; Ververis et al., 2004; Mohan et al., 2004; Lora, 2008).

2.2.7 Structure of lignin

Lignin has a complicated structure as its composition is dependent on various factors, such as the species of hardwood and softwood, the growing conditions of the trees, and the processing conditions of extracting/producing lignin from wood species. Softwood plant species have more lignin than hardwood species (Azadi et al., 2013). Softwood contains 26-32% (spruce approx. 27%) and hardwood contains 20-26% (birch approx. 22%) of lignin. Around 70% of softwood (spruce) lignin and 60% of hardwood (birch) lignin are found in the secondary cell wall (Sjöström, 1993). In addition, lignin differs from other natural biopolymers (cellulose, chitin) by its unique chemical characteristics and the presence of aromatic heteropolymers instead of glucose units (Feofilova and Mysyakina, 2016; Wang et al., 2013).

This complicated structure of lignin produced by oxidative coupling of three main phenylpropanoid building blocks subunits, the so-called monolignols, namely *p*-coumaryl,

coniferyl, and sinapyl (Figure 2.3). Correspondingly, upon oxidative polymerization, each monolignol produces p-hydroxyphenyl (H), guaiacyl (G), and syringyl (S) residues in the polymer. These phenyl propane units in lignin molecule differ by the quantity and nature of the substitutes in aromatic rings. Lignins of different plants (softwood and hardwood) can considerably differ in the ratio of these phenyl propene subunits. In particular, the major components of the lignin of coniferous wood are G unit with trace amounts of S and small amount of H units; whereas, hardwood lignin is composed of a near equal amounts of S and G units with a traces of H units.

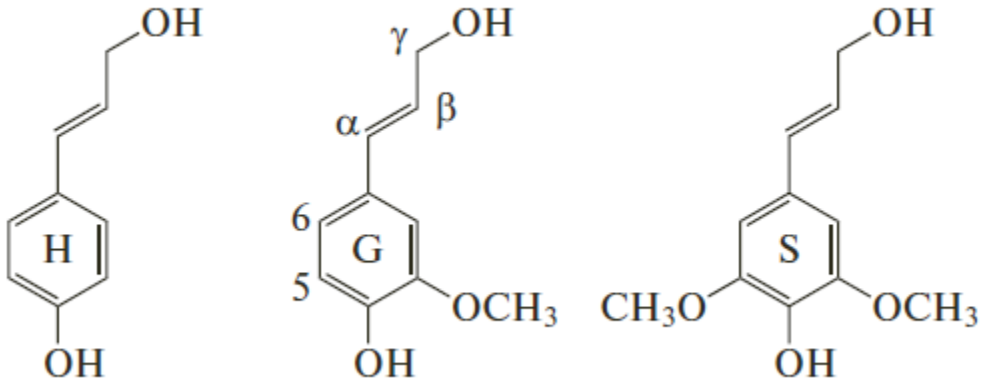

Figure 2.3. The three building blocks of lignin (Feofilova and Mysyakina, 2016)

The commonly recognized chemical structure of lignin is exhibited in Figure 2.4. It is observable that ether bonds, marked in circles, are most susceptible for chemical attacking during chemical conversion processes (Wang et al., 2013). The phenylpropane units are joined together both with C-O-C (ether) and C-C linkages; the ether linkage is the dominant type, accounting for about two thirds of the total linkages (Sjöström, 1993). Figure 2.5 illustrates some of the common types of linkage found in lignin and their approximate proportion are summarized in Table 2.4.

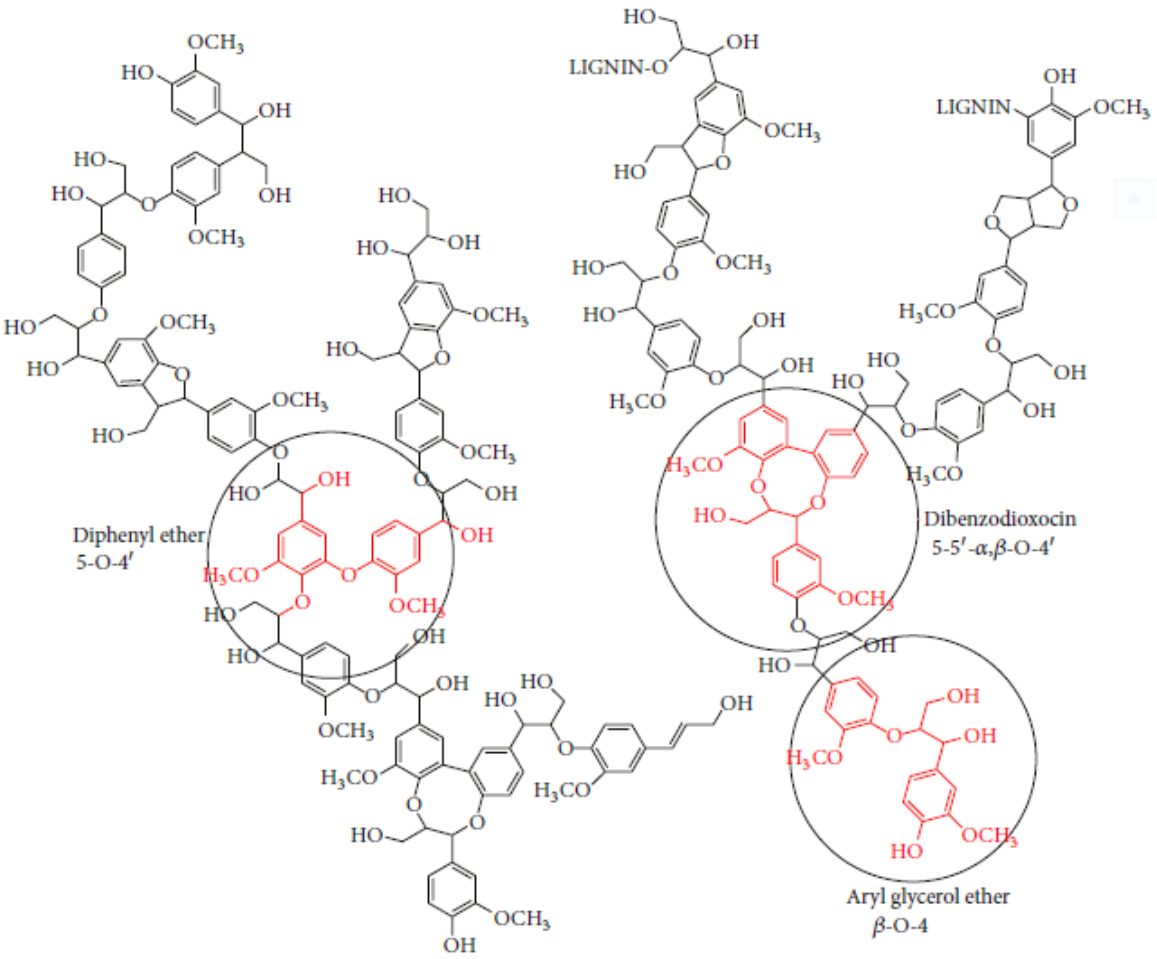

Figure 2.4. The chemical structure of lignin (Wang et al., 2013).

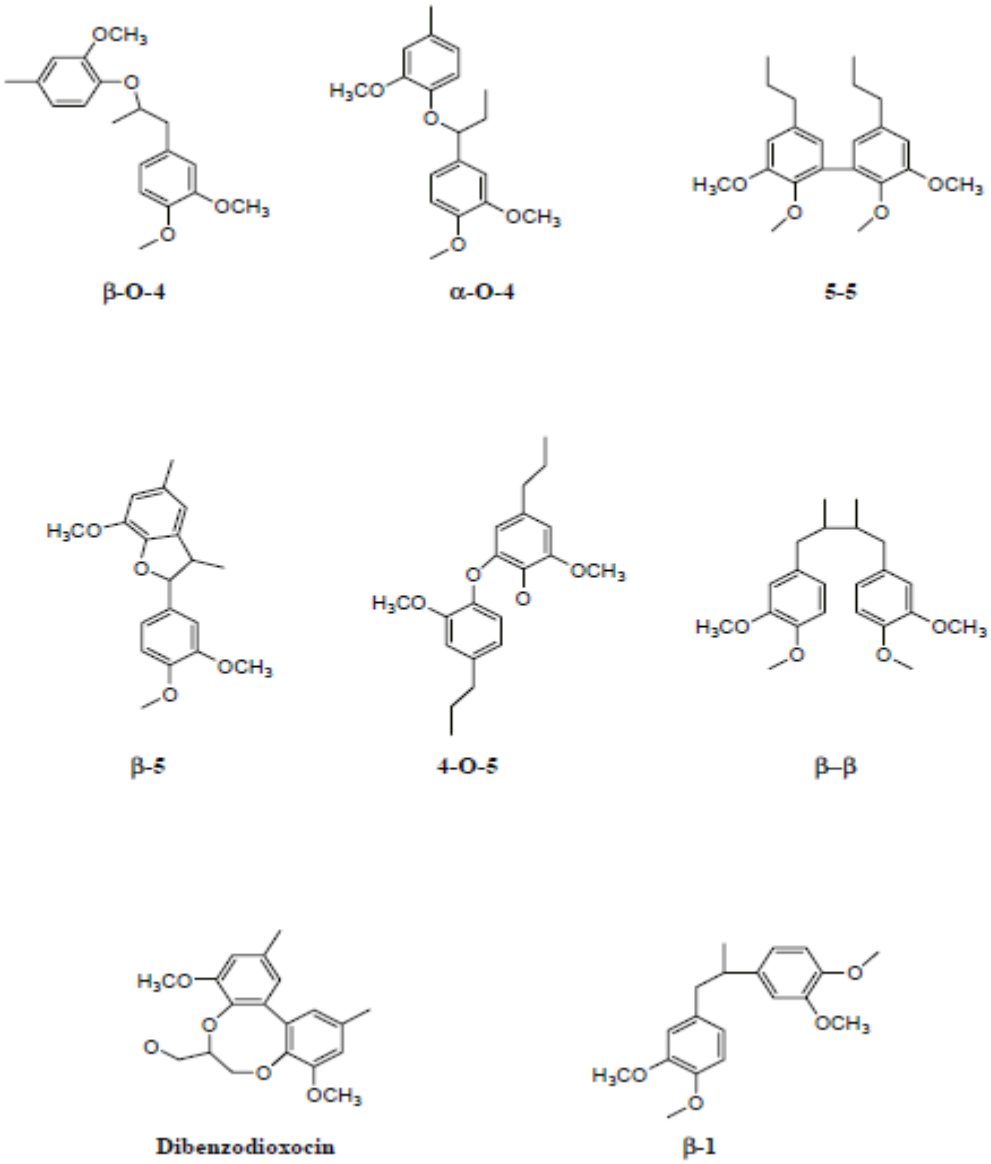

Figure 2.5. Common linkages between phenylpropane units in lignin (Sjostrom, 1981).

Table 2.4. The approximate percentages of linkages connecting the phenylpropane units in lignin (Sjostrom, 1993).

Linkage type	Dimer structure	Softwood (%)	Hardwood (%)
β-O-4	Arylglycerol-β-aryl-ether	50	60
α-O-4	Noncyclicbenzyl aryl ether	2-8	7
β-5	Phenylcoumaran	9-12	6
5-5	Biphenyl	10-11	5
4-O-5	Diarylether	4	7
β-1	1,2 –Diarylpropane	7	7
β-β	Linked through side chain	2	3

The main functional groups of lignin, such as aliphatic hydroxyl, phenolic hydroxyl, carbonyl, methoxyl groups, and some terminal aldehyde groups are important for the reactivity of the lignin. The number of functional groups present in lignin is illustrated in Table 2.5. The hydroxide group situated at para position on all three of the different subunits (p-coumaryl, coniferyl and sinapyl) is of great interest for lignin modification, which provides many changes in lignin properties (e.g., solubility) when reacted with reagents in chemical reactions (Chudakov, 1961; Gellerstedt and Lindfors, 1984).

Table 2.5. Functional groups in lignin (per 100 C6-C3 units) (Sjostrom, 1993).

Functional group	Softwood lignin	Hardwood lignin
Methoxyl	92–97	139–158
Phenolic hydroxyl	15–30	10–15
Benzyl alcohol	30–40	40–50
Carbonyl	10–15	-

2.2.8 Lignin production

Industrially, lignin is mainly produced as a by-product in the pulping industry, which generates between 40 to 50 million tons of lignin a year as a mostly non commercialized waste product (Sahoo et al., 2011). This huge amount of lignin, however, has not received much attention yet. Only 2 % of the produced lignin has been used commercially and the remaining part of lignin is burned as a solid fuel to supply energy for the pulping process and to recover the inorganic chemicals used in the kraft process (Varanasi et al., 2013). In order to meet the goal to replace 30% of fossil fuels by biofuels by 2030, about 225 million tons of lignin as a byproduct of fermentation processes would be generated (Sahoo et al., 2011). In addition, lignin is produced and dissolved in black liquor in the kraft pulping process when wood is pulped to cellulose fibers. The invention of the LignoBoost process has enabled the large-scale purification of lignin from the black liquor, so that the lignin becomes available for downstream applications.

Despite some promising avenues of research into lignin utilization, the highly variable and complex nature of lignin have allowed only limited success so far in developing lignin-based products from a laboratory scale to an industrial scale. However, by developing a better understanding of lignin molecule and by continuing research on its utilization, lignin's potential as a renewable and widely available raw material for value-added product generation can be unlocked (Meister, 2012; Varanasi et al., 2013).

However, the low reactivity of kraft lignin limits its chemical modification, owing to the aryl ether linkages cleavage, the disappearance of the reactive functional groups and condensation of polyphenyl propene units during kraft pulping process (Zakzeski et al., 2010). Hydrophobicity and low molecular weight are the two main factors influencing the application of kraft lignin (Ahvazi et al., 2011). Therefore, this research work focuses on the chemical modification of kraft lignin through graft copolymerization to improve its solubility in aqueous solutions.

2.2.9 Modification of lignin

The numerous sites on the lignin backbone offer many opportunities for different modification reactions (Tripathy and Ranjan, 2006). In order to take advantage of this characteristic, choosing the modification reactions that would tailor lignin properties for a certain application is crucial.

Different types of modification have been proposed to increase lignin's chemical reactivity, reduce the brittleness of lignin-derived polymers, increase its solubility in aqueous solution, and improve the ease of processing lignin (Meister, 2012). The phenolic OH groups of these phenyl propene subunits of kraft lignin present the most reactive sites for any reaction. However, the β-O-4 aryl ether linkages and others interconnecting bonds create significant steric hindrance or occupy these reactive sites, which leads to limited reactivity of kraft lignin for modification. Therefore, depending on the application, a lignin molecule can be modified via copolymerization reaction to make it more reactive (Dilling and Samaranayake, 1999; Lin, 1985; Turunen et al., 2003; Matsushita and Yasuda, 2005; Hashem et al., 2007; Chen et al., 2010; Wang and Xie, 2010; Yue et al., 2011; Huang et al., 2012; Kong et al., 2015).

2.2.10 Free radical copolymerization

Many pathways have been reported to synthesize copolymers via polymerization. Previous studies attempted copolymerization reactions through chemo-enzymes (Mai et al., 2000), irradiation (Jamaliah et al., 2013), UV radiation (Liliana et al., 2009), and mechanical activation (Zuqiang et al., 2009) to produce copolymers for different applications.

Free radical copolymerization is considered as the simplest, economical, efficient and appropriate method for industrial purposes (Fang et al., 2010; Mohamad et al., 2010). This research work focused on free radical copolymerization of kraft lignin with a suitable cationic or nonionic monomer and offers an effective approach to increase the solubility, molecular weight and the charge density of kraft lignin without adversely affecting its molecular structure.

The copolymerization mechanism uses a chemical free radical initiator (e.g. ceric ammonium nitrate, potassium per sulfate or hydrogen peroxide) to generate free radical sites on the backbone polymer, where the monomer of the graft is linked to form a graft chain. It is crucial to choose an initiator system that would lead to maximum grafting efficiencies with minimum or no homopolymer formation (Liliana et al., 2009; Mohamad et al., 2010; Da Silva et al., 2010; Wang et al., 2016).

Kraft lignin-based copolymers can be synthesized by copolymerization of either one- or two-monomers. In recent years, based on one-monomer polymerization reaction, cationic DMC monomer or nonionic AM monomer has been copolymerized onto starch, xylan, chitosan, and

soda lignin in attempts to produce bio-based flocculants and dispersant to treat wastewater (Wang et al., 2016, 2009, 2013; Hsu et al., 2016; Abrar et al., 2011; Ram et al., 2014; Yue et al., 2008; Shen et al., 2006; Yu et al., 2008; Chen et al., 1986; Hongyan et al., 2013). However, the produced polymers had small molecular weights and charge densities.

The flocculation in many applications requires high charge densities and molecular weights. Based on two-monomers polymerization reaction, the bio-based flocculants of acrylamide and cationic DMC monomers are the most common copolymers having high molecular weight and higher charge density (Duygu et al., 2002). To treat the pulp and papermaking sludge, chitosan-poly (acrylamide- methacrylatoethyl trimethyl ammonium chloride) copolymer was produced by grafting acrylamide and methacrylatoethyl trimethyl ammonium chloride (DMC) onto chitosan (Ben et al., 2010). Starch-based cationic copolymer flocculants were also prepared via copolymerization of 2-trimethylammonium ethyl methacrylate chloride (DMC) and acrylamide (AM) on starch backbone for high density waste drilling mud (Wang et al., 2010). In this dissertation, we studied the free-radical copolymerization of kraft lignin and one or two monomers.

2.2.11 Free radical copolymerization of lignin with two monomers

The copolymerization of lignin with acrylamide (AM) and methacrylatoethyl trimethyl ammonium chloride (DMC) as raw material is carried out following a free radicle copolymerization mechanism to produce lignin-based copolymers (Hasan and Fatehi, 2018a). In this reaction, potassium per sulfate acts as an initiator in an aqueous solution. Sulfate radicles produced by potassium per sulfate in the reaction medium lead to the propagation of the copolymers by attacking hydroxyl group (OH) of lignin and double bonds of acrylamide and DMC to have them engaged in the copolymerization reaction. Copolymers of lignin-AM, lignin-DMC and DMC-AM may be produced in the reaction medium (Figure 2.6 a). The addition of AM will introduce functional groups to lignin, which could improve the chain length and bridging ability of the copolymers efficiently. The grafting of DMC increases the cationic content of the lignin copolymers. On the other hand, the DMC and AM can participate in side reactions to produce homopolymers of PDMC and PAM (Figure 2.6 b). Ideally no homopolymer reactions should occur in this reaction, which is difficult to avoid and is considered as a drawback of this method.

(a) Copolymers

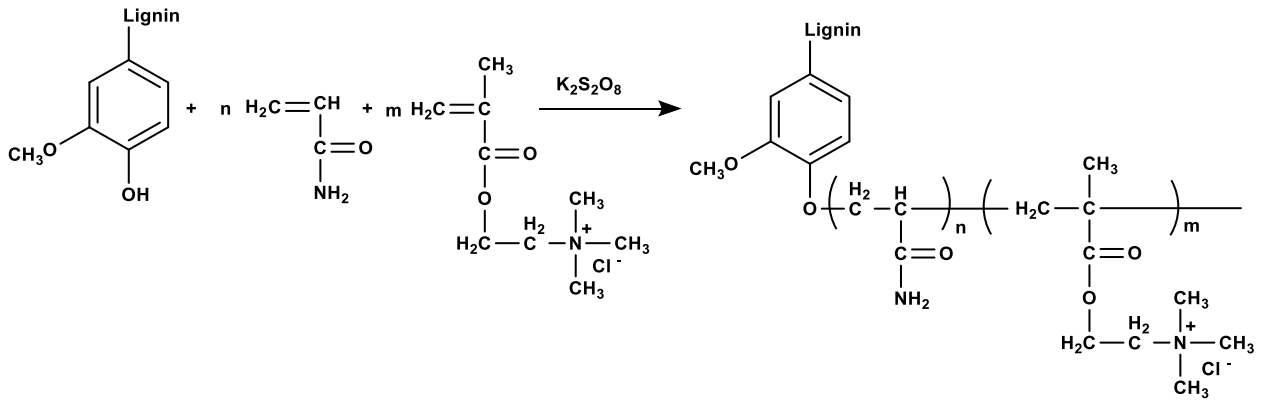

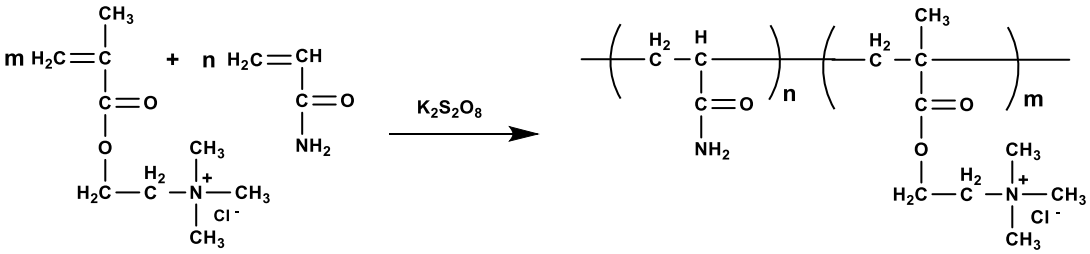

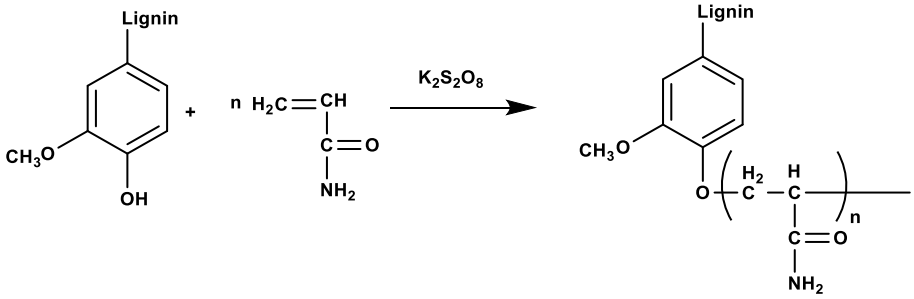

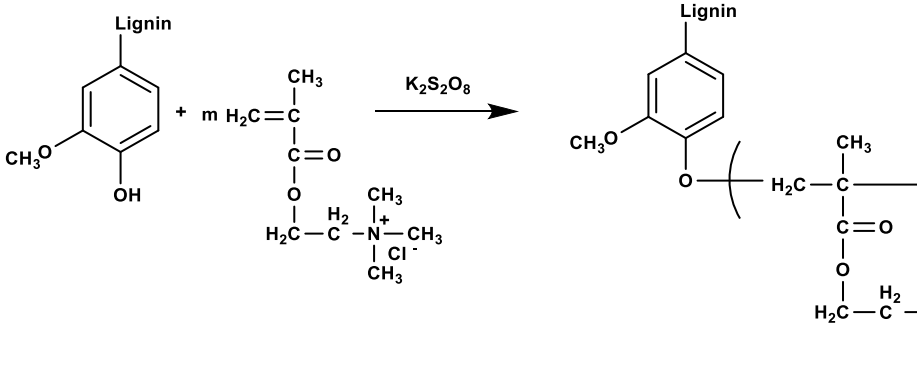

(b) Homopolymers

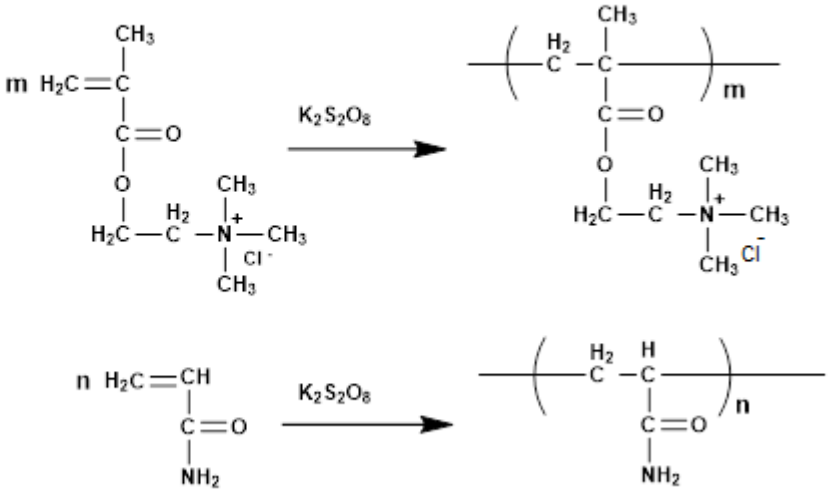

Figure 2.6. Copolymerization reaction of a) lignin, b) homopolymers (Hasan and Fatehi, 2018a).

2.2.12 Free radical polymerization of lignin with one monomer

The lignin polymers with different characteristics can be synthesized in similar fashion by using DMC cationic monomer as a raw material. The polymerization of kraft lignin and 2-[(methacryloyloxy) ethyl] trimethylammonium chloride (DMC) was carried out in this work following a free radicle polymerization mechanism to produce kraft lignin- DMC polymers with the possibility of homopolymerization of DMC to produce homopolymers (PDMC) as a by-product (Hasan and Fatehi, 2018). A general scheme corresponding to this reaction and the resulting kraft-lignin polymer structure obtained are shown in Figure 2.7.

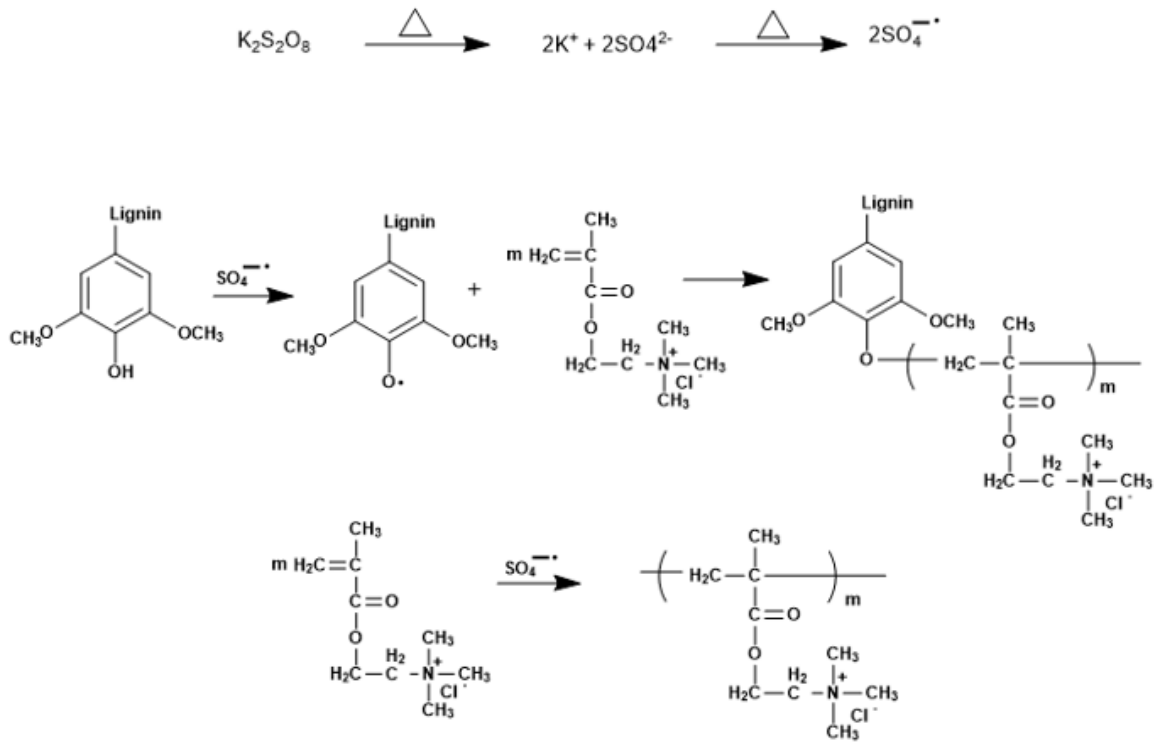

Figure 2.7. Mechanism of the polymerization reaction of lignin and DMC (Hasan and Fatehi, 2018b).

Similarly, the polymerization of lignin and acrylamide was carried out in order to prepare water soluble lignin-acrylamide polymers (Hasan and Fathi, 2018; Rong et al., 2013). In this reaction, potassium per sulfate acts as an initiator in an aqueous solution. As illustrated in Figure 2.8, sulfate radicles in the reaction medium converts lignin to phenoxy radicals and the radicals serve as reaction sites on the lignin backbone for the polymerization. These free radical sites then react with AM monomers to form the lignin polymers. Also, sulfate radicals can initiate the homopolymerization of AM, resulting in polyacrylamide (PAM) as a by-product.

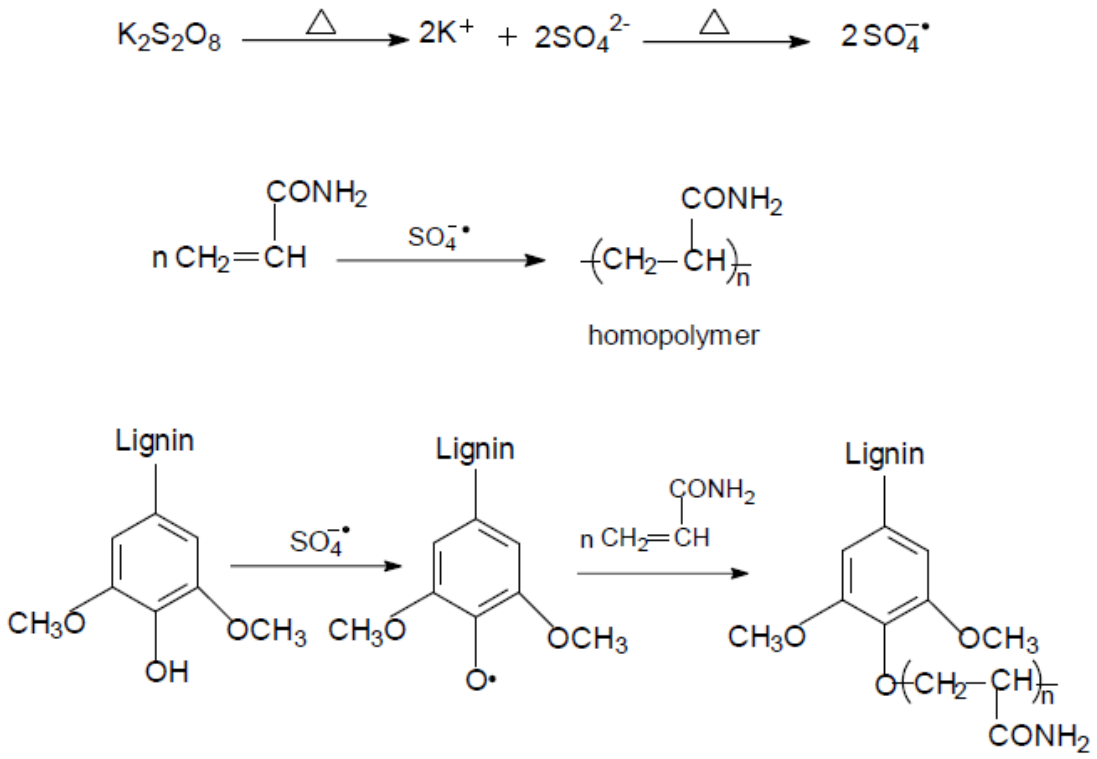

Figure 2.8. Polymerization of kraft lignin and acrylamide (Hasan and Fatehi, 2018b).

2.2.13 Kraft lignin application

Previously, lignin-acrylamide polymer, which was produced by reacting lignin originated from the sludge of a pulping process and acrylamide, was capable of removing 52% of turbidity from aluminum sulfate or poly aluminum chloride suspensions (Rong et al., 2013).The graft polymerization of enzymatically hydrolyzed (EH) lignin with acrylamide (AM) in an aqueous solution led to the production of a product that was able to remove 85% of azo-dyes from dye wastewater (Fang et al., 2009). Soda lignin-acrylamide polymers have been investigated as thinning agents for drilling mud (Ibrahim et al., 2006) and paper strength additives (Wang et al., 2016). In addition, sludge lignin has previously been used as a raw material to produce nonionic and cationic lignin based polymers (Mittal et al., 2014; Li et al., 2015a; 2015b; 2015c). In addition, kraft lignin has been industrially utilized in thermoplastic polymers, binder and resins, absorbent films and carbon fibers (Suhas et al., 2007; Jonsson et al., 2008; Holladay et al., 2007; Cruz et al., 2001; Reti et al., 2008; Kelley et al., 1989; Liu and Li, 2006). However, the

production of kraft lignin-based polymers as flocculants and dispersants was not studied fundamentally previously and was in fact one task of this PhD work.

2.3 Fundamentals

2.3.1 Polymer adsorption

The adsorption of cationic polymers on negatively charged clay particles' surface modify the surface properties of the particles, and hence the interparticle forces between the particles. The polymer adsorption characteristics and surface charge density of clay particles play important roles in determining the interparticle forces and magnitude of adsorption. The interaction with clay particles is a complex process due to simultaneous electrostatic forces, hydrogen bonding, and other forces. Therefore, understanding the relative significance of each of these phenomena is crucial for the explanation of the adsorption of polymers on clay particles. The interaction of cationic polymers with clay particles and their effect on adsorption also depends on the ionic strength, pH, charge density and molecular weight (Morris et al., 2002; Mekhamer et al., 2009; Farrokhpay et al., 2004; Nurmi et al., 2006). Studies have shown that polymer adsorption is promoted by increasing the salt concentration (Shirazi et al., 2003; Chibowski et al., 2009).

2.3.2 Effect of charge density and molecular weight

It has been reported that charge density is important in determining the magnitude of adsorption, and hence the predominant flocculation mechanism (Kam and Gregory, 1999; Rasteiro et al., 2015; Nurmi et al., 2006; Miranda et al., 2008). Previous studies showed that if the molecular weight of polymers is high and their charge density is low, the polymers conform on the clay particle surface in the manner shown in Figure 2.9. This conformation on particle surface is considered as tail and loop that can extend to the solution and interact with other particles to form bridging bonds (Morris et al., 2002; Mekhamer et al., 2009; Farrokhpay et al., 2004). It is generally believed that, the conformation of the adsorbed polymer depends greatly on its charges (Nurmi et al., 2006; Bratby et al., 2006). The adsorption of low charged polymers is based on tail and loop; as the charge density of polymers increases, the bridging capability of the polymers reduces because there is a tendency for the polymer chains to adopt a flatter configuration on the particle surface (Figure 2.9) (Nurmi et al., 2004).

In the same vein, low molecular weight flocculants have greater tendency to develop only charge neutralization mechanisms with particles (Yan et al., 2004; Zhou et al., 2006). Higher molecular weight flocculants developing bridging and charge neutralization facilitate the settlement of particles (Yan et al., 2004). It was reported that higher molecular weight polymers generated larger and stronger flocs with faster settling rates (Zhou et al., 2006). Molecular weight of the polymers is the dominant factor determining the floc strength and the size distribution of flocs (Miranda et al., 2008). Thus, a better understanding of the effect of the charge density and molecular weight of polymers on their flocculation and dispersion performance may lead to the development of more efficient flocculants and dispersants.

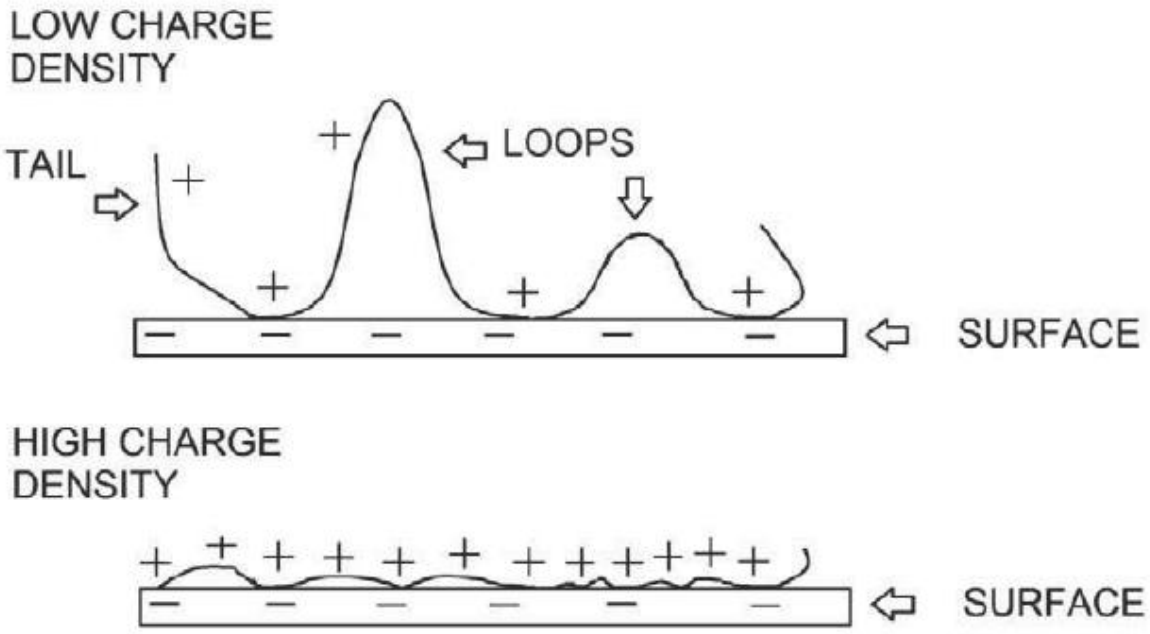

Figure 2.9. Adsorption configuration with low and high charged cationic polymers on a particle surface (Roberts, 2011).

2.3.3 Effect of ionic strength

Among the aforementioned factors, there is also an important one which concerns the potential impact of the solution ionic strength due to the presence of dissolved ions, simple or multivalent electrolyte (salt) in the solution. Polymer conformation in solution is significantly affected by salt concentration and thus the flocculation phenomenon (Shirazi, et al., 2003; Chibowski, et al., 2003). The presence of same charges on the polymer backbone lead to mutual charge repulsion

and cause the polymer chains to expand. Indeed, salt is expected to screen the electrostatic repulsive forces between the charged particles in solution and thus via short-range van der Waals interactions to promote the rate of particle flocculation. At high ionic strength, these charged sites become shielded and force the polymer to fold and adopt a smaller hydrodynamic volume (Miranda et al., 2008). These effects manifest themselves in the flocculation mechanism.

2.3.4 Effect of pH

As described previously, the surface of clay particles possesses both negative and positive charges, and the amount of respective charges varies with pH. The significance of the charges depends on the degree of ionization of the polymers' functional groups (Razali et al., 2015b). The extent of ionization itself depends on the pH of the medium. It has been reported that the pH of the solution has a direct impact on the behavior of the polymer's chains (Razali et al., 2015b). Adjusting the pH of the solution allows the clay suspension to be precipitated, which may directly interfere with flocculation. Hydrolysis, and therefore the ionic charge of the polymers depends on the pH (Jarvis et al., 2005). These changes will impact the adsorption of polymers on the surfaces, accordingly, the polymer activity and the mechanism. Consequently, it is crucial to investigate the adsorption behavior of polymers on clay particles at different pHs (Jarvis et al., 2005; Yoon and Deng, 2004).

2.3.5 Effect of particle size

The size of flocs depends on the polymer adsorption and the extent of flocculation (Yu et al., 2006; Zhou et al., 2006). The suspended negatively charged particles in clay suspension are aggregated into larger size flocs after the addition of cationic flocculants, and then these flocs can be effectively removed via filtration or sedimentation (Zhou et al., 2006). In suspensions, the size of particles depend on their aggregation behavior. As described in sections 2.3.2, the charge density and molecular weight of cationic polymers would impact the size of clay flocs, which in turn affects the stability of clay suspensions. In general, the size of clay particle increases with the increase in molecular weight and charge density of polymers (Zhou et al., 2006; Yu et al., 2006). This is likely possible because higher molecular weight polymers help the chain of polymers to adsorb onto several particles simultaneously by hydrogen bonding via bridging, which results in larger flocs (Wang et al., 2016).

Furthermore, as flocs become larger, its growth is usually prohibited by the disruptive forces created in turbulent environments resulting in floc breakage (Thill et al., 2001). Nevertheless, these broken flocs partially re-flocculate when the shear forces decrease (Chen et al., 1998). In order to achieve the higher removal efficiency, generally larger flocs are preferred as compared to smaller ones (Zhou et al., 2006). The floc strength is dependent on the inter particle bonding of colloid particles in the aggregates. The aggregate size and its strength are directly related to the floc structure, and they determine whether the flocs are suitable for a particular flocculation process. The formation of large flocs facilitates separation of solid particles from the suspension by means of sedimentation and the formation of open flocs facilitates their removal by filtration (Thill et al., 2001). Fractal dimension indicating floc compactness is considered as an essential parameter to describe the floc structure, which is influenced by the polymer's molecular weight, charge density, and types of colloidal suspension (Jin et al., 2014). In this thesis, the effects of charge density and molecular weight of lignin-based polymers on the size of flocs formed via interacting lignin polymers and clay particles are comprehensively studied.

2.3.6 Relative turbidity

The flocculation efficiency is evaluated by parameters, such as turbidity removal, because it is directly related to the industrial separation process and wastewater. It has been observed that cationic flocculants should be more effective than nonionic flocculants in dealing with negatively charged clay particles in reducing the turbidity in colloidal suspension. The compositional characteristics of the polymer-based flocculants including functional groups, charge density, and molecular weight of the polymers, are considered to be among the main factors affecting the flocculation efficiency. In addition, the relative turbidity of clay suspensions increases (dispersion) or decreases (aggregation) depending on the pH of the medium and charge of the polymers (Liimatainen et al., 2009; Shaw, 1992). The influence of shear after cationic flocculant addition on the relative turbidity of clay suspension is reported in literature (Wang et al., 2016; Jarvis et al., 2005). The shear force can break flocs (Thill et al., 2001; Hunter, 1993). Flocculation properties (settling rate, sediment thickness, supernatant clarity) of clay suspensions have been studied in the presence of cationic polymer. In addition, turbidity of suspensions depends on the size of particles. This process is characterized by parameters, settling velocity,

size and compactness of flocs for instance. Thus, it is worth investigating the effect of polymer characteristics on the relative turbidity of clay suspensions.

2.3.7 Zeta potential

The particles in a colloidal suspension usually carry an electrical charge. The charge on colloidal particles can arise from a number of different sources, e.g., dissociation of acidic or basic groups on the particle surface, and adsorption of a charged polymers from solution. Zeta potential is a function of the surface charge of the particle, any adsorbed layer at the interface, the nature and composition of the surrounding suspension medium (Chorom and Rengasamy, 1995; Salopek et al., 1992). It depends on the properties of liquid as well as properties of the surface. The development of a net charge at the particle's surface affects the distribution of ions in the surrounding interfacial region, resulting in an increased concentration of counter ions close to the surface. An increase in the concentration of the counter ions close to the surface results in the formation of an electrical double layer. The liquid layer surrounding the particle consists of two parts, i.e., an inner region (stern layer) where each particle is surrounded by oppositely charged ions, and is strongly bound; and an outer (diffuse) region, where ions move freely and become weaker and weaker and eventually decay to zero. Within the diffuse layer, there is a notional boundary (slip plane), inside which the ions and particles form a stable entity. When a particle moves in voltage field (electrophoresis), ions within the boundary move with it. Those ions beyond the boundary stay with the bulk solution. The potential at the boundary of the stern plane and the diffuse (shear) plane is known as the zeta potential (Figure 2.10). The thickness of this layer depends on the type and concentration of ions in solutions.

Zeta potential of particles is a good indicator of the magnitude of the interaction between colloidal particles, and it is commonly measured to assess the stability of colloidal systems. The change in clay's surface charge density as a result of cationic polymer adsorption has been observed as a change in zeta potential (Wang et al., 2016). Generally, the higher the value of absolute zeta potential, the stronger the repulsion, the more stable the system would be. The zeta potential of solution varies with the pH of the solution. For example, in the acidic colloidal dispersion (high concentration of H^+ ions in the solution), the adsorption of H+ ions on kaolinite particles will compress the diffuse electrical double layer resulting in lower zeta potential values. Under alkaline conditions (high concentration of OH^- in the solution), the adsorption of OH^- ions

on kaolinite water interface results a large diffuse double layer having a higher zeta potential value (Huang et al., 2016). Zeta potential technique has been conveniently applied to control the stability of the dispersions in many industries, such as the mining (Petroff et al., 1993), clay and drilling fluid (Lameirasa et al., 2008), ceramics (Schmut et al., 1964), and wastewater treatment and papermaking (Wang et al., 2016).

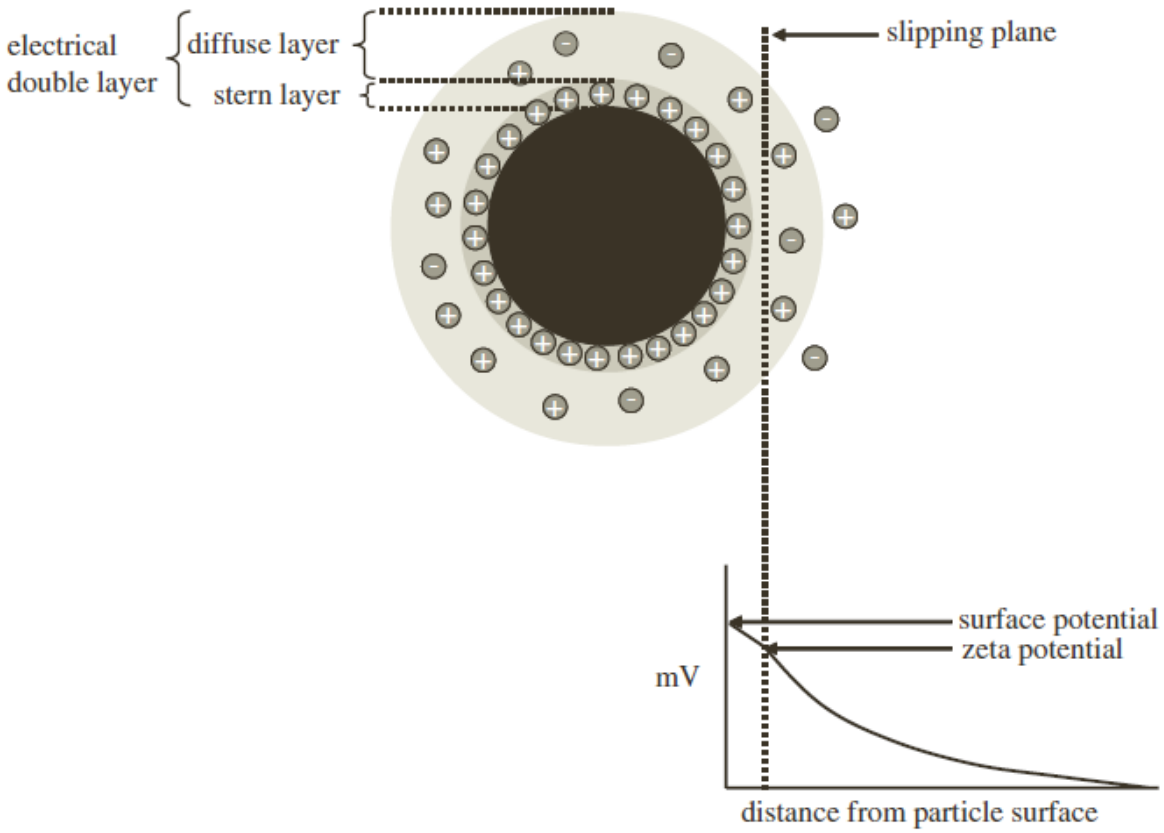

Figure 2.10. Schematic of the electrical double layer that surrounds a particle in an aqueous medium and the position of the slipping plane. The zeta potential is the electrical potential at the slipping plane (Kaszuba et al., 2010).

2.3.8 Effect of polymer characteristics on relative turbidity of clay suspensions

As stated in the literature, the addition of cationic polymers introduces more positive charges on the clay particles causing them to destabilize the negatively charged particles upon adsorption (Thill et al., 2001). This phenomenon results in sedimentation of particles from the suspensions, and reduces the turbidity of clay suspensions, as a result (Zhu et al., 2011; Farrokhpay et al., 2004). As described in section 2.2.9.2, the adsorption of the polymers on the surface of clay samples depends on the charge density and molecular weight of the polymers. To produce a novel flocculant, it is important to study the effect of charge density and molecular weight of kraft lignin based polymers on the relative turbidity of clay suspensions.

2.3.9 Effect of polymer characteristics on stability of clay suspensions

The stability of clay suspensions is crucial in the mining and mineral industries to achieve products with desired performance. However, suspended clay particles pose a major challenge due to their high concentrations (Schmidt and Lagaly, 1999; Wang et al., 2016). It is important to study the settling or stability characteristics of clay suspensions in the presence of kraft lignin based polymers in order to design effective flocculant. There are no reports on the effect of charge density and molecular weight of kraft lignin based polymers on the settling behavior of clay suspensions, which is one of the objectives of this thesis work.

2.4 Methodology

2.4.1 Charge density analysis

Charge density of the polymers were determined via colloidal titration using a particle charge detector (PCD). In this method, a solution or a cationic modified lignin is neutralized with an oppositely charged standard polymer solution potassium polyvinylsulfate (PVSK) using a Mütek PCD 03 particle charge analyzer. The titration is based on their interaction to form the complexes that are stoichiometric with respect to charge of polymers (Huang et al., 2013; Ma, 2011). A back titration method is applied to measure the surface charge density of clay (Lou et al., 2013). In this analysis, PVSK and PDADMAC solutions are employed as standard solutions since their interactions with the charges of clay particles are stoichiometrically controlled (Peng et al., 2011). The PDADMAC standard solution, which has an opposite charge density than that of clay particles, is added to colloidal suspensions to adsorb on the clay surface. After mixing

and filtering, the concentration of PVSK or PDADMAC solution is determined by the PCD, and is compared with the concentration of PVSK or PDADMAC in the control solutions (i.e. the solutions with no clay). The difference between the concentration of polymers in the filtrate and in its control solutions provides the surface charge density of clay particles (Lou et al., 2013), as the difference is due to the adsorption of PVSK or PDADMAC polymers on the surface of the clay particles.

The carboxylate groups generated during modification of lignin is determined by using potentiometric titration method as described in the literature (Peng et al., 2011; Gunther, 2014). Peng and coauthors (2011) reported that potentiometric titration is a reliable method to determine the concentrations of charged groups present in the unmodified and modified polymers.

2.4.2 Methods to characterize modified polymers

Nuclear magnetic resonance (NMR) spectroscopy is one of the most powerful and widely used techniques in chemical research for investigating structures and dynamics of molecules. The method is based on spectral lines of different atomic nuclei that are excited when a strong magnetic field and a radiofrequency transmitter are applied (Lou et al., 2013; Hong et al., 2016). These excited nuclei absorb some energy and subsequently release energy as the nuclei relax back to their original states. The released energy can be scanned and expressed as chemical shifts, and considered as fingerprints of chemical structures. This relaxation time of the nuclei depends on the surrounding chemical groups and occurs differently depending on the type of chemical groups (Griffiths and Haseth, 1986).

FTIR spectrometers (Fourier transform infrared spectrometer) is a simple, rapid and sensitive method applied in organic synthesis, polymer science, petrochemical engineering, pharmaceutical industry and food analysis (Konduri et al., 2017; Kim et al., 2004). It is an easy way to identify the presence of functional groups of polymers. In this analysis, infrared radiation is passed through a sample. Some of the infrared radiation is absorbed by the sample and some of it is passed through (transmitted). An infrared spectrum represents a fingerprint of a sample with absorption peaks, which corresponds to the frequencies of vibrations between the bonds of the atoms making up the material. Since each different material is a unique combination of atoms, no two compounds produce the exact same infrared spectrum. Therefore, infrared spectroscopy can result in a positive identification (qualitative analysis) of different materials. In addition, the size

of the peaks in the spectrum is a direct indication of the amount of material present. Infrared is an excellent tool for quantitative analysis with modern software algorithms (Kim et al., 2004). The FTIR spectrophotometer operates on a principle called Fourier transform (Kim et al., 2004); whose formula can be seen in Equation 2.1.

$$F(\omega) = \int_{\infty}^{\infty} f(x) e^{ix\omega} \qquad (2.1)$$

The reverse Fourier transform is

$$F(x) = \frac{1}{2\pi} \int_{-\infty}^{+\infty} f(\omega) e^{i\omega x} dx \qquad (2.2)$$

where ω is angular frequency (1/s) and x is the optical path difference. F (ω) is the spectrum and f(x) is called the interferogram. In this study, lignin based polymers were studied by FTIR to elucidate the difference in functional groups between unmodified and modified lignin.

Thermo gravimetric analyzer (TGA) is a technique in which the mass of a substance is monitored by gradually raising the temperature of a sample in a furnace as its weight is measured on an analytical balance that remains outside of the furnace (Heinze et al., 2005; Daniel and Musil, 2013). In TGA assessment, mass loss is observed as a function of temperature and/or time as the sample is subjected to a controlled temperature change in a controlled atmosphere. The weight of the sample is plotted against temperature or time to depict thermal transitions in the material, such as loss of solvent in polymers, water in inorganic materials, and decomposition of the material (Solberg and Wagberg, 2003). In this study, the TGA analysis of dried polymeric samples (lignin) were conducted. The difference of the mass of the polymers during this process is measured using micro-thermal balance. A mass loss indicates the degradation of polymers at a specific temperature (Thompson, 2008).

Elemental analyzer is a technique employed in determining the elemental compositions of polymers (Das et al., 2013; Forster and Schmidt, 1990). This method is used extensively for the determination of carbon, hydrogen, sulphur and nitogen elements of different samples across a wide range of applications, including pharmaceuticals, polymers, food and chemicals. Based on classical Pregl-Dumas method, the combustion process in pure oxygen and high temperature (furnace at 1000^{o} C) environment, carbon is converted to carbon dioxide; hydrogen to water; nitrogen to nitrogen gas, and sulphur to sulphur dioxide. If other elements, such as chlorine, are

present, they will also be converted to combustion products, such as hydrogen chloride. Eluted gases are sent to the detector where electrical signals processed by the software to provide percentages of nitrogen, carbon, hydrogen, and sulfur contained in the sample (Forster and Schmidt, 1990). Unmodified and modified lignin were combusted to determine the elemental compositions.

Dynamic light scattering (DLS) technique has been applied extensively for characterization of particles or molecules, which have been dispersed or dissolved in a liquid (Murphy, 1997; Rodd et al., 2000; Kostanski et al., 2004; Feng et al., 2015). The Brownian motion of particles or molecules in suspension causes laser light to be scattered at different intensities. Analysis of these intensity fluctuations yields the velocity of the Brownian motion. Due to the fact that large molecules or particles move slower than small molecules, a defined correlation function is generated. From the correlation function, the diffusion coefficient (D) of the molecules can be calculated by fitting the data. Finally the hydrodynamic radius (R_h) of the particles and molecules can be calculated using the Stokes-Einstein relationship according to equation 2.3 (Feng et al., 2015).

$$R_H = \frac{KT}{6\pi nD} \qquad (2.3)$$

where D is the diffusion coefficient, R_H is radius (nm), k is Boltzmann constant, T is temperature (°C), and η is solvent viscosity (Pa. s).

In this thesis, the hydrodynamic of lignin based polymers were determined in the presence of NaCl salt. The addition of salt prevents the aggregation of polymers by neutralizing their functional groups. After mixing, the polymer solutions are filtered and the filtrates containing polymer are subjected to the hydrodynamic size analysis using DLS.

Gel permeation chromatography (GPC) is a widely used technique for determining the molecular weights and molecular weight distribution of the polymers (Heinze and Koschella, 2005, Lu et al., 2002). When a sample is injected in the apparatus, the polymer molecules are separated with respect to their effective size. Separation occurs in columns with porous packings. The choice of columns depends upon the solvent and range of molecular weights.

In this analysis, a sample containing different polymeric molecules is introduced into a solvent flowing through the column. As the dissolved polymer molecules flow through the porous beads, they can diffuse into the internal gel to an extent depending on their size and the pore-size distribution of the gel. The principle of measurement is elution of components with mobile phase through the stationary phase. As the larger molecules cannot enter the pores of the GPC column, they pass quickly through the column and exit. Smaller molecules can enter some pores and they elute slower. In this arrangement, the different molecular species are eluted from the column in order of their molecular size as distinguished from their molecular weight. The elution behavior of sample produces reliable and reproducible chromatograms, which represents the time taken for a molecule of particular size (a fraction) to elute from column (retention time). The concentration of polymer molecules in each eluting fraction can be monitored by means of a polymer-sensitive detector, such as refractive, infrared or ultraviolet.

Moreover, a correlation can be made between size and molecular weight by plotting a graph between log molecular weight (M) and retention time for standard samples, and this correlation can be used for determining the molecular weight distribution of polymers. For a more precise determination of molecular weight of polymers, the chromatogram is divided into several equidistant slices. The weight average molecular weight (M_w), number average molecular weight (M_n) and polydispersity index (PDI) are calculated following equations 2.4, 2.5 and 2.6 (Kostanski, et al., 2004; Striegel et al., 2009).

$$M_w = \frac{\sum_i N_i M_i^2}{\sum_i N_i M_i} = \frac{\sum_i w_i M_i}{\sum_i w_i} \qquad (2.4)$$

$$M_n = \frac{\sum_i N_i M_i}{\sum_i N_i} \qquad (2.5)$$

$$PDI = \frac{M_w}{M_n} \qquad (2.6)$$

where N refers to the number of polymer chains, having molecular weight of M, and w_i corresponds to weight fraction distribution. The ratio of Mw over Mn provides information about

the distribution of the chain lengths, which is denoted as polydispersity index (PDI). The number or weight fraction distribution (N_i or M_i) can be obtained from the concentration of molecules measured by the viscometer and refractive index detectors associated with GPC. In this work, polymer samples (lignin) were dissolved in sodium nitrate salt solution, which was the mobile phase of the GPC system used in this work. After dissolving, the polymer solutions were filtered and the filtrates were subjected to molecular weight analysis. The molecular weight and polydispersity of the polymers were assessed using GPC, equipped with viscometer and refractive index detectors.

Tensiometer can be used to determine the wettability of polymers by measuring the contact angle of water on solid surfaces (Grundke et al., 1996; Kwok and Neumann, 2000; Rogers, 2005). Contact angle, θ, is a quantitative measure of the wetting of a solid by a liquid. Contact angle is the interior angle formed by the sample being used and the tangent to the drop interface at the apparent intersection of all three interfaces. This intersection is called the contact line. Figure 2.11 shows the tangent line and contact angle of a liquid drop on a surface. More specifically, a contact angle less than 90° indicates that wetting of the surface is favorable, and the fluid will spread over a large area on the surface; while, the contact angles greater than 90° generally means that wetting of the surface is unfavorable so the fluid will minimize its contact with the surface and form a compact liquid droplet. For example, complete wetting occurs when the contact angle is 0°, as the droplet spread completely (Yuan et al., 2013).

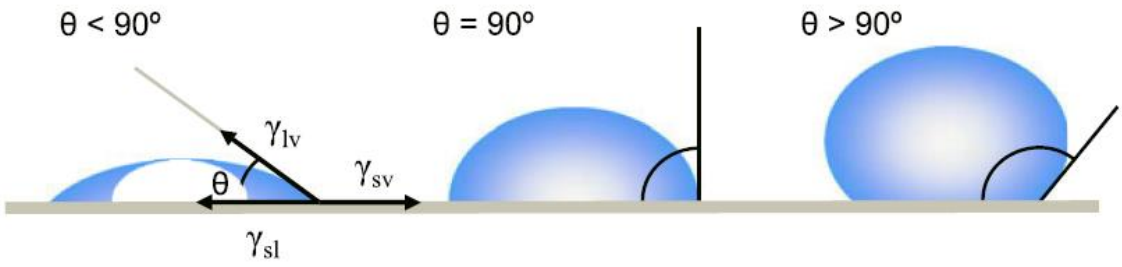

Figure 2.11. Illustration of contact angles formed by sessile liquid drops on a smooth homogeneous solid surface (Yuan et al., 2013).

Historically, a static contact angle on a flat surface is defined by the Young Equation (2.7). Theoretically, the contact angle is a distinctive property of a given solid-liquid system under specific conditions (Loginov et al., 2008). As described by Young in 1805, the contact angle of a liquid droplet on an ideal solid surface is defined as the mechanical equilibrium of the droplet balanced by the action of three interfacial tensions as represented in Equation 2.7 (Rogers, 2005).

$$\gamma_{lv}\, cos\theta_Y = \gamma_{sv} - \gamma_{sl} \qquad (2.7)$$

where, γ_{lv}, γ_{sv}, and γ_{sl} represent the liquid-vapor, solid-vapor, and solid-liquid interfacial tensions, respectively, and θ_Y is the contact angle in degrees (°).

In this thesis, polymers (lignin) or clay samples were coated on microscopic glass slides using a spin coater under controlled conditions in nitrogen atmosphere. After coating, the slides were wetted with required volume of water droplets by the sessile drop technique, and the wettability of the polymers or clay samples were determined by contact angle and interfacial measurements using an optical tensiometer.

2.4.3 Clay properties

Brunauer-Emmett-Teller (BET) instrument determines the specific surface area (m^2/g) of clay samples (Tombac and Szekeres, 2006; Howang and Barron, 2011). The volume of gas adsorbed to the surface of the particles is measured at the boiling point of nitrogen. The amount of adsorbed gas is correlated to the total surface area of the particles including pores in the surface. The specific surface area of a sample is determined by physical adsorption of a gas on the surface of the solid particle and by calculating the amount of adsorbate gas corresponding to a monomolecular layer on the surface of the particle. Physical adsorption results from relatively weak forces (van der Waals forces) between the adsorbate gas molecules and the adsorbent surface area of the particle. The determination is usually carried out at the temperature of liquid nitrogen. The amount of gas adsorbed can be measured by a volumetric or continuous flow procedure. In this method, a monolayer adsorption of the gas is determined on the surface, from which the surface area is measured by the BET equation (Equation 2.8) (Cartula and Sabio, 1991; Hussein et al., 1996).

$$\frac{p}{V_a(p_0 - p)} = \frac{1}{V_m c} + \frac{c-1}{V_m c}\left(\frac{p}{p_0}\right) \qquad (2.8)$$

where P (Pa) and P_0 (Pa) are the equilibrium and the saturation pressure of the gas at the temperature of adsorption, representivley, v (mL) is the gas adsorption amount (for example, in volume units), and v_m (mL) is the amount of gas adsorbed in a monolayer form on the surface and c is the BET constant.

By plotting $\frac{p}{V_a(p_0 - p)}$ against $\frac{p}{p_0}$, the BET plot can be obtained. The intercept and slope of the BET plot can be identified, from which V_m and c can be calculated.

The total surface area (BET) of the solid can be calculated from Equation 2.9.

$$a_s = \frac{V_m}{22414} L\sigma_g \qquad (2.9)$$

where L is the Avogadro constant and σ_g is the cross-section area of the adsorbed gas molecules (σ_g for nitrogen is 0.162 nm^2).

Scanning electron microscopy (SEM) in tandem with energy dispersive X-ray spectroscopy (EDX) was used to determine the chemical composition of kaolin (Tombac and Szekeres, 2006; Wu et al., 2012; Vie et al., 2007). In this thesis, the clay samples were initially mixed in acetone under ultrasonic vibrations to disperse the particles and allowed to dry. After drying, the samples were coated with carbon under vacuum using carbon coating technique and analyzed using SEM-EDX technique. In EDX Analysis, the particles (specimen) is bombarded with an electron beam inside the scanning electron microscope. The bombarded electron beam collides with the electrons of specimen's atoms and moves the electrons present in the inner shell of atoms to the outer shell. In this process, the void generated in the lower shell is occupied by a higher-energy electron from an outer shell of specimen atom by releasing energy in the form of X-rays. Furthermore, the atom of every element in the particles releases X-rays with unique amounts of energy in the transferring process. Thus, by measuring the amounts of energy present in the X-rays released by the sample in electron beam bombardment, the identity of the atom can be established (Zhou et al., 2016; Zhu, et al., 2012).

According to the literature, X-ray diffractometer (XRD) is described as a powerful tool in assessing the mineral compositions of substances (Penkavova et al., 2015; Hu, 2002; Roh, 1995). In this analysis, the samples were dried to remove any moisture and loaded on the spinner of the XRD

and scanned for mineral compositions. The three-dimensional structure of crystalline materials, such as clay minerals, is defined by regular, repeating planes of atoms that form a crystal lattice. When an X-ray beam interacts with these planes of atoms, one part of the beam is transmitted, one part is absorbed by the sample, one part is refracted and scattered, and another part is diffracted. Diffraction of an X-ray beam by a crystalline solid produces spectra, and furthermore each mineral diffracts the X-ray beam differently, depending on what atoms present in the crystal lattice and how they are arranged. When an X-ray beam hits the clay sample and is diffracted, the distances (d-spacings) between the planes of the atoms that constitute the sample can be measured by applying Bragg's Law using Equation 2.10 (Mishra et al., 2002; Peng-wei et al., 2008)

$$n\lambda = 2d \sin\theta \qquad (2.10)$$

where the integer n is the order of the diffracted beam, λ is the wavelength of the incident X-ray beam in nm, d is the distance between adjacent planes of atoms (the d-spacings) in nm, and θ is the angle of incidence of the X-ray beam in degrees (°).

The configuration of an XRD unit is aimed to perform this measurement. The distinctive set of d-spacings generated in a typical X-ray scan provides a unique feature of the mineral or minerals present in the clay sample. When properly interpreted, by comparison with standard reference patterns and measurements, minerals present in the clay sample can be identified.

2.4.4 Properties of clay suspensions

The zeta potential is an important parameter to evaluate the colloidal stability of a system. As described in literature, zeta potential, which is also referred to as electrokinetic potential of particles in the suspension, can be measured by zeta potential analyzer. This technique includes an electrophoresis principle. When an electric field is applied across an electrolyte solution, charged particles suspended in the electrolyte are attracted towards the electrode of opposite charges, while viscous forces acting on the particles tend to oppose this movement. However, when an equilibrium is reached between these two opposing forces, the particles move with constant velocity. This velocity of the particle is also referred to as electrophoretic mobility. Based on this principle, the zeta potential of particles can be measured by the Smoluchowski equation (Equation 2.11) (Riddick, 1961; Araki et al., 1992).

$$U_E = \frac{2\varepsilon z f(ka)}{3\eta} \quad (2.11)$$

where z is zeta potential (mV), U_E is electrophoretic mobility (m/s), Ɛ is dielectric constant, η is viscosity of suspension (mPa.s) and f (ka) is Smoluchowski constant (either 1 or 1.5). In this study, the zeta potential of clay suspensions in the presence or absence of lignin-based polymers was determined at a constant electric filed.

Relative turbidity is one of the important criteria used for studying the stability of colloidal suspensions (He and Fatehi, 2015). Colloidal particles in the suspensions possess charges on their surfaces, which may result in dispersion (due to more repulsion forces) or aggregation (due to more aggregation forces) of the particles. If the repulsion forces between the particles dominate, the particles tend to repel each other and be more distributed within the system, which is accompanied by an increase in the relative turbidity. On the other hand, if the repulsion forces diminish, the particles tend to aggregate and settle, which results in decreased relative turbidity of the colloidal suspensions. As described elsewhere, a dynamic drainage jar (DDJ) equipped with photometric dispersion analyzer (PDA) is widely employed to analyze the dispersion of colloidal suspensions via measuring the relative turbidity of colloidal suspensions. PDA is a fibre-optical monitor that measures the fluctuation in the intensity of light transmitted through a flowing suspension. The fluctuations in the intensity of light were quantified in terms of direct current (DC) voltage signals (Petzold et al., 2006). In this analysis, distilled water was transferred to DDJ and circulated from DDJ to PDA for a required period of time and the corresponding DC voltage values were recorded. Later, clay suspension in the presence or absence of polymers (lignin or xylan) was added to DDJ and allowed for passing through PDA. The change in DC voltage signals were recorded and used further to calculate the relative turbidity of clay suspensions by Equation 2.12.

$$\text{Relative turbidity, } \tau_r = \frac{\tau_f}{\tau_i} = \frac{ln(\frac{V_0}{V_f})}{ln(\frac{V_0}{V_i})} \quad (2.12)$$

where τ_f is denoted as the final suspension turbidity, and τ_i is denoted as initial suspension turbidity, V_0 is initial base DC voltage, V_i stands for unflocculated suspension DC voltage, and V_f is final suspension DC voltage.

In laser diffraction instrument, particle size distributions were calculated by the scattering pattern of a clay suspension (Loginov et al., 2008; Nonrorv, 1997; Zhang et al., 2014). In this technique, an intense laser beam of fixed wavelength passes through the clay sample and a series of detectors to measure the light pattern produces over a wide range of angles. The Mie theory was considered to calculate the particle size distributions from light scattering data. It interprets the scattering intensities for all the particles with different sizes and transparencies based on Equation 2.13 (Zhang et al., 2014).

$$I = \frac{2\pi r N_m}{\lambda} \qquad (2.13)$$

In this equation, I is denoted the intensity of incident light, r is the radius of the particles (nm), N_m is the refractive index of the medium and λ is the wavelength of incident light (nm).

The fractal dimensions (structure) of the flocs were determined by small-angle laser light scattering technology (SALLS) (De Boer and Weerd, 1987; Waite et al., 2001; Tang et al., 2002; Jarvis et al., 2008). In this experiment, the incident light was directed onto a sample containing the particles/flocs and then the light was scattered at different angles with respect to the incident direction. The intensity of the lights scattered at the angles of 0.01° and 40.6° is a function of the scattering vector (Q) (Teixeira, 1988; Bushell et al., 2002). This vector is defined as the difference between the incident and scattered wave vectors of the radiation light in the medium (i.e., water). The magnitude of the wave vector can be approximated following equation 2.14:

$$Q = \frac{4\pi n \sin(\theta/2)}{\lambda} \qquad (2.14)$$

where, n is the refractive of the medium (i.e., n=1.33 as deionized water is used), θ is the scattered angle (from 0.01° to 40.6°), and λ is the wavelength of radiation (633 nm).

It has been shown that for a mass fractal aggregate that satisfies the conditions for the Rayleigh-Gans-Debye (RGD) theory, Equation 2.14 can be used to correlate the scattered light intensity (I) with the scattering wave vector (Q) (Farias et al., 1996). Therefore, Equation 2.15 is classically used to determine the mass fractal dimension from the negative slope of the linear region of the log-log plot of I vs Q.

$$I \propto Q^{-D_f} \qquad (2.15)$$

In this equation, D_f is fractal dimension of the flocs (Jarvis et al., 2008).

In addition, the stability of kaolin suspensions in the presence and absence of lignin polymer was determined using a vertical scan analyzer, Formulation, France as described in the literature (Ryan and Gschwend, 1994; Senoussi et al., 2016). In this analysis, kaolin or clay suspensions with required concentration were prepared under aqueous conditions in the presence or absence of polymers (lignin). The suspensions were transferred to vial and the analysis was performed by allowing light beams pass through a clay dispersion. The light passes through a transmission zone of the samples, while it cannot pass throughout the sediment zone of the samples. Two synchronous optical sensors receive light transmitted through the sample (180° from the incident light, transmission sensor) and light backscattered by the sample (45° from the incident radiation, backscattering detector). The higher transmission zone implies less stable kaolin dispersions due to the sedimentation of particles. These transmittance and backscattering signals were recorded as a percentage of transmittance signals in regard to that of the reference chemical, silicon oil.

The transmission and backscattering data was used for determining the destabilization index (DSI) and average particle diameter using the turbisoft software by equations 2.16 and 2.17 (Senoussi et al., 2016).

$$\mathrm{DSI} = \Sigma_i \frac{\Sigma_h |scan_i(h) - scan_{i-1}(h)|}{H} \qquad (2.16)$$

where $scan_i$ (h) and $scan_{i-1}$ (h) are the transmission signals for two consecutive time intervals at a given height and H is the total height of the sample.

Correlation between the particle migration velocity and the properties of the suspensions can be determined using Equation 2.17.

$$V(\Phi, \mathrm{d}) = \frac{|p_p - p_c| g d^2}{18 v p_c} \times \frac{[1-\Phi]}{\left[1 + \frac{4.6\,\Phi}{(1-\Phi)^2}\right]} \qquad (2.17)$$

where V is the particle migration velocity (μm/min), p_c is the continuous phase density (g/mL), p_p is the particle density (g/mL), d is the particle mean diameter (μm), v is the continuous phase

dynamic viscosity (mPa.s), and Φ is the volume fraction of dispersed particles (i.e., kaolin particles) in %.

The size of kaolin particles in the dispersed state (i.e. not settled) and their volume fractions can be obtained based on the backscattering data collected. Based on the Mie theory, the backscattering data measured by the instrument can be expressed as a function of photo transport mean free path, I* in Equation 2.18.

$$BS = \frac{1}{\sqrt{I^*}} \quad (2.18)$$

In addition, the photo transport mean free path, I* (μm), could be obtained via following Equation 2.19:

$$I^*(d, \theta) = \frac{2d}{3\theta\,(1-g)Q_s} \quad (2.19)$$

where, d is the particle mean diameter (μm), θ is the particle volume fraction (%), g and Qs are the dimensionless scattering efficiency factors, depending on the particle diameter (d), wave length of light (λ) in nm, refractive index of dispersed kaolin particles (n_p), and the refractive index of continuous phase (n_f). In this work, the refractive indices of kaolin particles and water were considered to be 1.54 and 1.33, respectively. According to Eqs. 2.18 and 2.19, backscattering data is directly dependent on the particle mean diameter, d, and their volume fraction, θ (Sarwar et al., 2012). By providing refractive indices of kaolin and water, the turbisoft 2.1 software associated with the instrument would generate a correlation between the size of kaolin particles and their volume fraction in the dispersion from the backscattering data.

Recently, the number of optical techniques available to monitor the flocculation behavior in industrial separation processes has been expanded by employing non-imaging scanning laser microscopy, also called focused beam reflectance measurement, FBRM. This methodology allows for studying and optimizing the flocculation and coagulation processes (determination of mechanism and floc properties, selecting the optimal flocculant, dosage and conditions) in a faster and more efficient way (Thapa et al., 2009; Zhu et al., 2011; Senaputra et al., 2013; Klein et al.,

2013). The FBRM measurement principle is based on backscattering light using a probe where a revolving laser beam is projected through a sapphire window. The beam is highly focused just outside the window surface and rotates in order to perform measurements in a circular path. As particles pass by the window surface, the focused beam intersects the edge of a particle as illustrated in Figure 2.12. The particle then begins to backscatter laser light until the focused beam reaches the opposite edge of the particle. The backscattered light is collected by FBRM optics and converted into an electronic signal. Particle backscattering time is multiplied by scan speed resulting in a chord length, which is a straight line between any two points on the edge of a particle. During a specified measurement time, recorded chord lengths are displayed in the form of chord length distribution (CLD). Thousands of chord length measurements are collected per second, producing a histogram in which the number of the observed counts is sorted in several chord length bins over the range 0.5 to 1000 or 2000 μm. From the data, total counts, counts in specific size regions (population), mean chord length, and other statistical parameters can be calculated and analyzed using the FBRM software (Clain et al., 2015). This machine was used for studying the flocculation performance of lignin polymers in clay suspensions.

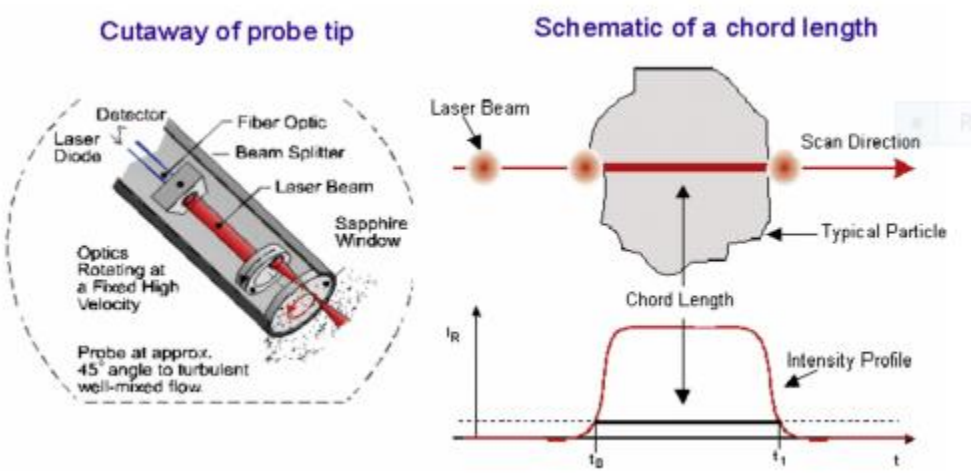

Figure 2.12. FBRM chord length measurement (from Mettler Toledo, USA).

Quartz crystal microbalance with dissipation (QCM-D) technique was widely applied in the field of biological and non-biological systems (polymers, polymer-brushes, electro-polymerization) (Nomura and Minemura, 1980; Duner et al., 2013; McNamara and Blanford, 2013). The

viscoelastic properties of the polymer in liquid have studied extensively by QCM-D to allow for real-time analysis of polymer adsorption and/or interactions on various surfaces (Dixon, 2008). QCM-D measures the resonance frequency (f) of a quartz crystal at its fundamental resonance frequency recorded at 5 MHz with sensitivity constant (C) of 0.177 mg/m^2 Hz and at several overtones. The quartz crystal sensor is a thin piezoelectric plate with gold coated on each side as electrodes. When AC voltage is applied to crystal causing the sensor crystal to oscillate at its specific resonance frequency. The resonance frequency of a crystal is dependent to its mass. The principle of the QCM-D is that any mass of polymers added or removed lead to change in resonance frequency Δf (Duner et al., 2013). The equation that correlates frequency change (Δf) and mass change (Δm) is named Sauerbrey equation, where negative frequency shift related to the mass increase:

$$\Delta m = - \frac{C\Delta F}{n} \qquad (2.20)$$

where C is the mass sensitivity constant that depends on the crystal properties (17.7 ng/ Hz ×cm^2) for a 5 MHz quartz crystal sensor and n is the overtone number (1, 3, 5, 7, 9, 11, and 13), which is the natural resonance or vibration frequency of QCM-D system. However, the Sauerbrey relation is only applicable for rigid and evenly distributed thin adsorbed films that do not exhibit energy losses during oscillation. A way to determine the validity of the Sauerbrey equation is to look at the viscoelastic properties of the adsorbed layer through the change in dissipation energy of the adsorbed layer. More viscoelastic material leads to the higher dissipation (energy release) (Czandema and LU, 1984; Rodahl et al., 1995). The dissipation of sensors' energy, D, which results from adsorption of a viscous or loose layer, is also measured (Rodahl et al., 1995). This dissipation energy is given by equation 2.21:

$$D = \frac{E_d}{2\pi E_s} \qquad (2.21)$$

where Ed is the energy dissipated during one oscillation and Es is the energy stored in the oscillating system. Thus, changes in adsorbed mass of, for example, a rigid polymer provide a

change in frequency, but for viscoelastic polymers, there is a change both in frequency and dissipation. This instrument was used for studying the self-assembly of lignin based polymers.

The LUMiSizer is an analytical centrifuge that uses the principle of centrifugal separation analysis to measure particle size, demixing, and consolidation. It combines a centrifuge with an optics system (NIR or blue light source and a linear high resolution detector) to monitor the concentration profile over the entire length of a sample, while it is being subjected to centrifugation using STEP-technology (space and time resolved extinction profiles technology). A light source sends parallel NIR-light (λ of 880 nm), which is passed through the sample cells lying on the rotor. The distribution of local transmission is recorded over the entire sample length by a CCD-line detector. Finally, space and time resolved transmission profiles are obtained, from which the integral value indicates the sedimentation progress with time (Chang and Liao, 2016). This instrument was used for determining the dispersion affinity of lignin polymers in clay suspension.

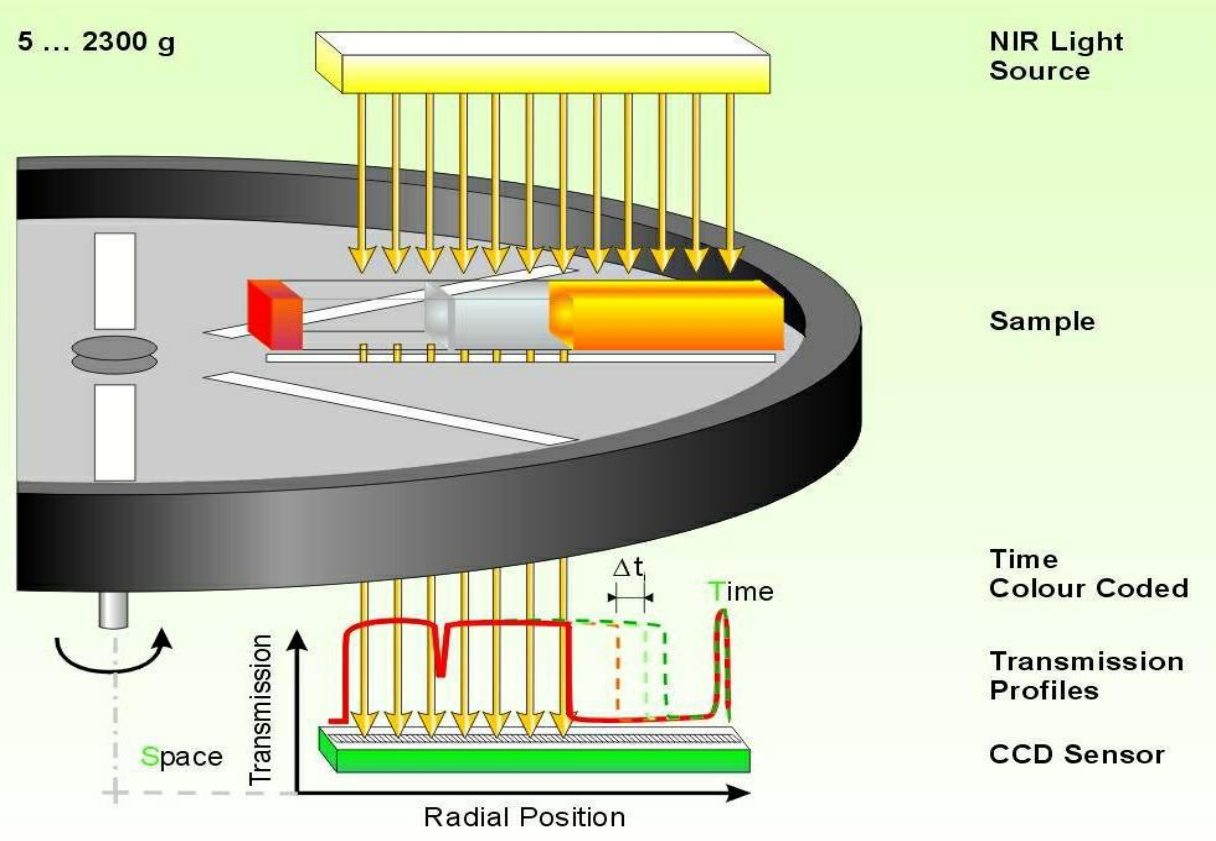

Figure 2.13. Principle of STEP-Technology (from LUM-Gmbh).

2.5 References

Abrar, S., Pedram, F., Yonghao, N. 2011. Chitosan as a flocculant for pre-hydrolysis liquor of kraft-based dissolving pulp production process, Carbohydr. Polym., 86, 1630– 1636.

Ahvazi, B. Wojciechowicz, O., Ton-That, T.M., Hawari, J. 2011. Preparation of lignopolyols from wheat straw soda lignin. J. Agric. Food Chem., 59, 10505-10516.

Araki, J., Wada, M., Kuga, S., Okano, T. 1992.Flow properties of microcrystalline cellulose suspension prepared by acid treatment of native cellulose. Colloids and Surf. A., 142, 75-82.

Atesok, G., Somasundaran, P., Morgan, L.J. 1998. Charge effects in the adsorption of polyacrylamides on the sodium kaolinite and its flocculation. Powder. Technol., 54, 77-83.

Azadi, P., Inderwildi, O.R., Farnood, D.A, King, D.A. 2013. Liquid fuels, hydrogen and chemicals from lignin: A critical review, Renewable and Sustainable Energy Reviews, 21, 506-523.

Baurhoo, B., Ruiz-Feria, C.A., Zhao, X. 2008. Purified lignin: nutritional and health impacts on farm animals-a review. Anim. Feed Sci. Technol., 144, 175-184.

Blanco, A., Fuente, E., Negro, C., Tijero, J. 2002. Flocculation Monitoring: Focused Beam Reflectance Measurement as a Measurement Tool. Can. J. Chem. Eng., 80, 1-7.

Bushell, G. C., Yan, Y. D., Woodfield, D., Raper, J. U. D. Y., Amal, R. 2002. On Techniques for the Measurement of the Mass Fractal Dimension of Aggregates. Adv. Colloid Interface Sci., 95, 1-50.

Cartula, F., Molina-Sabio, M., Reinoso, F.R. 1991. Preparation of activated carbon by chemical activation with ZnCl2. Carbon, 29, 999-100.

Chang, C.W., Liao, Y.C. 2016. Accelerated Sedimentation Velocity Assessment for Nanowires Stabilized in a Non-Newtonian Fluid. Langmuir, 32, 13620−13626.

Chena, Y., Shaoying, L., Wang. G. 2007. A kinetic investigation of cationic starch adsorption and flocculation in kaolin suspension. J. Chem. Eng., 133, 325–333.

Chen, W.J., 1998. Effects of surface charge and shear during orthokinetic flocculation on the adsorption and sedimentation of kaolin suspensions in polyelectrolyte solutions. Sep. Sci. Technol., 33(4), 569- 590.

Chen, M. J., Gunnells, D. W., Gardner, D. J., Milstein, O., Gersonde, R., Feine, H. J. 1996. Graft copolymers of lignin with 1-ethenylbenzene. Macromol., 29(5), 1389–1398.

Chen, Y., Liu, S., Wang, G. 2007. Kinetic investigation of cationic starch adsorption and flocculation in kaolin suspension. J. Chem. Eng., 33, 325-333.

Chen, Q.Y., Wu, Y.G., Pu, Y.T., Zheng, Z.K., Shi, C.Z., Huang, X.Z. 2010. Synthesis and characterization of quaternized beta-chitin. Carbohydr. Res., 345(11), 1609–12.

Chibowski, S., Grządka, E., Patkowski., J. 2009. Influence of a type of electrolyte and its ionic strength on the adsorption and the structure of adsorbed polymer layer in the system: polyacrylic acid/SiO_2. Croat. Chem. Acta, 82, 623–631.

Chorom, M., Rengasamy, P. 1995. Dispersion and zeta potential of pure clays as related to net particle charge under varying pH, electrolyte concentration and cation type. Eur. J. Soil Sci., 46, 657–665.

Chudakov, M.I., 1961. LIGNIN. Russ. Chem. Rev., 30, 61-78.

Clain, P., Ndoye, F.T., Delahaye, A., Fournaison, L., Lin, W., Dalmazzone, D. 2015. Particlesize distribution of TBPB hydrates by focused beam reflectance measurement (FBRM) for secondary refrigeration application. Int. J. Refrig., 50, 19-31.

Cruz, J.M., Dominguez, J.M., Dominguez, H., Parajo, J.C. 2001. Antioxidant and antimicrobial effects of extracts from hydrolysates of lignocellulosic materials. J. Agric. Food Chem., 49, 2459-2464.

Czandema, A.W. and LU, C. 1984. Applications of piezoelectric quartz crystal microbalances. Amsterdam: Elsevier Science Publishers.

Da Silva, D.A., de Paula, R.C.M., Feitosa, J.P.A., 2007. Graft copolymerization of acrylamide onto cashew gum. Eur. Polym. J., 43, 2620–2629.

Daniel, R.., Musil, J. 2013. Novel nanocomposite coatings-Advances and industrial applications. Taylor & Francis group.

Das, D., Dash, U., Meher, J., Misra, P.K. 2013. Improving stability of concentrated coal-water slurry using mixture of a natural and synthetic surfactants. Fuel Process. Technol., 113, 41-51.

De Boer, G.B.J., Weerd, C. Thoenes, D., Goossens, H.W.J. 1987. Laser diffraction spectroscopy: Fraunhofer diffraction versus Mie scattering. Particles, 4, 14-19.

Dilling, P., and Samaranayake, G. S. 1999. "Mixtures of amine modified lignin with sulfonated lignin for disperse dye," US Patent 5,989,299.

Dixon, M. 2008. Quartz Crystal Microbalance with Dissipation Monitoring: Enabling Real Time. Characterization of Biological Materials and Their Interactions. J. Biomol. Tech., 19, 151-158.

Dispersion Analyser LUMiSizer. 2011. "The complete Dispersion Lab in one Instrument," L.U.M. GmbH.

Duygu, A., Nuri, M., Levent, D. 2002. New cationic polyelectrolytes for flocculation processes of baker's yeast waste water. Polym. Bull., 48, 353-359.

Duner, G., Thormann, E., Dedinaite, A. J. 2013. Quartz Crystal Microbalance with Dissipation (QCM-D) studies of the viscoelastic response from a continuously growing grafted polyelectrolyte layer. Colloid Interf. Sci., 408, 229–234.

Fang, R., Cheng, X., Xu, X. 2010. Synthesis of lignin-base cationic flocculant and its application

in removing anionic azo-dyes from simulated wastewater. Bioresour. Technol., 101, 7323−9.

Fang, R., Cheng, S.U., Fu, J., Zheng, Z. B. 2009. Research on the Graft Copolymerization of EH-lignin with acrylamide. Natural Science, 1, 17-22.

Fang, R., Cheng, X., Xu, X. 2010. Synthesis of lignin-base cationic flocculant and its application in removing anionic azo-dyes from simulated wastewater. Bioresour. Technol., 101(19), 7323-9.

Fanta., G.F., Burr, R.C., Doane, W.M., Russel, C.R. 1972. Graft Copolymers of Starch With Mixtures of Acrylamide and the Nitric Acid Salt of Dimethylaminomethyl Methacrylate. J. Appl. Poly. Sci., 16, 2835

Farias, T.L., Koylu, U.O., Carvalho, M.G., 1996. Range of validity of the Rayleigh-Gans Debyetheory for optics of fractal aggregates. Appl. Opt., 35(33), 6560-6567.

Farrokhpay, S., Morris, G., Fornasiero, D. P. 2004. Role of polymeric dispersant functional groups in the dispersion behaviour of titania pigment particles. Progress in Colloid and Polymer Science, 128, 216–220.

Farrokhpay, S., Morris, G.E., Fornasiero, D. 2006. Titania Pigment Particles Dispersion in Water Based Paint Films. JCT Research, 3(4), 275-283.

Feng, L., Stuart, M.S., Adachi, Y. 2015. Dynamics of polyelectrolyte adsorption and colloidal flocculation upon mixing studied using mono-dispersed polystyrene latex particles. Adv. Colloid Int. Sci., 226, 101–114.

Feofilova, E.P., Mysyakina, I.S. 2016. Lignin: Chemical Structure, Biodegradation, and Practical Application (a Review). Appl. Biochem. Microbiol., 52, 573–581.

Forster, S., Schmidt, M. 1990. Static and dynamic light scattering by aqueous polyelectrolyte solutions: effect of molecular weight, charge density and added salt. Polymer, 31 (5), 781-792.

Gan, L., Zhou, M., Yang, D., Qiu, X. 2013. Preparation and Evaluation of Carboxymethylated Lignin as Dispersant for Aqueous Graphite Suspension Using Turbiscan Lab Analyzer. J. Dispers. Sci. Technol., 34:644–650.

Gellerstedt, G., Lindfors, E. 1984. Structural changes in lignin during kraft pulping. Part Phenolic hydroxyl groups in wood and kraft pulps. Svensk Papperstidning, 15, R115–R117.

Ghimici, L., Constantin, M., Fundueanu, G. 2010. Novel biodegradable flocculating agents based on pullulan. J. Hazardous Mat., 181,351–358.

Ghorai, S., Sarkar, A., Panda, A.B., Pal, S., 2013. Evaluation of the Flocculation Characteristics of Polyacrylamide Grafted Xanthan Gum/Silica Hybrid Nanocomposite. Ind. Eng. Chem. Res., 52, 9731−9740.

Gill., R.I.S., Herrington, T.M., 1987. The flocculation of kaolin suspensions using polyethylenimine and cationic polyacrylamides of the same molar mass but different charge density. Colloids Surf., 28, 41-52.

Grundke, K., Bogumil, T., Gietzelt, T., Jacobasch H-J., Kwok D. Y., Neumann A. W. 1996. Wetting measurements on smooth, rough and porous solid surfaces. Prog. Colloid Polym. Sci., 101, 58–67.

Gunther, H., 2014. NMR Spectroscopy: Basic Principles, Concepts and Applications in Chemistry. Wiley & Sons, USA. 138. Griffiths, P.R.; J.A. de Haseth. 1986. Fourier Transform Infrared Spectrometry. Wiley, NewYork, 1986.

Gregory, J., Barany, S., 2011. Adsorption and flocculation by polymers and polymer mixtures. Adv. Colloid. Int. Sci., 169, 1-12.

Hasan, A., Fatehi, P. 2018 a. Synthesis and characterization of lignin- polyacrylamide-(2-methacryloyloxyethyl) trimethyl ammonium chloride copolymer. J. appl. polym. Sci., 135, 46338.

Hasan, A., Fatehi, P. 2018 b. Stability of kaolinite dispersion in the presence of lignin-

acrylamide polymer. Appl. Clay Sci., 158, 72-82.

Hashem, A., Abdel-Halim, E., Sokker, H. 2007. Bi-functional starch composites prepared by c irradiation for removal of anionic and cationic dyes from aqueous solutions. Polymer Plastic Technology 46(1), 71–7.

He, W., Fatehi, P. 2015. Preparation of sulfomethylated softwood kraft lignin as a dispersant for cement admixture. RSC Adv., 5, 47031-47039.

Heinze, T., Koschella, A. 2005. Carboxymethylesters of cellulose and starch-A review. Macromolecular Symposium, 223, 13-40.

Hofmann, U., Endell, K., Wilm, D. 1933. Kristallstruktur und Quellung von Montmorillonit. *Z.* Kristall. 86,340–349.

Holladay, J. E., Bozell, J. J., White, J. F., Johnson, D. 2007. Top value-added chemicals from biomass. Volume II- Results of screening for potential candidates from biorefinery lignin, a report. Available via: http://www1.eere.energy.gov/biomass/pdfs/pnnl-16983.pdf.

Hong, N., Zhang, S., Yi, C., Qiu, X., 2016. Effect of polycarboxylic acid used a high performance dispersant on low rank coal water slurry. J. Disp. Sci. Technol., 37 (3), 415-422.

Hongyan, R., Baoyu, G., Yanxia, Z., Shenglei, S., Zhonglian, Y., Yan, W., Qinyan, Y., Qian, L. 2013. Advanced lignin-acrylamide water treatment agent by pulp and paper industrial sludge: Synthesis, properties and application. J. Env. Sci., 25(12) 2367–2377.

Howang, M., Barron, A.R., BET Surface Area Analysis of Nanoparticles. OpenStax-CNX module: m3827. 1-11.

Hsu, K.C., Chen, C.H., K.T. Hsu, K.T. 2016. Acrylamide-based Polymeric Dispersants for Barium Titanium Suspensions. International Conference on Material Science and Civil Engineering (MSCE 2016), 269-274.

Hu, T.Q., 2002. Chemical modification, properties, and usage of lignin; Kluwer Academic Plenum Publishers: New York.

Huang, R.H., Yang, B.C., Zheng, D.S., Wang, B. 2012. Preparation and characterization of a quaternized chitosan. J. Mat. Sci., 47(2), 845–51.

Huang, W., Leong, Y.K. Chen, T., Au, P.I., Liu, X., Qiu, Z. 2016. Surface chemistry and rheological properties of API bentonite drilling fluid: pH effect, yield stress, zeta potential and ageing behavior. J. Pet. Sci. Eng., 146, 561–569.

Huang, J., Xu, J., Wang, D., Li, L., Guo, X. 2013. Effects of amphiphilic copolymer dispersants on rheology and stability of coal water slurry. Ind. Eng. Chem. Res., 52 (25), 8427-8435.

Hunter, R. J. 1993. Introduction to modern colloid science. Oxford, UK: Oxford Science Publications.

Hussein, M. Z., Tarmizi, R. S. H., Zainal, Z., Ibrahim, R., Badri, M. 1996. Preparation and characterization of active carbons from oil palm shell. Carbon, 34, 1447-1454.

Ibrahim, M.N.M., Azeena, N., Nadiah, M.Y.N., Saaid, M. 2006. Lignin graft copolymer as a drilling mud thinner for high temperature well. J. App. Sci., 6, 1808-1813.

Jarvis, P., Jefferson, B., Parsons, S. A. 2005. Breakage, Regrowth, and Fractal Nature of Natural Organic Matter Flocs. Env. Sci. Technol., 39, 2307-2314.

Jarvis, P., Parsons, S. A., Henderson, R., Nixson, N., Jefferson, B., 2008. The Practical Application of Fractal Dimension in Water Treatment Practice–the Impact of Polymer Dosing. Sep. Sci. Technol., 43, 1785-1797.

Jin, L., Wei, Y., Xu, Q., Yao, W., Cheng, Z. 2014. Cellulose Nanofibers Prepared from TEMPO-oxidation of Kraft Pulp and Its Flocculation Effect on Kaolin Clay. J. App. Polym. Sci.,131, 40450.

Jonsson, A.S., Nordin, A.K., Wallberg, O. 2008. Concentration and purification of

lignin in hardwood kraft pulping liquor by ultrafiltration and nanofiltration. Chem. Eng. Rese. Des., 86(11), 1271-1280.

Kam, S.K, Gregory, J. 1999. Charge determination of synthetic cationic polyelectrolytes by colloid titration. Colloid surface A, 159 (1), 165 - 179.

Karmakar, G.P., Singh, R.P. 1998. Flocculation studies using amylose-grafted polyacrylamide. Colloids Surf. A Physicochem. Eng. Asp., 133, 119 -124.

Karnland, O., Olsson, S., Nilsson, U. 2006. Mineralogy and Sealing Properties of Various Bentonites and Smectite-Rich Clay Materials. Swedish Nuclear Fuel and Waste Management Company Report, SKB TR 06-30.

Kaszuba, M., Corbett, J., Watson, F.M., Jones, A. 2010. High-concentration zeta potential measurements using light-scattering techniques. Philosophical Transaction Royal Society A, 368, 4439–4451

Kelley, S. S., Glasser, W. G., Ward, T. C. 1989. Effect of soft-segment content on the properties of lignin-based polyurethanes. In "Lignin: Properties and Materials" (W. G. Glasser and S. Sarkanen, eds.), ACS Symposium Series No. 397, 402-413, American Chemical Society, Washington, D.C.

Klein, C., Harbottle D, Alagha L, Xu Z. 2013. Impact of Fugitive Bitumen on Polymer Based Flocculation of Mature Fine Tailings. Can. J. Chem. Eng., 91, 1427–1432.

Kim, H.S., Yang, S.H., Kim, H.J., Park, H.J. 2004. Thermogravimetric analysis of rice husk flour filled thermoplastic polymer composites. Journal of Thermal Analysis and Calorimetry, 7, 395 404.

Kirk, T.K. 1971. Effects of microorganisms on lignin. Annu. Rev. Phytopathol., 9,185 210.

Konduri, M.K.R., Fatehi, P. 2017. Dispersion of kaolin particles with carboxymethylated xylan. Appl. Clay Sci., 137, 183–191.

Kong, F., Parhiala, K., Wang, S. Fatehi, P. 2015. Preparation of cationic softwood kraft lignin and its application in dye removal. Eur., Polym. J., 67, 335–345.

Kostanski, L.K., Keller, D.M., Hamielec, A.E. 2004. Size-exclusion chromatography-a review of calibration methodologies. J. Biochem. Biophys. Methods, 58 (2), 2159-186.

Kwok, D.Y., Neumann, A. W. 2000. Contact angle interpretation in terms of solid surface tension. Colloids Surf. A Physicochem. Eng. Asp., 161, 31–38.

Lameirasa, F.S., De Souzaa, A.L., De Meloa, V.A.R., Nunesa, E.H.M, Bragaa, I.D. 2008. Measurement of the Zeta Potential of Planar Surfaces with a Rotating Disk. Mat. Res., 11, 217-219.

Li, R., Gao, B., Sun, S., Wang, H., Liu, Y., Yue, Q. 2015. Wang Y. Coagulation behavior and floc structure characteristics of cationic lignin-based polymerpolyferric chloride dual-coagulants under different coagulation conditions. RSC Adv., 5, 100030–100038

Li, H., Cai, T., Yuan B., Li R., Yang H., Li, A. 2015a. Flocculation of Both Kaolin and Hematite Suspensions Using the Starch-Based Flocculants and Their Floc Properties, Ind. Eng. Chem. Res., 54, 59−67.

Li, R., Gao, B., Sun, S., Wang, H., Liu, Y., Yue, Q. 2015b. Wang Y. Coagulation behavior and floc structure characteristics of cationic lignin-based polymerpolyferric chloride dual coagulants under different coagulation conditions. RSC Adv., 5, 100030–100038.

Li, R., Gao, B., Sun, S., Yue, Q., Li, M., Yang, X, Song, W., Jia, R. 2015c. Amine-Cross Linked Lignin-Based Polymer: Modification, Characterization, and Flocculating Performance in Humic Acid Coagulation. ACS Sust. Chem. Eng., 3, 3253−326.

Li, Z., Ge, Y., 2011. Extraction of Lignin from Sugar Cane Bagasse and its Modification into a High Performance Dispersant for Pesticide Formulations. J. Braz. Chem. Soc., 22 (10), 1866-1871.

Li, H., Long, J., Xu, Z., Masliya, J.H. 2008. Effect of molecular weight and charge density on the performance of polyacrylamide in low-grade oil sand ore processing. Can. J. Chem. Eng., 86, 177–185, doi:10.1002/cjce.20029

Liimatainen, H., Haapala, A., Tomperi, J. Niinimaki, J. 2009. Fibre floc morphology and dewater ability of a pulp suspension: role of flocculation kinetics and characteristics of flocculation agents. BioResource, 4(2), 640-658.

Liliana, R., Constantin N. C., Dan, R. P. 2009. Effect of UV radiation on some polymeric networks based on vinyl ester resin and modified lignin. Polymer Testing, 28, 296–300

Lin, S. Y. 1985. "Reaction product of lignosulfonate and unsaturated fatty amine," US Patent 4,562,236.

Liu, Y., Li, K., 2006. Preparation and characterization of demethylated lignin-polyethylenimine adhesives., J. Adhes. 82, 593–605.

Loginov, M., Larue, O., Lebovk, N., Vorobeiv, E. 2008. Fluidity of highly concentrated kaolin suspensions: Influence of particle concentration and presence of dispersant. Colloid Surf. A 325, 64-71.

Lora, J. 2008. Industrial commercial lignins: Sources, properties and applications. In: Belgacem, M., and Gandini, A. (eds.), Monomers, Polymers and Composites from Renewable Resources, Elsevier, ISBN: 978-0-08-045316-3.

Lou, H., Lai, H., Wang, M., Pang, Y., Yang, D., Qiu, X., Wang, B., Zhang, H. 2013. Preparation of lignin-based superplasticizer by graft sulfonation and investigation of the dispersive performance and mechanism in a cementitious system. Ind. Eng. Chem. Res., 52, 16101-16109.

Lu, J. H., Wu, L., Letey, J. 2002. Effects of Soil and Water Properties on Anionic Polyacrylamide Sorption. Soil Science Society American Journal, 66, 578–584.

Ma, X. 2011. Effect of a low-molecular-weight polyacrylic acid on the coagulation of kaolinite particles. Int. J. Min. Process., 99, 17-120.

Mabire, F., Audebert, R., Quivoron, C. 1984. Synthesis and solution properties of water soluble copolymers based on acrylamide and quaternary ammonium acrylic comonomer. Polymer, 25, 1317-1322.

Machida, S., Narita, H., Katsur, T. 1971. Flocculation properties of cellulose-acrylamide graft copolymers. Macromol. Mat. Eng., 20, 47–56.

Mai, C., Majcherczyk. A., Huttermann, A. 2000. Chemo-enzymatic synthesis and characterization of graft copolymers from lignin and acrylic compounds. Enz. Microb. Tech., 27, 167- 175.

Mansfield, S.D., Mooney, C., Saddler, J.N. 1999. Substrate and enzyme characteristics that limit cellulose hydrolysis. Biotechnol. Progr., 15, 804-806.

Matsushita, Y., Yasuda, S. 2005. Preparation and evaluation of lignosulfonates as a dispersant for gypsum paste from acid hydrolysis lignin. Bioresour. Technol., 96,465–470.

Mekhamer, W.K., Andis, N. A., Shabanat, M. l. 2009. Kinetic study on the sedimentation behavior of Na- and Ca-kaolinite suspension in the presence of polyethyleneimine. Journal of King Saud University (Science), 21, 125–132.

McNamara, T.P., Blanford, C.F. 2016. A sensitivity metric and software to guide the analysis of soft films measured by a quartz crystal microbalance. Analyst, 141, 2911.

Meister, J.J., 2002. Modification of lignin. Journal of Macromolecules Science. Polym. Rev., 42, 235–289.

Miranda, R., Blanco, A., Fuente, E., Negro, C. 2008. Separation of contaminants from deinking process water by dissolved air flotation: effect of flocculant charge density. Sep. Sci. Technol., 43, 3732–3754.

Mishra, S.K., Senapati, P.K., Panda, D. 2002. Rheological behaviour of coal-water slurry. Energy Sources. 24, 159-167.

Mishra, S., Mukul, A., Sen, G., Jha, U. 2011. Microwave assisted synthesis of

polyacrylamide grafted starch (St-g-PAM) and its applicability as flocculant for water treatment. Int. J. Biol. Macromol., 48, 106–111.

Mittal, H., Jindal, R., Kaith, B. S., Maity, A., Ray, S. S. 2014. Synthesis and flocculation properties of gum ghatti and poly (acrylamide-coacrylonitrile) based biodegradable hydrogels. Carbohyd. Polym. 114, 321−9.

Mohamad, I., Haras, A., Rashid, M., Sipaut, C., Enein, A., Mohamad. BA. 2010. Preparation and characterization of a newly water soluble lignin graft copolymer from oil palm lignocellulosic waste. Carbohydr. Polym., 80, 1102-1110.

Mohan, D., Pittman, C.U. Jr., Steele, P.H. 2006. Pyrolysis of wood/biomass for bio-oil: a critical review. Energy & Fuels, 20, 848-889.

Morris G. E., Fornasiero, D., Ralston, J. 2002. Polymer depressants at the talc–water interface: adsorption isotherm, microflotation and electrokinetic studies. Int. J. Miner. Process. 67, 211–227.

Murphy, R.M. 1997. Static and dynamic light scattering of biological macromolecules: what can we learn. Current opinion in Biotechnology, 8 (1), 25-30.

Nsib, F., Ayed, N., Chevaliar, Y. 2006. Dispersion of hematite suspensions with sodium polymethacrylate dispersants in alkaline medium. Colloids and Surfaces A: Physicochem. Eng. Aspects 286, 17–26

Nomura, T., Minemura, A. 1980. Behavior of a piezoelectric quartz crystal in an aqueous solution and its use for the determination of minute amounts of cyanide. Nippon Kagaku Kaishi, 1621–1626.

Nonrorv, F. H. 1979. Critical study of the differential thermal method for the identification of the clay minerals. J. Am. Ceram., 22, 54-63.

Nurmi, M., Byskata, J., Eklund, D. 2004. Factors influencing flocculation of dissolved and colloidal substances in thermomechanical pulp water. Journal of pulp and paper science A., 30, 41-44.

Nurmi, N., Wallin, S., Eklund, D., 2006. The effect of molar mass and charge density of cationic polyacrylamide on the flocculation of dissolved and colloidal substances in thermomechanical pulp water. Journal of pulp and paper science, 32(1) 43-46.

Okieimen, F.E., 2003. Preparation, characterization, and properties of cellulose–polyacrylamide graft copolymers. J. Appl. Poly. Sci., 913–923.

Ouyang X., Qiu X., Chen, P. 2006. Physicochemical characterization of calcium lignosulfonate —A potentially useful water reducer. Colloids and Surfaces A: Physicochem. Eng. Asp., 282, 489–497.

Pal, S., Mal, D., Singh, R.P., 2006. Synthesis, characterization and flocculation characteristics of cationic glycogen: a novel polymeric flocculant. Colloids Surf A Physicochem. Eng. Asp., 289, 193–199.

Pawlik, M. 2005. Polymeric dispersants for coal–water slurries. Colloids and Surfaces A: Physicochem. Eng. Aspects, 266, 82–90.

Pawlik, M., Laskowski, J.S., Ansari, A. 2003.Effect of carboxymethyl cellulose and ionic strength on stability of mineral suspensions in potash ore flotation systems. J. Coll. Interf. Sci., 260, 251-258.

Peng, X.W., Ren, J.L., Zhong, L.X., Cao, X.F., Sun, R.C. 2011. Microwave-induced synthesis of carboxymethyl hemicelluloses and their rheological properties. J. Agric. Food Chem., 59, 570-576.

Peng-wei, L., Dong-jie, Y., Hong-ming, L., Xue-king, Q. 2008. Study on the stability of coal water slurry using dispersion-stability analyzer. J. Fuel Chem. Technol., 36 (5), 524−529.

Penkavova, V., Guerreiro, M., Tihon, J., Teixeira, J. A. C. 2015. Deflocculation of kaolin suspensions – the effects of various electrolytes. Appl. Rheol., 25, 24151-24160.

Petroff, T.E., Sayer, M., Hesp, S.A.M. 1993. Zeta potential modification of ceramic powders using zirconium hydrogel. Colloids Surf. A Physicochem. Eng. Asp., 78, 235-243.

Petzold, K., Schwikal, K., Gunther, W., Heinze, T. 2006. Carboxymethyl xylan-control of properties by synthesis. Macromolecular Symposium, 232, 27-36.

Pusch, R., Karnland, O. 1983. Aspects of the physical state of smectite absorbed water. SKB TR 83-37.

Qin, Y., Yang, D., Qiu, X. 2015. Hydroxypropyl Sulfonated Lignin as Dye Dispersant: Effect of Average Molecular Weight. ACS Sustainable Chem. Eng., 3 (12), 3239–3244.

Qin, Y., Yang, D., Gu, F., Li, X., Xiong, W., Zhu, J.Y. 2016. Biorefinery lignosulfonates as a dispersant for coal water slurry. Sustainable Chem. Pro., https://doi.org/10.1186/s40508-016-0050-0

Ram. P., Sagar P., Ali. S.K. 2014. Novel biodegradable polymeric flocculants based on cationic polysaccharides. Adv. Mat. Lett., 5(1), 24-30.

Rasteiro, G. M., Pinheiro, I., Ahmadloo, H., Hunkeler, D., Fernando, A.P. Garcia, F.A.P., Ferreira, P., Wandrey, C. 2015. Correlation between flocculation and adsorption of cationic polyacrylamides on precipitated calcium carbonate. Chem. Eng. Res. Des., 95, 298–306.

Rath, S.K., Singh, R.P. 1997. Flocculation characteristics of grafted and ungrafted starch, amylose, and amylopectin. J. Appl. Polym. Sci., 66, 1721–1729.

Ravi, K., Rao, S.M. 2013. Influence of Infiltration of Sodium Chloride Solutions on SWCC of Compacted Bentonite–Sand Specimens. Geotechnical and Geological Engineering 31, 1291-1303.

Reti, C., Casetta, M., Duquesne, S., Bourbigot, S., Delobel, R. 2008. Flammability properties of intumescent PLA including starch and lignin. Polymers for Advanced Technology, 19 (6), 628- 635.

Riddick, M. T. 1961.Control of colloid stability through Zeta-potential, Inc., New York.

Roberts, J.C. (ed.) (1996): The chemistry of paper. Royal Society of Chemistry, Cambridge, UK, 64-82.

Shaw, D. J., 1992. Introduction to colloid and surface chemistry. London, UK: Butterworth

Heinemann.

Rodahl, M., F. Hook, A. Krozer, P. Brzezinski, and B. Kasemo. 1995. Quartz crystal microbalance setup for frequency and Q-factor measurements in gaseous and liquid environments. Rev. Sci. Instrum., 66, 3924 –3930

Rodd, A.B., Dunstan, D.E., Boger, D.V. 2000. Characterization of xanthan gum solutions using dynamic light scattering and rheology. Carbohydr. Polym., 42 (2), 159-174.

Rogers, K., Takacs E., Thompson M. R. 2005. Contact angle measurement of select compatibilizers for polymersilicate layer nanocomposites. Polymer Testing, 24, 423–427.

Roh, N.S., Shin, D.H., Kim, D.C., Kim, J.D. 1995. Rheological behaviour of coal water Mixtures. Fuel, 74 (8), 1220-1225.

Rong, H., Gao, B., Zhao, Y., Sun, S., Yang, Z., Wang, Y., Yue, Q., Li, Q. 2013. Advanced lignin-acrylamide water treatment agent by pulp and paper industrial sludge: Synthesis, properties and application. J. Environ. Sci. Health Part C, 25, 2367–2377.

Ryan, J.N, Gschwend, P.M. 1994. Effect of solution chemistry on clay colloid release from an iron oxide-coated aquifer sand. Env. Sci. Technol., 28, 1717-1726.

Saake, B., Lehnen, R. 2012. Lignin. Wiley-VCH Verlag GmbH and Co. KGaA, Weinheim.

Sahoo, S., Seydibeyoglu, M.O., Mohanty, A.K., Misra, M. 2011. Characterization of industrial lignins for their utilization in future value added applications. Biomass Bioenergy 35: 4230- 4237.

Salopek, B., Krasi, D., Filipovi, S., 1992. Measurement and application of zeta-potential. Rudarsko-geoloSko-naftni zbornik, 4, 147 -151.

Santisteban, J. I., Mediavilla, R., Lopez-Pamo, E., Dabrio, C. J., Zapata, M. B. R., García, M. J. G., Castano, S., Martínez-Alfaro, P. E. 2004. Loss on ignition: a qualitative or quantitative method for organic matter and carbonate mineral content in sediments? J. Paleolimnol., 32 (3), 287-299.

Sarwar, J. M., Liu, Z., Wang, H., Saeed, A., Ni, Y. 2012. Isolation and characterization of lignin from prehydrolysis liquor of kraft based dissolving pulp production. Cellul. Chem. Technol., 46, 261-267.

Schmidt, C.U., Lagaly, G.V. 1999. Surface modification of bentonites I. Betaine montmorillonites and their rheological and colloidal properties. Clay Miner., 34, 447-458.

Schmut , R. 1964. Zeta potential measurement - Applications in the Paper Industry, Ind. Eng. Chem., 56, 28–33.

Senaputra, A., Jones, F., Fawell, P.D., Smith, P.G. 2013. Focused Beam Reflectance Measurement for Monitoring The Extent And Efficiency of Flocculation in Mineral Systems, AIChE J., 1-15.

Senoussi, H., Osmani, H., Courtois, C. Bourahli, M.H. 2016. Mineralogical and chemical characterization of DD3 kaolin from the east of Algeria. J. Spanish Ceram. Glass Soc., 55, 121-126.

Shen, J.J., Ren, L.L., Zhuang, Y.Y. 2006. Interaction between anionic dyes and cationic flocculant P (AM-DMC) in synthetic solutions. J. Hazard. Mat., 136, 809–815.

Shirazi, M., Van de Ven, T.G.M., Garnier, G. 2003. Adsorption of Modified Starches on Pul Fibers. Langmuir 19, 10835-10842.

Sjöström, E. 1993. Wood chemistry: Fundamentals and Applications, Gulf Professional Publishing.

Sjostrom, E., 1981. Wood Chemistry: Fundamentals and Applications. Academic Press, Orlando, pp. 68–82.

Solberg, D., Wagberg, V. 2003. Adsorption and flocculation behavior of cationic polyacrylamide and colloidal silica. Colloids Surf A Physicochem. Eng. Asp., 219, 161-172.

Striegel, A. M., Yau, W., Kirkland, J. J., Bly, D. D. 2009. Modern Size Exclusion Liquid

Chromatography; John Wiley and Sons, Inc.

Suhas, P.J.M., 2007. Lignin-From natural absorbent to activated carbon-A review. Bioresour. Technol., 98, 2301-2312.

Tang, P., Greenwood, J., Raper J. A. 2002. A Model to Describe the Settling Behavior of Fractal Aggregates. J. Colloid Interface Sci., 247, 210-219.

Teixeira, J., Small-angle scattering by fractal systems. 1988. J. Appl. Crystallogr., 21, 7.

Thapa, K.B., Qi, Y., Hoadley, A.F. 2009. Using FBRM to Investigate the Sewage Sludge Flocculation Efficiency of Cationic Polyelectrolytes. Water Sci. Technol., 59.3: 583 593.

Thill, A., Moustier, S., Aziz, J., Wiesner, M.R., Bottero, J.Y. 2001. Flocs restructuring during aggregation: experimental evidence and numerical simulation, J. Colloid Interface Sci., 243, 171–182.

Thompson, M., 2008. AMC technical briefs. CHNS elemental analyzers. AMCTB No 29, http://www.rsc.org/images/CHNS-elemental-analysers-technical-brief-29_tcm18-214833.pdf.

Tombac, E., Szekeres, M., 2006. Surface charge heterogeneity of kaolinite in aqueous suspension in comparison with montmorillonite. Appl. Clay Sci., 34, 105-124.

Tripathy, T., Ranjan, B. 2006. Flocculation: A New Way to Treat the Waste Water. J. Phys. Sci., 10, 93 – 127

Turunen, M., Alvila, L., Pakkanen, T. T., and Rainio, J. 2003. Modification of phenol formaldehyde resol resins by lignin, starch and urea. J. Appl. Polym. Sci., 88(2), 582-588.

Vanholme, R., Demedts, B., Morreel, K., Ralph, J., Boerjan, W. 2010. Lignin biosynthesis and structure. Plant Physiol., 153(3), 895-905.

Varanasi, P., Singh, P., Auer, M., Adams, P.D., Simmons, B.A., Singh, S. 2013. Survey of

renewable chemicals produced from lignocellulosic biomass during ionic liquid pretreatment. Biotechnol. Biofuels, 6, 14.

Ververis, C., Georghiou, K., Christodoulakis, N., Santas, P., Santas, R. 2004. Fiber dimensions, lignin and cellulose content of various plant materials and their suitability for paper production. Ind. Crops Prod.,19(3), 245-254.

Vie, R., Azema, N., Quantin, J.C., Touraud, E., Fouletier, M. 2007. Study of suspension settling: A approach to determine suspension classification and particle interactions. Colloids Surf. A., 298, 192-200.

Waite, T. D., Cleaver, J. K., Beattie, J. K., 2001. Aggregation Kinetics and Fractal Structure of γ alumina Assemblages. J. Colloid Interface Sci., *241*, 333-339.

Wang, K.T., Audebert, R. 1988. Adsorption of Cationic Copolymers of Acrylamide at the Silica-Water Interface: Hydrodynamic Layer Thickness Measurements. J. Colloid. Interface Sci., 121, 32-41.

Wang, J.P., Chen, Y.Z., Wang, Y., Yuan, S.J., Yu, H.Q. 2011. Optimization of the coagulation-flocculation process for pulp mill wastewater treatment using a combination of uniform design and response surface methodology. Water Res., 45, 5633-5640.

Wang, J.P., Chen, Y.Z., Yuan, S.J., Sheng, G.P., Yu, H.Q. 2009. Synthesis and characterization of a novel cationic chitosan-based flocculant with a high water-solubility for pulp mill wastewater treatment. Water Res., 43, 5267-5275.

Wang S., Hou Q., Kong F., Fatehi P. 2015. Production of cationic xylan–METAC copolymer as a flocculant for textile industry. Carbohyd. Polym., 124, 229-236.

Wang, B., Yulian, Z., Chunbao, M., 2011. Preparation of cationic chitosan-polyacrylamide flocculant and its properties in wastewater treatment. Journal of Ocean University of China. 10. 42-46. 10.1007/s11802-011-1741-5.

Wang, J.P., Chen, Y.Z., Wang, Y. 2012. A novel efficient cationic flocculant prepared through

grafting two monomers onto chitosan induced by gamma radiation. RSC Adv., 2, 494-500.

Wang, J.P., Yuan, S.J., Wang, Y., Yu, H.Q. 2013. Synthesis, characterization and application of a novel starch-based flocculant with high flocculation and dewatering properties. Water Res., 2013, 47(8):2643-8.

Wang, J.P., Chen, Y.Z., Zhang, S.J., Yu, H.Q. 2008. A chitosan-based flocculant prepared with gamma-irradiation-induced grafting. Bioresour. Technol., 99, 3397- 3402.

Wang, H., Tucker, M., Ji, J. 2013. Recent Development in Chemical Depolymerization of Lignin. A Review. J. Appl. Chem., 9 pages. http://dx.doi.org/10.1155/2013/838645

Wang, Y.B., Xie, W.L. 2010. Synthesis of cationic starch with a high degree of substitution in an ionic liquid. Carbohyd. Polym., 80(4), 1172–7.

Wang, S., Sun, Y., Kong, F., Yang, G., Fatehi, P., 2016. Preparation and characterization of lignin-acrylamide copolymer as a paper strength additive. BioResour., 11(1), 1765-1783.

Wang, S., Konduri, M. K. R., Hou, Q., Fatehi, P. 2016. Cationic xylan–METAC copolymer as a flocculant for clay suspensions. RSC Adv., 6, 40258.

Wong, S.S., Teng, T.T., Ahmad, A.L., Zuhairi, A., Najafpour, G. 2006. Treatment of pulp and paper mill wastewater by polyacrylamide (PAM) in polymer induced flocculation. J. Hazard. Mat., 135, 378–388.

White, R.E., 1987.Introduction to the Principles of Soil Science, 2nd ed., Blackwell, Boston.

Wu, H., Chen, F., Feng, Q., Yue, X., 2012. Oxidation and sulfomethylation of alkali extracted lignin from corn stalk. Bioresour., 7, 2742-2751.

Xiumei, Q, Yadong, L., Aref, A., Xiaoyan, Z., Chunjie, Y., 2017. Viscosity of Kaolin Slurries: Effects of Dispersant and Urea-Intercalation. Journal of Wuhan University of Technology-Mater. Sci. Ed., 32 (1), 51-57. DOI 10.1007/s11595-017-1557-2.

Yan, Y.D., Glover, S.M., Jameson, G.J., Biggs, S. 2004. The flocculation efficiency of

polydisperse polymer flocculants. International J. Miner. Process., 73,161 – 175.

Yang., Z., Li, H.J., Yan, H., Wu, H., Yang, H., Wu, Q., Li, H.B., Li, A.M., Cheng, R.S. 2014. Evaluation of a novel chitosan-based flocculant with high flocculation performance. low toxicity and good floc properties. J. Hazard. Mat., 276, 480-488.

Yoon, S., Deng, Y. 2004. Flocculation and reflocculation of clay suspension by different polymer systems under turbulent conditions. J. Colloid Interface Sci., 278, 139–145.

Yoshihara, H., 1999. Graft Copolymers as Dispersants for CWM. 21:1, 93-103, DOI: 10.1080/07349349908945611

Yu, J., Wang, D., Ge, X., Yan, M., Yang, M. 2006. Flocculation of kaolin particles by two typical polyelectrolytes: A comparative study on the kinetics and floc structures. Colloids and Surf. A Physicochem. Eng. Asp., 290, 288-294.

Yuan, B., Shang, Y.B., Lu, Y.B., Qin, Z.Q., Jiang, Y.X., Chen, A.M., Qian, X.Z., Wang, G.Z., Yang, H., Cheng, R.S. 2010. The flocculating properties of chitosan-graft polyacrylamide flocculants and effect of the grafting ratio. J. Appl. Polym. Sci., 117, 1876-1882.

Yuan, Y., Lee, T.R., Bracco, G. 2013. Holst (eds.), Surface Science Techniques, Springer Series in Surface Sciences 51, DOI 10.1007/978-3-642-34243-1_1.

Yue, X., Chen, F., Zhou, X. 2011. Improved interfacial bonding of PVC/Wood-flour composites by lignin amine modification. Bioresour., 6, 2022–34.

Yue. Q.Y., Gao, B. Y., Wang, Y., Zhang, H., Sun, X., Wang, S.G., Roy R. G. 2008. Synthesis of polyamine flocculants and their potential use in treating dye wastewater. J. Hazard. Mat., 152,
221–227.

Zakzeski, J., Bruijnincx, P. C. A., Jongerius, A. L., Weckhuysen, B. M. 2010. The Catalytic Valorization of Lignin for the Production of Renewable. Chem. Rev., 110, 3552–3599.

Zhang, W.X., Shang, Y.B., Yuan, B., Jiang, Y.X., Lu, Y.B., Qin, Z.Q., Chen, A.M., Qian, X.Z., Yang, H., Cheng, R.S. 2010. The flocculating properties of chitosan-graftpolyacrylamide flocculants (II)-test in pilot scale. J.Appl. Polym. Sci., 117, 2016-2024.

Zhang, G., Li, J. Zhu, J., Wu, Q., Xiong, W. 2014. Synthesis and evaluations of three sulfonated polycondensate dispersants for coal-water slurries. Powder Technol., 254, 572-578.

Zhu, Z., Li, T., Lu, J., Wang, D., Yao, C. 2009. Characterization of kaolin flocs formed by polyacrylamide as flocculation aids. International J. Miner. Process., 9, 94–99.

Zhou, Y., Franks, G.V. 2006. Flocculation Mechanism Induced by Cationic Polymers Investigated by Light Scattering. Langmuir, 22(16), 6775-6786.

Zhou, G., Qiu, H., Zhang, Q., Xu, M., Wang, J., Wang, G. 2016. Experimental investigation of coal dust wettability based on surface contact angle. J. Chem., http://dx.doi.org/10.1155/2016/9452303.

Zhou, M., Qiu X., Yang D., Lou H., Ouyang X. 2007. High-performance dispersant of coal–water slurry synthesized from wheat straw alkali lignin. Fuel Pro. Technol., 88, 375–382

Zhu, J., Zhang, G., Miao, Z., Shang, T. 2012. Synthesis and performance of a comb like amphoteric polycarboxylate dispersant for coal–water slurry. Colloids Surf. A., 412, 101-107.

Zhu, R., Liu, Q., Xu, Z., Masliyah, J.H., Khan, A., 2011. Role of Dissolving Carbon Dioxide in Densification of Oil Sands Tailings. Energy Fuels, 25, 2049–2057.

Zou, J., Zhu, H., Wang, F., Sui, H., Fan, J. 2011. Preparation of a new inorganic–organic composite flocculant used in solid–liquid separation for waste drilling fluid. J. Chem. Eng., 171, 350–356.

Zuqiang, H., Xingtang, L., Huayu, H., Li, G., Yongjun C., Zhangfa T. 2009. Influence of mechanical activation on the graft copolymerization of sugarcane bagasse and acrylic acid. Polym. Degrad. Stab., 94, 1737–

Chapter 3: Synthesis and characterization of lignin- poly (acrylamide) - poly (2-methacryloyloxyethyl) trimethyl ammonium chloride copolymer

3.1 Abstract

In this work, two monomers, acrylamide (AM) and (2-methacryloyloxyethyl) trimethyl ammonium chloride (DMC) were copolymerized from kraft lignin (KL) in an aqueous suspension, initiated by free radical copolymerization in the presence of potassium persulfate. The impact of copolymerization conditions on the charge density and molecular weight of the copolymers was investigated. The molecular weight and mass balance analyses confirmed that the homopolymer (polyDMC (PDMC) and polyAM (PAM)) and undesired copolymer (AM-DMC) productions dominated as the time, initiator and DMC dosage increased more than the optimum values. The activation energy of the polymerization of KL and AM (43.02 kJ mol^{-1}), KL and DMC (21.99 kJ mol^{-1}), AM (14.54 kJ mol^{-1}), DMC (10.34 kJ mol^{-1}), and AM and DMC (18.13 kJ mol^{-1}) was determined. Proton nuclear magnetic resonance (1H-NMR), Fourier transform infrared spectroscopy (FTIR), thermogravimetric analysis, and elemental analysis confirmed the production of KL-AM-DMC copolymer.

3.2 Introduction

Lignin is the second most abundant biopolymer in the world after cellulose and its content in wood varies from 20 wt. % to 30 wt. % (Kuhire et al., 2017; Bernardini et al., 2015; Ma et al., 2016). It is mainly produced as a by-product in kraft pulping process (i.e., the dominant pulping process in the world) (Windt et al., 2009), where the spent liquor (i.e., black liquor) from the pulping process is combusted to recover the pulping chemicals, and its lignin is utilized as a fuel source (Voitl et al., 2010). However, kraft lignin has potential to be converted to value-added products. In recent years, kraft lignin has attracted much attention for its potential use in green material productions because of its renewability, nontoxicity, and biodegradability (Gooselink et al., 2014). The utilization of kraft lignin in the production of value-added products contributes to considerable economic and environmental benefits (Levasseur et al., 2011). However, the low reactivity of kraft lignin limits its chemical modifications and thus its commercial use (Zakzeski et al., 2010).

Several methods are common for wastewater treatments, among which coagulation–flocculation process is one of the most popular one because of its economic feasibility and effectiveness (Sing et al., 2014). Although high molecular weight acrylamide based polymers are extensively used as flocculants for various wastewater systems (Junren et al., 2013), they are reported to have biodegradation, environmental and economic issues. The copolymerization of acrylamide (AM) with anionic and cationic monomers was investigated for producing efficient flocculants for wastewater treatments (Fanghui et al., 2014; Duygu et al., 2002; Jamshidi et al., 2014; Wang et al., 2012). In one study, a cationic monomer, 2-[(methacryloyloxy) ethyl] trimethylammonium chloride (DMC), was copolymerized with acrylamide and the resultant copolymer was used as a flocculant for dye removals from wastewater (Shen et al., 2006). Polyamine, polydiallyldimethylammoniumchloride (PDADMAC), and the copolymer of acrylamide and 2-[(methacryloyloxy) ethyl] trimethylammonium chloride (AM-DMC) were also reported as effective cationic flocculants for removing color from wastewater (Yue et al., 2008; Abdollahi et al., 2011). However, these polymers were not very environmentally friendly. The production of an environmentally friendly, cationic, water soluble and high molecular weight flocculant is a challenging task (Ben et al., 2011). In the past, various green copolymers were produced for this purpose. In one study, chitosan-AM-DMC with the charge density of 1.02 meq g^{-1} was produced and used as a flocculant for treating papermaking wastewater, which resulted in 84.3% lignin removal, 80.1% chemical oxygen demand (COD) removal, and 93.9% water recovery (Ben et al., 2011). In another study, starch-based copolymer (starch-PAM- PDMC) was used as a flocculant for pulp mill wastewater treatment, which led to turbidity and lignin removals of 95.7 % and 83.4 %, respectively, along with 72.7% of water recovery efficiency(Wang et al., 2001). In another study, a starch-AM-DMC flocculant was produced for treating wastes of drilling mud, and its application led to the reduction in water content of the drilling mud from 50 % to 27.6 % (Fanghui et al., 2010). The demand for green flocculants utilized in various wastewater and industrial effluent applications is expected to rise over the next few years. Despite the acceptable efficiency of cationic starch-based flocculants, the industrial applications of starch-based polymers may be restricted as it is a main food resource (Lee et al., 2014; Sriroth et al., 2013). On the other hand, lignin is a non-food source and available abundantly, which can be used for the production of cost effective and efficient cationic flocculants.

Kraft lignin can be modified to produce various chemicals used in the paper, mining, textile, and wastewater systems. Lignin can be catatonically modified to produce asphalt emulsifiers, cationic surfactants, flocculants, and strength additives for composites (Meister, 2002; Savy et al., 2014; Silva et al., 2009). Previously, different modification pathways, such as amination (Mannich reaction) and grafting were proposed to increase lignin's chemical reactivity and solubility in organic solvents (Xueyu et al., 2014; Maziero et al., 2012). In one report, lignin-acrylamide copolymer was produced by reacting lignin, originated from the sludge of a pulping process, and acrylamide, where the copolymer was capable of removing 52 % of turbidity from aluminum sulfate or poly aluminum chloride suspensions (Rong et al., 2013). In another study, the graft copolymerization of enzymatically hydrolyzed (EH) lignin with acrylamide (AM) was investigated in an aqueous solution, and the product was able to remove 85% of azo-dyes from dye wastewater when the dosage of the copolymer was 200 mg L^{-1} (Fang et al., 2009).

However, the production of kraft lignin-based copolymer with cationic charges in aqueous environments was rarely reported in the past, which is a more cost-effective and non-toxic method for lignin copolymer production. The novelties of this work were the i) production of water soluble kraft lignin based copolymer via free radical copolymerization of kraft lignin, AM and DMC, and ii) investigation on the impact of the modification conditions on the solubility and charge density of the copolymer. In this work, the produced copolymer was analyzed by means of Fourier-transform infrared (FTIR), thermogravimetric analysis (TGA), ^{1}H-NMR and an elemental analyzer. To understand the kinetics of the copolymerization reaction, the activation energy (E_a) of the copolymers (AM-DMC, KL-AM, KL-DMC) and homopolymers (PAM, PDMC) were also determined.

3.3 Materials and Methods

3.3.1 Materials

Softwood kraft lignin (KL) was produced via LignoForce^{TM} technology of FPInnovations in Thunder Bay, ON (Kouisni et al., 2012). The molecular weight (M_w) of this lignin sample was reported to be 17,900 g mol^{-1} (Kong et al., 2015). (2-methacryloyloxyethyl) trimethyl ammonium chloride (DMC), 80 wt. % in water, acrylamide (AM) with 99.0 % purity, potassium persulfate, $K_2S_2O_8$ (analytical grades), and trimethylsilyl propanoic acid were all obtained from Sigma-Aldrich company. Cellulose acetate dialysis membrane with the molecular weight cut off of 1,000

g mol^{-1} was obtained from Spectrum Labs Inc., USA. Potassium polyvinyl sulfate (PVSK) was provided by Wako Pure Chem. Ltd. Japan and was diluted to 0.005 M prior to use. Ethanol (95 vol. %) was received from Fisher Scientific company. All chemicals were applied without further purification.

3.3.2 Copolymerization of AM and DMC from kraft lignin

First, 2 g of KL was dissolved in 40 mL of deionized water in a 250 mL three neck round bottom glass flask while stirring at 300 rpm. Predetermined quantities of AM and DMC were added to the flask and stirred at 300 rpm for 5 min. The reaction solution was continuously purged with nitrogen at room temperature for 30 min to remove any residual oxygen. Subsequently, potassium persulfate was added as an initiator to the system and the reaction solution purged for another 5 min. The copolymerization of KL, AM, and DMC was processed by placing the flask in a preheated water bath after adjusting the pH of the medium. The copolymerization reaction of KL, AM, and DMC was conducted at different pHs (2-10), temperatures (50 °C- 90 °C), times (2 h – 6 h), initiator dosages (0.036 mmol – 0.22 mmol), 0.011 mol of KL, 0.028 mol of AM, and 0.024 mol of DMC. In another set of experiments, the copolymer of AM and DMC was prepared under the reaction conditions of pH 4, temperatures range of 40 °C and 80 °C, 2 h, initiator dosage of 0.11 mmol, 0.028 mol of AM, and 0.024 mol of DMC. The copolymer of KL-AM was synthesized at pH 4, temperature range of 50 °C and 90 °C, 2 h, initiator dosage of 0.11 mmol and 0.028 mol of AM. Similarly, the copolymer of KL and DMC was prepared under the reaction conditions of pH 4, temperature range of 50 °C and 90 °C, 2 h, initiator dosage of 0.11 mmol and 0.024 mol of DMC. In addition, the homopolymers of PDMC and PAM were produced under the reaction conditions of pH 4, temperature range of 40 °C to 80 °C, 3 h, initiator dosage of 0.11 mmol, 0.024 moles of DMC and 0.028 moles of AM. All experiments were repeated three times, and the average data is presented via error bars in this work.

3.3.3 Polymer purification and mass balance

Once the required reaction conditions attained, the flask containing the reaction solutions was submerged in cold tap water for 20 min. The solutions were then mixed with 95% ethanol in order to separate the lignin-based copolymers (KL-AM-DMC) from the rest of the reaction media. Ethanol precipitation was carried out for separating AM and DMC monomers from chitosan-AM-DMC copolymer in the past (Wang et al., 2012; Ben et al., 2012). By adding ethanol to the reaction

media, the solutions became suspensions. The suspensions were centrifuged at 3500 rpm for 10 min to collect the agglomerated copolymers (e.g., KL-AM-DMC). In this case, the homopolymers (i.e., PAM, PDMC), copolymer of AM-DMC and unreacted monomers (i.e., AM, DMC) would remain in the supernatants. These supernatants were dialyzed with membrane for 2 days, while changing water of dialysis every 12 h, which removed the unreacted monomers from the hydrolyzed samples. The dried (at 105 °C) samples collected at this step were considered as homopolymers of PAM and PDMC and copolymer of AM-DMC. H-NMR analysis was conducted on these samples to determine the properties of PAM, PDMC, and AM-DMC. Also, the amounts of KL, KL-DMC, KL-AM and KL-AM-DMC in the supernatants were determined using UV/vis spectrophotometer, Gensys S10, at 280 nm, via considering a calibration curve made for KL at predetermined concentrations.

On the other hand, the precipitates of ethanol treatment were remixed with ethanol (95 %v) for 5 min. Then, the mixtures were centrifuged at 3500 rpm for 10 min and this process was repeated 3 times. The supernatants of last cycle of ethanol treatment were collected for identifying if any AM-DMC, PDMC or PAM was remained in the precipitates (with the help of H-NMR analysis). The collected precipitates of ethanol treatment were also collected and dialyzed with membrane for 2 days, while changing the water of dialysis every 12 h. The samples were dried at 105 °C and considered as final copolymer products containing KL-AM-DMC, KL-DMC and KL-AM. The dried mass was considered for determining the yield of copolymer products.

The aforementioned purification method was repeated to obtain the copolymers of KL-DMC, and KL-AM via copolymerization reactions of KL with DMC and AM, respectively. It should be stated that the entire purification process was repeated for the products of homopolymerization reactions of AM and DMC separately, but no precipitates were obtained via ethanol treatment and thus the analysis for these homopolymers was based on assessing only the supernatants. In the copolymerization of three component systems of KL, AM and DMC, it was not possible to distinguish KL-AM, KL-DMC and KL-AM-DMC as there was no procedure to separate KL-AM, KL-DMC and KL-AM-DMC.

Also, the yield of homopolymers and copolymers were determined by considering the dried mass of homopolymer products and copolymer products after dialysis, and the total mass of monomers used in the reactions. As unreacted monomers were removed via dialysis, it was not possible to

determine the mass of unreacted monomers directly. Therefore, the mass of unreacted monomers was determined via developing a mass balance for all monomers used in the reactions and the mass of copolymers and homopolymers collected after dialysis and drying, and this analysis helped determine the yield of unreacted monomers.

3.3.4 Activation energy analysis

In different sets of experiment, the copolymerization of KL-AM, KL-DMC, AM-DMC and the homopolymerization of AM or DMC were conducted under the reaction conditions described previously, but at the temperature range of 40 °C to 90 °C and the time interval of 15 to 120 min. Then, the steps described previously were followed to purify the homopolymer or copolymer products. The activation energy (E_a) was determined according to the procedure stated in previous studies via considering Arrhenius equation, as well as the reaction yield, temperature and time of the reactions (Taghizadeh and Khosravy, 2003; Goel et al., 2009; Gupta et al., 2002; Ge et al., 1997; Leowandowska et al., 2007; Bi and Zhang, 2012)

3.3.5 Solubility and charge density determination

To measure the solubility of the copolymer products, 0.2 g of copolymer of KL-AM-DMC was suspended in 20 mL of deionized water by stirring at 100 rpm and 30 °C for 1 h in a water bath shaker (Innova 3100, Brunswick Scientific, Edison, NJ, USA). Then, the suspensions were centrifuged at 1000 rpm for 5 min. The supernatants were collected and used for analyzing the charge density and solubility of KL-AM-DMC. The concentration of copolymers in the supernatants was determined by drying the supernatants at 105 °C, and the solubility was determined based on equation 3.1:

$$\text{Solubility (wt. \%)} = \frac{\text{Mass of dissolved lignin in supernatants}}{\text{Initial mass of lignin}} \times 100 \qquad (3.1)$$

The charge density of KL-AM-DMC was measured by a particle charge detector, Mütek PCD 04 titrator (Herrsching, Germany) with a PVSK solution (0.0050 M) following equation 3.2. Three repeats were carried out, and the average values were reported in this work**.**

$$\text{Charge density (meq g}^{-1}) = \frac{\text{Volume of PVSK} \times \text{concentration of PVSK}}{\text{Mass of lignin in the titrator}} \qquad (3.2)$$

3.3.6 Molecular weight analysis

About 5 mg sample of dried KL-AM-DMC copolymer was dissolved in 10 mL of 5.0 wt. % acetic acid solution by stirring at 600 rpm for 48 h and 35 °C. The solution was then filtered with a 13 mm diameter nylon filter (pore size 0.2 μm) and the filtered solutions were used for molecular weight analysis. The molecular weight analysis of the samples was carried out using Malvern, GPCmax VE2001 Module, Viscotek system with viscometer and RI detectors. PolyAnalytic columns were used, and 5.0 wt. % acetic acid was used as solvent and eluent with the flow rate of 0.7 mL min^{-1}. The column temperature was set to 35 °C. Poly ethylene oxide was used as a standard in this system. The molecular weights of PAM, PDMC, and AM-DMC were also determined as stated above.

3.3.7 Elemental analysis

The elemental analysis was performed for KL and KL-AM-DMC copolymers using an elemental analyzer, Elementar Vario EL Cube, by the combustion method (Jahan et al., 2012). The samples were first dried in an oven at 105 °C overnight to remove any moisture prior to analysis. Approximately, 2 mg of dried samples were transferred into the carousel chamber of the elemental analyzer and combusted at 1200 °C to reduce the generated gasses to analyze carbon, hydrogen and nitrogen contents of the samples. The oxygen content of the samples was determined by developing a mass balance for carbon, hydrogen, sulfur, nitrogen, and oxygen, assuming no inorganic impurities existed in the KL and KL-AM-DMC products.

3.3.8 Fourier transform infrared (FTIR)

The Fourier transform infrared spectroscopy (FTIR) analysis was conducted for confirming the copolymerization. The samples were dried in an oven at 105 °C overnight and 0.05 g of the sample was used for analysis using a Bruker Tensor 37 (Germany) ATR accessory FTIR instrument. The spectra were recorded in a transmittance mode in the range of 600 cm^{-1} and 4000 cm^{-1} with a 4 cm^{-1} resolution via collecting 32 scans per sample.

3.3.9 Thermogravimetric analysis (TGA)

Thermogravimetric analysis was performed using a TGA (TGA i1000 Series System) to investigate the change in the thermal behavior of KL and KL-AM-DMC. The samples were dried in the oven at 105 °C overnight prior to testing. The analysis was carried out in nitrogen at a steady

flow rate of 100 mL min^{-1}. Each sample (7.5 mg) was heated from room temperature to 800 °C at the rate of 5°C min^{-1}.

3.3.10 ^{1}H-NMR analysis

Sixty milligrams of the dried samples were dissolved in D_2O at a 40-50 g L^{-1} concentration and stirred for 30 min. Then, 30 mg of TSP was used as an internal reference standard in the NMR analysis. The NMR spectra of the samples were recorded using an INOVA-500 MHz instrument (Varian, USA) with a 45° pulse and relaxation delay time of 1.0 s. This analysis was repeated to determine the properties of PAM and PDMC in the dried supernatants, KL-AM, KL-DMC and KL-AM-DMC in the precipitates. In another set of experiments, 60 mg of dried precipitate and dried supernatant of the reaction (after dialysis), which was performed under the conditions of 2 h, 0.11 mmol of initiator, 0.011 mol of KL, 0.028 mol of AM, 0.024 of DMC, pH 4.0 and 80 °C, were dissolved in D_2O at a 40-50 g L^{-1} containing 30 mg of TSP, and their NMR spectra were recorded.

3.3.11 SEM analysis

Scanning electron microscopy (SEM) images of KL and KL-AM-DMC were taken by Hitachi SU-70 Field emission SEM in tandem with Oxford Xmax energy dispersive X-ray spectroscopy (EDX). The powder forms of the samples were mounted on double side carbon tapes on the specimen stubs and coated with gold. The voltage was 5 kV and the images were taken at a magnification of 10000.

3.4 Results and Discussion

3.4.1 Reaction mechanism

Figure 3.1 shows the reaction scheme of KL, AM, and DMC. In the reaction mixture, $K_2S_2O_8$ generates two sulfite radical anions by thermal decomposition. These sulfite radicals lead to the propagation of the copolymer by attacking hydroxyl group (OH) of KL and double bonds of acrylamide and DMC to have them engaged in the copolymerization reaction (Figure 3.1a). On the other hand, the DMC and AM can participate in side reactions to produce homopolymers of PDMC and PAM (Figure 3.1b). Both copolymerization and homopolymerization are affected bythe reaction conditions (Rong et al., 2013; Kong et al., 2015). This radical polymerization may

lead to the generation of random products, such as copolymers of KL-AM, KL-DMC and AM-DMC.

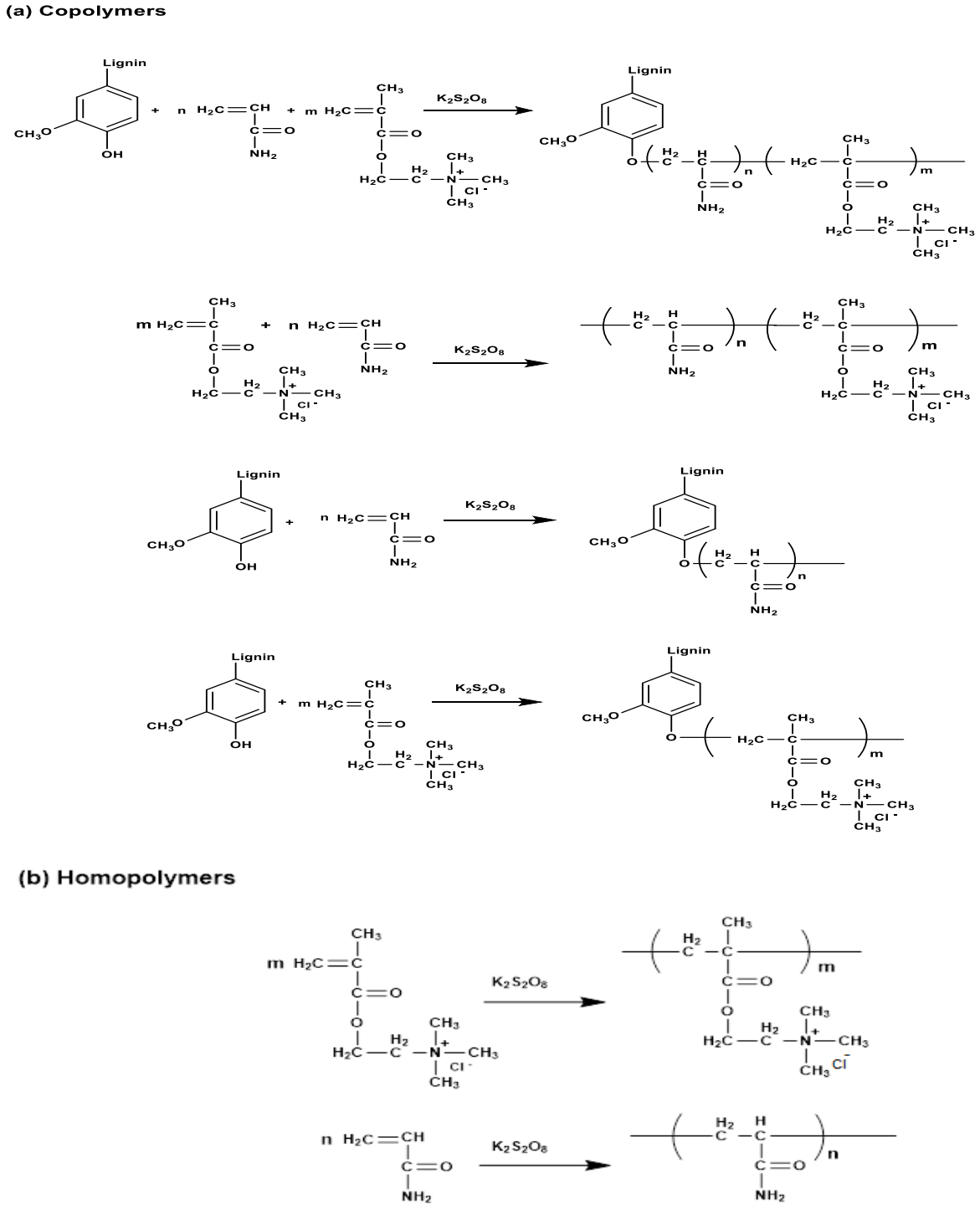

Figure 3.1. Copolymerization reaction of KL, DMC and AM; (a) copolymers of KL-AM-DMC, AM-DMC, KL-AM, KL-DMC, (b) homopolymers of PDMC and PAM.

3.4.2 Activation energy analysis

The activation energies of homopolymers and copolymers obtained following the procedure stated in the methodology section and listed in Table 3.1. It is evident that the E_a of KL-AM and KL-DMC were 43.02 kJ mol^{-1} and 21.99 kJ mol^{-1}, respectively. These results were close to those reported for starch-AM (48.16 kJ mol^{-1}) and 2-hydroxyethylmethacrylate-co-[2-(methacryloyloxy) ethyl] trimethylammonium chloride (HEMA-MAETC) polyelectrolyte hydrogels (26.84 kJ mol^{-1}) (Taghizadeh and Khosravy, 2003; Goel et al., 2009). In another study, the E_a of cellulose-ethyl acrylate copolymerization was 28.9 kJ mol^{-1}(Gupta et al., 2002). The E_a of AM-DMC was 18.13 kJ mol^{-1}, which is close to the reported value (16.9 kJ mol^{-1}) for AM-DMC in another study (Ge et al., 1997). The E_a of PAM was 14.54 kJ mol^{-1}, which is close to that reported elsewhere (12.5 kJ mol^{-1}) (Leowandowska, 2007). The E_a value of 10.34 kJ mol^{-1} was obtained for PDMC. The results indicated that the E_a of KL-AM, KL-DMC were greater than those of PAM, PDMC and AM-DMC, which implied that the homopolmerization reactions were favored and required less energy than KL-AM, KL-DMC and AM-DMC to proceed (Bi et al., 2012; Jahan et al., 2012).

Table 3.1. Activation energy of copolymers or homopolymers

Polymer	Temperature, (°C)	Time, min	R^2	Ea (kJ mol^{-1})
KL-AM	50-90	15-120	0.93	43.02
KL-DMC	50-90	15-120	0.96	21.99
AM-DMC	40-80	15-120	0.88	18.13
PAM	40-80	15 -120	0.96	14.54
PDMC	40-80	15-120	0.99	10.34

3.4.3 Effect of pH

The charge density and solubility of KL-AM-DMC as functions of reaction pH are presented in Figure 3.2. The charge density of KL-AM-DMC was constant between pH 2 and 3. At pH 4, the charge density and solubility of KL-AM-DMC reached the highest values of 1.76 meq g^{-1} and 50 wt. %, respectively. The decrease in the charge density may be ascribed to the decomposition of

quaternary ammonium group of DMC under alkaline conditions at a higher pH. It was stated in the literature that the quaternary ammonium group of DMC could be attacked by hydroxyl ion, which could convert quaternary ammonium groups into tertiary ammonium groups and this might result in a charge density decrease (Wang et al., 2015; Komkova et al., 2004).

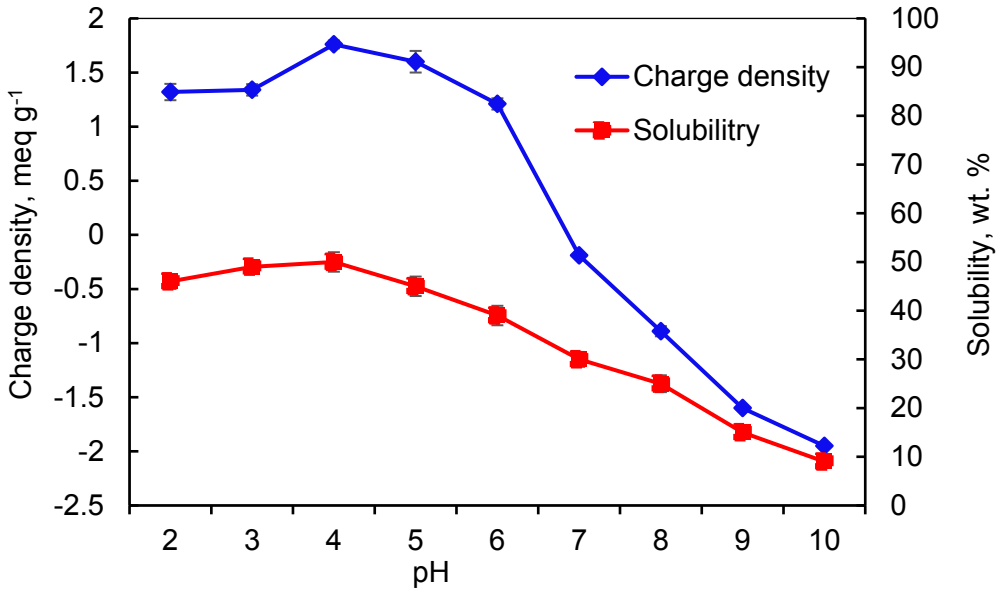

Figure 3.2. The effect of pH on the solubility and charge density of KL-AM-DMC. The reaction conditions were the initiator dosage of 0.11 mmol, 80 °C, 2 h, 0.011 mol of KL, 0.024 mol of DMC, 0.028 mol of AM.

3.4.4 Reaction temperature

The charge density and solubility of KL-AM-DMC are presented as functions of reaction temperature in Figure 3.3. As can be seen, they reached the maximum at 80 °C. The increase in the temperature improved the efficiency of the reaction as more radicals transferred to the polymer backbone (Thakur et al., 2010). However, the higher temperature of 90 °C probably hydrolyzed the products or facilitated the homopolymerization of DMC or AM or the copolymerization of AM-DMC (Sabhapondit et al., 2010), which in turn led to charge density and solubility reductions. It was reported in the past that the amide group attached to polyacrylamide could be hydrolyzed at 80–90 °C (Jamshidi et al., 2014; Sabhapondit et al., 2010)

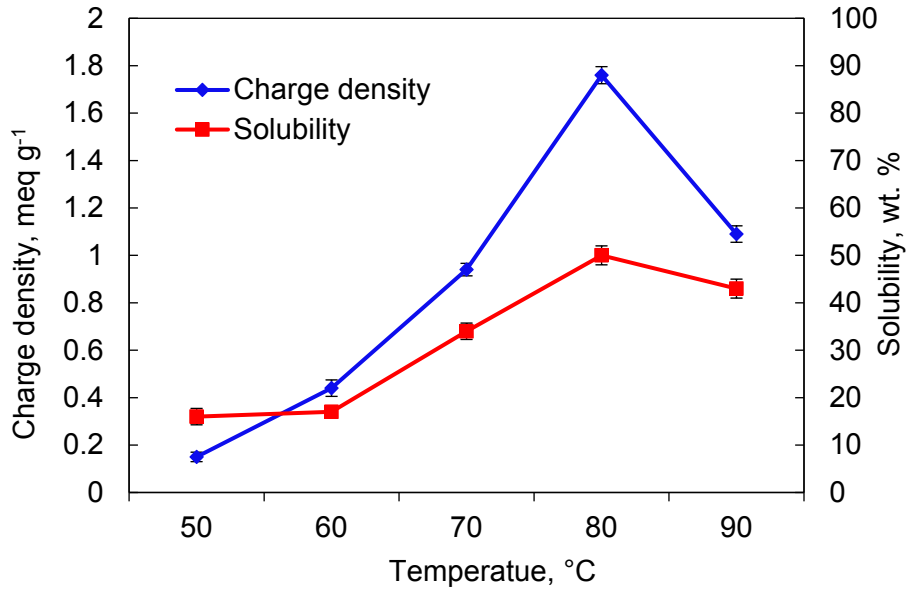

Figure 3.3. The effect of temperature on the solubility and charge density of KL-AM-DMC. The reaction conditions were initiator dosage of 0.11 mmol, pH 4.0, 2 h, 0.011 mol of KL, 0.024 mol of DMC, and 0.028 mol of AM.

3.4.5 Reaction time

The charge density and solubility of KL-AM-DMC are depicted as functions of time in Figure 3.4. The optimum reaction time was found to be 2 h that generated the KL-AM-DMC product with 50 wt. % solubility and 1.76 meq g^{-1} charge density. With increase in the reaction time from 2 h to 6 h, the charge density of KL-AM-DMC was reduced from 1.76 meq g^{-1} to 0.31 meq g^{-1}, and the solubility of the product decreased from 50 wt. % to 9.0 wt. %, respectively, which could be due to the progress in PAM, PDMC or AM-DMC production.

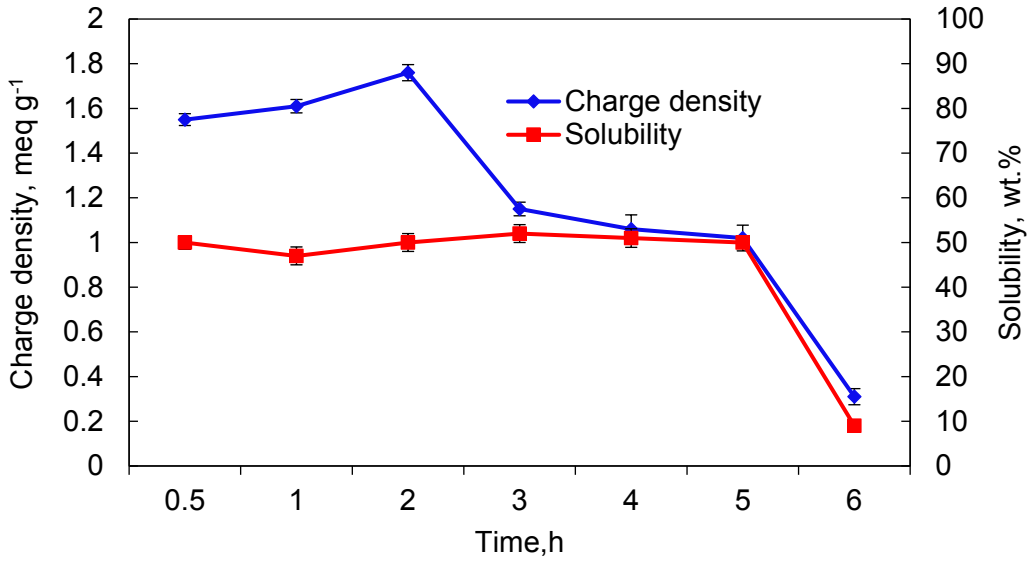

Figure 3.4. The effect of reaction time on the charge density and solubility of KL-AM-DMC. The reaction conditions were pH 4.0, initiator dosage of 0.11 mmol, 80 °C, 0.011 mol of KL, 0.024 mol of DMC, 0.028 mol of AM.

Table 3.2 lists the reaction conditions and the properties of the homopolymer or copolymer products produced under different conditions. By extending the reaction time of KL-AM-DMC, AM-DMC, PAM, and PDMC production 1) the monomer yield (KL, AM, DMC) in reaction media decreased in the copolymerization reactions and was undetectable in the homopolymerization reactions, 2) the molecular weight, charge density, and/or nitrogen content of homopolymers as well as those of AM-DMC increased significantly, implying that the progress in side reactions hampered the progress in the KL-AM-DMC production. Figure 3.5 shows the response of light scattering detector of the GPC instrument as a function of retention time of polymers of sample 1 and sample 8 produced under different reaction conditions in Table 3.2. It is seen that sample 1 and sample 8 have a similar retention time and thus molecular weight. The broader peak of sample 8 than sample 1 implies that the KL-AM-DMC had a wider molecular weight distribution than sample 1.

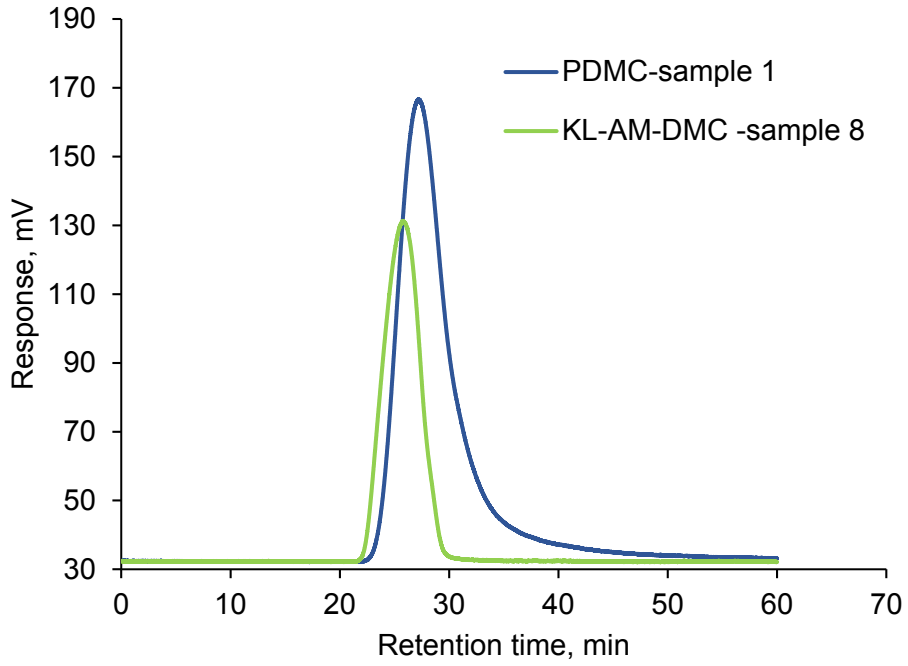

Figure 3.5. Response of light scattering detector of GPC as a function of retention time of polymers in GPC column for determining the molecular weight of KL-AM-DMC, and homopolymers (PAM, DMC) after purification.

Table 3.2. Reaction conditions and properties of the products in the reaction media

Name	Sample ID	Time, h	Initiator ,mmol	Lignin,mol	AM, mol	DMC, mol	N%	Charge density ,meq/g	Mw, g/mol	Yield of copolymers in precipitates , wt.%	Yield of homopolymers and AM-DMC in supernatants , wt.%	Yield of Unreactive monomer , wt.%	Yield of copolymers in Supernatants, wt.%
PDMC	1	0.5	0.11	-	-	0.024	-	3.86	103, 287	NA	72	ND	NA
	2	3	0.11	-	-	0.024	-	4.43	114,162	NA	85	ND	NA
PAM	3	0.5	0.11	-	0.028	-	17.33	-	383,661	NA	70	ND	NA
	4	3	0.11	-	0.028	-	18.69	-	438,752	NA	90	ND	NA
AM-DMC	5	0.5	0.11	-	0.028	0.024	-	1.8	112,194	NA	79	ND	NA
	6	3	0.11	-	0.028	0.024	-	2.4	143,257	NA	84	ND	NA
KL-AM-DMC	7	2h	0.11	0.011	0.028	0.0048	-	0.44	70,740	78	16	2.3	3.14
	8	2h	0.11	0.011	0.028	0.024	-	1.76	117,882	80	15	0.87	3.88
	9	2h	0.11	0.011	0.028	0.038	-	0.86	133,779	36	50	2.7	10.4
KL-AM-DMC	10	2h	0.036	0.011	0.028	0.024	-	0.35	153,766	66	28	2.9	2.15
	11	2h	0.22	0.011	0.028	0.024	-	0.37	86,122	50	47	0.32	2.6
KL-AM-DMC	12	0.5h	0.11	0.011	0.028	0.024	-	1.55	462,352	65	32	0.4	2.5
	13	6h	0.11	0.011	0.028	0.024	-	0.31	54,896	53	44	0.21	2.21
KL-AM-DMC	14	2h	0.11	0.011	0.007	0.024	-	2.08	123,878	-	-	-	ND
	15	2h	0.11	0.011	0.056	0.024	-	1.01	522,021	-	-	-	ND

ND: not detec NA: Not available

The results in Table 3.2 confirmed that, under optimal reaction conditions (2 h, 0.11 mmol of initiator, 0.011 mol of KL, 0.028 mol of AM, 0.024 of DMC, pH 4.0 and 80 °C), the yield of KL-AM-DMC in precipitates, homopolymers (PAM, PDMC) and copolymer (KL-AM, KL-DMC, KL-AM-DMC) in supernatants as well as unreacted monomers were 80 %, 15 %, 3.88 %, and 0.87 %, respectively. Although the presence of homopolymers (PAM, PDMC) and copolymers (AM-DMC) in the supernatant was confirmed by ^{1}HNMR analysis of dialyzed supernatant, it was not possible to differentiate these polymers to identify the exact yield of each one. Furthermore, ^{1}HNMR confirmed the absence of the peaks for AM, DMC and KL in the supernatant of final ethanol washing of the precipitates, confirming the absence of homopolymers and AM-DMC in the precipitates of KL-AM-DMC, KL-DMC and KL-AM.

3.4.6 Effect of initiator concentration

The impact of initiator concentration on the KL-AM-DMC copolymerization was depicted in Figure 3.6. The charge density and solubility increased from 0.35 to 1.76 meq g^{-1} and from 11 % to 50 % with an increase in the initiator concentration to 0.11 mmol, respectively. However, as the concentration of the initiator further increased, the charge density and solubility decreased. The results in Table 3.2 show that, by increasing the initiator concentration in the KL-AM-DMC copolymerization reaction, the molecular weight and copolymer yield of KL-AM-DMC as well as the amount of unreacted monomers decreased, while the homopolymer yield increased. Hence, at the initiator dosage of more than 0.11 mmol, the reaction rate of KL-AM-DMC decreased, while that of homopolymers increased. It was reported in the literature that the molecular weight of polymers in the polymerization reaction inversely depended on the initiator concentration, and the higher initiator dosages resulted in a lower molecular weight, which in turn would reduce the copolymerization yield (Zohuriaan et al., 2005; Sadeghi et al., 2012). This may be attributed to the fact that the higher initiator dosages result in side-chain reactions of monomers that facilitate homopolymerization and cause the chain terminations of KL-AM-DMC (Thakur and Singha, 2010).

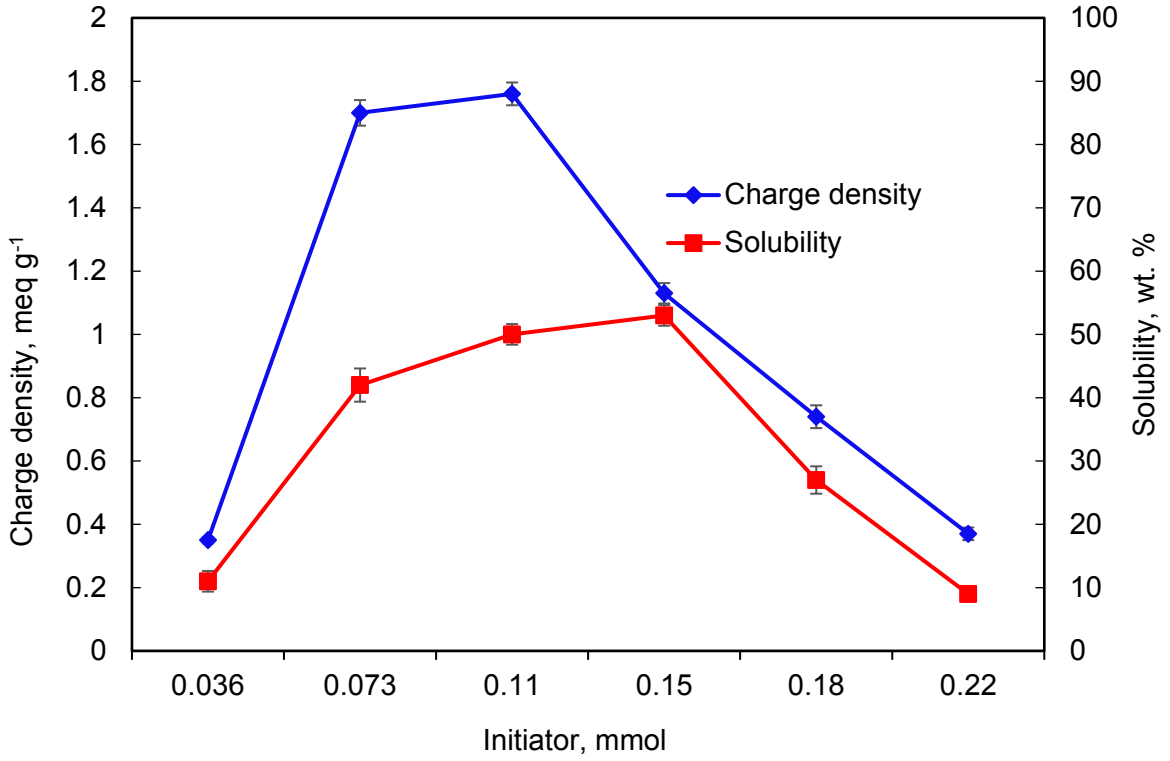

Figure 3.6. The effect of initiator concentration on the charge density and solubility of KL-AM-DMC. The reaction conditions were pH 4.0, 80 °C, 2 h, 0.011 mol of KL, 0.024 mol of DMC, 0.028 mol of AM.

3.4.7 Effect of DMC dosages

The impact of DMC on the copolymerization of KL-AM-DMC was investigated in Figure 3.7. The charge density and solubility of KL-AM-DMC was significantly increased by increasing the DMC amount in the reaction from 0.2 to 0.9 mol mol^{-1}. By adding more DMC to the reaction mixture, the produced copolymer would have a higher percentage of DMC monomers (i.e., cationic hydrophilic monomer), and in turn the product would have a higher charge density and solubility. However, at a DMC concentration that was higher than 0.6 mol mol^{-1}, the charge density and solubility decreased as the contents of KL and AM decreased. This is due to the fact that the reaction mixture would have less AM and lignin radicals compared with DMC, which would significantly hamper the copolymerization of KL-AM-DMC, as a result. Therefore, the reaction would have an excess amount of unreacted DMC monomers, which may improve the homopolymerization of PDMC (Junren et al., 2013; Rong et al., 2013). The results in Table 3.2

also show that the increase in the DMC dosage from 0.0048 to 0.038 wt. % (corresponds 0.2 to 0.9 mol mol^{-1}) led to a remarkable increase in the homopolymerization of PDMC (i.e., 16 to 50 %). However, the molecular weight of KL-AM-DMC insignificantly increased, and the yield of KL-AM-DMC reduced when the DMC dosage was increased. At the dosage of 0.9 mol mol^{-1}, most of the unreacted DMC monomers converted to homopolymers of PDMC (Table 3.2).

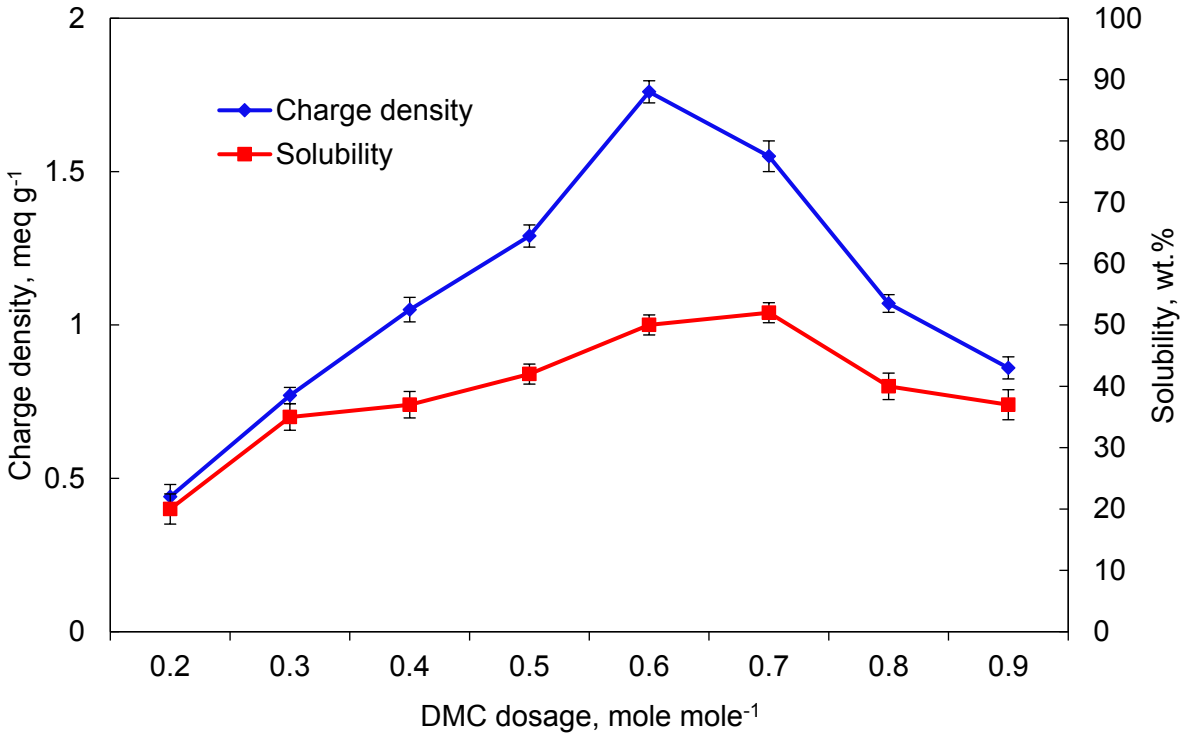

Figure 3.7. The effect of DMC/KL-AM molar ratio on the charge density and solubility of KL-AM-DMC. The reaction conditions were initiator dosage of 0.11 mmol, pH 4.0, 80 °C, 0.011 mol of KL, 0.028 mol of AM, 0.2-0.9 mol mol-1 of DMC/KL-AM.

3.4.8 Effect of acrylamide dosages

Figure 3.8 shows the impact of acrylamide dosage on the charge density and solubility of KL-AM-DMC. It is seen that KL-AM–DMC had a charge density of 1.76 meq g^{-1} and solubility of 50 wt. % at 0.011 mole of KL, 0.028 mole of AM, and 0.024 mole of DMC. The solubility of copolymer increased with the increase in AM from 0.2 to 1.5 mole ratio. However, the charge density dropped by increasing the AM ratio because a higher dosage of AM would facilitate more bridging of KL and DMC monomers, which would promote water solubility of KL-AM-DMC but reduce the

charge density of KL-AM-DMC, as AM did not carry a cationic charge density. Further increase in AM dosage (beyond 1.5 mole ratio) would trigger the homopolymerization of AM. The higher AM concentration would enhance the probability of AM chain extension instead of grafting onto KL. Table 3.2 shows that the molecular weight of KL-AM-DMC was significantly increased by increasing the dosage of AM from 0.007 to 0.056 wt. % (corresponds to 0.2 and 1.5 mole mole^{-1}).

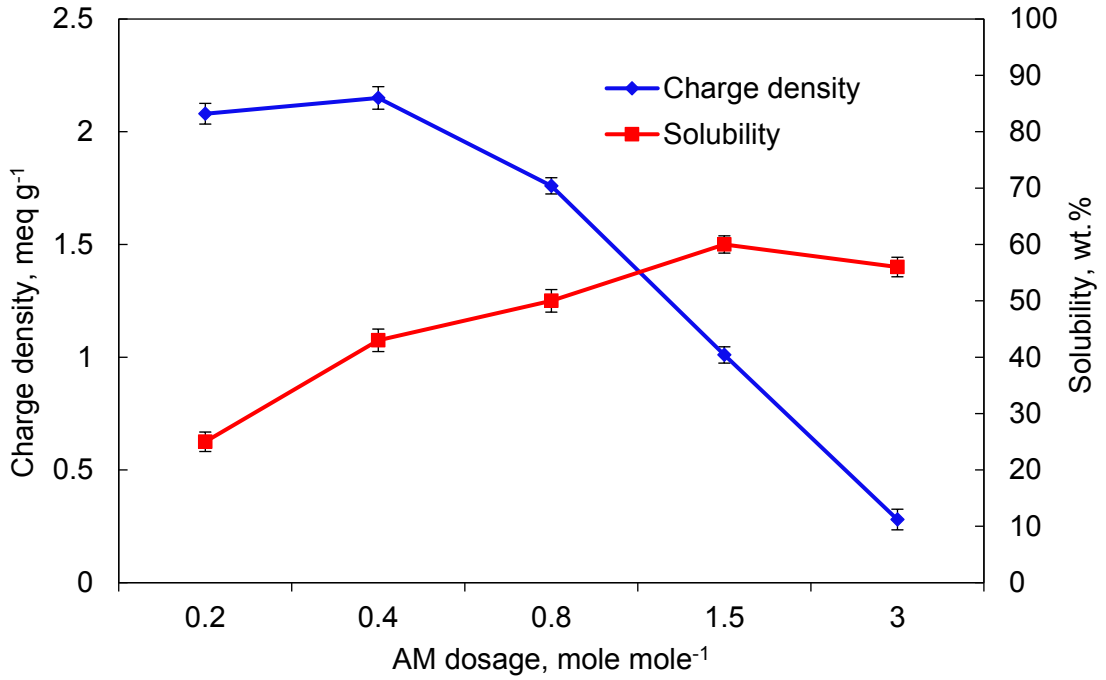

Figure 3.8. The effect of AM/KL-DMC molar ratio on the charge density and solubility of KL-AM-DMC. The reaction conditions were initiator concentration of 0.11 mmol, pH 4.0, 80 °C, 0.011 mol of KL, 0.024 mol of DMC.

3.4.9 FTIR analysis

The FTIR spectra of KL and KL-AM-DMC are shown in Figure 3.9. The sample produced under the optimal conditions of 0.011 moles of KL, 0.024 moles of DMC, 0.028 moles of AM, 80°C, 2 h and the initiator dosage of 0.11 mmol was selected as the best sample. The broad band around 3400 cm^{-1} was assigned to the O-H stretching absorption in the phenolic and aliphatic compounds of KL (Sun et al., 2010). The C-H vibration absorption band of the aromatic ring appeared at 1590 cm^{-1}, 1510 cm^{-1}, and 1448 cm^{-1}, which represent the existence of the aromatic skeletal structure in KL and KL-AM-DMC (Xu et al., 2008) The bands at 1448 cm^{-1} and 1421 cm^{-1} are assigned to methoxyl groups (Mansouri et al., 2011). The absorbance bands at 1261 cm^{-1} and 1140 cm^{-1} are

assigned to the C-O and C-H stretch of guaiacyl unit (Mansouri and Salvado, 2006; Zhou et al., 2010).

Furthermore, in spectrum of KL-AM-DMC, a broad band at 3400–3100 cm^{-1} corresponds to O-H stretching in the phenolic and aliphatic compounds in modified lignin. A considerable decrease in the absorption intensities in this band for modified kraft lignin have been observed previously (Konduri et al., 2015). The KL-AM-DMC spectrum indicated an absorption peak at 3327 cm^{-1}, which was due to the stretching vibrations for $–NH_2$ bond in amide groups and C–O in ester groups. A strong adsorption peak at 1670 cm^{-1} is related to carbonyl group (NH_2 -C-O of amide group) in AM (Zhou et al., 2010). The bands indicated at 1475 and 952 cm^{-1} belong to the carbonyl (C=O) of ester groups and the methyl groups (-N-CH_3) of the ammonium in the quaternary ammonium group of DMC, respectively (Fanghui et al., 2010; Wang et al., 2012; Mansouri et al., 2011). The absorption peaks at 1450 cm^{-1} and 2930 cm^{-1} originated from $–CH_3$ and $–CH_2$ groups of ammonium in DMC (Fanghui et al., 2010; Shang et al., 2009; He et al., 2007). These spectra demonstrated that both DMC and AM were successfully participated in the copolymerization of KL, AM and DMC.

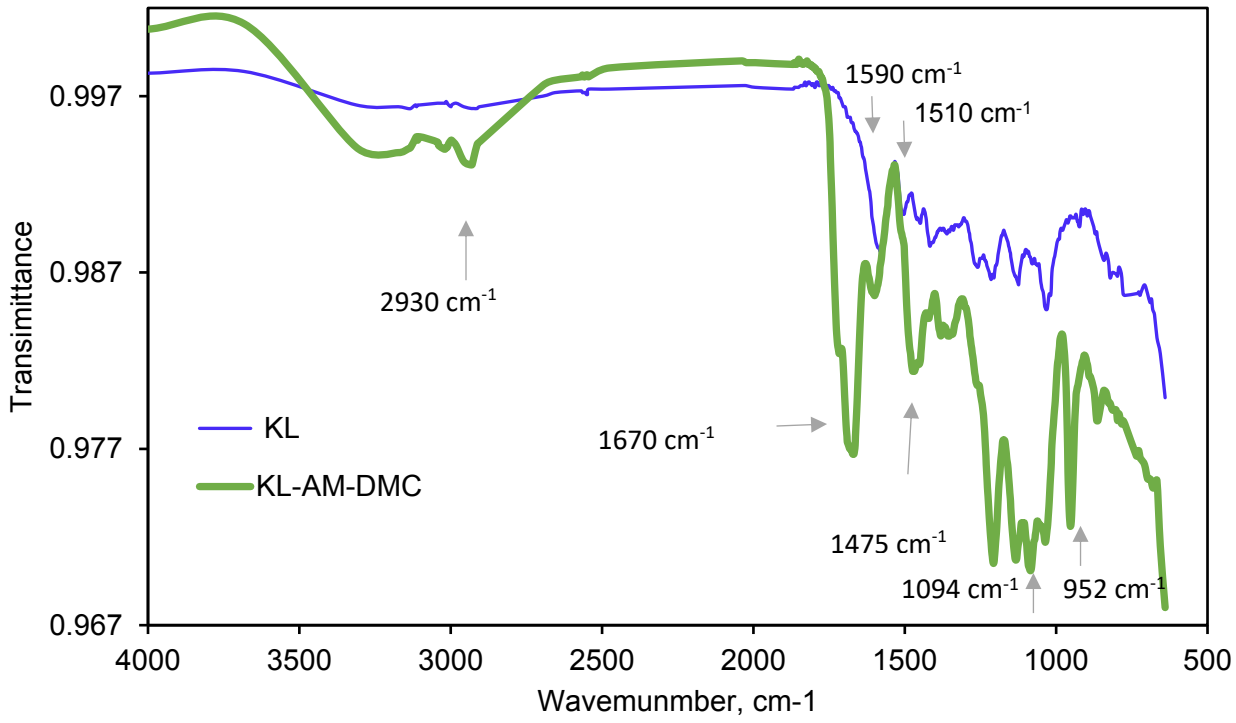

Figure 3.9. FTIR spectra of KL and KL-AM-DMC.

3.4.10 Elemental analysis

The elemental contents of KL and KL-AM-DMC are presented in Table 3.3. The results depict that KL originally had 0.03 wt. % of nitrogen; whereas, its nitrogen content increased to 7.02 wt. % in the KL-AM-DMC copolymer. The DMC contains one nitrogen atom in its quaternary ammonium group, thus the increase in the nitrogen content in KL-AM-DMC confirmed the copolymerization of KL, AM, and DMC. The overall nitrogen content of KL-AM-DMC can be attributed to the nitrogen elements of DMC and AM. Based on the charge density and nitrogen content of the KL-AM-DMC, the contributions of KL, AM, and DMC in the products were determined and the results showed that KL-AM-DMC had 40 wt. % KL, 36.5 wt. % DMC, and the rest was AM. Also, the hydrogen and oxygen contents of KL-AM-DMC were higher than those of KL, which was due to the high hydrogen content of DMC and AM monomers.

Furthermore, based on the elemental compositions of KL (Table 3.3), those of DMC and AM participating in the reaction, as well as the proportion of AM, DMC, and KL in the KL-AM-DMC, the theoretical elemental compositions of KL-AM-DMC can be determined. The theoretical carbon, hydrogen, oxygen, and nitrogen contents of KL-AM-DMC were determined to be 55.7 wt.%, 7.2 wt. %, 27.2 %, and 7.4%, respectively. These results are close to the experimental results obtained for KL-AM-DMC in Table 3.3.

Table 3.3. Elemental analysis of KL and KL-AM-DMC

Sample	**KL**	**KL-AM-DMC**
Nitrogen wt. %	0.03	7.02
Carbon wt.%	54.63	55.22
Hydrogen wt.%	4.60	7.77
Oxygen wt.%	38.63	28.03
Sulfur wt.%	2.10	1.96
DMC wt.%	0	36.5
AM wt.%	0	23.5
KL wt.%	100	40
Formula	$C_9H_{9.10}O_{3.25}N_{0.00}S_{0.129}$	$C_9H_{15.21}O_{4.32}N_{0.98}S_{0.11}$

3.4.11 Thermal decomposition analysis

The thermal behavior of KL and KL-AM-DMC copolymers are shown in Figure 3.10. The initial weight loss of KL (below 200 °C) is probably attributed to the loss of adsorbed and bound water. The changes in the thermal behavior of KL are presented by two peaks at 288 °C and 322 °C, where the results showed that 60 wt. % of KL remained as ash. In addition, it is observable that part of KL-AM-DMC copolymer remained as ash after incinerating at 668 °C. It is also seen in this figure that temperatures for the weight loss of KL-AM-DMC were at 280 °C, 351°C, and 399 °C. This investigation indicates that the grafting of the AM and DMC onto the KL backbone varied the thermal stability of KL-AM-DMC.

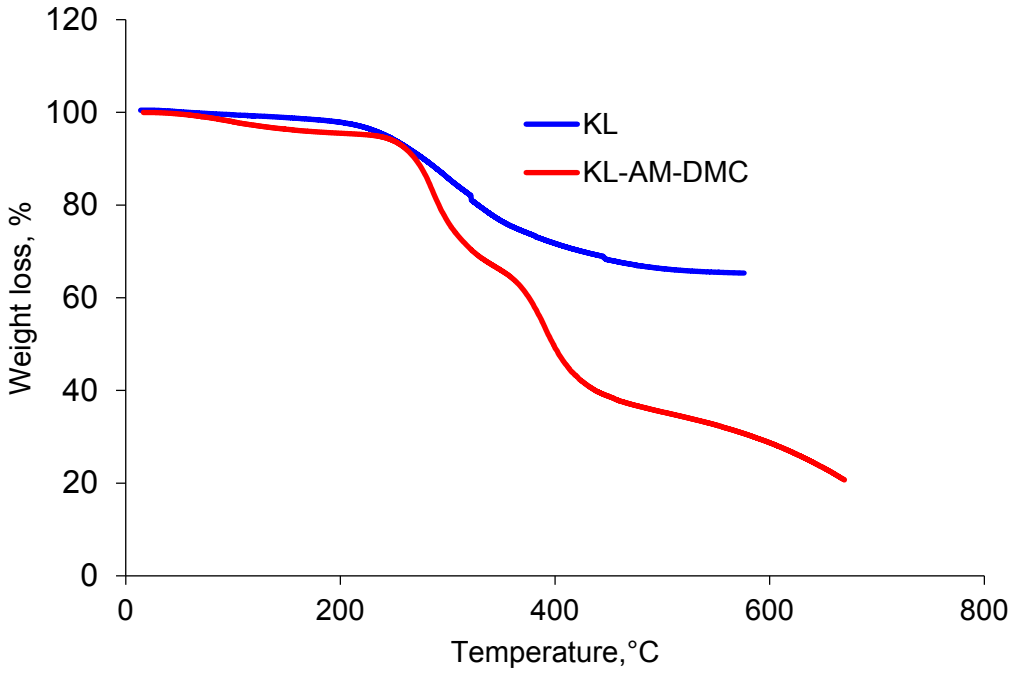

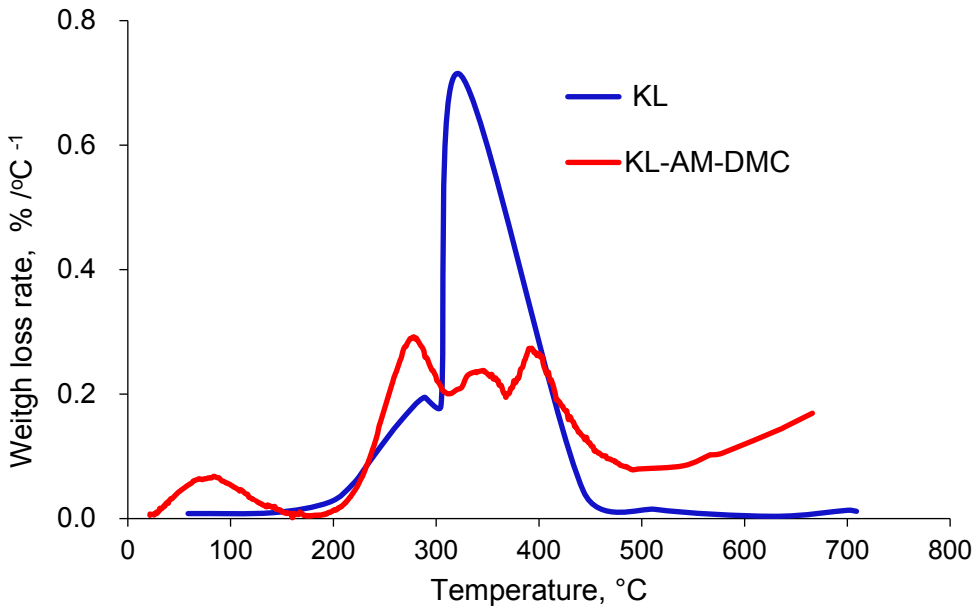

Figure 3.10. Weight loss and weight loss rate of KL, KL-AM-DMC copolymers.

3.4.12 ^{1}H-NMR

The dried and dialyzed precipitates and the supernatants of the reaction products yielded under the conditions of 2h, 0.11 mmol of initiator, 0.011 mol of KL, 0.028 mol of AM, 0.024 of DMC, pH 4.0 and 80 °C, were analyzed by NMR and presented in Figure 3.11. As shown, in KL spectrum (i.e., raw material) the peak at 8.5 ppm is attributed to unsubstituted phenolic protons; at 7.42–5.99 ppm is attributed to aromatic protons; at 4.5–3.05 ppm is attributed to protons in methoxyl groups of lignin; at 3.6- 3.2 ppm is assigned to the methylene protons in β-β structure; and at 3.3-1.75 ppm is assigned to the aliphatic protons in lignin (Sun et al., 2010; Mansouri et al., 2011). Peaks appeared at 4.7 ppm is assigned to the solvent of D_2O.

In case of KL-AM-DMC (i.e., dried and dialyzed precipitates), the methenyl (-CH-) and methylene –CH_2- connected to the amide group in AM, as is evidenced by the peaks around 1.05 to 1.3 ppm, respectively (Abdollahi et al., 2011; Yang et al., 2010; Chen et al., 2006). The peak of $–N^{+}(CH_3)_3$ was observed at 3.3 ppm. The methylene groups connected to the ammonium group and ester carbon were detected at 3.4 - 3.8 ppm (Abdollahi et al., 2011). In addition, the methyl (-CH_3-) group connected to ammonium group in DMC was shown by the peak at 0.8 ppm. The small peak for KL segment was also presented at 7.2 ppm spectrum of KL-AM-DMC copolymer (Sun et al.,

2010; Mansouri et al., 2011). These peaks indicated that both AM and DMC participated in the copolymerization of KL, AM, and DMC (Abdollahi et al., 2011; Chen et al., 2006).

In the case of dried and dialyzed homopolymers (PAM and PDMC) as well as AM-DMC in supernatants, few new peaks were revealed between 1-2 ppm and 4-6 ppm. These peaks also confirmed the presence of homopolymers in the supernatant. The peaks at 3.7 and 4.3 ppm confirmed the presence of AM-DMC copolymer in the supernatant (Abdollahi et al., 2011).

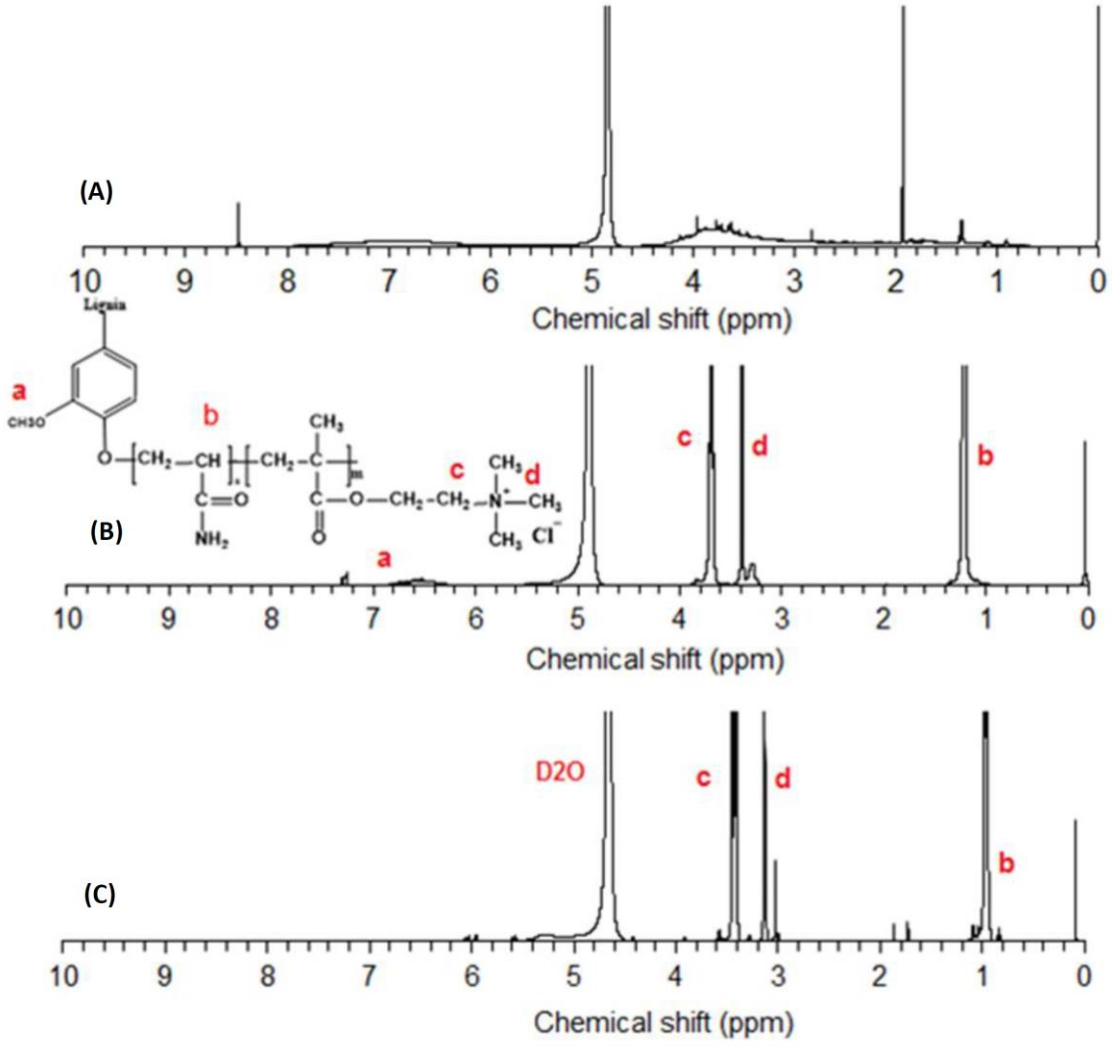

Figure 3.11. 1H-NMR spectrum of (A) KL, (B) precipitates (KL-AM-DMC, KL-DMC and KL-AM) and (C) homopolymers of PAM, PDMC and copolymer of AM-DMC produced under

optimized conditions of 2h, initiator 0.11 mmol, KL 0.011 mol, AM 0.028 mol, DMC 0.024, pH 4.0, temperature 80 °C.

3.4.13 SEM assessment

The SEM images of KL and KL-AM-DMC were shown in Figure 3.12. As can be seen, the surfaces of KL and KL-AM-DMC were significantly different, that is to say KL particles were larger and smooth. After the copolymerization reaction, it appears that KL-AM-DMC had a rough and porous surface.

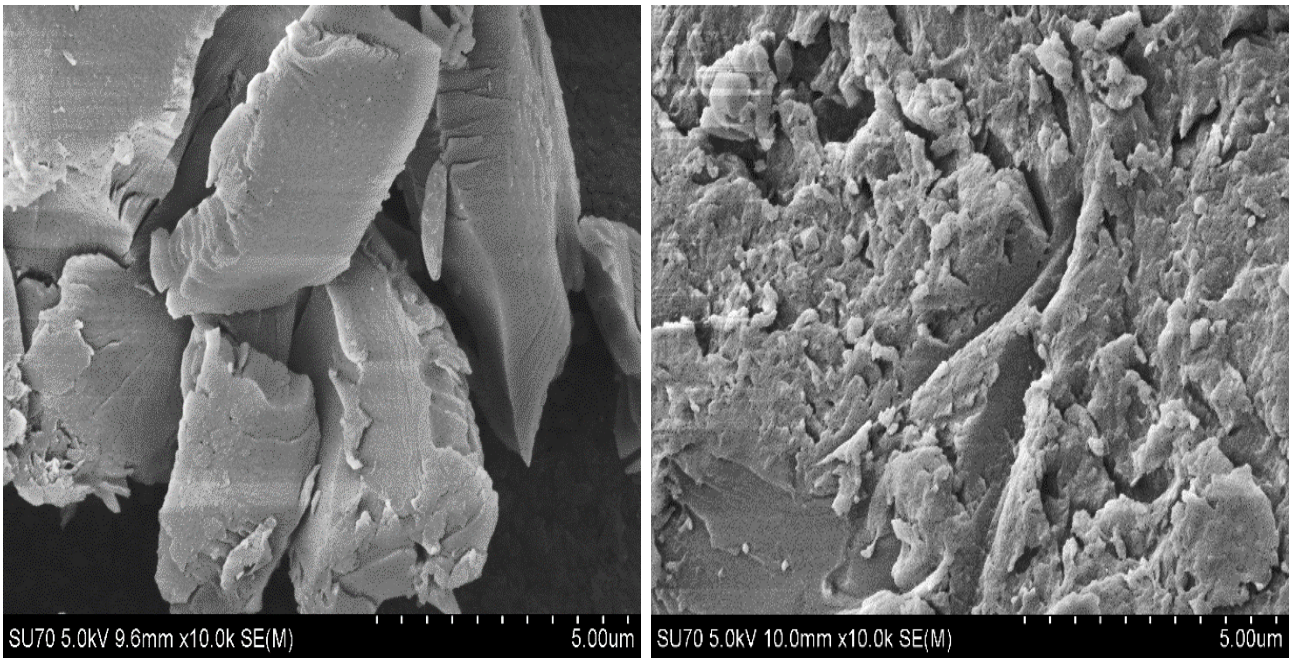

Figure 3.12. SEM images of (a) KL and (b) KL-AM-DMC polymers

3.5 Conclusions

In this work, KL was copolymerized with AM and DMC in order to produce cationic copolymerized kraft lignin based product. The optimal conditions were pH 4.0, initiator concentration of 0.11 mmol, 80 °C, 2 h, 0.011 mol of KL, 0.024 mol of DMC, 0.028 mol of AM, which generated KL-AM-DMC with the charge density of 1.76 meq g^{-1} and M_w of 118 kg mol^{-1}. The activation energy of KL-DMC, KL-AM, and AM-DMC were 21.99, 43.03, and 18.13 kJ mol^{-1}, while that of PAM and PDMC were 14.54 and 10.34 kJ mol^{-1}, respectively. The increase in

temperature improved the charge density and solubility of the copolymer, beyond optimum temperature the homopolymerization of PAM and PDMC dominated. The maximum charge density and solubility were obtained at 2 h of reaction, but further extension of reaction time declined the charge density and solubility of the copolymer due to the formation of homopolymers (PAM, PDMC). The increase in the initiator dosage beyond the optimum led to the progress in homopolymerization reaction. The copolymerization of KL, AM, and DMC was successfully confirmed by ^{1}H NMR, FTIR, TGA and elemental analyses. The TGA analysis depicted that the grafting of AM and DMC onto the KL greatly altered the thermal stability of KL. The elemental analysis also confirmed that the nitrogen, hydrogen, and oxygen contents of KL were increased via copolymerization with AM and DMC.

3.6 References

Abdollahi, Z., Frounchi, M., Dadbin, S. 2011. Synthesis, characterization and comparison of PAM, cationic PDMC and P (AM-co-DMC) based on solution polymerization. J. Ind. Eng. Chem., 17, 58 0–586.

Ben, W. Yulian, Z., Chunbao, M. 2011. Preparation of cationic chitosan-polyacrylamide flocculant and its properties in wastewater treatment. J. Ocean Univ. Chin., 10, 42-46.

Bernardini, J., Anguillesi, I., Coltelli, M.B., Cinelli, P., Lazzeri, A. 2015. Optimizing the lignin based synthesis of flexible polyurethane foams employing reactive liquefying agents. Polym. Intl., 2015, 64, 1235-124.

Bi, K., Zhang Y., 2012. Kinetic study of the polymerization of dimethyldiallylammonium chloride and acrylamide. J. App. Polym. Sci., 125, 1636–1641.

Chen, D., Liu, X., Yue, Y., Zhang, W., Wang, P. 2006. Dispersion copolymerization of acrylamide with quaternary ammonium cationic monomer in aqueous salts solution. Eur. Polym. J., 42, 1284–1297.

Duygu, A., Nuri, M., Levent, D. 2002. New cationic polyelectrolytes for flocculation processes of baker's yeast waste water. Polymer Bulletin, 48, 353-359.

Fanghui. W., Jing, Z., Hong, Z., Kefei, H., Jiantao, F. 2010. Preparation of high effective flocculant for high density waste drilling mud. J. Environ. Prot., 1, 179-182.

Fang, R., Cheng, S.U., Fu, J., Zheng, Z.B., 2009. Research on the graft copolymerization of EH-lignin with acrylamide, Natural Sci., 1, 17-22.

Ge, X., Ye, Q., Xu, X., Zhang, Z., Sun, S. 1997. Kinetics of emulsion copolymerization of (2-methacryloyloxyethyl) trimethyl ammonium chloride and acrylamide with gamma rays. Radiat. Phys. Chem., 50, 253-258.

Goel, K., Kumar, V., Bhardwaj, Y., Chaudhari, C., Dubey, K., Sabharwal, S. 2009. Swelling response of radiation synthesized 2-Hydroxyethylmethacrylate-co-[2-(methacryloyloxy) ethyl] Trimethylammonium chloride hydrogels under various in vitro conditions. J. Biomater. Sci. Polym. Ed., 20, 785–805.

Gooselink, R.J., Snijder, M.H., Kranenbarg A., Keijsers, E.R., Jong, E., Stigsson, L.L. 2010. Characterization and application of NovaFiber lignin. Ind. Crops. Prod., 20, 191-203.

Gupta, K.C., Sahoo, S., Khandekar, K., 2002. Graft copolymerization of ethyl acrylate onto cellulose using ceric ammonium nitrate as initiator in aqueous medium. *Biomacromol.* 3, 1087-1094.

He, Y., Li, G., Yang, F., Yu, X., Cui, Y., Ren, F. 2007. Precipitation polymerization of acrylamide with quaternary ammonium cationic monomer in potassium carbonate solution initiated by plasma. J. Appl. Polm. Sci.,104, 4060-4067.

Jahan, M.S., Liu, Z., Wang, H., Saeed, A., Ni, Y. 2012. Isolation and characterization of lignin from prehydrolysis liquor of kraft based dissolving pulp production. Cellul. Chem. Technol., 46, 261–267.

Jamshidi, H., Rabiee A. 2014. Synthesis and characterization of acrylamide-based anionic copolymer and investigation of solution properties. Adv. Mater. Sci. Eng., 1-6.

Junren, Z., Huaili, Z., Zhenzhen, J., Tshukudu, T. 2013. Synthesis and characterization of a dewatering reagent: cationic polyacrylamide (P (AM–DMC–DAC)) for activated sludge dewatering treatment, Desalin. Water Treat., 51, 2791–2801.

Komkova, E.N., Stamatialis, D.F., Strathmann, H., Wessling, M. 2004. Anion-exchange membranes containing diamines: preparation and stability in alkaline solution. J. Memb. Sci., 244, 25-34.

Konduri, M.K., Kong, K., Fatehi, K. 2015. Production of carboxymethylated lignin and its application as a dispersant. Eur. Polym. J., 70, 371-383.

Kong, F., Wang, S., Price, J.T., Konduri, M., Fatehi, P. 2015. Synthesis and characteristics of water soluble lignin copolymer from Kraft lignin and acrylic acid. Green Chem., 17, 4355-4366.

Kouisni, L., Holt-Hindle, P., Maki, K., Paleologou, M. 2012. The lignoforce system (TM): a new process for the production of high-quality lignin. J. Sci. Tech. Forest Prod. Pro., 2, 6– 10.

Kuhire, S.S., Nagane, S.S., Wadgaonkar, P.P., 2017. Poly (ether urethane) s from aromatic diisocyanates based on lignin-derived phenolic acids. Polym. Intl., 66, 882-891.

Lee, C.S., Robinson, J., Chong, M.F., 2014. A review on application of flocculants in wastewater treatment process. Process Saf. Environ. Prot., 92, 489-508.

Leowandowska, L., 2007. Comparative studies of rheological properties of polyacrylamide and partially hydrolyzed polyacrylamide solutions. J. App. Polym. Sci., 103, 2235–2241.

Levasseur, Z., Savulescu, L., Benali, M. 2011. Lignin production path assessment: energy, water, and chemical integration perspective J. Sci. Technol. Forest Prod. Proc., 1, 25-30.

Ma, S., Li, T., Liu, X., Zhu, J.2016. Research progress on bio-based thermosetting resins. Polym. Intl., 65, 164-173.

Mansouri, E., Yuan, Q., Huang, F. 2011. Characterization of alkaline lignin for use in phenol form-aldehyde and epoxy resin. BioResources, 6, 2647- 2662.

Mansouri, E., Salvado, J. 2006. Structural characterization of technical lignins for the production of adhesives: Application to lignosulfonate, kraft, soda-anthraquinone, organosolv and ethanol process lignins. Ind. Crops Prod., 24, 8-16.

Maziero, P., Neto, M.O., Machado, D., Batista, D., Cavalheiro, C.S. 2012. Structural features of lignin obtained at different alkaline oxidation conditions from sugarcane baggase. Ind. Crops Prod., 35, 61-69.

Meister, J.J., 2002. Modification of lignin. J. Macromol. Sci. Polym. Rev., 42, 235–289.

Rong, H., Gao, B., Zhao, Y., Sun, S., Yang, Z., Wang, Y., Yue, Q., Li, Q. 2013. Advanced lignin-acrylamide water treatment agent by pulp and paper industrial sludge: Synthesis, properties and application. J. Environ. Sci., 25, 2367– 2377.

Sabhapondit, A., Borthakur, A., Haque, I. 2003. Characterization of acrylamide polymers for enhanced oil recovery. J. Appl. Polym. Sci., 87, 1869–1878.

Sadeghi, M., Mohammadinasab, E., Shafie, E. 2012. APS-initiated graft copolymerization of N-Vinyl pyrollidone onto gelatin: Preparation, characterization, and optimization of grafting parameters. Sci. Res. Essays, 7, 511-521.

Savy, A., 2014. Physical–chemical characteristics of lignin separated from biomasses for second-generation ethanol. Biomass Bioenerg., 62, 58-67.

Shang, H., Liu, J., Zheng, Y., Wang, J. 2009. Synthesis, characterization, and flocculation properties of poly (acrylamide-methacryloxyethyltrimethyl ammonium chloride-methacryloxypropyltrimethoxy Silane). J. Appl. Polym Sci., 111, 1594–1599.

Shen, J.J., Ren, L.L., Zhuang, Y. 2006. Interaction between anionic dyes and cationic flocculant P (AM-DMC) in synthetic solutions. J. Hazard Mater., 136, 809–815.

Silva, E.A., Zabkova, M., Araujo, J.D., Cateto, C.A., Barreiro, M.F., Belgacem, M.N., Rodrigues, A.E. 2009. An integrated process to produce vanillin and lignin-based polyurethanes from kraft lignin. Chem. Eng. Res. Des., 87, 1276–1292.

Sing, R.P., Pal, S., Ali, S.K. 2014. Novel biodegradable polymeric flocculants based on cationic polysaccharides. Adv. Mater. Lett., 5, 24-30.

Sriroth K., Piyachomkwan K. 2013.The outlook of sugars and starch crops in biorefinery. in bioprocessing technologies in biorefinery for sustainable production of fuels. Yang, S.T., El-Enshasy, H.A., Thongchul, N., Eds.; Wiley J. & Sons, New Jersey, Chapter 2, pp 27-46.

Sun, Y.C., Xu, F., Sun, R.C. 2010. Fractionation and structural characterization of lignin isolated by organic solvents and alkaline solutions from Tamarix spp. Sci. Res. Essays, 5, 3850-3864.

Taghizadeh, M., Khosravy, M., 2003. Kinetics and mechanism of graft copolymerization of vinyl monomers (acrylamide, acrylic acid, and methacrylate) onto starch by potassium dichromate as redox initiator. Iran Polym. J., 12, 497- 505.

Thakur, V.K., Singha, A.S. 2010. KPS-initiated graft copolymerization onto modified cellulosic biofibers. Int. J. Polym. Anal. Charact., 15, 471-485.

Voitl, T., Von, P. 2010. Demonstration of process for the conversion of kraft lignin into vanillin and methyl vanillate by acidic oxidation in aqueous methanol. Ind. Eng. Chem. Res., 49, 520-525.

Wang. J.P., Chen, Y.Z., Wang, Y., Yuan, S.J., Sheng, J.P. 2012. A novel efficient cationic flocculants prepared through grafting two monomers onto chitosan induced by gamma radiation. RSC. Adv., 2, 494–500.

Wang, S., Hou, Q., Kong, F., Fatehi, P., 2015. Production of cationic xylan–METAC copolymer as a flocculant for textile industry. Carbohyd. Polym., 124, 229–236.

Wang, J.P., Chen, Y.Z., Wang, Y., Yuan, S.J., Yu, H.Q., 2001. Optimization of the coagulation-flocculation process for pulp mill wastewater treatment using a combination of uniform design and response surface methodology. Water Res., 45, 5633-56-40

Windt, M., Meie, D., Marsman, J.H. Heeres, J.H., Koning, S. 2009. Micro pyrolysis of technical lignins in a new modular rig and product analysis by GC-MS/FID and GCXGC-TOFMS/FID. J. Anal. Appl. Pyrolysis., 85, 38-46.

Xueyu, D., Jiebing, L., Mikael, E., 2014. Modification of industrial softwood kraft lignin using Mannich reaction with and without phenolation pretreatment. Ind. Crops Prod., 52, 729–735.

Xu, F., Sun, R.C., Mei-Zhai, Z., Sun, J.J., Jiang, J.X., Zhao, G.J. 2008. Comparative study of three lignin fractions isolated from mild ball-milled Tamarix austromogoliac and Caragana sepium. J. Appl. Polym. Sci., 108, 1158-1168.

Yang, Z.H., Gao, B.Y. Li, C.X., Yue, Q.Y., Liu, B., 2010. Synthesis and characterization of hydrophobically associating cationic polyacrylamide. Chem. Eng. J., 161, 27–33.

Yue, Q.Y., Gao, B.Y., Wang, B.Y., Zhang, H., Sun, X., Wang, S.G., Roy, R. 2008. Synthesis of polyamine flocculants and their potential use in treating dye wastewater. J. Hazard Mater., 152, 221–227.

Zakzeski, J., Bruijnincx, P.C., Jongerius, A.L., Weckhuysen, B.M. 2010. The catalytic valorization of lignin for the production of renewable Chem. Rev., 110, 3552–3599.

Zhou, S., Xu, J., Zhao, W., Wang, C., Wu, Y. 2010. Microwave-enhanced extraction of lignin from birch in formic acid: Structural characterization and antioxidant activity study. eXPRESS Polym. Lett., 4, 275–283.

Zohuriaan, M.J., Pourjavad, A., Sadeghi, M. 2005. Modified CMC: Part1- Optimized synthesis of carboxymethylcellulose-g-polyacrylonitrile. Iran Polym. J., 14, 131-138.

Chapter 4: Optimization of kraft lignin-p (AM) –p (DMC) production following Taguchi method

4.1 Abstract

Lignin produced in the kraft pulping process is insoluble in water at neutral pH, which limits its application in industry. In this chapter, kraft lignin (KL) was copolymerized with acrylamide (AM) and (2-methacryloyloxyethyl) trimethyl ammonium chloride (DMC) in an aqueous solution to produce a water soluble lignin- P (AM)-P (DMC) copolymer. Reaction time, temperature, pH, and monomers concentrations were optimized using Taguchi L^{16} (orthogonal array) design to get maximum charge density and solubility of kraft lignin. The optimal reaction conditions for KAD copolymer were as follows: 0.011 mol of KL, 0.014 mol of AM, 0.024 mol of DMC, pH 3, 3 h and 80 °C. At optimized conditions, lignin- P (AM)-P (DMC) copolymer showed charge density of 2.13 meq/g with solubility of 56% in an aqueous solution. The copolymers were well characterized by Thermogravimetric analysis (TGA). Analysis of variance (ANOVA) revealed that the reaction temperature and reaction pH were the most influential factors in maximizing the charge density and solubility of lignin copolymer, respectively.

4.2 Introduction

The gradual depletion of fossil resources and the environmental pollutions are getting even more serious throughout the world. Great attention has been paid to the development of sustainable technologies based on renewable raw materials (Fang et al., 2009; Kumar et al., 2009). Lignin is the most abundant aromatic sustainable polymer in nature after cellulose (Pouteau et al., 2003). Kraft lignin is produced via acidification of black liquor that is generated in the kraft pulping process (Lora and Glasser, 2002). The industrial applications of kraft lignin are limited due to its poor water solubility (Sun et al., 2001), whose improvement can widen its application in flocculent, dispersants, painting, oil, pulp and paper, as a biodegradable substitution for current petroleum based polymers (Fang et al., 2010; Kong et al., 2015).

Inorganic salts (Alum, $FeCl_3$) or synthetic acrylamide polymers (PAM) have been used extensively to treat industrial wastewater. However, many of the inorganic salts and synthetic polymers are considered carcinogenic (Miranda et al., 2013). In this context, kraft lignin is not

currently consumed effectively, and therefore, can be modified to produce cationic lignin copolymers for wastewater treatment.

A well-established and most effective technique to tailor new and desired properties of lignin is copolymerization. The copolymerization of lignin using various monomers, such as N,N-dimethyldiallyl ammonium chloride (DADMAC), N,N′-methylenebisacrylamide, methyl methacrylate, acrylamide, vinyl acetate or vinyl acetate via free radical polymerization were also studied (Agarwal et al., 2013; Lu et al., 2004; Ren et al., 2008; Feng et al., 2011; Dacunha et al., 1993; Panesar et al., 2013). Various reaction parameters such as the temperature, time, pH, etc., have been reported to influence the lignin copolymerization reaction, and hence the properties of the resultant copolymer. The increase in reaction time and temperature might increase polymer's charge density (Konduri et al., 2015). The pH of reaction mixture may also affect the solubility of the resultant copolymer (Kong et al., 2015). Therefore, it is highly necessary to optimize the copolymerization process to obtain a copolymer with high charge density and solubility. Therefore, the impacts of time, temperature, pH, and monomer concentrations on the copolymerization acrylamide and (2-methacryloyloxyethyl) trimethyl ammonium chloride (DMC) onto kraft lignin in an aqueous medium requires investigation and are the objectives of this study.

Taguchi orthogonal array design uses a special set of predefined arrays to study a maximal number of factors at selected levels with a minimal set of experiments (Rafizadeh et al., 2005). It allows for investigating the influence of individual factors involved in the study and finally calculating the performance at the optimum levels obtained (Taguchi, 1987; Montgomery, 2013). This methodology is applied in many areas such as environmental sciences, agricultural sciences, medicine, and biotechnology (Daneshvar et al., 2007; Du Plessis and de Villiers, 2007; Tasirin et al., 2007).

The main novelty of this work was the production of cationic kraft lignin via copolymerization. In this context, the influence of reaction parameters on the preparation of cationic lignin from softwood kraft lignin using acrylamide and DMC in aqueous solution were studied in order to obtain cationic kraft lignin with a high charge density and solubility. The characterization of the synthesized copolymer was examined by TGA.

4.3 Materials and Methods

4.3.1 Materials

Softwood kraft lignin (KL) was produced via LignoForce^{TM} technology of FPInnovations in Thunder Bay, ON (Kouisni et al., 2012). (2-methacryloyloxyethyl) trimethyl ammonium chloride (DMC) 80 wt. % in water, acrylamide (AM) with 99.0 % purity, potassium persulfate, $K_2S_2O_8$ (analytical grades), and trimethylsilyl propanoic acid were all obtained from Sigma-Aldrich company. Cellulose acetate dialysis membrane with the molecular weight cut off of 1,000 g/mol was obtained from Spectrum Labs. Inc., USA. Potassium polyvinyl sulfate (PVSK) was provided by Wako Pure Chem. Ltd. Japan, it and was diluted to 0.005 M prior to use. Ethanol (95 vol. %) was received from Fisher Scientific company. All chemicals were applied without further purification.

4.3.2 Copolymerization of lignin

First, 2 g of KL was dissolved in 40 mL of deionized water in a 250 mL three neck round bottom glass flask while stirring at 300 rpm. Predetermined quantities of AM and DMC were added to the flask and stirred at 300 rpm for 5 min. The reaction solution was continuously purged with nitrogen at room temperature for 30 min to remove any residual oxygen. Subsequently, potassium persulfate was added as an initiator to the system and the reaction solution purged for another 5 min. The copolymerization of KL, AM, and DMC was processed by placing the flask in a preheated water bath after adjusting the pH of the medium. The reaction was allowed to proceed for different time intervals under nitrogen. The copolymerization was repeated under varying reaction conditions including varying time (2, 3, 4 and 5 h), temperature (60, 70, 80 and 90 °C), pH (2, 3, 4 and 5), DMC concentration (0.009, 0.014, 0.019 and 0.024 moles), and AM concentration (0.014, 0.028, 0.042 and 0.056 moles). Upon reaction completion, the flask containing the reaction solutions was submerged in cold tap water for 20 min. The solution was then mixed with ethanol in order to separate the lignin based copolymers (KL-AM-DMC) from the rest of the reaction medium. Ethanol precipitation was carried out for separating AM and DMC monomers from chitosan-AM-DMC copolymer in the past (Wang et al., 2012; Ben et al., 2011). By adding ethanol to the reaction medium, the solution reactions became suspension. Then, the suspension was centrifuged at 3500 rpm for 10 min using a Sorvall ST 16 laboratory centrifuge (Thermo Fisher) in order to separate copolymers from the suspension. This

precipitation/centrifugation process was performed three times to remove KL-AM-DMC from the suspension. After centrifugation, the precipitated copolymers were mixed with 200 mL deionized water and the pH of the solution was adjusted to 7.0. The samples were dialyzed using the dialysis membrane for 48 h in order to remove other impurities (e.g., inorganic salts and monomers) from the copolymer solutions. The deionized water used for dialysis was changed every 12 h for 2 days. After dialysis, the solution containing the copolymer (KL-AM-DMC) was dried at 105 °C, and the dried samples were kept for further analysis. This copolymer is denoted as KAD, while unmodified kraft lignin is denoted as KL in this work.

4.3.3 Experimental design

To optimize the experimental conditions, Taguchi orthogonal test was designed to observe the impact of reaction parameters on the charge density and solubility of KAD copolymer. On the basis of Taguchi orthogonal design $L_{16}(4^5)$, a total of 16 runs were conducted to determine the optimum conditions for producing KAD with the maximum charge density and solubility. The experimental conditions conducted in the orthogonal design and responses are listed in Table 4.1. The factors and their levels were time of reaction (2, 3, 4 and 5 h), temperature of reaction (60, 70, 80 and 90 °C), DMC concentration (0.009, 0.014, 0.019 and 0.024 moles), AM concentration (0.014, 0.028, 0.042 and 0.056 moles), and pH (2, 3, 4 and 5). The experiments were repeated three times, and the average values were reported in this work.

Table 4.1. The Taguchi orthogonal parameters and levels (L^{16}) and the responses.

Run	Temp., °C	Time, h	AM, mol	DMC, mol	pH	Charge density, meq/g	Solubility, wt.%
1	80	5	0.028	0.009	4	0.5	8
2	90	3	0.042	0.009	5	0.12	42
3	80	2	0.042	0.024	3	1.43	59
4	70	3	0.014	0.024	4	1.37	56
5	90	5	0.014	0.019	3	1.15	50
6	90	4	0.028	0.024	2	1.05	45
7	60	5	0.056	0.024	5	-0.65	43
8	70	5	0.042	0.014	2	0	49
9	60	3	0.028	0.014	3	1.15	45
10	60	2	0.014	0.009	2	-1.41	60
11	70	2	0.028	0.019	5	-1.2	29
12	80	3	0.056	0.019	2	1.60	50
13	70	4	0.056	0.009	3	0.42	34
14	60	4	0.042	0.019	4	0.38	10
15	90	2	0.056	0.014	4	0.68	30
16	80	4	0.014	0.014	5	1.29	53
Optimum	80	3	0.014	0.024	3	2.13	56

4.3.4 Model fitting and statistical analysis

The experimental data were analyzed using the statistical software Design Expert version 8.0.7.1 (STAT-EASE Inc., Minneapolis, USA). An optimum condition of grafting percentage was performed based on three main steps, which were analysis of variance (ANOVA), a regression analysis, and plotting of experimental responses.

The model for producing the maximum charge density and solubility of kraft lignin-AM-DMC is presented in Eq. (4.1). The number of terms in the models depends on the main effects and their degree of freedom.

$$Y = b_0 + b_1A[1] + b_2A[2] + b_3A[3] + b_4B[1] + b_5B[2] + b_6B[3] + b_7C[1] + b_8C[2] + b_9C[3] + b_{10}D[1] + b_{11}D[2] + b_{12}D[3] + b_{13}E[1] + b_{14}E[2] + b_{15}E[3]. \ldots\ldots (4.1)$$

This model provides the best fitting to the experimental data points. In this equation, Y is the charge density or solubility of KAD, b_0 is the intercept, b_1 represents the model coefficients, while factor A, B, C, D, and E represent time, temperature, DMC concentration, AM concentration, and pH of the reactions, respectively. The analysis provides the best estimates for b_0 and b_1. The numbers in brackets represent first, second and third levels of each primary factor.

4.3.5 Solubility and charge density determination

To measure the solubility of the KAD, 0.2 g of the copolymer was added in 20 mL of deionized water by stirring at 100 rpm and 30 °C for 1 h in a water bath shaker (Innova 3100, Brunswick Scientific, Edison, NJ, USA). Then, the suspensions were centrifuged at 1000 rpm for 5 min. The supernatants were collected and used for analyzing the charge density and solubility of the copolymer. The concentration of copolymers in the supernatants was determined by drying the supernatants at 105 °C, and the solubility was determined based on the concentration of KAD in the supernatants and the initial concentration of KAD in solutions. The charge density of the copolymers was measured by a particle charge detector, Mütek PCD 04 titrator (Herrsching, Germany) with a PVSK solution (0.0050 M) (Wang et al., 2016). Three repeats were carried out, and the average values were reported**.**

4.3.6 Thermogravimetric analysis (TGA)

Thermogravimetric analysis was performed using a TGA (TGA i1000 Series System) to investigate the change in the thermal behavior of KL and KL-AM-DMC. The samples were dried in the oven at 105 °C overnight prior to testing. The analysis was carried out in nitrogen at a steady flow rate of 100 mL/min. Each sample (7.5 mg) was heated from room temperature to 800 °C at the rate of 5 °C/min.

4.4 Results and Discussion

4.4.1 Reaction mechanism

Figure 4.1 shows the reaction scheme of KL, AM, and DMC. In the reaction mixture, thermal decomposition of $K_2S_2O_8$ generates two sulfite radical anions by thermal decomposition. These

sulfite radicals lead to the propagation of the copolymer by attacking hydroxyl group (OH) of KL and double bonds of acrylamide and DMC to have them engaged in the copolymerization reaction (Figure 4.1a). On the other hand, the DMC and AM can participate in side reactions to produce homopolymers of PDMC and PAM (Figure 4.1b). Both copolymerization and homopolymerization are affected by the reaction conditions.

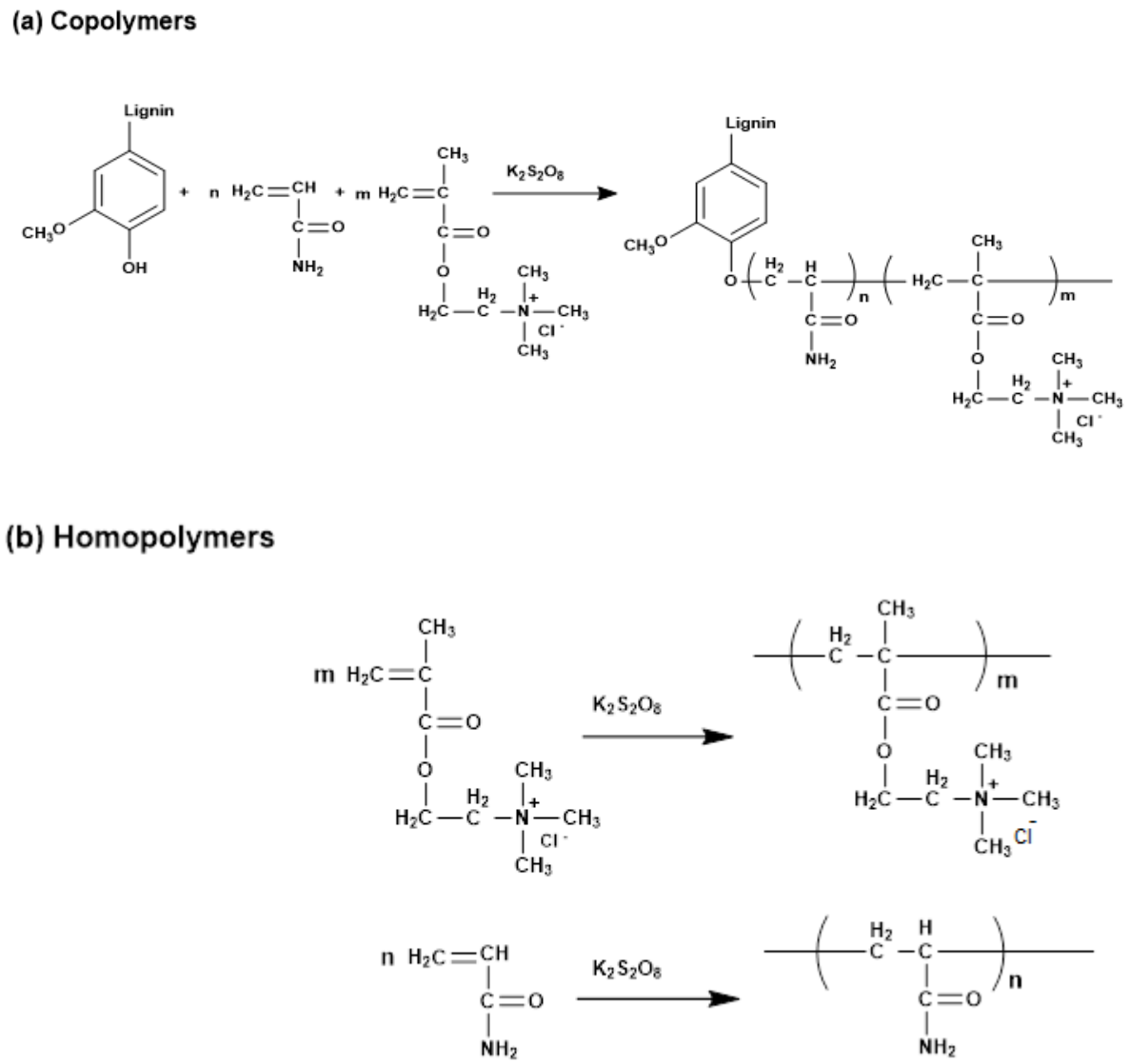

Figure 4.1. Mechanism of the copolymerization reaction (a) Copolymers of KL-AM-DMC (b) Homopolymers of PDMC and PAM

4.4.2 Thermogravimetric (TGA) analysis

Figure 4.2 shows the results of TGA analysis for KL and KL-AM-DMC polymers. KL decomposed continuously above 200 °C and was completely degraded around 600 °C. The weight loss at a temperature lower than 200 °C in Figure 4.2 is attributed to the evaporation of water (Yang et al., 2014). The weight loss rate of kraft lignin shows two peak at 288 °C and 322 °C, and the results showed that 60 wt. % of KL remained as ash. The weight loss peaks of KL-AM-DMC were at 237 °C, 334 °C, and 470 °C. Compared with degradation behavior of KL at 288 °C, KL-AM-DMC exhibited a lower degradation temperature (235 °C). On the other hand, the degradation peak of KL at 322 °C was found to be lower than that for KL-AM-DMC. These results showed that the grafting of the AM and DMC onto the KL backbone varied the thermal stability of KL-AM-DMC.

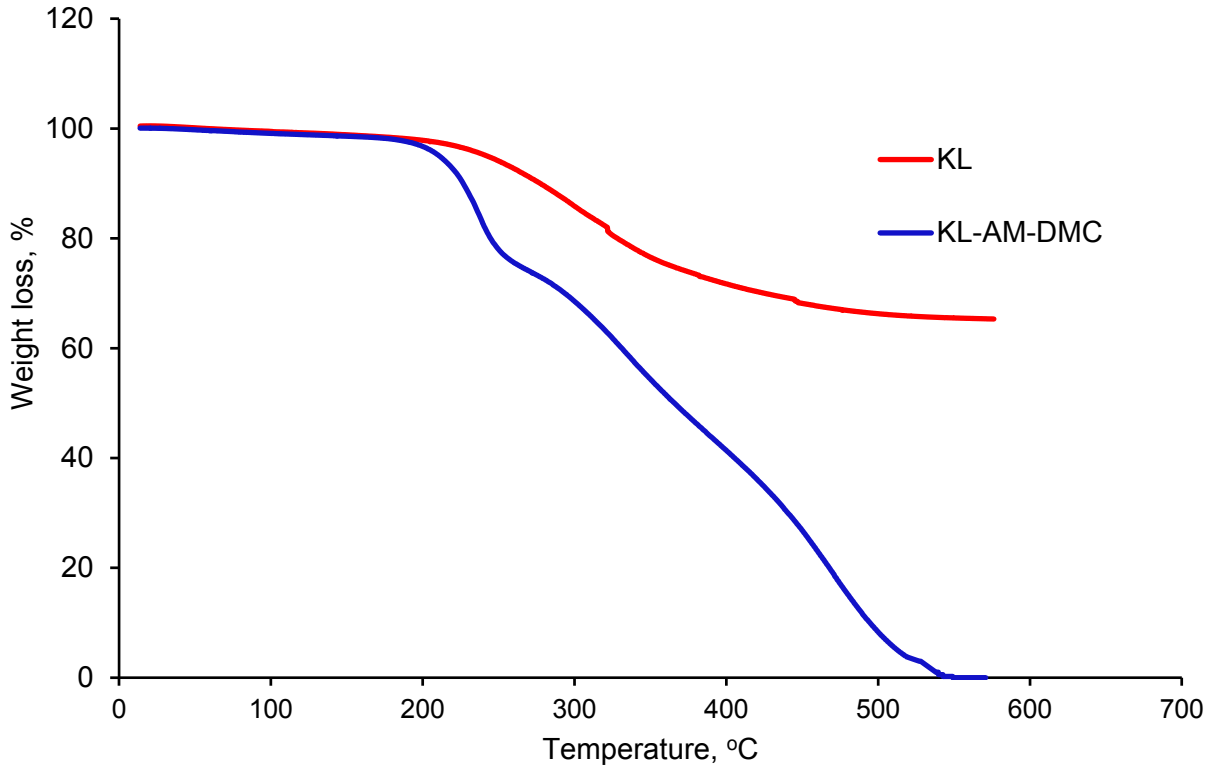

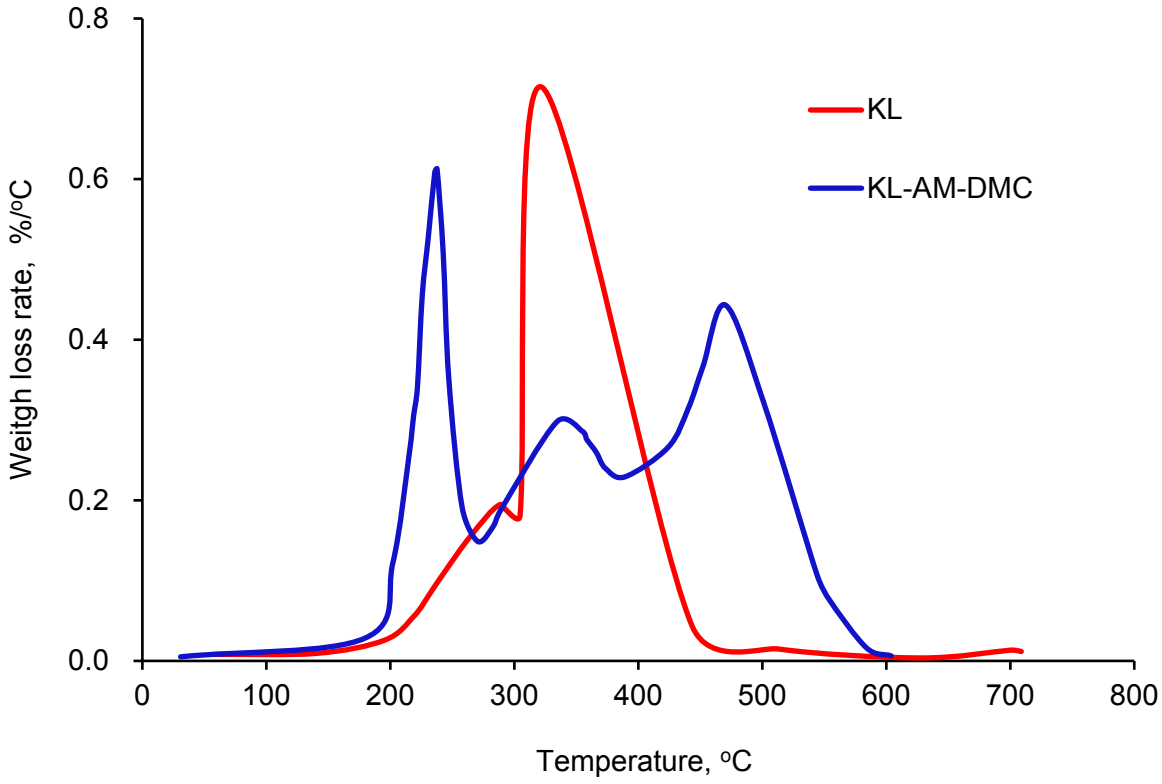

Figure 4.2. Weight loss and weight loss rate of KL, KL-AM-DMC copolymers.

4.4.3 Analysis of variance (ANOVA)

The ANOVA statistical analysis is carried out to inquire the statistical significance of the experimental factors impacting the responses (charge density and solubility). This was attained by comparing the mean square with the estimate of the experimental error at specific confidence levels (Cl). Table 4.2 shows the predicted data generated by the models, F-test, and the regression coefficients for the analysis (R^2). F-test was used to check which factor has a significant effect on the charge density and solubility of KAD copolymer (Bi et al., 2009). F-test represents the ratio of the mean square error to the residual error. When the F-value is high, the process parameters have pronounced effects on the charge and solubility of KAD copolymers.

The results confirmed that the level of significance of reaction conditions on the charge density decreases in the order of Temperature > Time > pH > DMC > AM. On the other hand, following the magnitude of F-value for solubility, the influence of reaction conditions on solubility decreases in the order of pH > AM > DMC > Time > Temperature. The optimal reaction conditions for KAD copolymer were as follows: 0.011 mol of KL, 0.014 mol of AM, 0.024 mol of DMC, pH 3, 3 h, and 80 °C. The maximum charge density (2.13meq/g) and solubility (56 wt. %) was achieved under the optimized synthetic conditions.

Table 4.2. ANOVA analysis for charge density and solubility of cationic lignin

Factor	**Sum of squares**		**Mean Square**		**F-Value**	
	Charge density, meq/g	Solubility, wt.%	Charge density, meq/g	Solubility, wt.%	Charge density, meq/g	Solubility, wt.%
Model	12.81	3536.75	1.07	294.73	30.95	54.62
Temperature, °C	4.33	16.19	1.44	5.40	41.90	0.018
Time, h	3.39	533.19	1.13	177.73	32.78	32.94
DMC, mol	2.08	642.69	0.69	214.23	20.09	39.70
pH	3.0	1450.19	1.0	483.40	29.04	89.59
AM, mol	0.10	910.69	0.034	303.56	0.032	56.26

Standard deviation		Coefficient of variation,%		R^2		Predicted R^2		Adjusted R^2	
Charge density, meq/g	Solubility, wt.%	Charge density, meq/g	Solubility, wt.%	Charge density, meq/g	Solubility, wt.%	Charge density, meq/g	Solubility, wt.%	Charge density, meq/g	Solubility, wt.%
0.19	2.32	37.7	5.67	0.9946	0.9954	0.7721	0.8704	0.9599	0.9772

The smaller values of standard deviation (SD) and coefficient of variation (CV) for the charge density (0.19 and 37.70 meq/g) and solubility (2.32 and 5.67 %) reveal that the experimental results obtained are reliable (Zhang et al., 2011). The reliability of results was further confirmed

by the regression coefficients (R^2) values for the charge density (0.994 meq/g) and solubility (0.995 %). Both predicted R^2 and adjusted R^2 determined how well the model fitted into the experimental data. The former assumes all the independent variables impacted the dependent variables, and the latter considers only the independent variables affected the dependent variable (Kosikova et al., 2000). The predicted R^2 values of the charge density and solubility were found to be in agreement with adjusted R^2 values. The regression analysis was employed to fit the experimental data (Table 4.1) into the first order polynomial equation Eq. (4.1) using Taguchi orthogonal model. The results obtained were shown in Table 4.3.

Table 4.3. Model coefficients estimated by regression analysis.

	Charge density, meq/g				**Solubility, wt.%**			
Term	Coefficient Estimate	Standard Error	95% Cl Low	95% Cl High	Coefficient Estimate	Standard Error	95% Cl Low	95% Cl High
Intercept	0.49	0.046	0.34	0.64	40.94	0.58	39.09	42.79
A[1]	-0.63	0.080	-0.88	-0.37	3.56	1.01	0.36	6.76
A[2]	-0.34	0.080	-0.60	-0.089	7.31	1.01	4.11	10.51
A[3]	0.71	0.080	0.46	0.97	-7.44	1.01	-10.64	-4.24
B[1]	-0.62	0.080	-0.87	-0.36	11.81	1.01	8.61	15.01
B[2]	0.57	0.080	0.31	0.82	-9.19	1.01	-12.30	-5.99
B[3]	0.29	0.080	0.037	0.55	-0.94	1.01	-4.14	2.26
D[1]	-0.59	0.080	-0.84	-0.33	-4.94	1.01	-8.14	-1.74
D[2]	0.29	0.080	0.032	0.54	1.31	1.01	-1.89	4.51
D[3]	-0.010	0.080	-0.27	0.25	-6.19	1.01	-9.39	-2.99
E[1]	-0.18	0.080	-0.44	0.073	10.06	1.01	6.86	13.26
E[2]	0.55	0.080	0.29	0.80	6.06	1.01	2.86	9.26

E[3]	0.24	0.080	0.016	0.50	-14.94	1.01	-18.14	-11.74

The small standard errors of regression indicated that the experimental data well fitted into the first order polynomial equation. The coefficient values predicted for the terms also found to be in the 95% confidence interval (CI) range. These results suggested that the models can be used to predict the charge density and solubility of lignin polymer. ANOVA analysis confirmed that the temperature and pH were the major factors for charge density and solubility responses, respectively. To confirm that the models can adequately predict the charge density and solubility of the resultant lignin copolymer, the predicted charge density and solubility results were plotted against the experimental results in Figure 4.3. As can be seen, the predicted results were in good agreement with the experimental data (Sasmal et al., 2011).

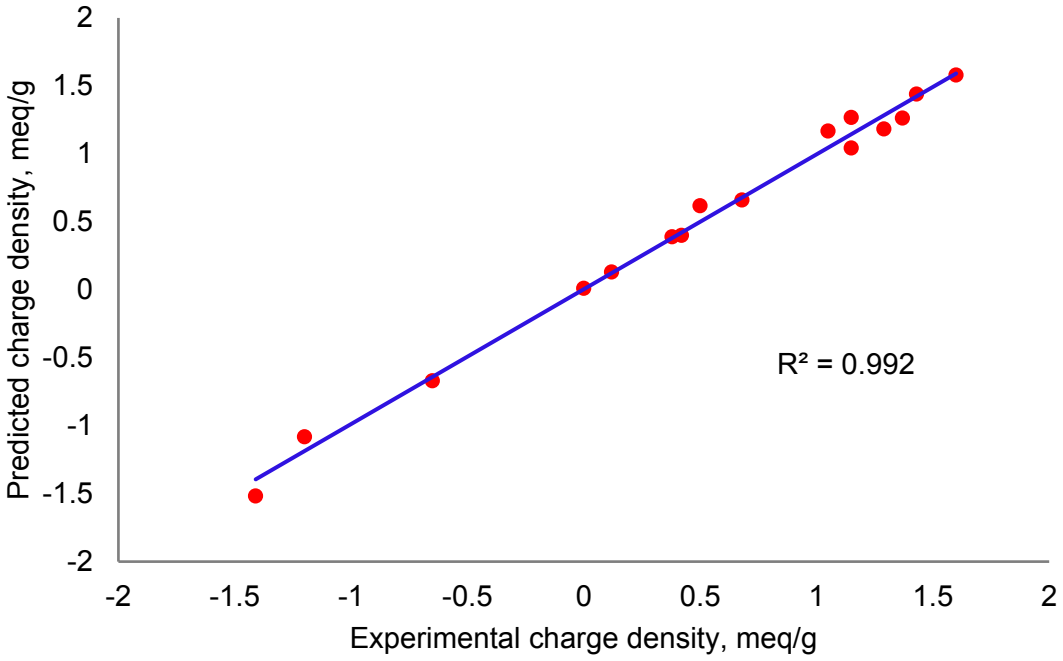

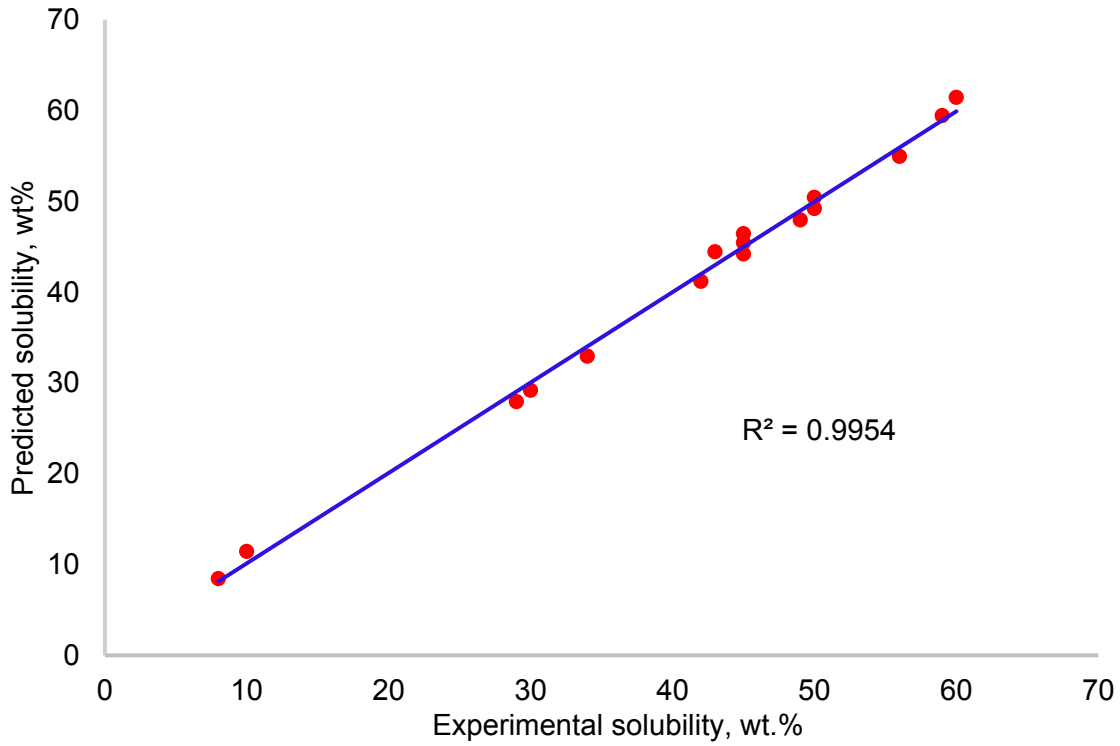

Figure 4.3. Relationship between the predicted values and experimental values for (a) charge density and (b) solubility based on Taguchi orthogonal design.

4.5 Conclusions

The copolymerization of AM and DMC with lignin was conducted to produce kraft lignin-AM-DMC polymer and its characterization has been done using TGA. The reaction conditions of kraft lignin-AM-DMC were optimized by Taguchi method. The optimal reaction conditions for KAD copolymer were as follows: 0.011 mol of KL, 0.014 mol of AM, 0.024 mol of DMC, pH 3, 3 h and 80 °C. The higher charge density (2.13meq/g) and solubility (56 wt. %) was obtained under the optimized synthetic conditions. The ANOVA was carried out to inquire the statistical significance of the process parameters impacting the response. It was found that the predicted charge density and solubility was in a very good agreement with the experimental data.

4.6 References

Agarwal, V., McLean, D., Horne, J., Richardson, D., Stack, K., 2013. Chemometric study of graft copolymerization of guar-g-(acrylamide-co-diallyl dimethylammonium chloride, Journal Applied Polymer Science 127, 3970-3979.

Ben, W., Yulian, Z., Chunbao, M., 2011. Preparation of Cationic Chitosan-Polyacrylamide Flocculant and Its Properties in Wastewater Treatment. Journal Ocean Univversity China (Oceanic and Coastal Sea Research) 10, 42-46.

Bi, Y., Liu, M., Wu, L., Cui, D. 2009. Optimization of preparation conditions of carboxymethyl potato starch through orthogonal experimental design, Journalof Applied Polymer Science. 113, 24–39.

Dacunha, C., Deffieux, A., Fontanille, M., 1993. Synthesis and polymerization of lignin-based macromonomers .3. Radical copolymerization of lignin-based macromonomers with methyl-methacrylate, J. Appl. Polym. Sci. 48, 819-831.

Daneshvar, N., Khataee, A.R., Rasoulifard, M.H., Pourhassan, M. 2007. Biodegradation of dye solution containing Malachite Green: Optimization of effective parameters using Taguchi method. J. Hazard. Mat., 143(1-2), 214-219.

Du Plessis, B.J., de Villiers, G.H. 2007. The application of the Taguchi method in the evaluation of mechanical flotation in waste activated sludge thickening. Resources, Conservation and Recycling 50(2), 202-210.

Fang, R., Cheng, S.U., Fu, J., Zheng, Z. B. 2009. Research on the Graft Copolymerization of EH-lignin with acrylamide, Nat. Sci., 1, 17-22.

Fang, R., Cheng, X., Xu, X. 2010. Synthesis of lignin-base cationic flocculant and its application in removing anionic azo-dyes from simulated wastewater. Bioresour. Technol. 101, 7323−9.

Feng, Q.H., Chen, F.G., Wu, H.R. 2011. Preparation and characterization of a temperature-sensitive lignin-based hydrogel. Bioresour., 6, 4942-4952.

Kong, F. Parhiala, K., Wang, S., Fatehi, P., 2015. Preparation of cationic softwood kraft lignin and its application in dye removal. Eur. Polym. J., 67, 335–345.

Kong, F., Wang, S., Price, J.T., Konduri, M., Fatehi, P. 2015. Synthesis and characteristics of water soluble lignin copolymer from Kraft lignin and acrylic acid. Green Chem., 17, 4355-4366

Konduri, M.K., Kong, F., Fatehi, P. 2015. Production of carboxymethylated lignin and its application as a dispersant. Eur. Polym. J., 70, 371–383

Kosikova, B., Duris, M., Demianova, V., 2000. Conversion of lignin biopolymerinto surface active derivatives. Eur. Polym. J., 36(6), 1209–1212.

Kumar, M.N.S., Mohanty, A.K., Erickson, L., Misra, M. 2009. Lignin and its applications with polymers, J. Biobased Mat., 3, 1-24.

Lora, J.H., Glasser, W.G. 2002. Recent industrial applications of lignin: A sustainable alternative to nonrenewable materials. J. Polym. Environ., 10, 39-48.

Lu, S.J., Lin, S.B., Yao, K.D., 2004. Study on the synthesis and application of starch-graft-poly(AM-co-DADMAC) by using a complex initiation system of CS-KPS. Starch-Starke, 56, 138-143.

Miranda, R., Nicu, R., Latour, I., Lupei, M., Bobu, E., Blanco, A. 2013. Efficiency of chitosans for the treatment of papermaking process water by dissolved air flotation. Chem. Eng. J., 231, 304-313.

Montgomery, D.C., 2013. Design and Analysis of Experiments, eighth ed. John Wiley & Sons Inc, Hoboken, NJ.

Panesar, S.S., Jacob, S., Misra, M., Mohanty, A.K. 2013. Functionalization of lignin: Fundamental studies on aqueous graft copolymerization with vinyl acetate. Industrial Crop. Production 46, 191-196.

Pouteau, C., Dole, P., Cathala, B., Averous, L., Boquillon, N. 2003. Antioxidant properties of lignin

in polypropylene. Polym. Degrad. Stab. 81, 9-18.

Rafizadeh, M., Morshedian, J., Ghasemi, I., Bolouri, A. 2005. Experimental relationship for impact strength of PC/ABS blend based on the Taguchi method. Iran Polym., 14, 881-889.

Ren, Y., Luo, Y., Zhang, K., Zhu, G., Tan, X. 2008. Lignin terpolymer for corrosion inhibition of mild steel in 10% hydrochloric acid medium. Corros. Sci., 50, 3147-3153.

Sasmal, S., Goud, V. V., Mohanty, K. 2011. Optimization of the acid catalyzed pretreatment of areca nut husk fibre using the Taguchi design method. Biosyst. Eng., 110, 465–472.

Sun, R., Tomkinson, F., Mao, F., Sun, X. 2001. Physicochemical characterization of lignin from rice straw by hydrogen peroxide treatment. J. Appl. Polym. Sci., 79(4), 719–732.

Taguchi, G., 1987. System of experimental design: engineering methods to optimize quality and minimize costs. UNIPUB/Kraus International Publications. American Supplier Institute, White Plains, N.Y. Dearborn, Mich.

Tasirin, S.M., Kamarudin, S.K., Ghani, J.A., Lee, K.F. 2007. Optimization of drying parameters of bird's eye chilli in a fluidized bed dryer. J. Food Eng., 80(2), 695-700.

Wang, J. P., Chen, Y.Z., Wang, Y., Yuan, S.J., Sheng, G.P., Yu., H. Q. 2012. A novel efficient cationic flocculant prepared through grafting two monomers onto chitosan induced by Gamma radiation. RSC Advances., 2, 494–500.

Yang, J., Hu, D., Xue, M., Yang, X. 2014. Synthesis of P (AM-co-MAA)/AEM composite microspheres with lichi-like surface structure using porous microgel as template. J. Colloid Interface Sci., 418, 350-359.

Zhang, G. L., Zhang, L., Deng, H., & Sun, P. 2011. Preparation and characterization of sodium carboxymethyl cellulose from cotton stalk using microwave heating. Chem. Technol. Biotechnol., 86(4), 584–589.

Chapter 5: The effect of KL-AM-DMC molecular weight on the flocculation of clay suspensions

5.1 Abstract

Currently, kraft lignin is burned in the recovery cycle of the kraft pulping process; whereas, it can be extracted and modified to produce value-added products. In this work, kraft lignin (KL) was copolymerized with acrylamide (AM) and 2-[(methacryloyloxy) ethyl] trimethylammonium chloride (DMC) to produce cationic flocculants. Copolymers with two different molecular weights of 168, 200 g/mol (KAD-1) and 103, 000 g/mol (KAD-2), but with a similar charge density of 1.15 meq/g, were selected and their flocculation efficiency in two different clay suspensions was investigated. The adsorption and turbidity removal of clay suspension in the presence of the copolymer were found to be dependent on the pH of the suspension. At 8 mg/g dosage, KAD-1 adsorbed more than KAD-2 as it was larger and thus developing more bridging with clay particles. The size of kaolin particles increased from 4.7 to 16.3 and 15.1 μm, and that of bentonite particles increased from 6.1 to 18.97 and 15.35 μm via having 8 mg/g of KAD-1 and KAD-2 copolymers in the clay suspensions, respectively. The adsorption, zeta potential, and flocculation analyses confirmed that KAD-1 was a more effective flocculant. The effect of shear rate on KAD polymers revealed polymer bridging and electrostatic patch flocculation mechanisms.

5.2 Introduction

Today, the effluents produced in industrial processes contain a wide range of toxic materials; metals and other undesirable compounds, which are considered as main sources of environmental pollutions. Hence, the removal of these hazardous materials from the effluents has become a serious challenge for industry. In the past, a number of technologies were employed to remove the colloidal particles from wastewater including membrane filtration, adsorption, coagulation, biological, and electrolytic processes. Nevertheless, flocculation is an effective alternative for the removal of suspended and dissolved solids, colloids and organic matters present in industrial wastewater (Lee et al., 2014).

In the past few years, there has been increased interests in modifying biomaterials including starch, chitosan, cellulose and other natural materials to develop environmentally friendly flocculants for removing contaminants found in wastewater effluents (Sirvio et al., 2011; Ben et al., 2011; Wang et al., 2010). Cationic polymers are effective flocculants to treat the negatively charged particles present in effluents. Previous studies demonstrated that acrylamide (AM) and 2-[(methacryloyloxy) ethyl] trimethylammonium chloride (DMC) are two comonomers for rendering polysaccharides flocculants for treating wastewater (Abdollahi et al., 2011). In the past, the copolymer of chitosan-AM-DMC at a dosage of 1 mg/L was reported to reduce the turbidity of a clay suspension by 90 % (Wang et al., 2012), while the same copolymer at the dosage of 8 mg/L reported to reduce the turbidity of wastewater effluent by 95 % (Ben et al., 2011). In a similar work, starch-AM-DMC copolymer was used to concentrate a drilling mud suspension with the water content decrease from 35 % to 21.34 % when polymer at 0.3 wt. % dosage was used (Zou et al., 2011). In another study, 23 mg/L of starch-AM-DMC reduced the turbidity of a pulp mill effluent by 95.7 % (Wang et al., 2011).

Today, the consumption of starch and chitosan based food has been increased due to the population growth. In addition, cellulose is used as a platform material for producing other value-added materials, chemicals, and biofuels. As these materials, e.g., starch, chitosan and cellulose are heavily used for other purposes worldwide, their usage in producing new chemicals may not be an excellent option in future. Interestingly, other under-utilized chemicals such as lignin can be used for this purpose. Lignin is a natural polymer that currently has a very limited industrial use and is available in a large quantity (Pouteauet al., 2010; Zakzeski et al., 2010). However, it can be modified to produce environmentally friendly flocculants to treat paper, mining, textile, and wastewater systems. In one report, lignin-AM copolymer removed 52 % of turbidity from aluminum sulfate or poly aluminum chloride suspensions (Rong et al., 2013). In another investigation, the copolymer of hydrolysis lignin and AM removed 85 % of azo-dyes from dye wastewater when the dosage of the copolymer was 200 mg/L (Fang et al., 2009). However, lignin-AM copolymer is uncharged and thus may not be very effective for wastewater treatment. Previously, lignin was catatonically modified by introducing quaternary ammonium group to produce asphalt emulsifiers, cationic surfactants, and strength additives for composites (Meister, 2002; Silva et al., 2009; Zhang et al., 2013; Du et al., 2014). However, the production of lignin-AM-DMC as a flocculant for treating kaolin and bentonite suspensions has not been

reported. Therefore, the first objective of this work was to study the flocculation behavior of lignin-AM-DMC in these suspensions.

It is well-known that the properties of polymers impact their adsorption performance on surfaces (Tekin et al., 2006; Razali et al., 2011). In one study, an increase in the cationic charge of cationic polyacrylamide from 10 to 50 mol % increased the turbidity removal of a clay suspension by 90 % (Chen, 1998). The adsorbed polymers may neutralize and bridge the particles, and thus facilitate their settlement. However, unadsorbed polymers would also affect the chemistry of the suspension systems, which may affect the attraction/repulsion force developed between particles and thus their settlement. However, it is unclear if the adsorbed or unadsorbed polymers would impact the flocculation performance of a polymer. The effect of molecular weights and charge densities on the flocculation performance have been investigated previously (Zhu et al., 2009; Gill and Herrington, 1987). In one study, the flocculation performance of polydiallyldimethylammonium chloride (PDADMAC) in pulping effluents was reported to improve by 92 % when its molecular weight increased from 8.5×10^4 to 15.7×10^4 g/mol (Razali et al., 2011). In another study, when the molecular weight of cationic polyacrylamide increased from low to high, the flocculation performance of particles in the effluent of a pulp and paper mill was improved from 63 % to 95 % (Wong et al., 2006). Lignin-based copolymers are different from synthetic polymers, however, the impact of the properties of lignin based copolymers on their flocculation performance was not studied earlier. The second objective of the present study was to investigate the flocculation efficiencies of cationic lignin-AM-DMC polymers with different molecular weights in a clay suspension.

In our previous chapter, the production of kraft lignin-AM-DMC was investigated (Hasan and Fatehi, 2018). In this study, kraft lignin-AM-DMC copolymers with the same charge densities but two different molecular weights were produced, and their flocculation behavior was investigated in kaolin and bentonite suspensions for the first time.

5.3 Materials and Methods

5.3.1 Materials

Softwood kraft lignin was produced via LignoForce^{TM} technology of FPInnovations in Thunder Bay, ON (Kouisni et al., 2012). 2-[(methacryloyloxy) ethyl] trimethylammonium chloride

(DMC) (80 % in water), acrylamide (99.0 %), potassium persulfate ($K_2S_2O_8$) (analytical grades), kaolin and bentonite were obtained from Sigma-Aldrich company. Cellulose acetate dialysis membrane (molecular weight cut off of 1,000 g/mol) was supplied by Spectrum Labs. Inc., USA. Polydiallyldimethylammonium chloride (PDADMAC) was obtained from Sigma Aldrich Company and diluted to 0.005 M prior to use. Potassium polyvinyl sulfate (PVSK) was provided by Wako Pure Chem. Ltd. Japan. All the chemicals were applied without further purification. Moreover, Ethanol (95 vol. %) was received from Fisher Scientific company.

5.3.2 Lignin-AM-DMC production and purification

Kraft lignin-AM-DMC copolymers were synthesized in 250 mL three-neck glass flasks under the reaction conditions listed in Table 5.1. After the reactions, the flasks were submerged in cold tap water for 20 min. Then, ethanol (95 vol. %) was mixed with the reaction media in order to precipitate the lignin-based copolymers from the system. Previously, ethanol precipitation was carried out for separating chitosan-AM-DMC copolymer from homopolymers (PAM, PDMC) and monomers (AM, DMC) in reaction media (Ben et al., 2011; Wang et al., 2012; He et al., 2007). By adding ethanol to the reaction media, the solution reactions became suspensions. The suspensions were then centrifuged at 3500 rpm for 10 min using a Sorvall ST 16 laboratory centrifuge (Thermo Fisher) in order to separate copolymers from the suspensions. This precipitation/centrifugation process was repeated three times so that purified lignin-AM-DMC was obtained. After centrifugation, the precipitated copolymers were mixed with 200 mL of deionized water and the pH of the solution was adjusted to 7. The samples were dialyzed using the dialysis membrane for 48 h in order to remove other impurities (e.g. inorganic salts and monomers) from the copolymer solutions. The deionized water used for dialysis was changed every 12 h for 2 days. After dialysis, the solution containing the copolymer was dried at 105 °C, and the dried samples were kept for flocculation studies. This copolymer is denoted as KAD, while unmodified kraft lignin is denoted as KL in this work.

5.3.3 Solubility and charge density determination

To measure the solubility of lignin-AM-DMC copolymers, 0.2 g of the copolymers was added to 20 mL of deionized water by stirring at 100 rpm and 30 °C for 1 h in a water bath shaker (Innova 3100, Brunswick Scientific, Edison, NJ, USA). Then, the suspensions were centrifuged at 1000 rpm for 5 min. The supernatants were collected and used for analyzing the charge density and

solubility of the copolymer. The concentration of the copolymers in the supernatants was determined by drying the supernatants at 105 °C, and the solubility was determined based on the concentration of lignin in the supernatants and the initial concentration of lignin. The charge density of the copolymers was measured by a particle charge detector, Mütek PCD 04 titrator (Herrsching, Germany) with a PVSK solution (0.0050 M) following equation 5.1 [26]:

$$\text{Charge density}\left(\frac{\text{meq}}{\text{g}}\right) = \frac{\text{Volume of PVSK (mL)} \times \text{concentration of PVSK}\left(\frac{\text{mol}}{\text{L}}\right)}{\text{Mass of lignin (g)}} \qquad (5.1)$$

Three repeats were carried out, and the average values were reported**.** The surface charge density analysis of bentonite and kaolin clay particles was determined via a back titration method using a particle charge detector (Mütek PCD-04, Germany). Approximately, 0.2 g of clay was suspended in 50 mL of PDADMAC (0.005M) solution and the suspensions were incubated at 30 °C for 2 h at 150 rpm. After the incubation, the samples were filtered using Whatman#1 filter membranes and the filtrates were titrated against the PVSK (0.0055 M) solution. Similarly, the titration analysis was conducted for the control sample (i.e. the PDADMAC solution with no clay addition), and the difference was considered for quantifying the surface charge density of the clay particles.

5.3.4 Molecular weight analysis

About 5 mg sample of dried KAD copolymers was dissolved in 10 mL of 5.0 wt. % acetic acid solution by stirring at 600 rpm for 48 h and 35 °C, then the solutions were filtered with a 13 mm diameter nylon filter (pore size 0.2 μm). The filtered solutions were used for the molecular weight analysis, which was carried out using Malvern, GPCmax VE2001 Module + Viscotek system with viscometer and RI detectors. In this analysis, PolyAnalytic columns were used, and a 5.0 wt. % acetic acid was used as a solvent and eluent with the flow rate of 0.7 mL/min. The column temperature was set to 35 °C. Poly ethylene oxide was used as standard polymers for calibration of this system.

5.3.5 Elemental analysis

The elemental analysis of the samples was performed for KL and KAD copolymers using an elemental analyzer, Elementar Vario EL Cube, by the combustion method (Jahan et al., 2012). The samples were first dried in an oven at 105 °C overnight to remove any moisture prior to analysis. Approximately, 2 mg of dried samples were transferred into the carousel chamber of the elemental analyzer and combusted at 1200 °C to reduce the generated gasses to analyze carbon, hydrogen, oxygen, and nitrogen contents of the samples.

5.3.6 Surface area analysis of clay particles

The surface area of bentonite and kaolin particles was determined by using Quantachrome surface area analyzer, a Nova2200e instrument. In this experiment, the samples were initially dried in an oven at 105 °C overnight, and approximately 0.05 g of sample was pretreated for 4 h at 250 °C prior to analysis. The specific surface area of the samples was then analyzed according to Brunauer-Emmett-Teller (BET) method via adsorption-desorption isotherms using nitrogen gas at -180 °C within relative pressure range of 0.01 to 0.99 (Oveissi and Fatehi, 2014).

5.3.7 Particle size distribution analysis

The size distribution of bentonite and kaolin particles was analyzed using a MasterSizer 2000 particle size analyzer (Malvern Instruments), which was equipped with a light scattering detector. In this study, 1.0 g of clay suspension (20 g/L) was added to 50 mL of deionized water or 50 mL of KL or KAD solution containing the copolymers with the dosage of 8 mg/g (based on clay) and stirred at 300 rpm and room temperature for 2 h. After stirring, the samples were analyzed for their particle size distribution.

5.3.8 Adsorption studies

In this set of experiments, different amounts (0.5 to 64 mg/g based on clay) of KL or KAD were added to 50 mL of clay suspensions (0.4 g/L) in order to study the adsorption of KL or KAD on clay particles. The suspensions were stirred at 300 rpm for 2 h at room temperature. Afterward, the suspensions were centrifuged for 15 min at 3500 rpm and then the concentrations of KAD remaining in the supernatants were determined by UV/Vis spectrophotometer (Genesys 10S UV–vis, Thermo FisherScientific, USA) at a wavelength of 205 nm. The impact of pH on the adsorption of KAD on clay particles was also studied. The pH of the suspensions (ranging 2 to

12) was adjusted with 0.1 M NaOH solution or H_2SO_4. Three repeats were carried out, and the average values were reported in the study.

5.3.9 Impact of KL or KAD on clay removal

In this set of experiments, different amounts of KL or KAD were mixed with 50 mL of clay suspensions (0.4 g/L) at 30 °C for 2 h. After mixing, clay suspensions were allowed to settle for 1 h. A 10 mL sample was collected from the upper half of the suspension before and after the settlement period and dried in an oven at 105 °C overnight. The concentration of clay particles in the samples was determined, which helped measure the removal of clay from the suspensions by developing a mass balance. This analysis was repeated at different copolymer dosages (0.5-64 mg/g based on clay) and pHs (2-12). The pH of the clay suspension was adjusted by using 0.1 M NaOH. Three repeats were carried out, and the mean values were reported in the study.

5.3.10 Zeta potential analysis

The zeta potential of the clay suspensions was characterized by using a compact automatic zeta potential analyzer (Laval labs Inc). In this study, 1 g of clay suspension (20 g/L) was added to 50 mL of deionized water and stirred at 300 rpm for 2 h and room temperature, and its zeta potential was then measured in a 1.0 mM KCL aqueous solution. The pH of the clay suspensions was adjusted by using 0.1 M NaOH or H_2SO_4. All the measurements were carried out at room temperature with a constant electric field (8.4 V/cm). Three repeats were carried out for the zeta potential measurement and the mean value was reported.

5.3.11 Flocculation analysis

The efficiency of the flocculation was determined using a photometric dispersion analyzer (PDA 3000, Rank Brothers Ltd) connected to a dynamic drainage jar (DDJ) fitted with a 70 mm mesh screen (Fatehi et al., 2013). The flocculation performance of the clay suspension was measured from the variation in the direct current (DC) voltage of the PDA instrument. In this study, 500 mL of distilled water was first added into the DDJ container and circulated from the DDJ to the PDA through a 3 mm plastic tube until a steady flow rate of 20 mL/min was achieved. The flow rate was regulated by a peristaltic pump throughout the experiment. Then, 10 mL of a 20 g/L clay suspension was added into DDJ (to make a 0.4 g/L clay concentration in DDJ) while stirring at 300 rpm. This caused a decrease in the initial base DC voltage (V_0) to a

new DC voltage (V_i) in PDA analysis. After 100 s, optimal dosage amount of 8 mg/g (based on clay) of KL or KAD was maintained in the DDJ. The increase in DC voltage was represented as the DC voltage (V_f) of the final suspension. The effects of copolymer dosage and pH of the clay suspensions on the flocculation were studied. The pH of the clay suspensions adjusted by using 0.1 M NaOH or H_2SO_4. The relative turbidity of the clay suspensions was measured using equation 5.2 (Wang et al., 2009).

$$\text{Relative turbidity, } \tau_r = \frac{\tau_f}{\tau_i} = \frac{ln(\frac{V_0}{V_f})}{ln(\frac{V_0}{V_i})} \qquad (5.2)$$

where τ_f is denoted as the final suspension turbidity, and τ_i is denoted as the initial suspension turbidity.

To study the strength of the clay flocs after copolymer addition, 10 mL of a 20 g/L clay suspension was added into DDJ (to make a 0.4 g/L clay concentration in the DDJ) while stirring at 300 rpm. After 100 s, KL or KAD was added to the DDJ. After 500 s and forming flocs, the shear rate was increased from 300 to 3000 rpm and maintained for another 100 s, during which the flocs would break. Subsequently, the shear rate was decreased to 300 rpm and maintained for another 500 s which might help the reflocculation of the broken small flocs. This process was repeated twice to study the flocculation behavior of the clay suspensions in the presence of KAD. The degree of breakage and reflocculation was represented by flocculation index (FI), which is the ratio of the mean square root (RMS) of the voltage that flocculation occurs to the direct (DC) voltage of the PDA instrument. The flocculation index was used as an indication of flocculation and breakage of clay particles in the suspensions in the past (Wang et al., 2012; Yu et al., 2013; Ramphal and Sibiya, 2014). All the experiments were performed in triplicates, and the mean values were reported in the study.

5.4 Results and Discussion

5.4.1 Properties of KAD

Figure 5.1 shows the reaction scheme of KL, AM and DMC. In this copolymerization reaction, $K_2S_2O_8$ is used as an initiator for the free radical copolymerization. The details of reaction mechanisms of KL, AM and DMC were discussed in the previous chapter (Hasan and Fatehi, 2018), where the AM and DMC would attach to the phenolic hydroxide group.

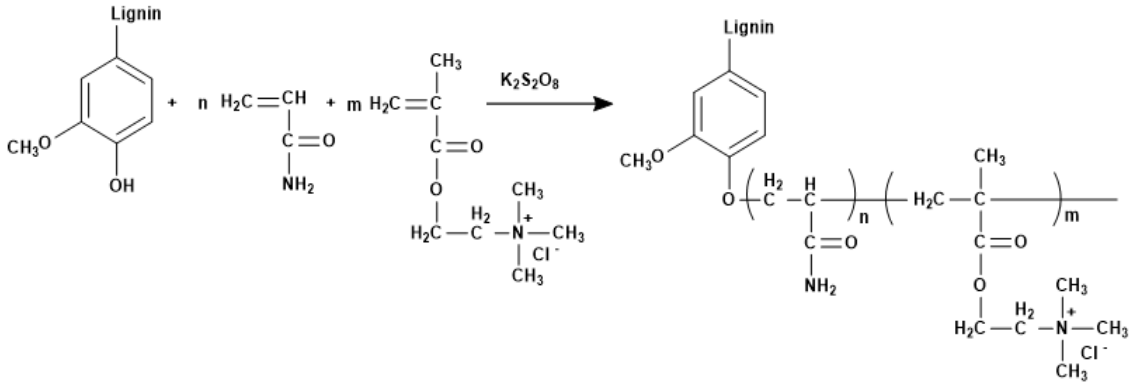

Figure 5.1. The copolymerization reaction of KL, DMC and AM for KAD production.

The properties of KAD are listed in Table 5.1. The reaction conditions were controlled so that two copolymers with a similar charge density but different molecular weights, were produced (Table 5.1). The increase in the nitrogen content confirmed the grafting of AM and DMC onto lignin backbone, which ultimately increased the molecular weight of KADs (compared to unmodified KL) (Wang et al., 2013). KAD-1 had more nitrogen and higher molecular weight than KAD-2, confirming that the copolymerization was more extensively conducted for KAD-1 than KAD-2. The similar charge densities of the two copolymers confirmed that both had very similar DMC content, as DMC was the only components that contributed to a cationic charge density of the copolymers.

Table 5.1. Reaction conditions and properties of KADs

Conditions	**KL**	**KAD-1**	**KAD-2**
Temperature, °C	-	60	90
Time, h	-	3	5
KL, mol	-	0.011	0.011
AM, mol	-	0.028	0.014
DMC, mol	-	0.014	0.019
pH	-	3	3
Charge density, meq/g	- 0.2	1.15	1.15
Solubility, wt.%	5	45	50
M_w, g/mol	17, 890	168,200	103,000

M_n, g/mol	5,150	117,400	82,000
M_w/M_n	3.473	1.432	1.256
Nitrogen, wt.%	0.03	5.12	4.49

5.4.2 Characterization of bentonite and kaolin clay

Table 5.2 presents the properties of kaolin and bentonite particles. The surface charge density of bentonite was more negative, which might be related to the montmorillonite layer structure of bentonite due to a greater percentage of oxide anions on the bentonite surface (Schmidt and Lagaly, 1999). Although, bentonite particles were larger, they had a smaller surface area and pore volume compared to kaolin particles.

Table 5.2. Properties of clays

Sample	Surface Charge, µeq/g	Particle Size, µm	BET Surface Area, m^2/g	Total Pore Volume, cm^3/g
Kaolin	-5.5	4.7	55.64	0.027
Bentonite	-9.4	6.1	20.12	0.012

5.4.3 Adsorption of polymers

The influence of KAD adsorption on clay particles as a function of copolymer dosage and pH is shown in Figure 5.2. As seen (Figure 5.2a), the KAD-1 and KAD-2 reached the saturation adsorption levels of 1.4 and 1.25 mg/g on kaolin and 1.08 and 0.99 mg/g on bentonite, respectively. KAD would interact with kaolin and bentonite particles through electrostatic charge interaction and thus adsorb on particles (Chen 1998; Solberg and Wagberg, 2003; Chen et al., 2007). The results also showed that KAD-1 adsorbed more than KAD-2 on particles. Although KADs had a similar charge density, KAD-1 had a higher molecular weight, which resulted in higher adsorption as compared to KAD-2 (Chen, 1998; Tian and Xie, 2008). The higher molecular weight of KAD-1 may indicate that KAD-1 had a longer chains and therefore higher chance for tail and loop configuration on particles upon adsorption, which would in turn promote polymer bridging. For effective bridging, the length of polymer chains should be sufficiently long that allows for extending from one particle surface to another (Pala et al., 2011). Previously,

it was reported that increasing molecular weight (1.4 x10^4 to 2.49 x 10^6 g/mol) would enhance the adsorption of cationic guar gum on bentonite surface (Levy et al., 1995). In addition, the slightly lower adsorption of KADs on bentonite may be due to its smaller surface area and larger particle size (Wang et al., 2016). Meanwhile, KL had marginal adsorption on kaolin and bentonite particles. Figure 5.2b shows that under strong acidic conditions (e.g. pH 2) the adsorption was limited; but it was enhanced at neutral or basic pHs, and the increase was more pronounced for KAD-1 than KAD-2. In one study, an increase in pH from 5.5 to 10 increased the adsorption of cationic polyacrylamide on clay from 15 to 75 mg/g at 25 °C temperature (Tekin et al., 2005).

Based on the results obtained from the adsorption analysis (Figure 5.2a) and considering the charge density of KADs, it was possible to theoretically calculate the change in the surface charge density of kaolin and bentonite particles after KAD adsorption. Figure 5. 2c shows the impact of the adsorbed KL and KAD on the theoretical surface charge density of kaolin and bentonite particles. This figure revealed that the overall surface charge density of kaolin and bentonite particles did not reach neutralization even after reaching the saturation level of adsorption. These findings indicated that KAD partly covered the surface of the clay particles; whereas, unadsorbed KAD was still available in the suspensions for adsorption. Therefore, the adsorption layer of KAD onto the clay particles was not evenly distributed, and theoretically, a part of particles contained anionic charges after saturation adsorption.

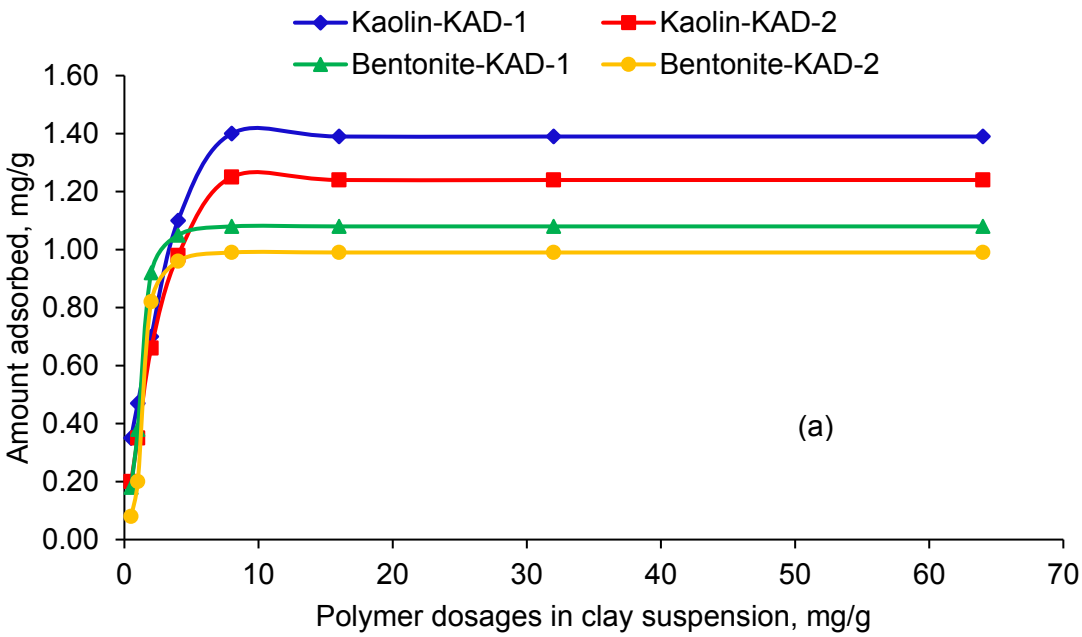
Kaolin-KAD-1
Kaolin-KAD-2
Bentonite-KAD-1
Bentonite-KAD-2
Amount adsorbed, mg/g
1.60
1.40
1.20
1.00
0.80
0.60
0.40
0.20
0.00
0
10
20
30
40
50
60
70
Polymer dosages in clay suspension, mg/g
(a)

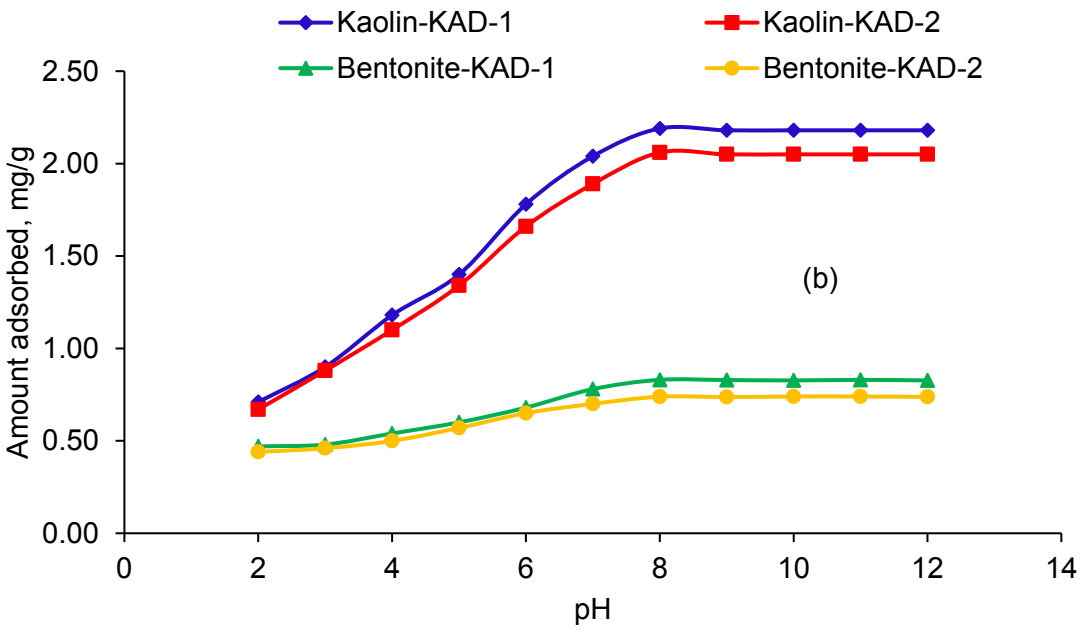
Kaolin-KAD-1
Kaolin-KAD-2
Bentonite-KAD-1
Bentonite-KAD-2
Amount adsorbed, mg/g
2.50
2.00
1.50
1.00
0.50
0.00
0
2
4
6
8
10
12
14
pH
(b)

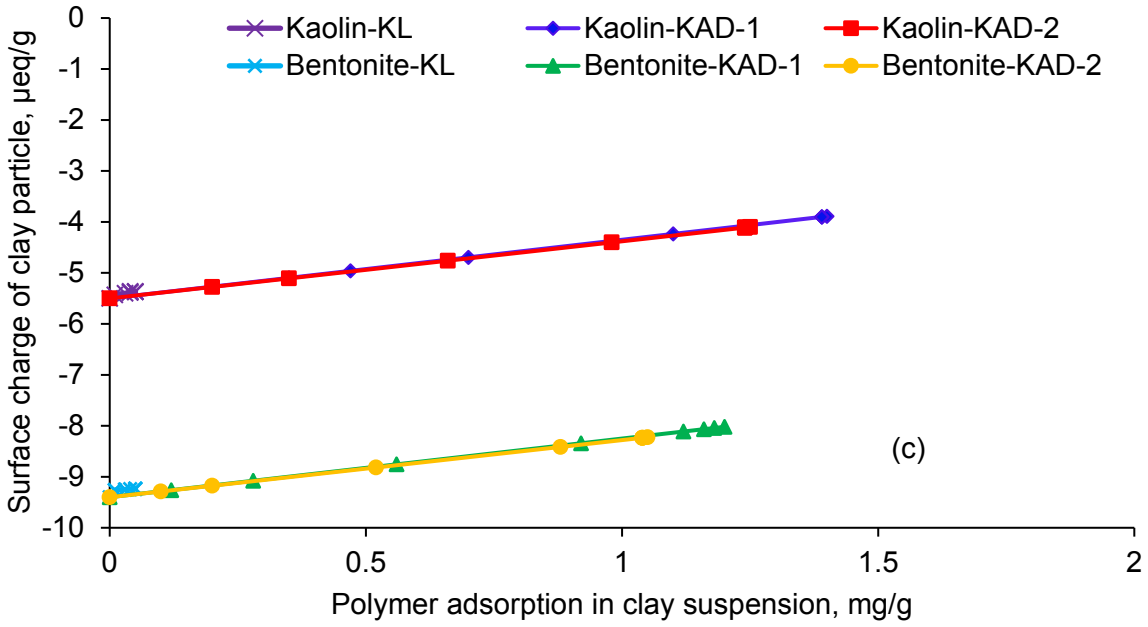

Figure 5.2. a) Adsorption of KL and KAD on kaolin and bentonite as a function of copolymer dosage, b) adsorption of KL and KAD on kaolin and bentonite particles as a function of pH c) theoretical surface charge density of kaolin and bentonite clay particles as a function of adsorbed KAD conducted under the conditions of pH 7, 25 °C, 2 h and 0.4 g/L clay concentration.

5.4.4 Particle size distribution

Figure 5.3 presents the particle size distribution of kaolin and bentonite particles at optimal dosage in the presence and absence of KL or KAD. The size of untreated kaolin and bentonite clay particles were originally 4.7 and 6.1 µm, respectively. Both KAD-1 and KAD-2 increased the size of kaolin particles from 4.7 to 16.3 and 15.1 µm, respectively. Furthermore, the size of the bentonite particles was increased to 18.97 and 15.53 µm in the presence of KAD-1 and KAD-2, respectively. In the past, the size of clay particles increased from 0.1 to 100 µm via treating with 0.8 mg/L of PDADMAC (with the molecular weight of 1.2×10^6 g/mol) in a clay suspension (Yu et al., 2006). In another study, the addition of 4 mg/g of polyacrylamide (with the molecular weight of 1.3×10^6 g/mol) increased the size of the clay particles from 9 to 28 µm at the clay concentration of 20 g/L and pH 5.8 (Zhou and Franks, 2006).

The larger increase in the size of the clay particles treated with KAD-1 could be attributed to the adsorption and bridging of particles with this larger polymer in the suspension. As studied previously, with the increase in the molecular weight of polymers, their adsorption on the clay particle increased, which facilitated the bridging mechanism (Zhu et al., 2009). The small peaks in the size range of 100-500 µm in Figure 5.3 may be indicative of flocs of coagulated particles (Ghimici et al., 2010).

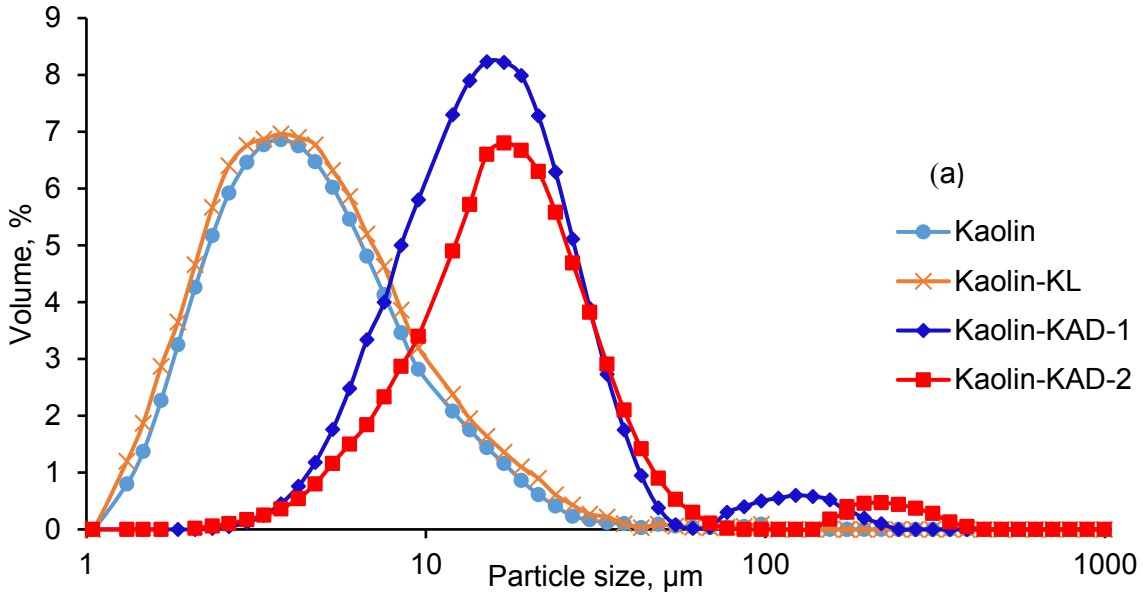

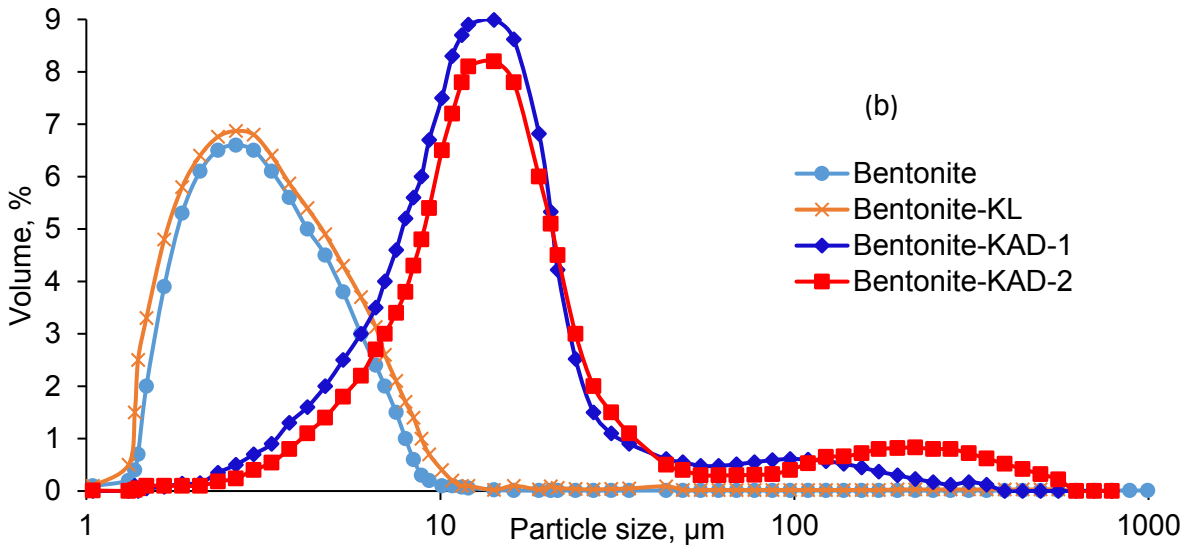

Figure 5.3. Particle size distribution of a) kaolin and b) bentonite particles in the presence and absence of KL or KAD conducted under the conditions of pH 7, 2 h, 8 mg/g of copolymer dosage, 25 °C and 0.4 g/L of clay concentration.

5.4.5 Influence of dosage on zeta potential

Figure 5.4 shows the effect of dosage of KAD on the zeta potential of kaolin and bentonite suspensions. The zeta potential of the suspensions was negative, but it increased substantially with an increase in cationic KAD dosage, which is due to the adsorption of KAD on the particles. As reported previously, the zeta potential of clay suspension was increased from -37.5 to +42.1 mV when the dosage of PDADMAC was increased from 0.16 to 3.2 mg/g in the clay suspension (Petzold et al., 2003). In another report, the zeta potential of a bentonite suspension was increased from -30.0 to +30.5 mV at 0.25 mg/g of polyethyleneimine dosage (Alemdar et al., 2005). Although KADs had similar charge densities, the higher adsorption of KAD-1 led to more positive zeta potential for both kaolin and bentonite suspensions. Untreated KL was not able to significantly affect the zeta potential of the clay suspension due to its insignificant adsorption capacity (not shown).

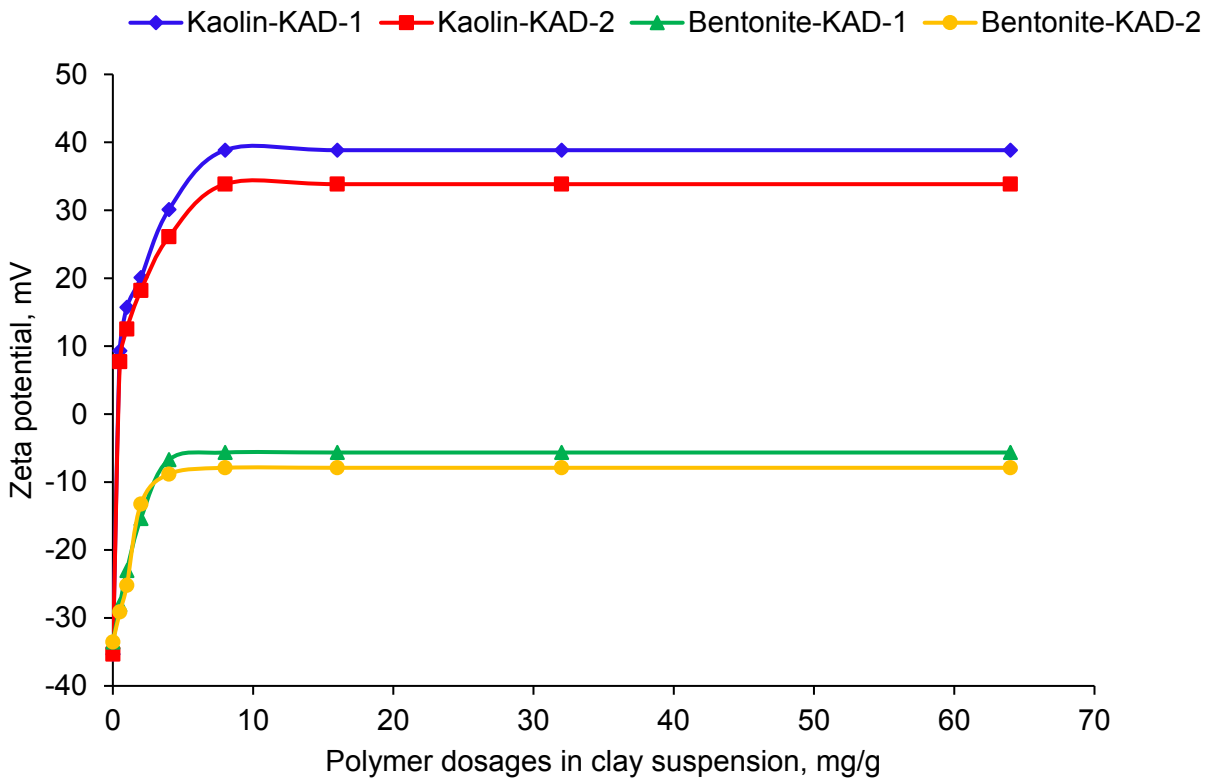

Figure 5.4. Zeta potential of kaolin and bentonite particles in the presence of KAD as a function of copolymer dosage conducted under the conditions of pH 7, 2 h, 25 °C, and 0.4 g/L of clay concentration.

Figure 5.5 shows the zeta potential of the suspensions as a function of theoretical charge density of clay particles. The zeta potential of untreated kaolin particles was -35 mV, when its surface charge density was -5.5 μeq/g. Interestingly, the surface charge density and zeta potential of particles for both KADs had a similar trend, regardless of the clay type. The zeta potential of kaolin particles became positive, but that of bentonite remained negative, via increasing the surface charge density of the particles (i.e., via adsorbing more KADs).

The adsorption of KAD led to neutralization and reversal of some of the charged sites on the surface of the particles. As the negative theoretical surface charge density of particles implies that not all anionic charges were neutralized or reached by KADs, the overall theoretical surface charge density of the particles remained negative. In other words, the interaction of charges on the clay particles and KAD was not one to one. The positive zeta potential of kaolin suspension suggested that the diffuse double layer of kaolin was overall positive after adsorption even when

there were still some sites on kaolin with no KAD adsorption. However, negative zeta potential of bentonite particles showed that the adsorption of KAD did not reverse the potential of diffuse double layer for bentonite particles.

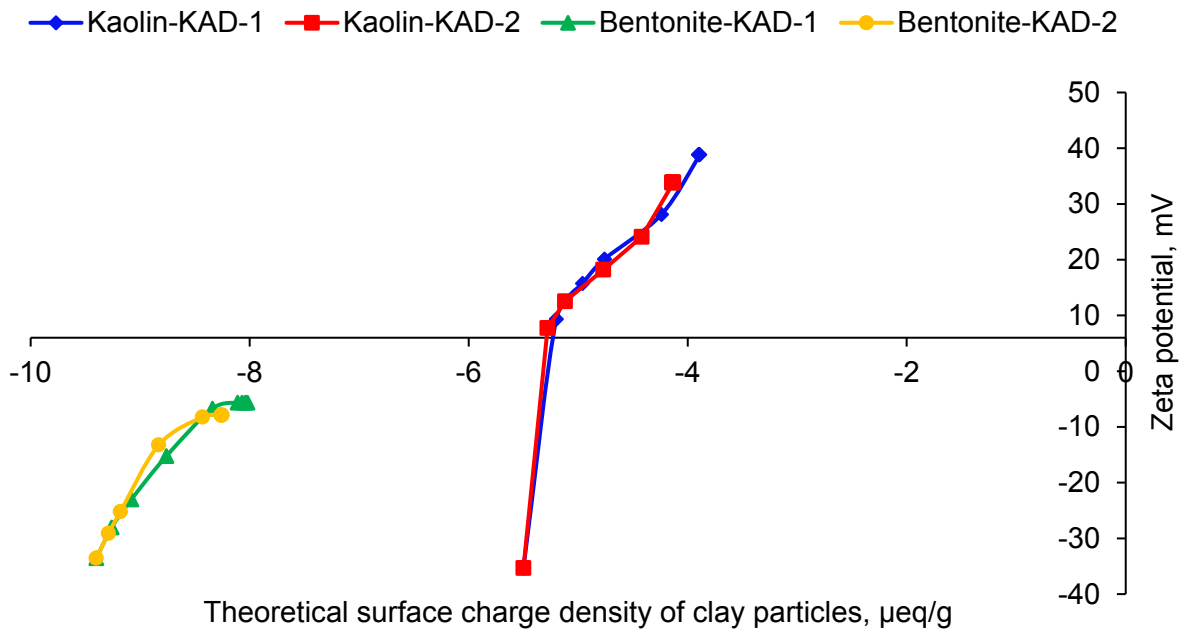

Figure 5.5. Zeta potential of kaolin and bentonite suspensions as a function of the theoretical surface charge density of particles, under the conditions of pH 7, 2 h, 25 °C and 0.4 g/L of clay concentration.

5.4.6 Influence of KAD on relative turbidity

The influence of KAD on relative turbidity and removal of kaolin and bentonite particles from the suspensions were presented in Figure 5.6. The relative turbidity of the clay suspensions decreased by increasing the concentration of KAD in suspensions. As can be seen, the minimum turbidity values for KAD-1 (0.62) and KAD-2 (0.68) were achieved at the dosage of 8 mg/g. These results were in agreement with the maximum adsorption of KADs on kaolin particles. By increasing the dosage to 8 mg/g in kaolin suspension, KAD-1 and KAD-2 caused 76.2 and 68.4 wt. % removals, respectively. Similarly, the minimum relative turbidity values for KAD-1 (0.41) and KAD-2 (0.47) for bentonite suspension was obtained at the concentration of 8 mg/g. The removal of bentonite particles for KAD-1 and KAD-2 were found to be 86.7 and 76.8 wt. %,

respectively, at 8 mg/g of dosage. A higher dosage of KAD-1 and KAD-2 did not affect the relative turbidity and removals of the suspensions' particles.

The higher efficiency of KAD-1 than KAD-2 in relative turbidity reduction and removal of clay particles was due to its higher adsorption (Figure 5.2a) and molecular weight (Pala et al., 2011; Chen, 1998; Wan et al., 2007). It was reported that the molecular weight of polymers had a critical role in bridging particles, and thus minimizing the turbidity of colloidal suspensions (Wong et al., 2006; Hocking et al., 1999; Divakaran and Pillai, 2001). In one research work, the flocculation performance of cationic guar gum polymers in a bentonite suspension was improved by reducing its turbidity from 50 to 5 NTU at a dosage of 5 ppm when molecular weight of the polymers increased from $1.4x10^4$ to $2.49x10^6$ g/mol (Levy, 1995).

The higher removal of bentonite particles was ascribed to the larger size of bentonite particles, which were easier to be removed than kaolin particles. In one study, with changes in the cationic xylan-2- (methacryloyloxy) ethyl] trimethylammonium chloride (DMC) dosages, from 0.25 to 8 mg/L and to 0.41 mg/L, the relative turbidity of the bentonite and kaolin suspension was decreased from 0.98 to 0.07 and 0.41, respectively (Besra et al., 2002). In another study, with an increase in the cationic pullulan dosage from 2 to 8 mg/L, the removal of clay was increased from 10 to 90 % (Wang, 2016). Unmodified lignin (KL) neither affected the relative turbidity, nor removed the particles from suspensions, which was due to the limited adsorption of KL on particles (not shown). The impact of pH on the relative turbidity (Figure 5.6c) and the removal of clay (Figure 5.6d) from the suspensions were also studied. The relative turbidity of kaolin and bentonite suspensions was decreased as pH increased. As these results indicated, with the increase in pH from 2 to 8, the relative turbidity of kaolin and bentonite suspensions was reduced to 0.48 and 0.28 via removing 80 and 88.5 wt. % of clay particles in the presence of KAD-1 polymer, respectively.

Furthermore, the results in Figure 5.6 revealed that, with the increase in the pH of the suspension, the overall negative charges of the clay suspensions increased, which resulted in more adsorption of KAD-1 via electrostatic interactions on clay particles (Figure 5.2b), and caused the relative turbidity to decrease (Chen, 1998).

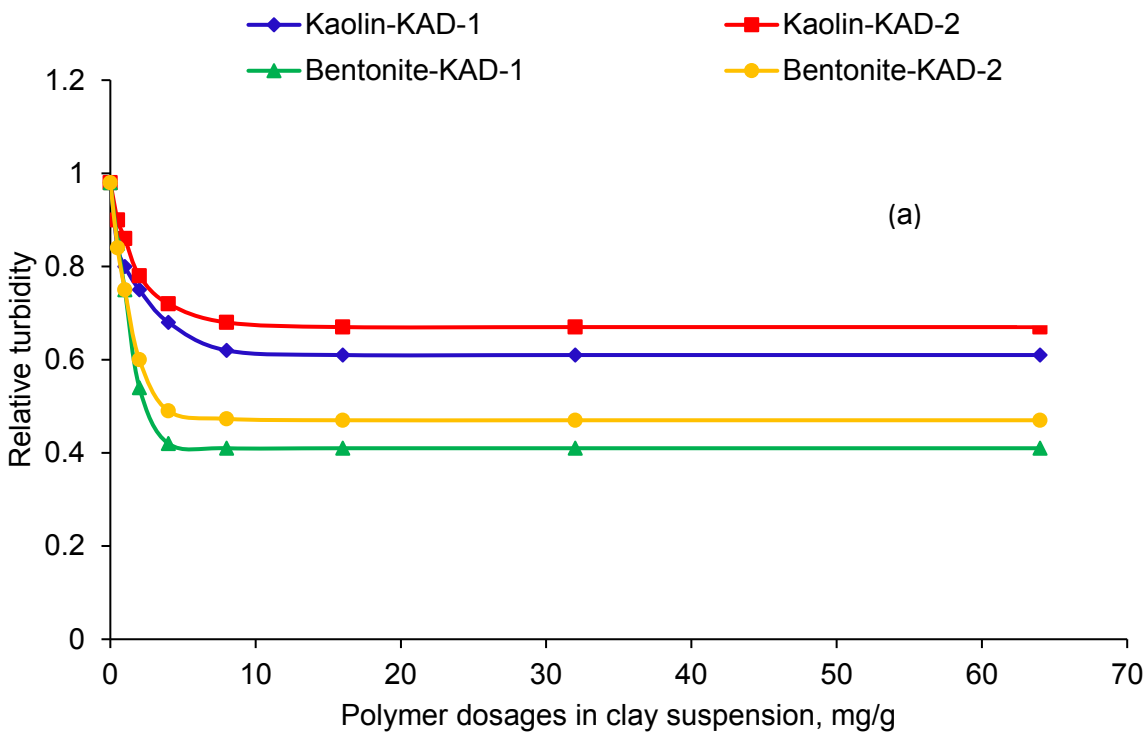
Kaolin-KAD-1
Kaolin-KAD-2
Bentonite-KAD-1
Bentonite-KAD-2
(a)
Relative turbidity
1.2
1
0.8
0.6
0.4
0.2
0
0
10
20
30
40
50
60
70
Polymer dosages in clay suspension, mg/g

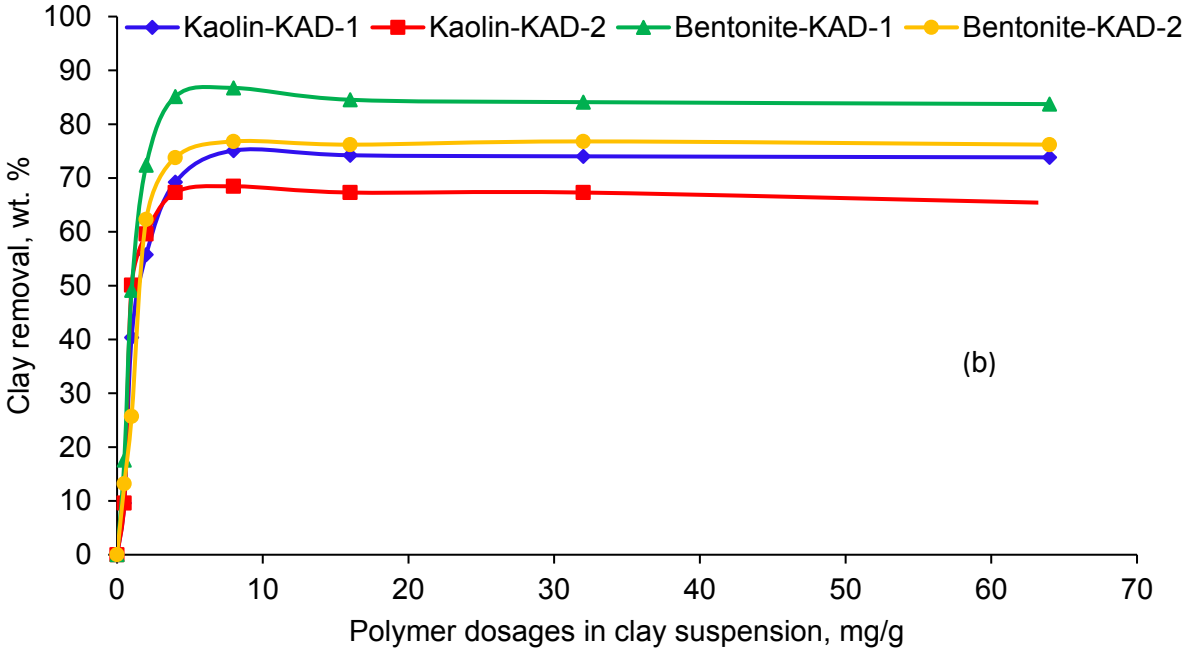
Kaolin-KAD-1
Kaolin-KAD-2
Bentonite-KAD-1
Bentonite-KAD-2
(b)
Clay removal, wt. %
100
90
80
70
60
50
40
30
20
10
0
0
10
20
30
40
50
60
70
Polymer dosages in clay suspension, mg/g

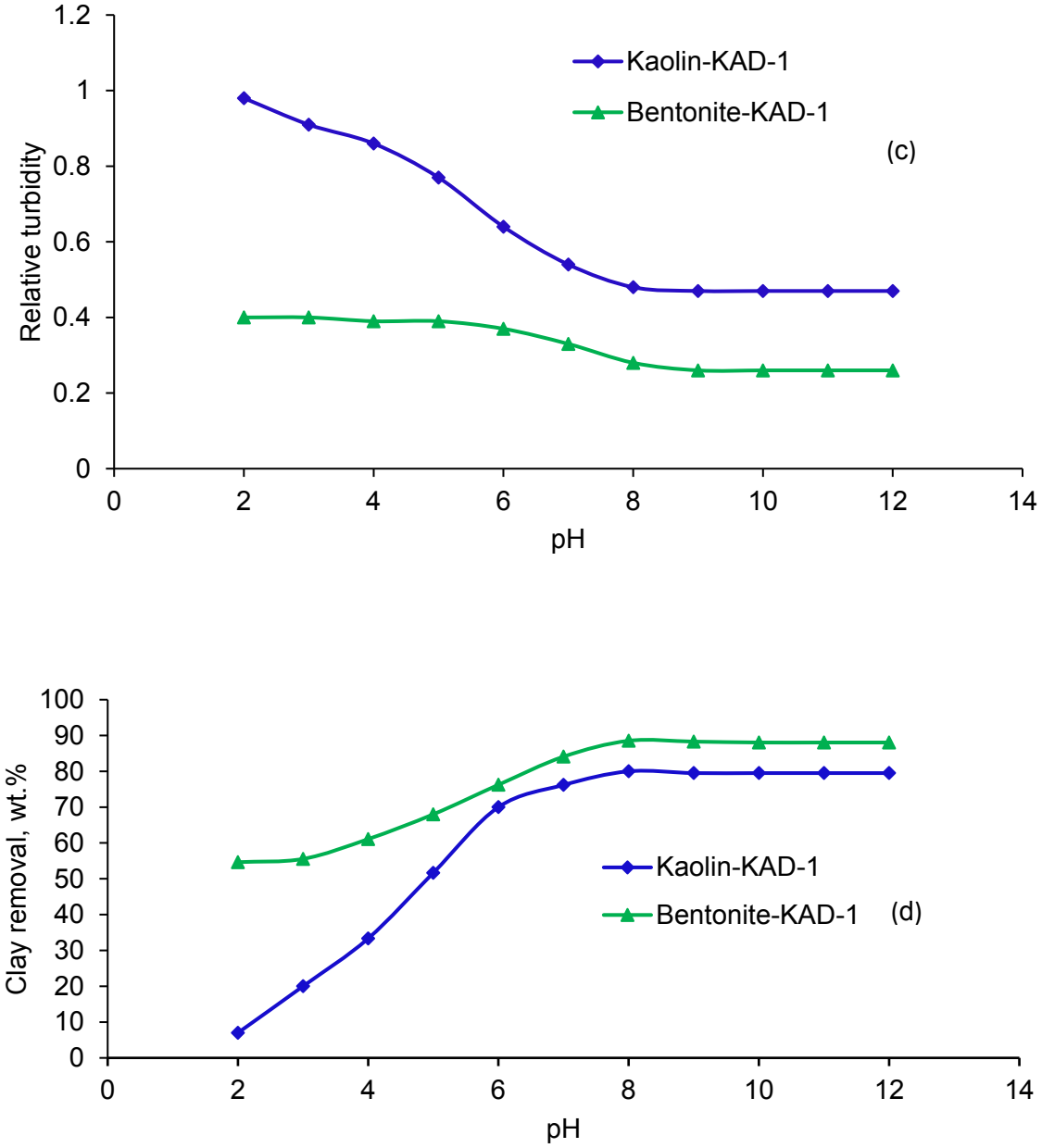

Figures 5.6. Influence of KAD dosage on the relative turbidity of a) kaolin and bentonite b) the removal of kaolin and bentonite particles from suspensions c) influence of pH on the relative turbidity of kaolin and bentonite suspension and d) removal of kaolin and bentonite from the suspensions in the presence of KAD, conducted under the conditions of 300 rpm, 2 h, 25 °C, and 0.4 g/L of clay concentration.

Figure 5.7 demonstrates the effect of adsorbed KAD amount on the relative turbidity of kaolin and bentonite suspensions. By increasing the adsorption of KAD on particles, the relative turbidity of suspensions dropped more significantly. Compared with KAD-2, a reduction in relative turbidity was slightly higher for KAD-1; this may be attributed to the higher molecular weight of KAD-1 that facilitated the bridging and flocculation of the particles in the suspension. Furthermore, KAD-1 adsorbed slightly more than KAD-2 (Figure 5.2a), and thus a lower relative turbidity was obtained for KAD-1 than KAD-2 for both kaolin and bentonite particles (Figure 5.6a). Also, the relative turbidity of bentonite suspension was lower than that of kaolin suspension, which indirectly implied a higher efficiency of KADs in bentonite suspension and this was ascribed to the larger size of bentonite particles than kaolin as explained earlier (Table 5.2).

Point "S" on Figure 5.7a shows the saturation level of KAD adsorption on particles. These points showed that, by adding more KADs to the suspensions, more unadsorbed KADs would remain after reaching the saturated level of adsorption. The results in Figure 5.7a for point "S" shows that the relative turbidity of the suspensions was not affected when more unadsorbed KADs were available in the suspensions, which was indeed affected only by the adsorbed KADs.

Based on the results obtained from the adsorption analysis (Figure 5.2a), and the charge density of KADs, it was possible to calculate the total charges introduced on the surface of kaolin and bentonite particles after KAD adsorption. Figure 5.7b depicts the impact of charges introduced to the particles via adsorbing KAD on the relative turbidity of the suspensions. It was seen that KADs showed a similar trend, regardless of KAD type. However, as KAD-1 introduced more charges to the particles, the relative turbidity was reduced more significantly. In addition, the introduction of charges to bentonite particles was more effective than to kaolin in terms of reducing its relative turbidity. As stated earlier, the larger size of bentonite particles was the reason for its more readily flocculation and thus relative turbidity reduction.

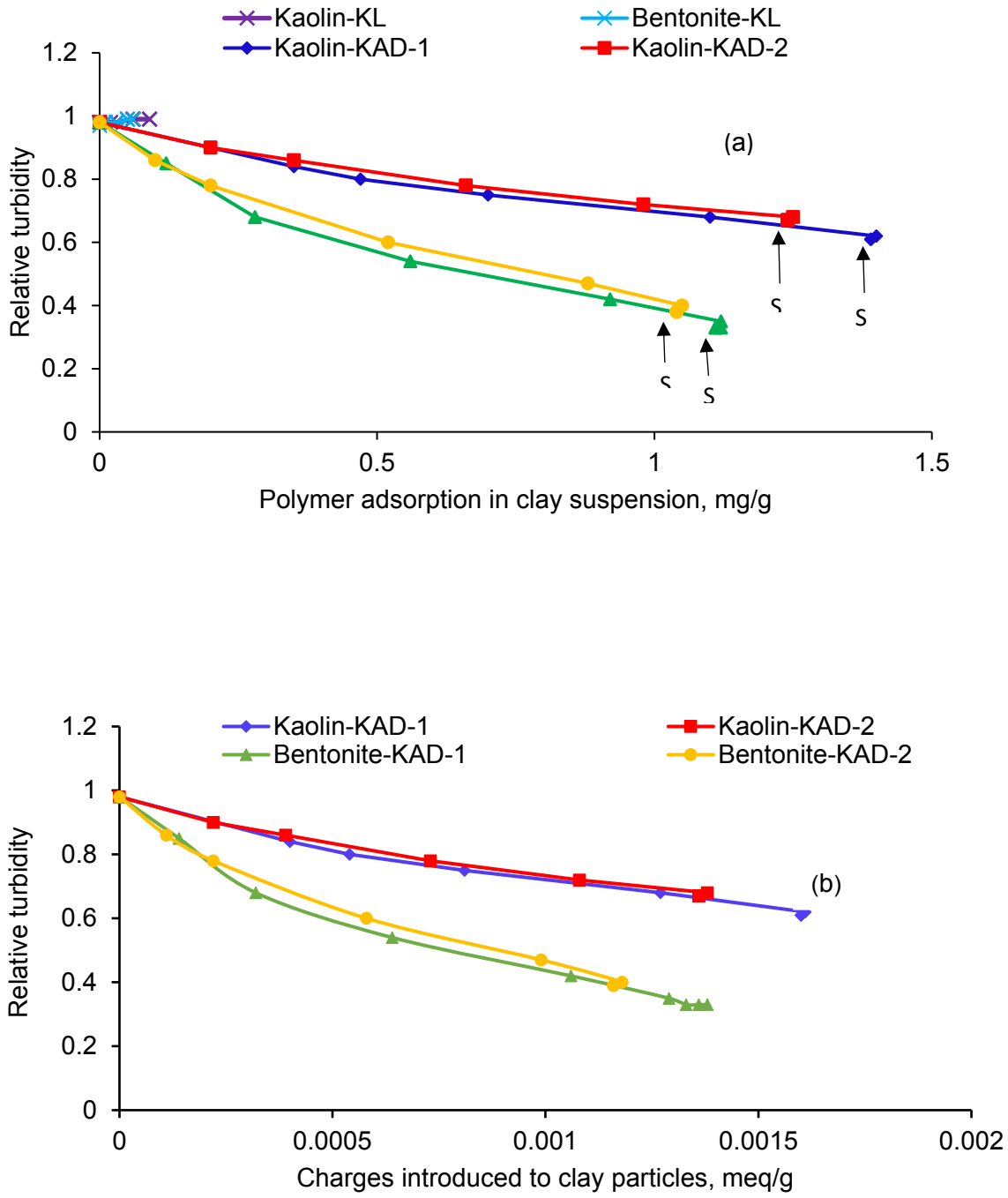

Figure 5.7. a) Effect of KAD dosage on the relative turbidity of kaolin and bentonite suspensions, b) effect of total charges introduced to particles on the relative turbidity of kaolin and bentonite suspensions, under the conditions of pH 7, 2 h, 25 °C and 0.4 g/L of clay concentrations.

To determine the flocculation mechanism of KAD in kaolin and bentonite suspensions, the relative turbidity of kaolin and bentonite suspensions was plotted as a function of zeta potential in Figure 5.8. In the case of kaolin suspension, the relative turbidity of the suspension gradually decreased when the zeta potential increased to positive values. In the case of bentonite suspension, the relative turbidity of the suspension dropped significantly when the zeta potential was still negative. Furthermore, slightly better results were obtained for KAD-1 than KAD-2. From these results, it is implied that 1) neutralization was a minor factor in flocculating kaolin particles as flocculation occurred more significantly at a higher positive zeta potential; 2) charge neutralization was a major factor in flocculating bentonite particles as flocculation was significantly improved via neutralizing the bentonite suspension.

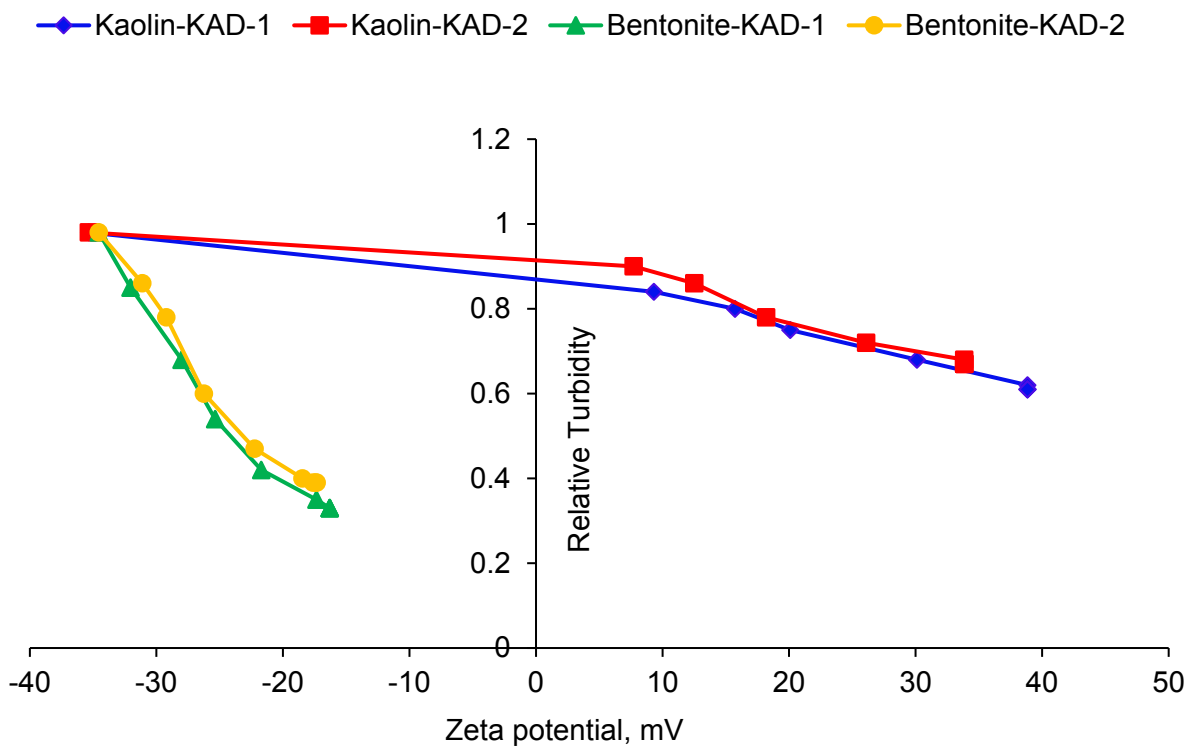

Figure 5. 8. Effect of zeta potential of kaolin and bentonite suspensions on the relative turbidity of clay suspensions conducted under the conditions of pH 7, 2 h, 25 °C and 0.4 g/L of clay concentration.

5.4.7 Influence of KAD on floc strength and recoverability

Figure 5.9 presents the formation, breakage, and reformation of flocs generated in kaolin and bentonite suspensions as a function of time in the presence of KAD. To investigate the impact of shear rate on the floc formation and breakage, different shear rates were applied to the formed flocs. The results of floc formation and breakage depicted that the flocculation index (FI) values of kaolin suspension reached plateau at 300 rpm in the presence of KAD, indicating a steady-state floc formation and representing a dynamic balance between floc growth and breakage (Liimatainen et al., 2009). When KAD was added, it neutralized and/or bridged the particles. Generally, the FI of the suspensions was reduced in the process of reducing and enhancing the shear rates. When the shear rate increased to 3000 rpm and maintained for 100 s, there was a rapid reduction in FI as a result of floc breakage. By increasing the shear rate, the particles could be disintegrated. The high shear rate would break the bridges between the particles; consequently, a part of the partly detached KADs from neighboring particles would reconfigure on one particle and KADs would lose their overall bridging affinity. The flocculation of particle would occur through charge neutralization and patch mechanism when reflocculated at a low shear rate, as the KADs can no longer perform bridging. In other words, the shear rate changes would impact the bridging performance of KAD and may introduce a patch mechanism for reflocculation (Yukselena and Gregory, 2004).

It is apparent in Figure 5.9a that the reflocculation of flocs was significant, but new plateaus were achieved when the shear rate was reduced for both KAD-1 and KAD-2. The results showed that the strength of flocs and the FI values for the re-grown flocs were larger for KAD-1 than KAD-2, which could be due to the higher molecular weight and thus ability of KAD-1 in bridging kaolin particles (Yu et al., 2011). Compared with kaolin suspension, bentonite suspension had a lower FI, indicating slower flocculation and weaker flocs. In addition, the FI values after refloccuation were lower for bentonite than for kaolin, indicating that these flocs were weaker than those formed by kaolin. Previously, the influence of shear on flocculating a clay suspension by 0.13 mg/g PDADMAC showed a decrease in the FI from 3.0 to 0.8, when the shear rate was increased from 50 to 400 rpm and FI increased again to 2.5 when shear rate decreased to 50 rpm (Hocking et al., 1999).

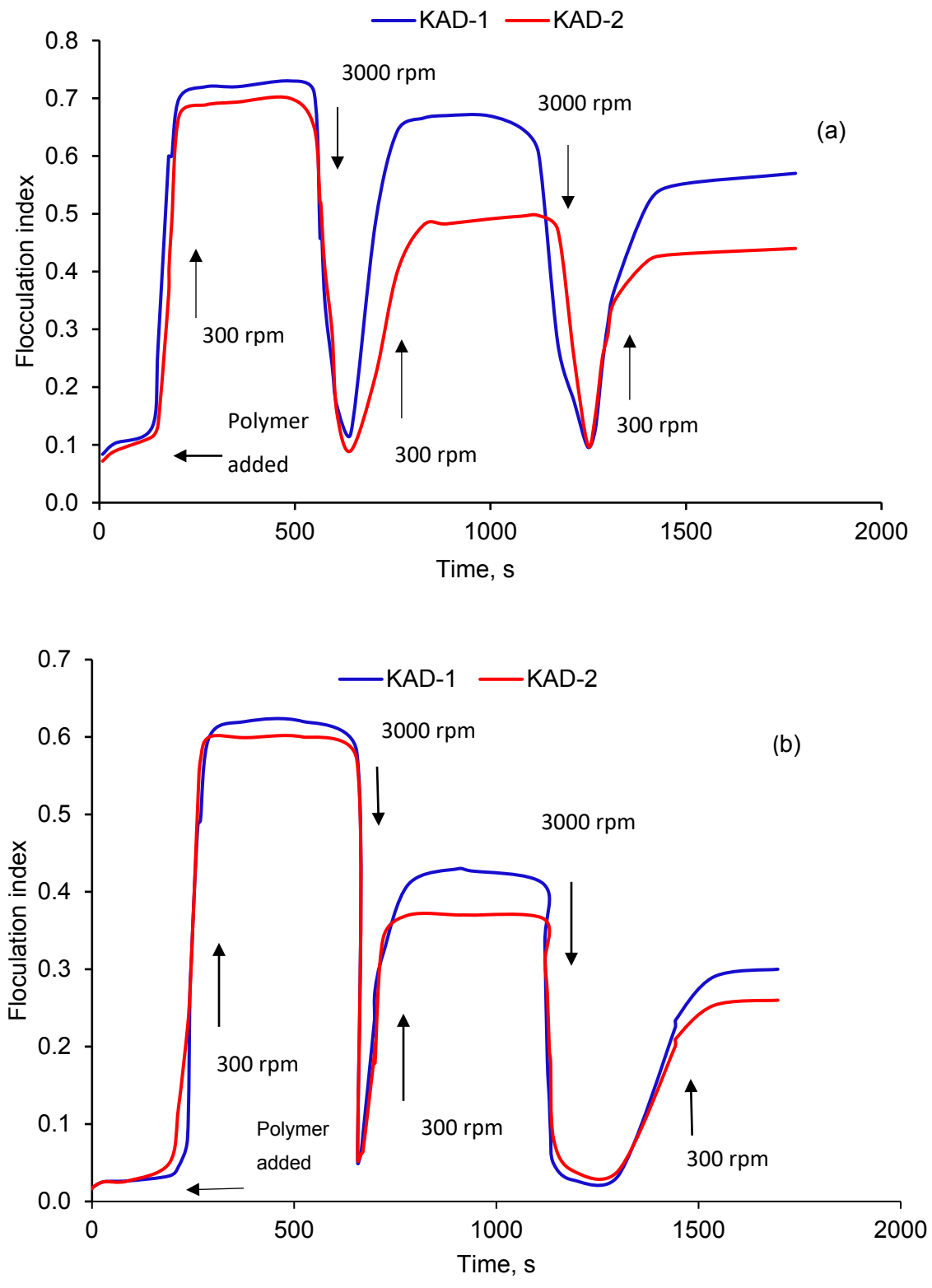

Figure 5.9. Flocculation index of a) kaolin and b) bentonite suspensions as a function of time conducted under the conditions of 8 mg/g KAD, 25 °C, and 0.4 g/L of clay concentration.

5.5 Conclusions

The adsorption capacity of KAD-1 and KAD-2 on kaolin particles (1.40 and 1.25 mg/g) was higher than that on bentonite (1.08 and 0.99 mg/g), and the adsorption of KAD-1 was higher at neutral or alkaline pH. The zeta potential of the kaolin suspensions increased significantly from -35.3 to 38.9 and 33.7 mV due to the adsorption of KAD-1 and KAD-2; while the zeta potential of bentonite particles increased slightly from -33.08 to -8.8 and – 7.9 mV due to the low adsorption of KAD-1 and KAD-2, respectively. A more significant change in the zeta potential of kaolin was due to the adsorption of more KAD on kaolin particles. KAD-1 was more effective than KAD-2 in flocculating kaolin and bentonite particles. However, the relative turbidity of bentonite reduced more significantly than kaolin as its particles were larger, which made it more affected by KADs. It was also observed that charge neutralization was the main factor in flocculating bentonite particles; whereas, polymer patching and/or bridging were the main factors for kaolin flocculation. The flocs of kaolin were stronger than those of bentonite, which were broken more easily by shear rates. KAD-1 was also induced the flocs with a higher strength than did KAD-2.

5.6 References

Abdollahi, Z., Frounchi, M., Dadbin, S. 2011. Synthesis, characterization and comparison of PAM, cationic PDMC and P (AM-co-DMC) based on solution polymerization. J. of Ind. and Eng. Chem., 17(3), 580–586.

Alemdar, A., Oztekin, N., Gungor, N., Ece, O.I., Erim, F.B. 2005. Effects of polyethyleneimine adsorption on the rheological properties of purified bentonite suspensions. Colloids and Surf. A: Physicochem. Eng. Asp., 252(2-3), 95–98.

Ben, W., Yulian, Z., Chunbao, M. 2011. Preparation of cationic chitosan-polyacrylamide flocculent and its properties in wastewater treatment. J. Ocean Univ. China (Oceanic and Coastal Sea Research), 10 (1), 42-46.

Besra, L., Senguptaa, D.K., Roy, S.K., Ay, P. 2002. Polymer adsorption: its correlation with flocculation and dewatering of kaolin suspension in the presence and absence of surfactants. Int. J. Miner. Process, 66, 183– 202.

Chen, W.J. 1998. Effects of surface charge and shear during orthokinetic flocculation on the adsorption and sedimentation of kaolin suspensions in polyelectrolyte solutions. Sep. Sci. Tech., 33(4), 569- 590.

Chen, Y., Liu, S., Wang, G. 2007. A kinetic investigation of cationic starch adsorption and flocculation in kaolin suspension. Chem. Eng. J., 133 (1-3), 325–333.

Divakaran, R., Pillai, V.N.S., 2001. Flocculation of kaolinite suspensions in water by chitosan, Water Res., 35(16), 3904-3908.

Du, X., Li, J., Lindstorm, M. E. 2014. Modification of industrial softwood kraft lignin using Mannich reaction with and without phenolation pretreatment. Indust. Crops Prod., 52, 729–735.

Fang, R., Cheng, S.U., Fu, J., Zheng, Z. B. 2009. Research on the graft copolymerization of EH-lignin with acrylamide. Nat. Sci., 1, 17-22.

Fatehi, P., Shen, J., Hamdan, F.C., Ni, Y. 2013. Improving the adsorption of lignocelluloses of prehydrolysis liquor on precipitated calcium carbonate. Carbohyd. Polym., 92 (2), 2103-2110.

Ghimici, L., Constantin, M., Fundueanu, G. 2010. Novel biodegradable flocculating agents based on pullulan, J. of Haza. Mat., 181 (1-3), 351–358.

Gill, R.I.S., Herrington, T.M. 1987.The flocculation of kaolin suspensions using polyethylenimine and cationic polyacrylamides of the same molar mass but different charge density. Colloid Surf. 28, 41-52.

Hasan, A., Fatehi, P., 2018. Synthesis and characterization of lignin-acrylamide-(2-methacryloyloxyethyl) trimethyl ammonium chloride copolymer. J. Appl. Polym. Sci., 135, 46338.

He, Y., Li, G., Yang, F., Yu, X., Cui, Y., Ren, F., 2007. Precipitation polymerization of acrylamide with quaternary ammonium cationic monomer in potassium carbonate solution initiated by plasma. J. of App. Polym. Sci., 104 (6), 4060–4067.

Hocking, M.B., Klimchuk, K.A., Lowen, S. 1999. Polymeric flocculants and flocculation. J. Macromol. Sci. Part C: Poly Rev., 39 (2), 177-203.

Jahan, M.S., Liu, Z., Wang, H., Saeed, A., Ni, Y. 2012. Isolation and characterization of lignin from prehydrolysis liquor of kraft based dissolving pulp production. Cell. Chem. Technol., 46 (3–4), 261–267.

Kouisni, L., Holt-Hindle, P., Maki, K., Paleologou, M. 2012. The lignoforcesystem ™: a new process for the production of high-quality lignin from black liquor. J. Sci. Tech. Forest Prod. Pro., 2 (4), 6–10.

Lee, C.S., Robinson, J., Chong, M.F. 2014. A review on application of flocculants in wastewater treatment. Pro. Safety and Env. Protec., 92 (6), 489–508.

Levy, N., Garti, N., Magdassi, S. 1995. Flocculation of bentonite suspensions with cationic guar. Colloids and Surfaces A: Phys. and Eng. Aspects., 97 (2), 91-99.

Liimatainen, H., Haapala, A., Tomperi, J. Niinimaki, J. 2009. Fibre floc morphology and dewaterability of a pulp suspension: role of flocculation kinetics and characteristics of flocculation agents. BioResour., 4(2), 640-658.

Meister, J.J. Modification of lignin. 2002. J. Macromol. Sci., Part C Poly. Rev., 42 (2), 235–289.

Oveissi, F., Fatehi, F., 2014. Isolating lignin from spent liquor of thermomechanical pulping process via adsorption. Env. Tech., 35(20), 2597-2603.

Pala, S., Ghorai, S., Dash, M.K., Ghosh, S., Udayabhanu, G. 2011. Flocculation properties of polyacrylamide grafted carboxymethyl guar gum (CMG-g-PAM) synthesized by conventional and microwave assisted method. J. Haz. Mat., 192, 1580– 1588.

Petzold, G., Mende, M., Lunkwitz, K., Schwarz, S., Buchhammer, H.M. 2003. Higher efficiency in the flocculation of clay suspensions by using combinations of oppositely charged polyelectrolytes. Colloids and Surf. A: Physicochem. Eng. Asp., 218 (1-3), 47-57

Pouteau, C., Dole, P., Cathala, B., Averous, L., Boquillon, N., 2003. Antioxidant properties of lignin in polypropylene. Polym. Degrad. Stab., 81(1), 9-18.

Ramphal, S.R., Sibiya, M.S. 2014. Optimization of coagulation-flocculation parameters using a photometric dispersion analyzer. Drink. Water Eng. Sci., 7, 73–82.

Razali, M.A.A., Ahmad, Z., Ahmad, M.S.B., Ariffin, A. 2011. Treatment of pulp and paper mill wastewater with various molecular weight of polyDADMAC induced flocculation. Chem. Eng. J., 166 (2), 529–535.

Schmidt, C.U., Lagaly, G. 1999. Surface modification of bentonites: I. Betaine montmorillonites and their rheological and colloidal properties, Clay Min., 34, 447-458.

Silva, E.A.B. D., Zabkova, M., Araujo, J.D., Cateto, C.A., Barreiro, M.F., Belgacem, M.N., Rodrigues, A. E. 2009. An integrated process to produce vanillin and lignin-based polyurethanes from Kraft lignin. Chem. Eng. Res. Des., 87 (9), 1276–92.

Sirvio, J., Honka, A., Liimatainen, H., Ninimaki, J., Hormi, O. 2011. Synthesis of highly cationic water-soluble cellulose derivative and its potential as novel biopolymeric flocculation agent. Carbohyd. Polym., 86 (1), 266-270.

Solberg, D. Wagberg, V. 2003. Adsorption and flocculation behavior of cationic polyacrylamide and colloidal silica. Colloids and Surf. A: Physicochem. Eng. Asp., 219 (1-3), 161-172.

Tekin, N., Dincer, A., Demirbas¸ O., Alkan, M. 2006. Adsorption of cationic polyacrylamide onto sepiolite. J. of Haz. Mat., 134(1-3), 211–219.

Tekin, N., Demirbas, O., Alkan, M. 2005. Adsorption of cationic polyacrylamide onto kaolinite Micro. and Meso. Mat., 85 (3), 340–350.

Tian, D. Xie, H.Q. 2008. Synthesis and flocculation characteristics of konjac glucomannan-g-polyacrylamide. Poly. Bull., 6, 277–285.

Wan, X., Li, Y., Wang, X., Gu, X. 2007. Synthesis of cationic guar gum-graft-polyacrylamide at low temperature and its flocculating properties. Eur. Polym. J., 43(8), 3655-3661.

Wang, F., Zou, J., Zhu, H., Han, K., Fan, F. 2010. Preparation of high effective flocculant for high density waste drilling mud. J. of Env. Prot., 1,179-182.

Wang, J. P., Chen, Y.Z., Wang, Y., Yuan, H. Q., Yu. H.Q. 2011.Optimization of the coagulation-flocculation process for pulp mill wastewater treatment using a combination of uniform design and response surface methodology. Water Res., 45 (17), 5633-5640.

Wang, J. P., Y. Z. Chen, Y.Z., Wang, Y., Yuan, S.J., Sheng, G.P., Yu. H. Q. 2012. A novel efficient cationic flocculent prepared through grafting two monomers onto chitosan induced by Gamma radiation. RSC Adv., 2 (2), 494–500

Wang S., Hou Q., Kong F., Fatehi P. 2015. Production of cationic xylan–METAC copolymer as a flocculant for textile industry. Carbohyd. Polym., 124,229-236.

Wang, S., Konduri, M.K.R., Hou., Q., Fatehi, P. 2016. Cationic xylan-METAC copolymer as a flocculant for clay suspensions. RSC Adv., 6(46), 1-34.

Wang, J.P., Yuan, S.J., Wang, Y., Yu, H.Q. 2013. Synthesis, characterization and application of a novel starch based flocculant with high flocculation and dewatering properties. Water Res., 47 (8), 2643-2648.

Wang, D., Gregory, J., Tang, H. 2008. Mechanistic difference of coagulation of kaolin between PACl and cationic polyelectrolytes: a comparative study on zone 2 coagulation. Dry. Technol., 26 (8), 1060–1067.

Wang, L.J., Wang, J.P., Zhang, S., Yu, H.Q. 2009. A water-soluble cationic flocculant synthesized by dispersion polymerization in aqueous salts solution. Sep. Purif. Technol., 67(3), 331-335.

Wong, S.S., Teng, T.T., Ahmad, A.L., Zuhairi, A., Najafpour, G. 2006. Treatment of pulp and paper mill wastewater by polyacrylamide (PAM) in polymer induced flocculation. J. Hazard. Mater., 135 (1-3), 378–388.

Yang, Z., Wang, Y., Yue, Q., Li, Q. 2013. Advanced lignin-acrylamide water treatment agent by pulp and paper industrial sludge: Synthesis, properties and application. J. Env. Sci., 25(12), 2367–2377

Yu, W.Z., Gregory, J., Campos, L., Li, G. 2011. The role of mixing conditions on floc growth, breakage and re-growth. Chem. Eng. J., 171 (2), 425-430.

Yu, J., Wang, D., Ge, X., Yan, M., Yang, M. 2006. Flocculation of kaolin particles by two typical polyelectrolytes: A comparative study on the kinetics and floc structures. Colloids and Surf. A: Physicochem. Eng. Asp., 290 (1-3), 288-294.

Yu, W., Gregory, J., Campos, L. 2010. The effect of additional coagulant on the re-growth of alum–kaolin flocs. Sep. Purif. Technol., 74 (3), 305–309.

Yukselena, M.A., Gregory, J. 2004. The reversibility of floc breakage, Int. J. Miner. Pro., 73 (2-4), 251– 259.

Zakzeski, J., Bruijnincx, P.C., Jongerius, A.L., Weckhuysen, B.M. 2010. The catalytic valorization of lignin for the production of renewable. Chem. Rev., 110 (6), 3552–3599.

Zhang, Q., Wang, D., Bei, Y., Ren, S., Fang, G. 2013. Flocculation performance of trimethyl quaternary ammonium salt of Lignin-alginate polyampholyte. BioResour., 8, 3544-3555.

Zhou, Y., Franks, G.V. 2006. Flocculation mechanism induced by cationic polymers investigated by light scattering. Langmuir., 22(16), 6775-6786.

Zhu, Z., Li, T., Lu, J., Wang, D., Yao, C. 2009. Characterization of kaolin flocs formed by polyacrylamide as flocculation aids. Int. J. Miner. Pro., 9 (3-4), 94–99.

Zou, J., Zhu, H., Wang, F., Sui, H., Fan, J. 2011. Preparation of a new inorganic–organic composite flocculant used in solid–liquid separation for waste drilling fluid. Chem. Eng. J., 171, 350–356.

Chapter 6: Flocculation of clay suspension with kraft lignin-AM-DMC polymers

6.1 Abstract

Lignin produced in the kraft pulping process is insoluble in water at neutral pH, which limits its application in industry. In this chapter kraft lignin (KL) was copolymerized with acrylamide (AM) and (2-methacryloyloxyethyl) trimethyl ammonium chloride (DMC) in an aqueous solution to produce a water-soluble lignin-based copolymer. Two cationic KAD polymers with the same molecular weights and different charge densities were produced and used as flocculants. KAD1 with a higher charge density showed a higher adsorption on kaolin (2.58 mg/g) and bentonite particles (1.83 mg/g) at 4 mg/g (based on clay) adsorption experiment. Furthermore, KAD1 changed the zeta potential and turbidity of the clay suspensions more effectively than KAD2 did, which was attributed to its higher charge density. The size of kaolin particles was increased from 4.7 to 22.3 and 16.2 μm, and that of bentonite particles increased from 6.1 to 31.9 and 19.8 μm at 4 mg/g of KAD concentration in the clay suspensions, respectively. In addition, the interfacial tension between KAD1 and kaolin and between KAD1 and bentonite reduced from 12.3 mN/m to 5.8 mN/m and 9.5 mN/m to 5.2 mN/m, respectively. Moreover, KAD1 produced stronger flocs and showed high regrowth ability at different shear rates.

6.2 Introduction

In recent years, fast industrialization along with unrestrained use and exploitation of natural resources have led to a significant increase in industrial effluent production, which makes the treatment of wastewater effluents a challenging issue (Razali et al., 2011). Amongst numerous solid–liquid separation processes, flocculation is an efficient and cost-effective method for wastewater treatment in many industrial processes, such as pulp and paper, mining and mineral processes (Wang et al., 2016; Nasser and James, 2006). Synthetic polymeric flocculants have been used for treating industrial wastes for years. However, these flocculants and their derivatives pose a number of environmental problems because some of these flocculants are non-biodegradable and some may be hazardous to human (Liimatainen et al., 2011; Razali et al., 2015; Xie et al., 2007). Taking in to account the above-mentioned issues, the incentives for producing green flocculants are high in industry. Natural products can be rendered flocculant via chemical modifications.

Previous studies demonstrated that acrylamide (AM) and 2-[(methacryloyloxy) ethyl] trimethylammonium chloride (DMC) are the two most explored and utilized monomers to produce polysaccharide based flocculants for treating effluents (Ye et al., 2003; Abdollahi et al., 2011). In addition, the modification of chitosan (Wang et al., 2010; Ben et al., 2011), starch (Lu et al., 2004; Razali et al., 2015) and cellulose (Wang et al., 2011) were reported for flocculant productions. As starch, chitosan and cellulose are heavily consumed in other industries (e.g., food, paper, medicine), they may have limited availability to be used for flocculant production (Wang, et al., 2016). On the other hand, lignin is a natural polymer that has currently limited industrial use (Pouteau et al., 2003; Zakzeski et al., 2010) but available in a large quantity. Therefore, the first objective of this work was to produce kraft lignin based flocculant via copolymerizing with water soluble AM and DMC monomers.

The adsorption of polymers on particles has been comprehensively studied in the past (Gregory and Barany, 2011; Wang et al., 2016). The magnitude of polymers adsorption on the particles would also be affected by the charge density of the polymers (Wang et al., 2016). It was stated that polymers with a higher charge density develop flattened configuration, while those with lower charge density develop tail and loop configurations, when adsorbed on surfaces (Nurmi et al., 2016). Also, the charge density of cationic polymers is considered as a key factor in determining their effectiveness as flocculants on mineral particles such as clay particle surface (Gregory and Barany, 2011; Nurmi et al., 2016; Miranda et al., 2008; Chen and Ovenden, 1998). The second objective of this study was to investigate how the charge density of lignin based flocculant would impact its flocculation performance.

This is the first attempt to produce kraft lignin based cationic polymers in an aqueous system for a flocculant application. To understand how this copolymer would act as a flocculant, a fundamental study of the adsorption behavior of this copolymer on the particle surface as well as investigating the zeta potential and flocculation efficiency of the copolymer in suspension systems were conducted in detail. The main focus of this work was to determine how kraft lignin based flocculant, with a similar molecular weight but varying charge densities, would function as flocculants in kaolin and bentonite suspension systems.

6.3 Materials and Methods

6.3.1 Materials

Softwood kraft lignin was produced via LignoForce^{TM} technology of FPInnovations in Thunder Bay, ON (Kouisni et al., 2012). (2-methacryloyloxyethyl) trimethyl ammonium chloride (DMC) (80% in water), acrylamide (99.0 %), potassium persulfate ($K_2S_2O_8$) (analytical grades), kaolin and bentonite were obtained from Sigma-Aldrich company. Cellulose acetate dialysis membrane (molecular weight cut off of 1,000 g/mol) was obtained from Spectrum Labs. Inc., USA. Poly diallyl dimethyl ammonium chloride (PDADMAC) was obtained from Sigma Aldrich Company and diluted to 0.005 M prior to use. Potassium polyvinyl sulfate (PVSK) was provided by Wako Pure Chem. Ltd. Japan. All the chemicals were used without further purification. Ethanol (95 vol. %) was received from Fisher Scientific company.

6.3.2 Lignin-AM-DMC production and purification

Kraft lignin-AM-DMC copolymers were synthesized in 250 mL three-neck glass flasks under the reaction conditions listed in Table 6.1. After the reactions, the flasks were submerged in cold tap water for 20 min. Then, ethanol (95 vol. %) was mixed with the reaction media in order to precipitate the lignin based copolymers from the reaction systems. Previously, ethanol precipitation was carried out for separating chitosan-AM-DMC copolymer from reaction media containing homopolymers (PAM, PDMC) and monomers (AM, DMC) (Wang et al., 2012; Ben et al., 2011). By adding ethanol to the reaction media, the solution reactions became suspension. The suspensions were centrifuged at 3500 rpm for 10 min in order to collect the precipitated copolymers (KL-AM-DMC) and remove the homopolymers (PAM, PDMC) and unreacted monomers (AM, DMC) present in the supernatants. In the next step, a 95 % ethanol was added to the collected precipitates after centrifuge, and it was gently mixed with the precipitates. These suspensions were centrifuged again to once again precipitate the produced KL-AM-DMC, and the supernatants containing homopolymers or monomers were removed. This step was repeated three times. Subsequently, the precipitated copolymers were mixed with 200 mL of deionized water and the pH of the solution was adjusted to 7.0 ± 0.2.

The samples were dialyzed using a membrane dialysis for 48 h in order to remove other impurities (e.g., inorganic salts and unreacted monomers) from the copolymer solutions. The deionized water

used for dialysis was changed every 12 h for 2 days. After dialysis, the solutions containing the copolymer were dried at 105 °C, and the dried samples were kept for flocculation studies. This copolymer was denoted as KAD, while unmodified kraft lignin was denoted as KL in this work.

6.3.3 Solubility and charge density determination

To measure the solubility of the KAD, 0.2 g of the copolymers were added to 20 mL of deionized water by stirring at 100 rpm and 30 °C for 1 h in a water bath shaker (Innova 3100, Brunswick Scientific, Edison, NJ, USA). Then, the suspensions were centrifuged at 1000 rpm for 5 min. The supernatants were collected and used for analyzing the charge density and solubility of the copolymers. The concentration of copolymers in the supernatants was determined by drying the supernatants at 105 °C, and the solubility was determined based on the concentration of KAD in the supernatants and the initial concentration of KAD in solutions. The charge density of the copolymers was measured by a particle charge detector, Mütek PCD 04 titrator (Herrsching, Germany) with a standard PVSK solution (0.0050 M) (Wang et al., 2016).

The surface charge density of bentonite and kaolin particles was determined via back titration method with a Mutek, PCD 04, particle charge detector (Germany). Approximately, 0.2 g of clay was suspended in 50 mL of PDADMAC (0.005M) solution and the suspensions were incubated at 30 °C for 2 h at 150 rpm. After the incubation, the samples were filtered using Whatman#1 and the filtrates were titrated against PVSK (0.0055 M) solution. Similarly, the titration analysis was conducted for the control sample (i.e., PDADMAC solution with no clay addition), and the difference in the concentration of PDADMAC in the control and actual samples was considered for quantifying the surface charge density of clay particles. Three repeats were carried out, and the average values were reported**.**

6.3.4 Molecular weight analysis

About 5 mg of dried KAD copolymer was dissolved in 10 mL of 5.0 wt. % acetic acid solution by stirring at 600 rpm for 48 h and 35 °C, and then the solutions were filtered with a 13 mm diameter nylon filter (pore size 0.2 μm). The filtered solutions were used for the molecular weight analysis, which was carried out using Malvern, GPCmax VE2001 Module + Viscotek system with viscometer and UV detectors. In this analysis, PolyAnalytic columns were used, and a 5.0 wt. % acetic acid was used as a solvent and eluent with the flow rate of 0.7 mL/min. The column

temperature was set to 35 °C. Poly ethylene oxide was used as standard polymers for calibration of this system.

6.3.5 Elemental analysis

The elemental analysis of the samples was performed for KL and KAD copolymers using an elemental analyzer, Elementar Vario EL Cube, by the combustion method (Jahan et al., 2012). The samples were first dried in an oven at 105 °C overnight to remove any moisture prior to analysis. Approximately, 2 mg of the dried samples were transferred into the carousel chamber of the elemental analyzer and combusted at 1200 °C to reduce the generated gasses to analyze carbon, hydrogen, oxygen, and nitrogen contents of the samples.

6.3.6 Surface area analysis of clay particles

The surface area of bentonite and kaolin particles was determined by using surface area analyzer, Quantachrome, Nova2200e instrument. In this experiment, the samples were initially dried in the oven at 105 °C overnight, and approximately 0.05 g of sample was pretreated for 4 h at 250 °C prior to analysis. The specific surface area of the samples was then analyzed according to Brunauer-Emmett-Teller (BET) method via adsorption-desorption isotherms using nitrogen gas at -180 °C within relative pressure range of 0.01 to 0.99 (Oveissi and Fatehi, 2014).

6.3.7 Particle size analysis

The size distribution of bentonite and kaolin particles was analyzed using a MasterSizer 2000 particle size analyzer (Malvern Instruments), which was equipped with a light scattering detector. In this study, 1.0 g of clay suspension (20 g/L) was added to 50 mL of deionized water or 50 mL of KL or KAD solution containing polymers at the dosage of 4 mg/g (based on clay) and stirred at 300 rpm and room temperature for 2 h. After stirring, the samples were analyzed for their particle size distribution.

6.3.8 Adsorption studies

In this set of experiments, different amounts of KL or KAD (from 0.25 to 32 mg/g, based on the clay) were added to 50 mL of clay suspensions (0.4 g/L) in order to study the adsorption of KL or KAD on the clay particles. The suspensions were stirred at 300 rpm for 2 h at room temperature. Afterward, they were centrifuged for 15 min at 3500 rpm and then the concentrations of KAD

remaining in the supernatants were determined by UV/Vis spectrophotometer (Genesys 10S UV–vis, Thermo FisherScientific, USA) at a wavelength of 205 nm. The impact of pH was also studied on the adsorption of KAD on clay particles. The pH of the suspensions (ranging 2 to 12) was adjusted with 0.1 M NaOH solution or H_2SO_4. Three repeats were carried out, and the average values were reported in the study.

6.3.9 Impact of KL or KAD on clay removal

In this set of experiments, different amounts of KL or KAD were mixed with 50 mL of clay suspensions (0.4 g/L) at 30 °C for 2 h. After mixing, clay suspensions were allowed to settle for 1 h. A 10 mL sample was collected from the upper half of the suspension before and after the settlement and dried in an oven at 105 °C overnight. The concentration of clay particles in the samples was determined, which helped measure the removal of clay from suspensions by developing a mass balance. This analysis was repeated at different polymer dosages (0.25-32 mg/g based on clay) and pHs (2-12). The pH of the clay suspension adjusted by using 0.1 M NaOH. Three repeats were carried out, and the average values were reported in the study.

6.3.10 Zeta potential analysis

The zeta potential of clay suspensions was characterized by a NanoBrook Zeta PALS (Brookhaven Instruments Corp, USA). In this study, 1 g of clay suspension (20 g/L) was added to 50 mL of deionized water and stirred at 300 rpm for 2 h and room temperature, then its zeta potential was measured in a 1.0 mM KCl aqueous solution. The pH of the clay suspensions was adjusted by using 0.1 M NaOH or H_2SO_4. All the measurements were carried out at room temperature at a constant electric field (8.4 V/cm). Three repeats were carried out for zeta potential measurement and the mean value was reported.

6.3.11 Flocculation analysis

The efficiency of the flocculation was determined using a photometric dispersion analyzer (PDA 3000, Rank Brothers Ltd) connected to a dynamic drainage jar (DDJ) fitted with a 70 mm mesh screen (Wang et al., 2016). The flocculation performance of the clay suspension was measured from the variation in the direct current (DC) voltage of the PDA instrument. In this study, 500 mL of distilled water was first added into the DDJ container and circulated from the DDJ to the PDA through a 3 mm plastic tube until a steady flow rate of 20 mL/min was achieved.

The flow rate was regulated by a peristaltic pump throughout the experiment. Then, 10 mL of a 20 g/L clay suspension was added into DDJ (to make a 0.4 g/L clay concentration in DDJ) while stirring at 300 rpm. This caused a decrease in the initial base DC voltage (V_0) to a new DC voltage (Vi) in the PDA analyzer. After 100 s, 4 mg/g dosage (based on clay) of KL or KAD was maintained in the DDJ. The increase in DC voltage was represented as the DC voltage of the final suspension (V_f). The effects of KAD dosage and pH of the clay suspensions on the flocculation were also studied. The pH of the clay suspensions adjusted by using 0.1 M NaOH or H_2SO_4. The relative turbidity of the clay suspensions was measured using equation 6.1 (Wang et al., 2009).

$$\text{Relative turbidity, } \tau_r = \frac{\tau_f}{\tau_i} = \frac{ln(\frac{V_0}{V_f})}{ln(\frac{V_0}{V_i})} \qquad (6.1)$$

where τ_f is denoted as the final suspension turbidity, and τ_i is denoted as the initial suspension turbidity.

To study the strength of clay flocs after copolymer addition, 10 mL of a 20 g/L clay suspension was added into DDJ (to make a 0.4 g/L clay concentration in the DDJ) while stirring at 300 rpm. After 100 s, KL or KAD was added to the DDJ. After 500 s and forming flocs, the shear rate in the DDJ was increased from 300 to 3000 rpm and maintained for 100 s, during which flocs would break. Subsequently, the shear rate was decreased to 300 rpm and maintained for another 500 s, which might help in the regrowth of broken flocs. This process was repeated twice to study the flocculation behavior of clay suspensions in the presence of KAD. The degree of breakage and regrowth was presented by flocculation index (FI), which is the ratio of the root-mean- square (RMS) and direct current (DC) of the PDA instrument. The flocculation index was used as an indication of flocculation and breakage of clay particles in the suspensions in the past (Wang et al., 2008; Yu et al., 2010; Ramphal and Sibiya, 2014). All the experiments were performed in triplicates, and the mean values were reported in the study.

Previously, it was demonstrated that the floc breakage or floc regrowth can be evaluated quantitatively in order to study the strength and regrowth ability of the broken flocs (Alfano, 1998; Alfano et al., 1999; Blanco et al., 2002; Blanco et al., 2001). The relationship between the floc breakage (T_{br}) at 3000 rpm (equation 6.2, 6.3) and regrowth (T_{gr}) at 300 rpm (equation 6.4, 6.5) for KAD in kaolin and bentonite suspensions were also developed:

$$Y = C_0 + A.e^{-t/T_{br}} \quad (6.2)$$

$$Y = A.e^{-B.t} \quad (6.3)$$

$$Y = C_\infty - K.e^{-t/T_{gr}} \quad (6.4)$$

$$Y = K.e^{-S.t} \quad (6.5)$$

where A and K are pre-exponential factor, C_0 and C_∞ are numerical constants, T_{br} and T_{gr} are the floc breakage and regrowth, Y is the mean floc size. By correlating equations (2) and (3), (4) and (5), $B = 1/T_{br}$ and $S = 1/T_{gr}$ are obtained. The parameters T_{br} and T_{gr} obtained are shown in Table 6.3.

6.3.12 Surface and interface tension analysis.

The surface tension of KAD polymers was measured using a tensiometer (Attension sigma 700), equipped with platinum loop (Ponnusamy et al., 2012). In this set of experiments, KAD with a lower charge density (KAD1) was added at different concentrations (2 to 32 mg/g) to deionized water (25 mL) and mixed for 1 h at 300 rpm and 30 °C. After mixing, 20 mL of KAD solution was transferred to glass container for surface tension analysis. Based on the input parameters (ring dimension, density of the sample and temperature), the surface tension of the samples was determined by the instrument. The surface tension of KAD1 and KAD2 solutions was measured for 3 min and each measurement was replicated 10 times within the time frame. The platinum loop was cleaned with ethanol and deionized water between each test. All the measurements were carried out at 25 °C and pH 7.

An optical tensiometer instrument, Theta lite (Biolin Scientific, Finland) equipped with camera was used to determine the wettability of kaolin samples (20 g/L). After mixing, 2 mL of each clay sample was coated on glass slides using a spin coater, WS-650 (Laurell Technologies Corp) under vacuum with 60 psi pressure at 250 rpm and 60 s. The contact angle of water droplet with kaolin and bentonite samples coated on the slides was measured by sessile drop method using an optical tensiometer (Cipriano et al., 2005). Approximately, 5 µL of water droplet was placed on the coated slides and the contact angles between droplets and the kaolin samples coated on slides were determined. In another set of experiments, a droplet (5 µL) of KAD1 or KAD2 solution was placed on the kaolin coated slides and the contact angle between the KAD1 or KAD2 droplet and kaolin

coated slides was measured as described above. Three replicates were performed for each experiment and average values were reported.

The surface tension of kaolin was analyzed using the tensiometer's OneAttension software via Zisman equation (Eq. 6.6) (Zhu et al., 2010).

$$\text{Cos}\,\theta = 1 + b\,(\gamma_{sv} - \gamma_{lv}) \qquad (6.6)$$

where γ_{lv} and γ_{sv} represent the surface tension of liquid (KAD1 or KAD2 solution) vapor and solid (kaolin) vapor in mN/m, θ represents contact angle between liquid and solid in degrees (°).

The interfacial tension between kaolin and KAD1 or KAD2 droplet was determined by using Young equation (Eq. 6.7)

$$\gamma_{lv}\,cos\theta = \gamma_{sv} - \gamma_{sl} \qquad (6.7)$$

where γ_{lv}, γ_{sv} and γ_{sl} represent the tensions of liquid vapor, solid vapor and solid liquid, respectively. The aforementioned procedures for contact angle, surface tension and interface tension analysis were repeated for bentonite, as well.

6.4 Results and Discussion

6.4.1 Properties of KAD

The copolymerization of KL from AM and DMC was carried out in an aqueous solution via free radical polymerization using potassium persulfate as an initiator (Figure 6.1). The details of reaction mechanisms of KL, AM and DMC were discussed in the previous chapter (Hasan and Fatehi, 2018). In this copolymerization reaction, the AM and DMC would attach to the phenolic hydroxide group of KL.

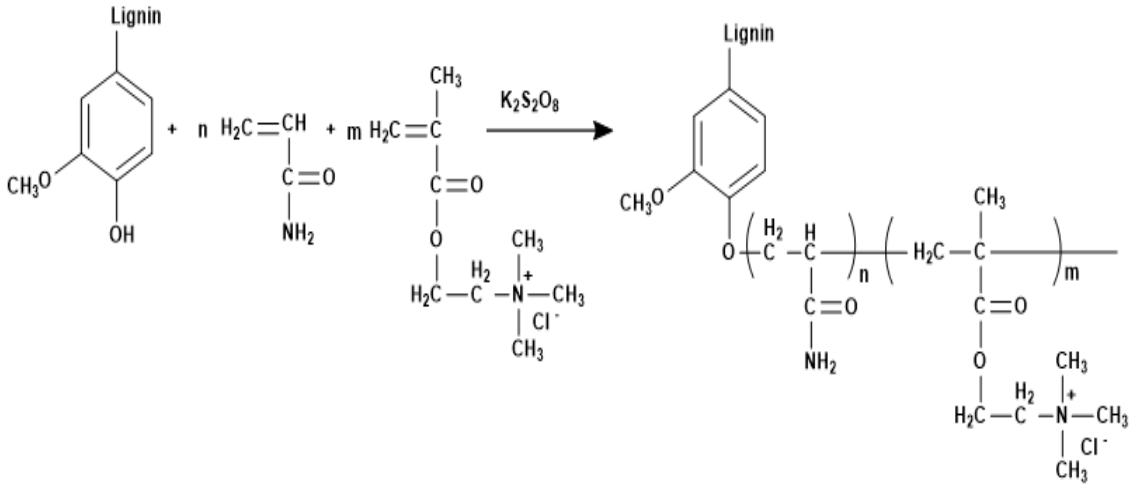

Figure 6.1. The copolymerization reaction of KL, DMC, and AM for KAD production.

Table 6.1 lists the reaction conditions and properties of the copolymers. Under controlled reaction conditions, the copolymers with varying charge densities of 1.3 and 2.1 meq/g but with a similar molecular weight of 185 kg/mol were produced. It is evident that the amount of nitrogen, charge density, and molecular weight increased in the KAD as compared to KL, confirming the grafting of AM and DMC onto lignin backbone (Wang et al., 2013). KAD1 had a higher nitrogen content and charge density than did KAD2, confirming that the copolymerization was accelerated more greatly for KAD1 than KAD2. The proportion of DMC, AM and KL in the KAD was presented in Table 6.1. The proportion of DMC was determined by the charge density analysis since a charge of +1 meq/g equals to 1 mmol/g of DMC in KAD, as only DMC contributes to the charge density of KAD. The proportion of AM and DMC in the KAD was measured by considering the total amount of nitrogen in KAD polymer. Finally, the proportion of KL in KAD was determined by developing a mass balance for the copolymer via considering the proportions of DMC and AM in the copolymer. As can be seen, KAD1 was composed of higher DMC content (44.2 %) as compared to KAD2 (26.79 %).

Table 6.1. Reaction conditions and properties of KADs

Conditions	KL	KAD1	KAD2
Temperature, °C	-	80	80
Time, h	-	3	4
KL, mol	-	0.011	0.011
AM, mol	-	0.014	0.014
DMC, mol	-	0.024	0.014
pH	-	3	5
Charge density, meq/g	- 0.2	2.13	1.29
Solubility, wt.%	5	56	53
M_W, g/mol	17, 890	185,900	185, 500
M_n, g/mol	5,150	128,500	135,700
M_w/M_n	3.473	1.442	1.367
Nitrogen, %	0.03	6.01	3.12
KL, %	-	40.2	66.51
AM, %	-	15.55	6.69
DMC, %	-	44.2	26.79

6.4.2 Kaolin and bentonite characteristics

Table 6.2 presents the properties of kaolin and bentonite particles. Bentonite mainly composed of two negatively charged silicon oxide and one positive charge aluminum oxide surfaces along with traces of other clay materials. Therefore, bentonite naturally possesses a negative charge due to the prevalence of the negatively charged oxide anions (Asselman and Garnier, 2000; Schmidt and Lagaly, 1999). Bentonite particles were larger with smaller surface area and pore volume than kaolin particles. However, kaolin contains one parallel layer of silicon dioxide and aluminum oxide sheets. It is apparent that kaolin particles possess a small net negative surface charge.

Table 6.2. Properties of clays

Sample	Surface charge density, μeq/g	Particle size, μm	BET surface area, m^2/g	Total pore volume, cm^3/g
Kaolin	-5.5	4.7	55.64	0.027
Bentonite	-9.4	6.1	20.12	0.012

6.4.3 Adsorption of polymers

Figure 6.2 shows the adsorption of KAD on clay particles as a function of KAD dosage and pH. It was observed that the adsorbed amount was increased with increasing the polymer charge density, implying the important role of electrostatic interaction in the adsorption process (Piana et al., 1987). As observed, the adsorption of cationic KAD1 and KAD2 onto kaolin particles approached a plateau at 4 mg/g (based on clay) dosage and the maximum polymer adsorptions were 2.58 and 2.11 mg/g, respectively. In case of bentonite, the adsorption for KAD1 and KAD2 was 1.83 and 1.63 mg/g, respectively. The lower adsorption capacity of bentonite than kaolin can be attributed to its smaller surface area and larger particle size (Asselman and Garnier, 2000; Wang et al., 2016). Meanwhile, KL had marginal adsorption on kaolin and bentonite particles. As indicated in Figure 6.2a, the adsorption behavior of a polymer onto clay particles is dependent on its charge density. The data presented here is consistent with previous findings in that increasing the charge density (10% to 35%) of a cationic poly acrylamide would enhance its adsorption from 1.5 to 3.4 mg/g in kaolinite suspension (Nasser and James, 2006). Wang et al. (2016) compared the flocculation efficiency of cationic polymers and reported that an increase in the charge density of cationic xylan (1.8 to 2.4 meq/g) enhanced its adsorption onto kaolin (3.1 and 4.6 mg/g) and bentonite (0.73 and 0.85 mg/g) particles. Similarly, the investigation of Barany et al. (2011) demonstrated that an increase in the charge density of cationic polymer (5 to 80 mol %) promoted the polymer adsorption onto kaolin (4 to 10 mg/g) and bentonite (8 to 16 mg/g) particles. Figure 6.2 also shows that the adsorption of KAD on kaolin and bentonite clay particles increased with the increase in the pH, indicating favorable adsorption in alkaline medium. Besra et al. (2002) illustrated that an increase in the pH of kaolin suspension from 2 to 10 led to an increase in the cationic polyacrylamide adsorption on clay from 1.09 to 1.98 mg/g at 2 mg/g of polymer dosage in the clay suspension. These findings also suggested that after polymer adsorption, the surface charge density of clay particles might change from negative to positive depending on the amount of polymer

adsorbed. The results obtained from the adsorption (Figure 6.2a), and the charge density of KADs facilitated the theoretical determination of a change in the surface charge density of kaolin and bentonite particles after KAD adsorption. Figure 6.2c shows the impact of the adsorbed KL and KADs on the theoretical surface charge density of kaolin and bentonite particles. The surface charge density of unmodified clay particles was experimentally determined as described in section 6.4.2; however, it was not possible to experimentally measure the surface charge density of the particles after KAD adsorption. As observed, the negative charges of kaolin and bentonite particles were not neutralized by a positively charged KAD segment even at the saturation level of adsorption. These results confirmed that KAD polymers were not able to fully cover the surface of clay particles because the adsorption sites might become inaccessible to KAD, even though unadsorbed KAD was still available in the suspensions.

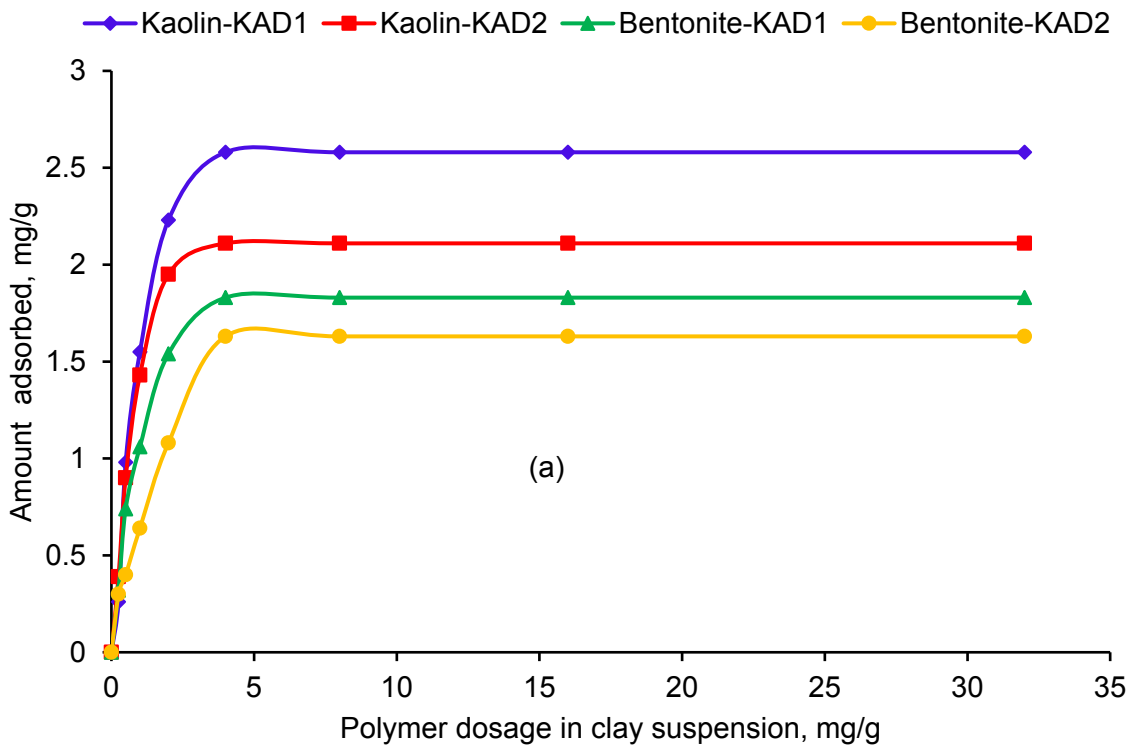

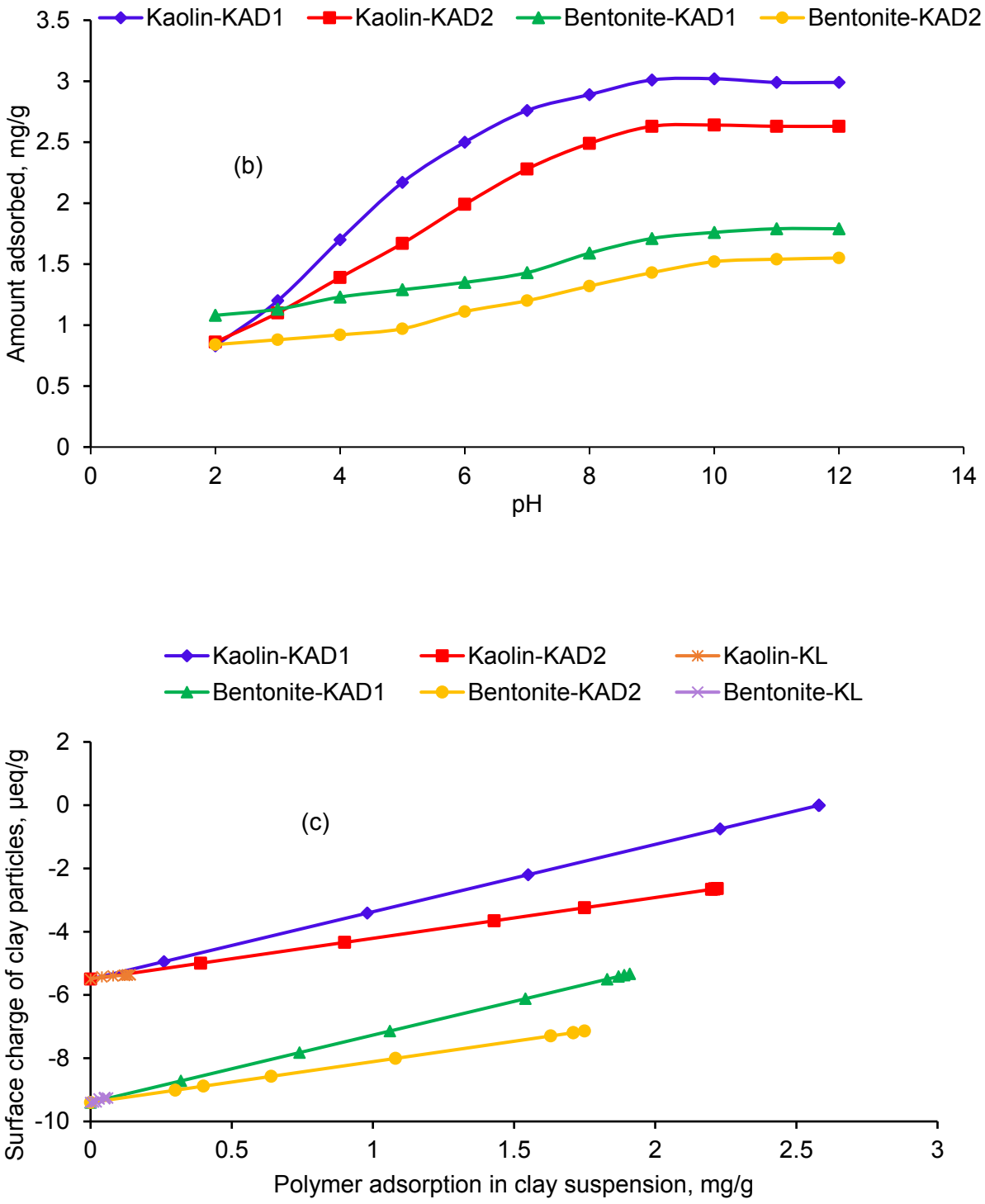

Figure 6.2. a) Adsorption of KL and KAD on kaolin and bentonite as a function of polymer dosage, b) adsorption of KL and KAD on kaolin and bentonite particles as a function of pH, c) theoretical surface charge density of kaolin and bentonite clay particles as a function of adsorbed KAD (conducted under the conditions of pH 7, 25 °C, 2 h and 0.4 g/L clay concentration).

6.4.4 Surface tension and interfacial tension analysis

Figure 6.3 shows the impact of KAD concentration on the surface tension of water. The surface tension of water in the absence of KAD was found to be 72.8 mN/m (Szymczyk and Jańczuk, 2011). It can be seen that the surface tension of water decreased to 65 and 67 mN/m via adding 32 mg/g KAD1 and KAD2 in the suspension, respectively. The KAD copolymer possesses a number of functional groups, such as quaternary ammonium, carbonyl, phenolic hydroxyl, and amide, which could alter the interactions developed between the water molecules and thus reducing the surface tension of water (Szymczyk and Jańczuk, 2011). The higher reduction in the surface tension of water caused by the KAD1compared to KAD2 can be attributed to its higher charge density; consequently, more interaction with water molecule would occur that impacts the surface tension. It is worth mentioning that, the surface tension of kaolin (γ_{sv}) (55 mN/m) was found to be greater than bentonite's (47 mN/m).

The interfacial tension between clay and water droplet was reduced with the addition of KAD (Figure 6.3). As observed, the interfacial tension between kaolin and water (12.35 mN/m) was decreased to 5.8 and 7.1 mN/m for KAD1 and KAD2, respectively, at 32 mg/g KAD concentration. This observation is in agreement with the significant reduction in contact angle of water (57°) for KAD1 (45°) and KAD 2 (47°) on the kaolin coated surfaces. On the contrary, the interfacial tension between water and bentonite (9.5 mN/m) was decreased to 5.2 and 6.6 mN/m for KAD1 and KAD2, respectively. However, no significant change in surface tension and interfacial tension between water and clay samples was observed in the presence of unmodified KL (not shown).

A smaller contact angle indicated more adhesion of liquid on solid surface (Somasundaran and Zhang, 2006). Evidently, adhesion (wettability) of KAD onto kaolin and bentonite surfaces increased with increasing the polymer concentration to 32 mg/g. As can be seen, the wetting behavior of KAD1 was better than KAD 2. This is because of higher charge density of KAD 1, which leads to enhanced electrostatic interaction with clay particles. As a result, the highest wettability (i.e., maximum drop in contact angle) of clay was achieved by KAD1, indicating that the decrease in the interfacial tension and contact angle was most likely associated with its increased adsorption onto the clay surface (Figure 6.2) (Somasundaran and Zhang, 2006). In addition, a decrease in KAD contact angle and interfacial tension was greater on kaolin than

bentonite surface because KAD polymers tend to adsorb less on the bentonite particles due to its smaller surface area (Table 6.2).

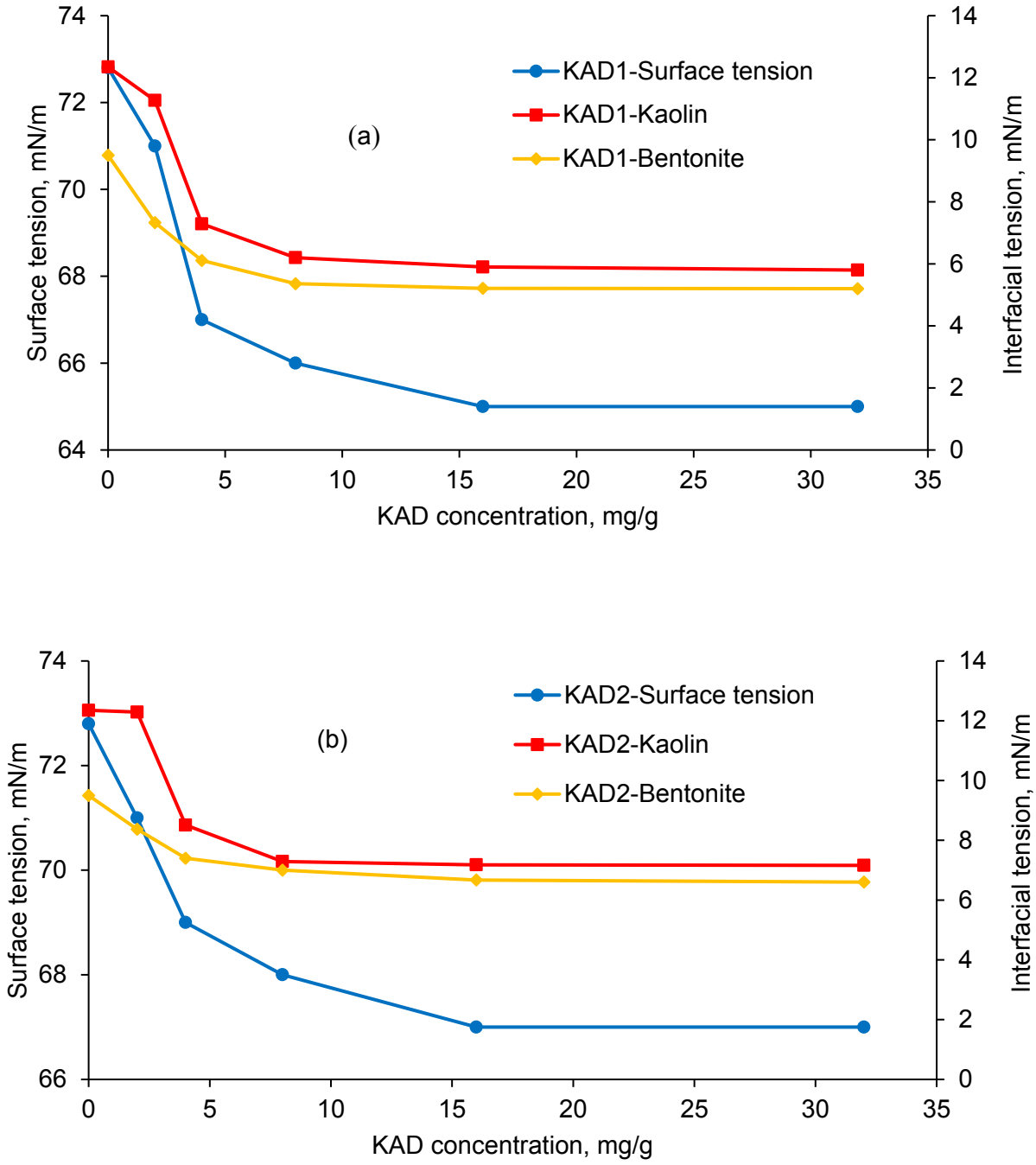

Figure 6.3. Effect of a) KAD1 concentration and b) KAD2 concentration on surface tension and interfacial tension of kaolin and bentonite particle under the conditions of pH 7 and 25 °C.

6.4.5 Particle size distribution

The volume fraction of particles in the presence and absence of KL or KAD at the dosage of 4 mg/g as a function of particle diameter is shown in Figure 6.4. The sizes of untreated kaolin and bentonite particles were 4.7 and 6.1 µm, respectively. Both KAD1 and KAD2 increased the size of kaolin particles from 4.7 to 22.3 and 16.2 µm, respectively. Furthermore, the size of the bentonite particles was increased to 31.9 and 19.8 µm in the presence of KAD1 and KAD2, respectively. The particle size was larger for the KAD1. As discussed previously, KAD1 exhibited more adsorption that led to a multilayer deposition of KAD1 on the particles and contributes to their larger sizes. Moreover, the small peaks seen in the figure demonstrate that some particles may be involved in inter-particle association to form flocs of coagulated particles (Ghimici et al, 2010). Wickramasinghe et al. (2002) observed that an increase in the charge density of cationic polyacrylamide led to an increase in the particle size for yeast suspension.

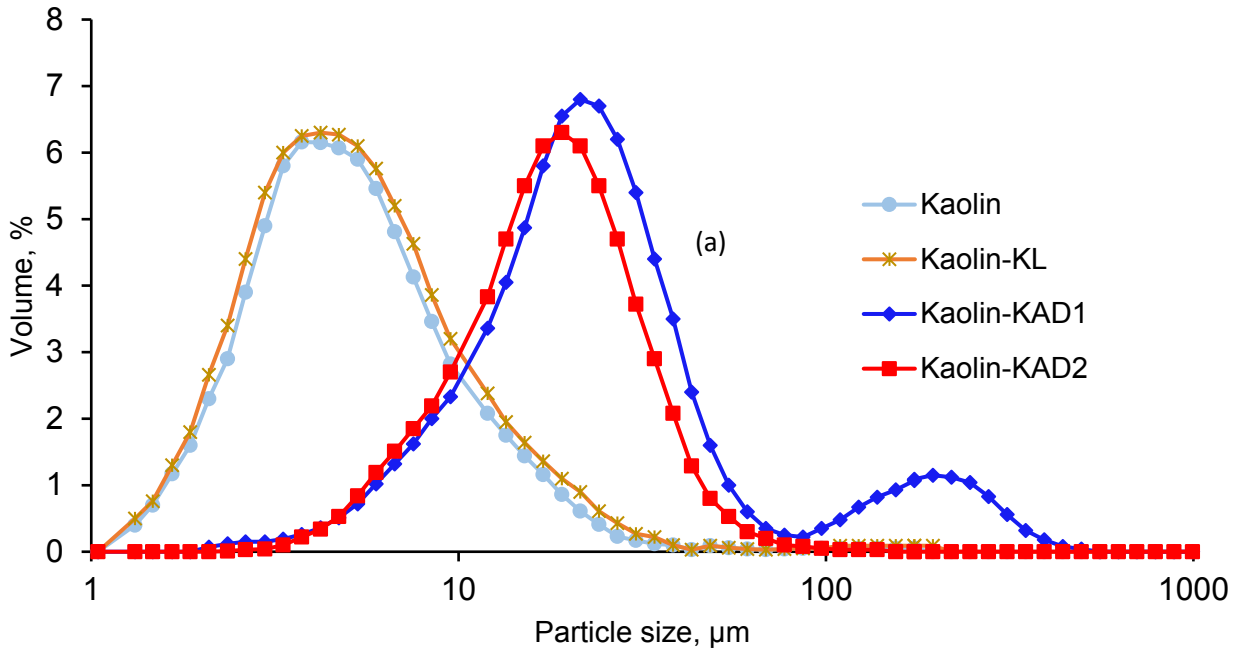

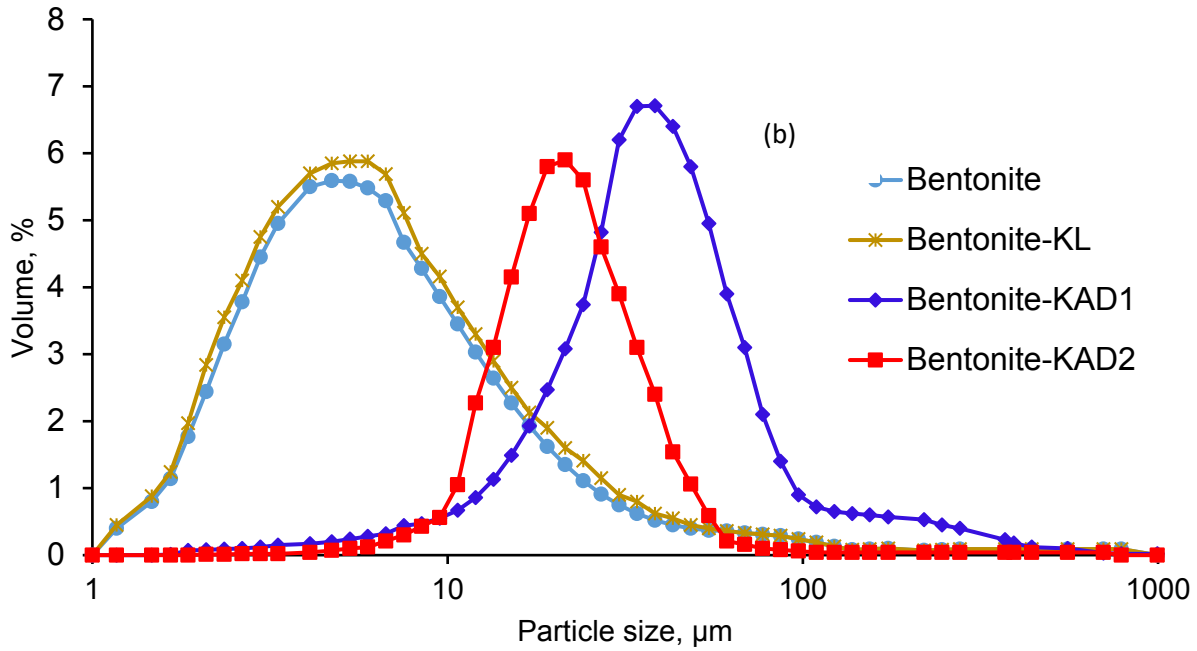

Figure 6.4. Particle size distribution of a) kaolin and b) bentonite particles in the presence and absence of KL or KAD conducted under the conditions of pH 7, 4 mg/g of polymer dosage, 25 °C and 0.4 g/L of clay concentration.

6.4.6 Influence of dosage on zeta potential

Figure 6.5 shows the effect of dosage of KAD on the zeta potential of kaolin and bentonite suspensions. The zeta potential of clay particles increased with increasing KAD dosages, indicating that the electrostatic attraction between the positively charged polymers and negative surface sites of the particle neutralized the surface charge of clay particles partly (Nasser and James, 2006). Changes in the zeta potential were more pronounced for KAD1 with the higher charge density as the zeta potential value reached +40 mV, while it reached 30 mV for KAD2 in the kaolin system. These results indicate the accumulation of higher amount of cationic charges in the diffused layer in the case of highly charged KAD1 sample (Gregory and Barany, 2011). Similar behavior was observed for bentonite particles, but the overall zeta potential remained anionic after adsorption of KADs. Untreated KL was not able to change the zeta potential of the clay suspension due to its insignificance adsorption (not shown). In one study, the zeta potential of cationic polymer

in bentonite suspension was reported to increase from -20 mV to +40 mV and +60 mV when its charge density increased from 5 to 35 mol % (Barany et al., 2010).

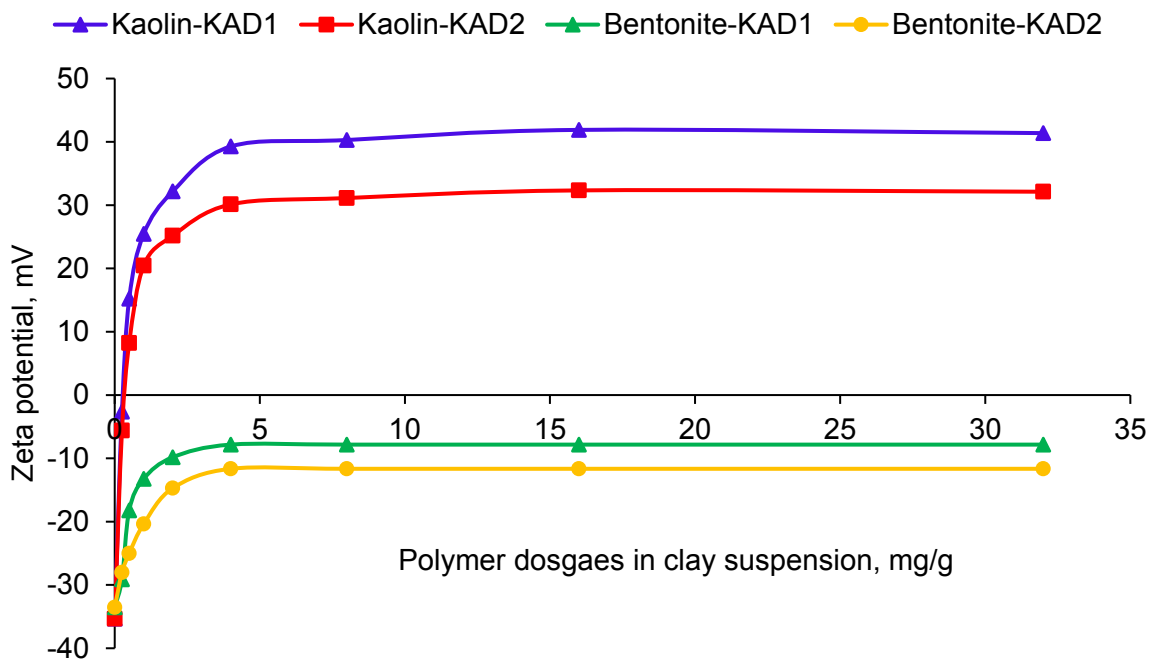

Figure 6.5. Zeta potential of kaolin and bentonite particles in the presence of KAD as a function of polymer dosage conducted under the conditions of pH 7, 2 h, 25 °C, and 0.4 g/L of clay concentration.

To understand if the zeta potential of clay particles is impacted by the overall surface charges of clay particles, the zeta potential of the suspensions was plotted as a function of theoretical surface charge density of clay particles (Figure 6.2c). In the absence of KADs, the zeta potential of the untreated kaolin suspension and the surface charge density of particles were -35 mV and -5.5 µeq/g, while those of bentonite were -33.5 mV and -9.4 µeq/g, respectively. Interestingly, both KADs impacted the zeta potential and surface charge density of particles in a similar fashion. After adsorption, the surface charge density of kaolin particles became positive and that of bentonite remained negative. As the surface charge density of kaolin theoretically remained negative but its zeta potential became positive, it is inferred that 1) a full surface coverage of KAD on kaolin particle was not required for a positive zeta potential, 2) adsorption of KAD on particles was such that it affected positively the potential of the diffused double layer of particles.

Contrarily, the negative zeta potential of bentonite particles indicated that the diffuse layer remained negatively charged due to less adsorption of KAD onto bentonite particles. As can be seen in Figure 6.6, KAD1 showed more pronounced zeta potential changes than did KAD2. This is due to the higher adsorption of KAD1, which could result in a higher surface charge density of the particles via charge neutralization and reversal of some of the charged sites on the surface of the particles. The negative theoretical surface charge density of particles indicated that the surface coverage provided by KADs was relatively small; thus, the overall theoretical surface charge density of the particles remained negative. This analysis provides evidence that the clay particles and KAD interaction was not based on stoichiometrical charge interaction.

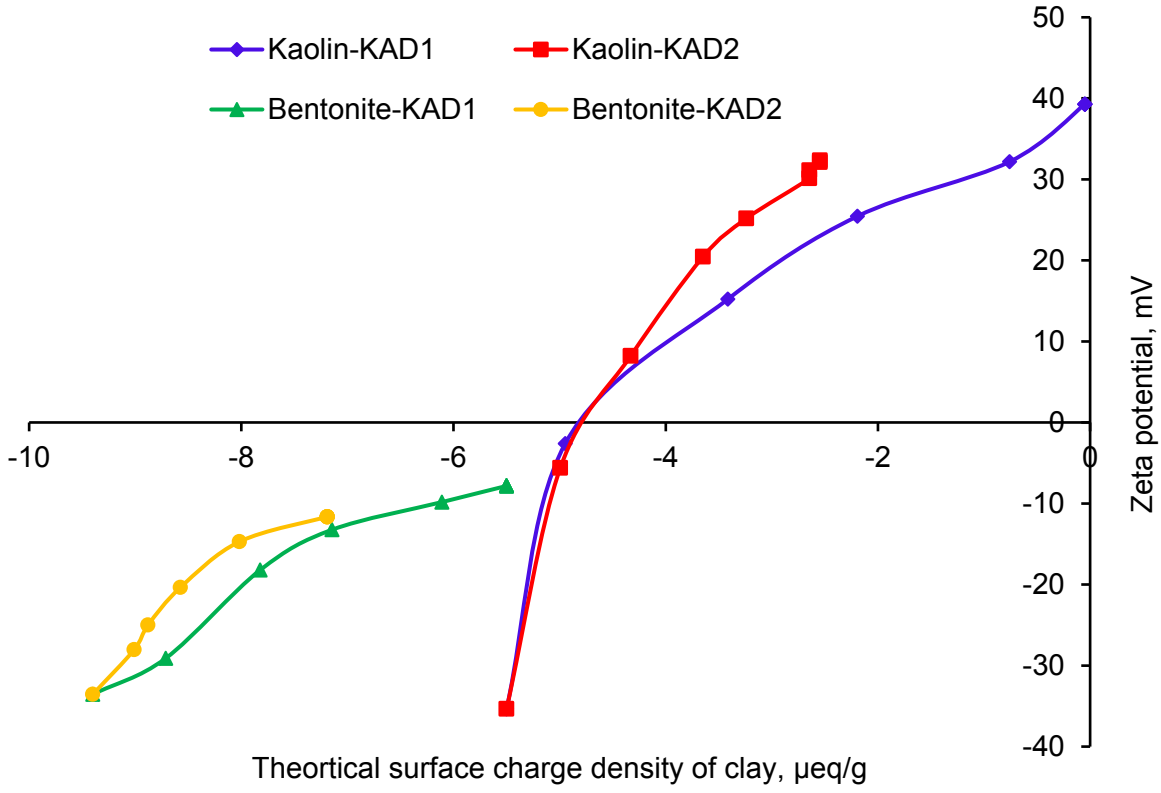

Figure 6.6. Zeta potential of kaolin and bentonite suspensions as a function of the theoretical surface charge density of particles, which was conducted under the conditions of pH 7, 2 h, 25 °C and 0.4 g/L of clay concentration.

6.4.7 Influence of KAD on relative turbidity

The influence of KAD on the relative turbidity and removal of kaolin and bentonite particles from the suspensions were presented in Figure 6.7. The relative turbidity of the clay suspensions decreased by increasing the concentration of KAD in suspensions. As can be seen, the minimum relative turbidity values for KAD1 (0.53) and KAD2 (0.61) were achieved at the dosage of 4 mg/g. By increasing the dosage to 4 mg/g in kaolin suspension, KAD1 and KAD2 led to 76.9 and 71.2 wt. % of clay removals, respectively. Similarly, the minimum relative turbidity values for KAD1 (0.20) and KAD2 (0.32) for bentonite suspension was obtained at 4 mg/g concentration. The removal of bentonite particles for KAD1 and KAD2 were found to be 96.2 and 84.6 wt. %, respectively (Figure 6.7b). These results were in agreement with their adsorption studies on kaolin and bentonite particles. Interestingly, a higher removal was obtained for bentonite particles than kaolin particles, which is possibly due to the large size of bentonite particles that could be removed more easily from the suspensions (Table 6.2 and Figure 6.4). It is also observable that the KAD1 induced a lower relative turbidity and more removal from the suspension systems, which could be attributed to its higher adsorption (Figure 6.2). Unmodified lignin (KL) did not affect the relative turbidity and removal of particles from the suspensions, which was due to its limited adsorption on particles (not shown). Chen (1998) showed that an increase in the cationic group of polyacrylamide from 10 to 50 mol % led to an increase in the turbidity removal of a clay suspension by 90 %. In one study, an increase in the charge density of cationic polyvinyl alcohol from 0.28 to 0.55 meq/g, led to 30 % clay removal at 3.0 wt. % polymer dosage (Sang and Xiao, 2008). In another report, the flocculation performance of polyacrylamide in palm oil mill effluents was reported to be improved by 98% when its cationic charge density increased from 9.6 to 97 % (Ariffin et al., 2005).

The effect of pH on the relative turbidity and removal of clay particles from the kaolin and bentonite suspensions was illustrated in Figure 6.7c. As pH increased from 2 to 10, the removal of bentonite (96.8 %) increased dramatically, while that of kaolin particles was 81.25 %. As discussed previously, a higher removal was achieved by bentonite because of its smaller surface area and larger particle size. Furthermore, these results suggested that, a higher suspension pH generated a higher overall negative charge on the clay particles, which resulted in more adsorption of KAD1

via electrostatic interactions on clay particles (Figure 6.2b) and a more pronounced reduction in the relative turbidity.

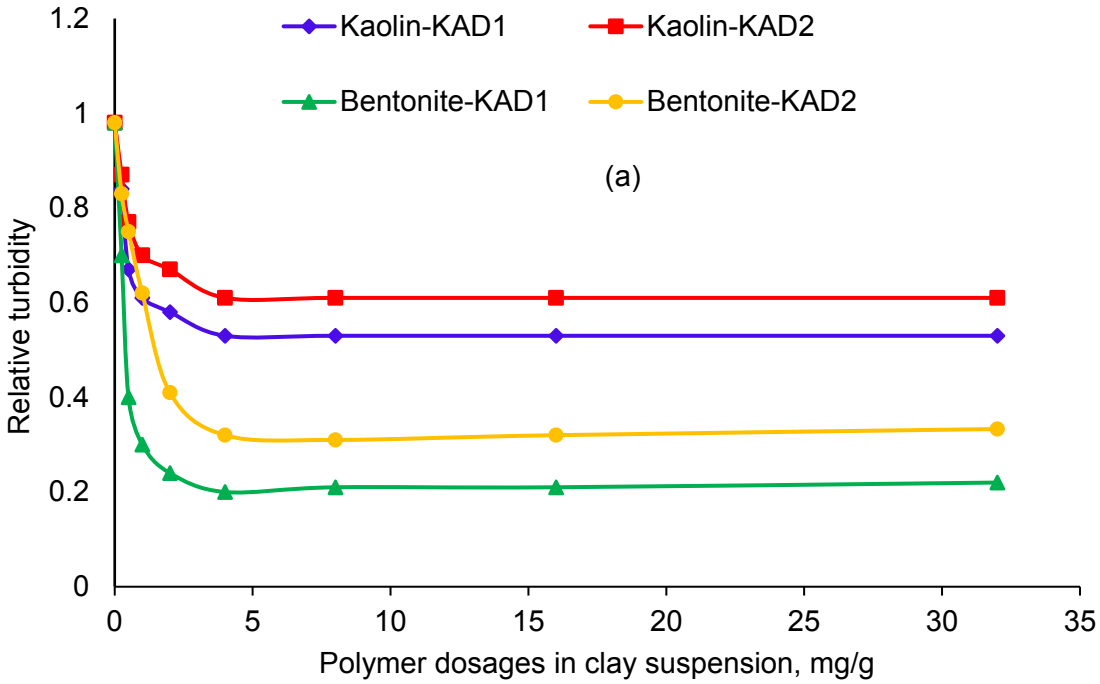

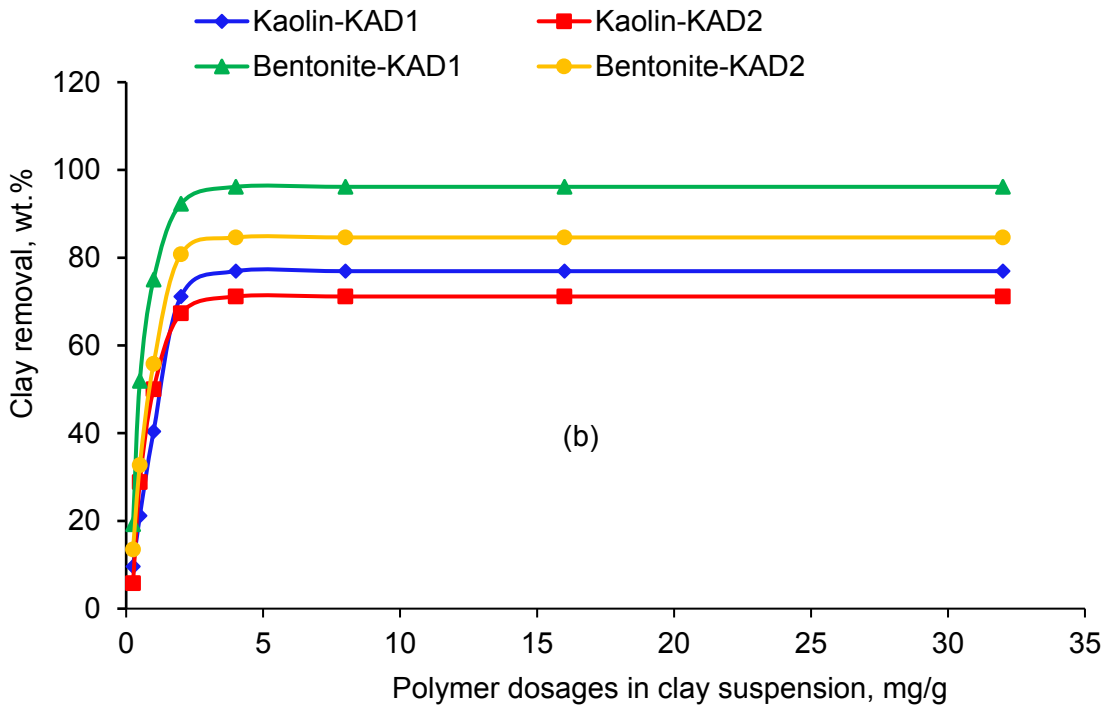

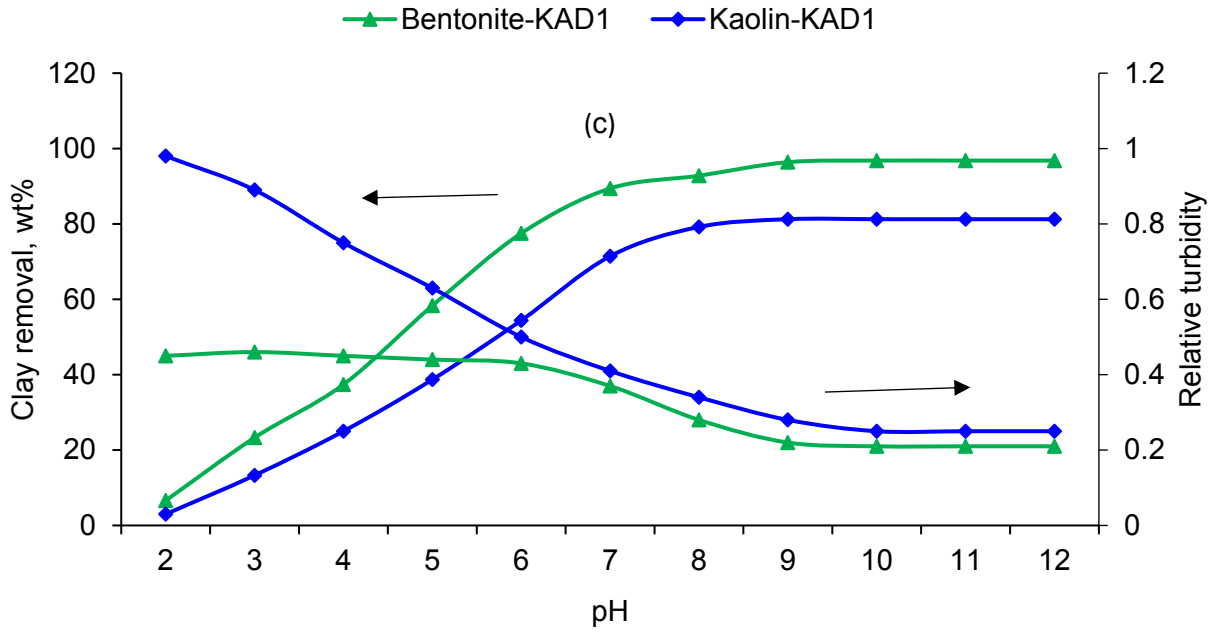

Figures 6.7. Influence of KAD dosage on the relative turbidity of a) kaolin and bentonite, b) the removal of kaolin and bentonite particles from suspensions, c) influence of pH on the relative turbidity and removal of kaolin and bentonite suspensions in the presence of KAD, under the conditions of 300 rpm, 2 h, 25 °C, and 0.4 g/L of clay concentration.

The effect of adsorbed KAD and the influence of the surface charge density of the particles on the relative turbidity of the suspensions are shows in Figure 6.8. At the same adsorption amount of KAD, a smaller relative turbidity was obtained for KAD1 than KAD2, which is due to the higher charge density and thus more effectiveness of KAD1 than KAD2 in flocculating particles. Thus, the higher adsorption affinity of KAD1 than KAD2 (Figure 6.2a) for kaolin and bentonite suspensions could be the reason for its more efficient flocculating performance (Figure 6.7a). However, due to larger size of bentonite particles (Table 6.2), the relative turbidity of bentonite suspension decreased more sharply than did that of kaolin. The points (S) in Figure 6.8a represent the saturation adsorption of KADs on particles. In this case, by adding more KADs to the suspensions, more unadsorbed KADs would remain in the suspensions (Figure 6.2). As the relative turbidity of the suspensions did not change for different KAD addition at this dosage, it can be claimed that the amount of adsorbed KAD played a crucial role in the relative turbidity of the particles, and unadsorbed KAD did not affect the relative turbidity of the suspensions.

Interestingly, the results in Figure 6.8b revealed that the surface charge density of the particles was a crucial factor in determining the relative turbidity of the particles, regardless of the charge density of KADs. To reach a certain level of surface charge density for particles, KAD2 was required to adsorb more than KAD1 as it had a lower charge density. However, the adsorption amount seems to only impact the overall adsorption of KADs and thereby affecting the surface charge density of particles (at a higher level of polymer adsorption), which remarkably affected the turbidity of the suspensions. At the same level of polymer adsorption, KAD1 was more effective as it introduced more charges to the surface of particles. Also, the influence of surface charges on the bentonite particles was more profound than on kaolin for reducing its relative turbidity.

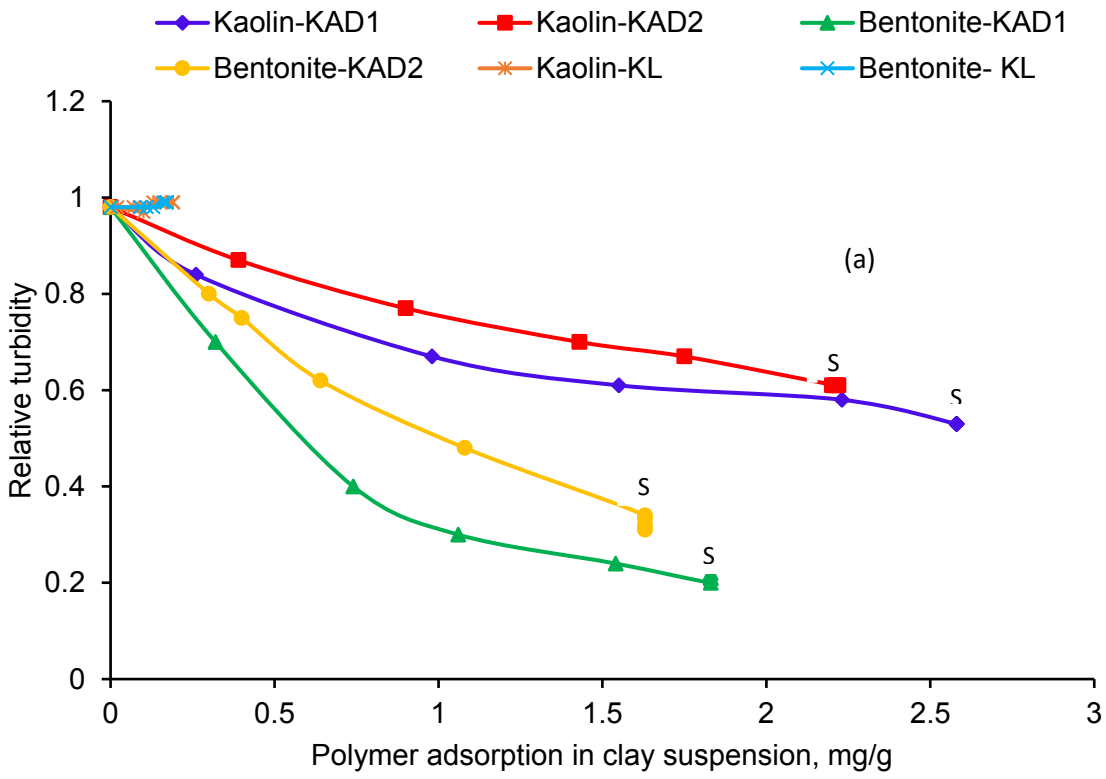

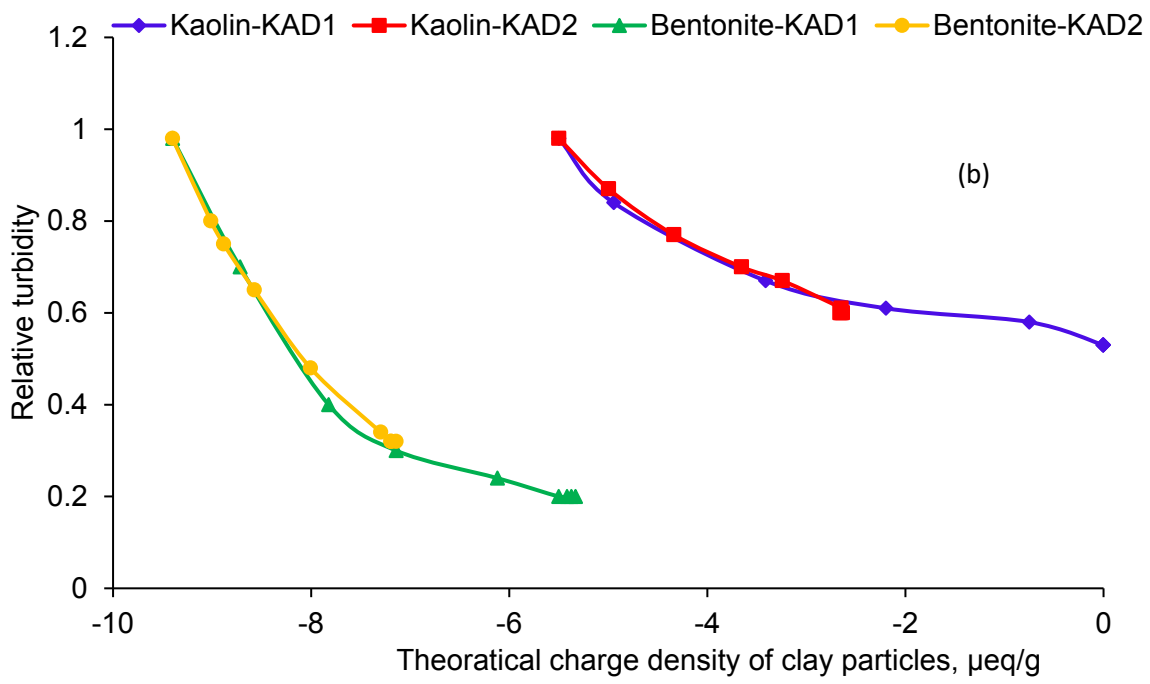

Figure 6.8. a) Effect of KAD adsorption amount on the relative turbidity of kaolin and bentonite suspensions, b) effect of the theoretical surface charges of the particles on the relative turbidity of kaolin and bentonite suspensions, under the conditions of pH 7, 2 h, 25 °C and 0.4 g/L of clay concentrations.

The flocculation mechanism of KAD in kaolin and bentonite suspensions can be predicted by plotting the relative turbidity of kaolin and bentonite suspensions as a function of zeta potential in Figure 6.9. In the case of kaolin suspension, the relative turbidity dropped gradually as the zeta potential of the suspensions was reversed. In contrast, the relative turbidity of bentonite suspension dropped more dramatically with a change in the zeta potential (even though the zeta potential was not reversed). Based on the results, it may be claimed that the charge neutralization was not a main factor for flocculation and the removal of kaolin particles, but it was for bentonite particles.

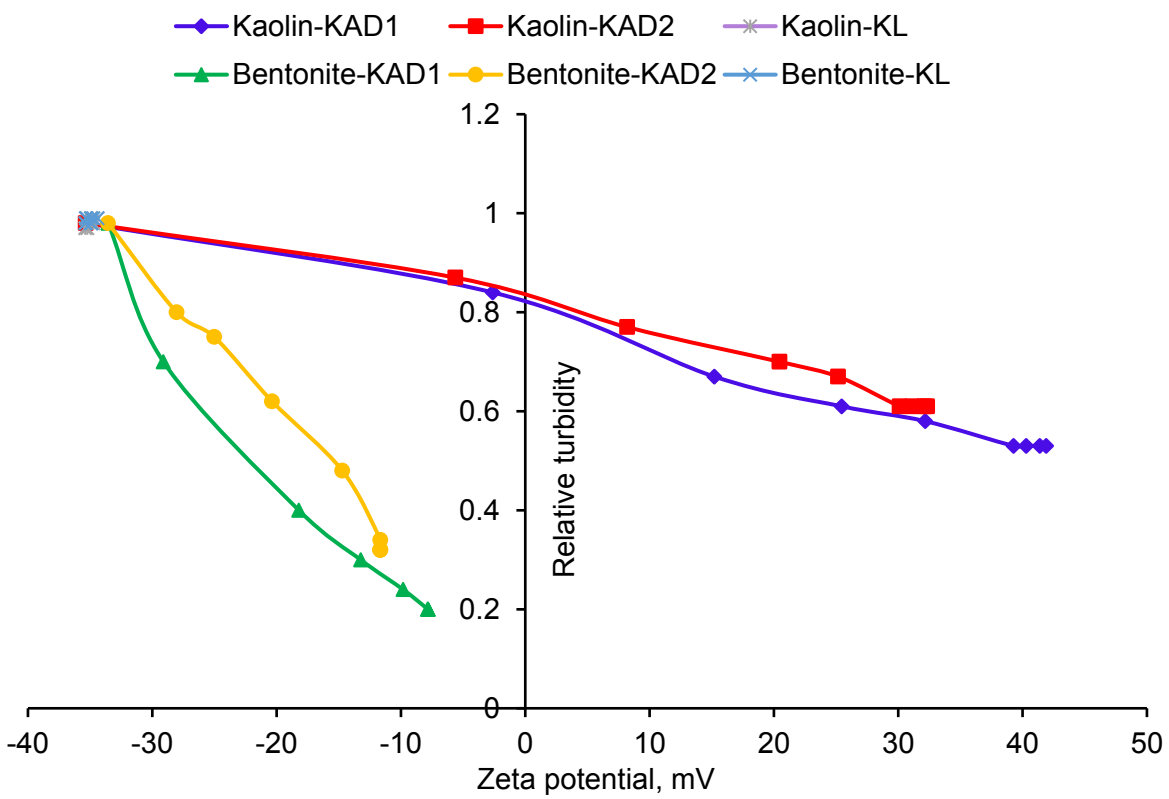

Figure 6.9. Effect of zeta potential of kaolin and bentonite suspensions on the relative turbidity of clay suspensions under the conditions of pH 7, 2 h, 25 °C and 0.4 g/L of clay concentration.

6.4.8 Influence of KAD on floc strength and recoverability

The variations in the FI of the suspension systems as a function of time were shown in Figure 6.10. The results show that the FI of kaolin suspension reached 1.4 at 300 rpm in the presence of KAD. This indicates the steady state floc growth, which depends on the dynamic balance between floc strength and the effective shear rate (Liimatainen et al., 2004). After adding KAD, both charge neutralization and bridging promote the aggregation of flocs. When the shear rate was enhanced to 3000 rpm, there was a rapid reduction in FI of the suspensions due to floc breakage. When the low shear rate was restored, floc regrowth occurred only to a limited extent. In order to analyze the floc breakage (T_{br}) and regrowth (T_{gr}), the floc strength and recovery of KAD polymers were calculated based on Eq. (6.3) and Eq. (6.5), respectively. As reported in Table 6.3, the higher value of T_{br} was obtained for KAD1 than for KAD2 at 3000 rpm in kaolin and bentonite systems, implying higher strength and resistance of the flocs for KAD1 system (Blanco et al., 2002). Since

regrowth takes place at 300 rpm, T_{gr} can be used as a means of determining the efficiency and the extent of regrowth. As can be seen at the 300 rpm, flocs formed via adding KAD1 achieved a more efficient regrowth compared to those formed via adding KAD2, indicating more efficient and a relatively faster regrowth capability. This phenomenon may be attributed to their aggregation mechanism. It was reported in the literature that polymer bridging is shear sensitive and nonrecoverable (Blanco et al., 2002). As the flocs are broken, the bridging polymer may undergo scission, and subsequently, a part of the partly detached KADs would reconfigure on the particles surface and lose their bridging affinity (Chen, 1998). However, polymer patching is less sensitive to shear and readily reforms the flocs (Gray and Ritchie, 2002). The results confirmed that KAD1 formed stronger flocs with a better regrowth efficiency. As stated earlier, polymers with a higher charge density tend to adsorb more strongly on the surface of particles and develop more flattened configuration. However, polymers with a lower charge density tend to develop tail and loop configuration promoting bridging. Therefore, stronger charge neutralization and polymer patching might be the reason for better performance of KAD1 than KAD2 (Zhu et al., 2009; Yukselena and Gregory, 2004).

Table 6.3. The floc breakage and regrowth of KADs under shear

	Sample	**T_{br}**	**T_{gr}**	**T_{br}**	**T_{gr}**
Shear rate (rpm)		3000	300	3000	300
Kaolin	KAD1	153	123	136	93
	KAD2	84	73	70	57
Bentonite	KAD1	90	75	59	33
	KAD2	77	60	55	27

On the other hand, as bentonite particles were larger than kaolin, KADs were generally weaker in patching or bridging them as the FI of bentonite system was lower than that of kaolin's and they were more sensitive to shear rates. Hence, flocs formed in bentonite suspension were weak and soft. However, the neutralization of their overall charges was helpful in their regrowth but not as much the flocs regrowth for kaolin systems. This was confirmed by lower floc breakage ($T_{br)}$ and regrowth (T_{gr}) values obtained for the bentonite system than for the kaolin system (Table 6.3).

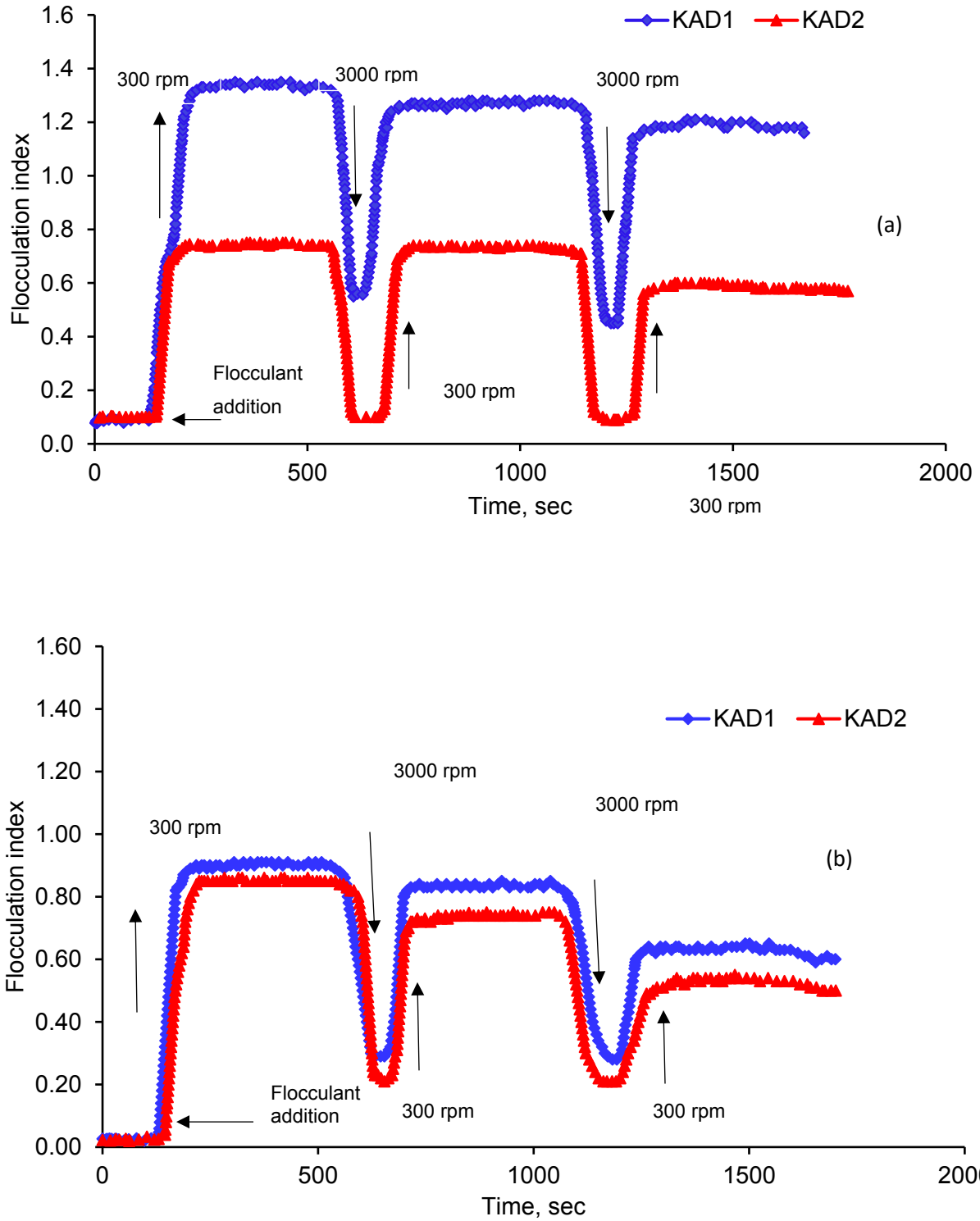

Figure 6.10. a) Flocculation index of a) kaolin and b) bentonite suspensions as a function of time conducted under the conditions of 8 mg/g KAD, 25 °C, and 0.4 g/L of clay concentration.

6.5 Conclusions

The interfacial tension between water and kaolin was reduced from 12.3 mN/m to 5.8 mN/m or 7.2 mN/m via adsorbing KAD1 or KAD2, indicating an increase in the wettability of the particles. Surface tension and contact angle results suggested an improved wettability of clay particles with increased adsorption of KAD1 or KAD2. The present study showed that the adsorption of KAD1 and KAD2 on kaolin particles (2.58 and 2.11 mg/g) was higher than that on bentonite (1.83 and 1.63 mg/g, respectively). The adsorption of KAD1 became more favorable by increasing pH. The zeta potential of the kaolin suspensions increased significantly from -35.3 to 39.3 and 30.1 mV due to the adsorption of KAD1 and KAD2; while, the zeta potential of bentonite particles was increased slightly from -33.5 to -7.8 and – 11.6 mV due to the low adsorption of KAD1 and KAD2, respectively. The more significant change in the zeta potential of kaolin was due to the higher adsorption of KAD on kaolin particles. KAD1 was more effective than KAD2 in flocculating kaolin and bentonite particles. However, the relative turbidity of bentonite was reduced more significantly than kaolin as its particles were larger, and thus more substantially affected by KADs. The relative turbidity of the particles was significantly affected by the overall charges introduced on the particles. It was observed that charge neutralization was the main factor in flocculating bentonite particles; whereas, polymer patching and/or bridging were the main factors for kaolin flocculation. The flocs formed by kaolin were stronger and showed better recovery than bentonite. KAD1 was also induced flocs with a higher strength than did KAD2.

6.6 References

Abdollahi, Z., Frounchi, Z., Dadbin, S. 2011. Synthesis, characterization and comparison of PAM, cationic PDMC and P (AM-*co*-DMC) based on solution polymerization. J. Ind. Engineering Chem., 3, 580-586.

Alfano, C.J., Carter, W.P., Gerli, A.1998. Characterization of the Flocculation Dynamics in a Papermaking System by Non-Imaging Reflectance Scanning Laser Microscopy. Nordic Pulp Paper Res. J., 13, 159–165.

Alfano, C.J., Carter, W.P., J.E. Whitten, J.E. 1999. Use of Scanning LaserMicroscopy to Investigate Microparticle Flocculation Performance. J. Pulp Paper Sci., 25, 189–195.

Ariffin, A., Shatat R.S.A., Norulaini, A.R.N., Omar, A.K.M. 2005. Synthetic polyelectrolytes of varying charge densities but similar molar mass based on acrylamide and their applications on palm oil mill effluent treatment. Desalination 173, 201-208.

Asselman, T., Garnier, G. 2000. Adsorption of model wood polymers and colloids on Bentonites, Colloids Surf. A Physicochem. Eng. Asp., 168, 175–182.

Barany, S., Meszaros, R., Marcinova, L., Skvarla, J. 2011. Effect of polyelectrolyte mixtures on the electrokinetic potential and kinetics of flocculation of clay mineral particles. Colloids Surf. A Physicochem. Eng. Asp., 383, 48–55.

Barany, S., Kozakova, I., Marcinova, L., Skvarla, J. 2010. Electrokinetic Potential of Bentonite and Kaolin Particles in the Presence of Polymer Mixtures. Colloid J., 72 (5), 595–601.

Ben, W., Yulian, Z., Chunbao, M., 2011. Preparation of Cationic Chitosan-Polyacrylamide Flocculant and Its Properties in Wastewater Treatment. J. Ocean Univ. China (Oceanic and Coastal Sea Research), 10, 42-46.

Besra, L., Senguptaa, D.K., Roy, S.K., Ay, P., 2002. Polymer adsorption: its correlation with flocculation and dewatering of kaolin suspension in the presence and absence of surfactants. Int. J. Miner. Process., 66, 183– 202.

Blanco, A., Fuente, E., Negro, C., Tijero, J. 2002. Flocculation Monitoring: Focused Beam Reflectance Measurement as a Measurement Tool, Can. J.Chem. Eng., 80, 1-7.

Blanco, A., Fuente, C., Negro, C., Monte, J., Tijero, J. 2001. FBRM as a Tool to Measure Flocculation**,** in TAPPI Papermakers Conf., Cincinnati, OH, March 11–14.

Chen, W. J., Ovenden, C. 1998. Effects of Surface Charge and ShearDuring Orthokinetic Flocculation on the Adsorption and Sedimentation of Kaolin Suspensions in Polyelectrolyte Solutions. Sep. Sci. and Tech. 33(4), 569- 590.

Chen, W.J., 1998. Effects of Surface Charge and Shear During Orthokinetic Flocculation on the Adsorption and Sedimentation of Kaolin Suspensions in Polyelectrolyte Solutions. Sep. Sci. technol., 33(4), 569-590.

Cipriano, B.H., Raghavan, S.R, McGuiggan, P.M. 2005. Surface tension and contact angle measurements of a hexadecyl imidazolium surfactant adsorbed on a clay surface. Colloids Surf. A Physicochem. Eng. Asp., 262, 8–13.

Ghimici, L., Constantin, M., Fundueanu, G., 2010. Novel biodegradable flocculating agents based on pullulan. J. of Haz. Mat., 351–358.

Gray, S.R., Ritchie, C.B., 2006. Effect of organic polyelectrolyte characteristics on floc strength. Colloids Surf. A Physicochem. Eng. Asp., 273,184–188.

Gregory, J., Barany, S. 2011. Adsorption and flocculation by polymers and polymer mixtures. Adv. in Coll. Inter Sci., 169, 1–12.

Hasan, A., Fatehi, P. 2018. Synthesis and characterization of lignin-acrylamide-(2-methacryloyloxyethyl) trimethyl ammonium chloride copolymer. J. Appl. Polym. Sci., 35, 46338.

Jahan, M. S., Liu, Z., Wang, H., Saeed, A., Ni, Y., 2012. Isolation and characterization of lignin from prehydrolysis liquor of kraft based dissolving pulp production. Cell. Chem. Technol., 46 (3–4), 261–267.

Kouisni, L., Holt-Hindle, P., Maki, K., Paleologou, M., 2012. The lignoforcesystem (TM): a new process for the production of high-quality lignin from black liquor. The Journal of Science & Technology for Forest Products and Processes, 2 (4), 6–10.

Liimatainen, H., Sirvio, J., Sundman, O., Visanko, M., Ninimaki, J., Hormi, O., 2011. Flocculation performance of a cationic biopolymer derived from a cellulosic source in mild aqueous solution. Bioresour. Technol., 102, 9626–9632.

Liimatainen, H., Haapala, A., Niinimaki, J. 2004. Fibre floc morphology and dewaterability of a pulp suspension: role of flocculation kinetics and characteristics of flocculation agents. BioResour., 4(2), 640-658.

Lu, S., Lin, S., Yao, K. 2004. Study on the synthesis and application of starch-graft poly (AM-co-DADMAC) by using a complex initiation system of CS-KPS. Starch– Starke, 56, 138–143.

Miranda, R., Blanco, A., Fuente, E., Negro, C. 2008. Separation of contaminants from deinking process water by dissolved air flotation: effect of flocculant charge density. Sep. Sci. Technol., 43, 3732–3754.

Nasser, M.S., James, A.E., 2006. The effect of polyacrylamide charge density and molecular weight on the flocculation and sedimentation behaviour of kaolinite suspensions. Sep. Pur. Technol., 52, 241–252.

Nurmi, N., Wallin, S., Eklund, D. 2006. The effect of molar mass and charge density of cationic polyacrylamide on the flocculation of dissolved and colloidal substances in thermomechanical pulp water. J. pulp and paper sci., 32(1), 43-46.

Oveissi, F., Fatehi, P. 2014. Isolating lignin from spent liquor of thermomechanical pulping process via adsorption. Env. Tech., 35(20), 2597-2603.

Ponnusamy, T., Lawson, L.B., Lucy C. Freytag., L.C., Blake, D.A., Ayyala, R.S., John, V.T. 2012. In vitro degradation and release characteristics of spin coated thin films of PLGA with a "breath figure" morphology. Biomatter, 2, 77–86.

Piana, G.D., Lafuma, S., Audebert, R. 1987. Flocculation and adsorption properties of cationic polyelectrolytes toward Na-montmorillonite dilute suspensions. J. Colloid Interf. Sci., 119(2), 474-480.

Pouteau, C., Dole, P., B. Cathala, B., Averous, L., Boquillon, N. 2003. Antioxidant properties of lignin in polypropylene. Polym. Degrad. Stab., 81, 9-18.

Ramphal, S.R., and Sibiya, M. S. 2014. Optimization of coagulation-flocculation parameters using a photometric dispersion analyser. Drink. Water Eng. Sci., 7, 73–82.

Razali, M. A. A., Ahmad, Z., Ahmad, M.S.B., Ariffin, A. 2011. Treatment of pulp and paper mill wastewater with various molecular weight of polyDADMAC induced flocculation. Chem. Eng. J., 166, 529–535.

Razali, M.A.A., Ariffin, A., 2015. Polymeric flocculant based on cassava starch Grafted polydiallyldimethylammonium chloride: Flocculation behavior and mechanism. M. Appl. Surf. Sci., 351, 89–94.

Razali, M.A.A., Ismail, H., Ariffin, A. 2015. Graft copolymerization of polyDADMAC to cassava starch: Evaluation of process variables via central composite design. Ind. Crops Prod., 65, 535–545.

Sang, Y., Xiao, H. 2008. Clay flocculation improved by cationic poly (vinyl alcohol)/anionic polymer dual-component system. J. Colloid and Interface Sci., 326, 420–425.

Schmidt, C.U., Lagaly, G.V. 1999. Surface modification of bentonites" I. Betaine montmorillonites and their rheological and colloidal properties. Clay Miner., 34, 447-458.

Somasundaran, P, Zhang, L. 2006. Adsorption of surfactants on minerals for wettability control in improved oil recovery processes, J. Pet. Sci. Eng., 52, 198–212.

Szymczyk, K., Jańczuk, B. 2011. Wettability of Polymeric Solids by Aqueous Solutions of Anionic and Nonionic Surfactant Mixtures. J. Adhes. Sci. Technol., 25, 2641-2657

Wang, J. P., Chen, Y.Z., Wang, Y., Yuan, S.J., Sheng, G.P., Yu. H. Q. 2012. A novel efficient cationic flocculant prepared through grafting two monomers onto chitosan induced by Gamma radiation. RSC Adv., 2, 494–500.

Wang, S., Konduri, M.K.R., Hou., Q., Fatehi, P. 2016. Cationic xylan-METAC copolymer as a flocculant for clay suspensions. RSC Adv., 6, 40258-40269.

Wang, J. P., Chen, Y.Z., Wang, Y., Yuan, H. Q., Yu., H.Q. 2011. Optimization of the coagulation-flocculation process for pulp mill wastewater treatment using a combination of uniform design and response surface methodology. Water Res., 45, 5633-5640.

Wang, L.J., Wang, J. P., Zhang, S. J., Chen, Y. Z., Yuan, S. J., Sheng, G. P., Yu, H. Q. 2009. A water-soluble cationic flocculant synthesized by dispersion polymerization in aqueous salts solution. Sep.Purif. Technol., 67(3), 331-335.

Wang, D., Gregory, J., Tang, H. 2008. Mechanistic Difference of Coagulation of Kaolin Between PACl and Cationic Polyelectrolytes: A Comparative Study on Zone 2 Coagulation. Dry. Technol., 26, 1060–1067.

Wang, J.P. Yuan, S. J., Wang, Y., Yu, H. Q. 2013. Synthesis, characterization and application of a novel starch based flocculant with high flocculation and dewatering properties. Water Res., 47 (8), 2643-2648.

Wickramasinghe, S.R., Wu, Y., Han, B. 2002. Enhanced microfiltration of yeast by Flocculation. Desalination, 147, 25-30.

Xie, C., Feng, Y., Cao, Xia, Y., Lu, Z. 2007. Novel biodegradable flocculating agents prepared by phosphate modification of Konjac. Carbohydr. Polym., 67, 566–571.

Yukselena, M.A., Gregory, J. 2004. The reversibility of floc breakage. Int. J. Miner. Process. 73, 251– 259.

Ye, Q., Zhang, Z., Ge, X. 2003. Highly Efficient Flocculant Synthesized through the Dispersion Copolymerization of Water Soluble Monomers Induced by γ-Ray Irradiation: Synthesis and Polymerization Kinetic. J. Appl. Polym. Sci., 89, 2108 –2115.

Yu, W., Gregory, J., Campos, L. 2010. The effect of additional coagulant on the re-growth of alum–kaolin flocs. Sep. Pur. Technol., 74, 305–309

Zakzeski, J., Bruijnincx, P.C., Jongerius, A. L., Weckhuysen, B.M. 2010. The Catalytic Valorization of Lignin for the Production of Renewable chemicals. Chem. Rev., 110, 3552–3599.

Zhu, R., Cui, S., Wang, X. 2010. Theoretical foundation of Zisman's empirical equation for wetting of liquids on solid surfaces. Eur. J. Phy., 31, 251-256.

Zhu, Z., Li, T., Lu, J., Wang, D., Yao, C. 2009. Characterization of kaolin flocs formed by polyacrylamide as flocculation aids. Int. J. Miner. Process. 9, 94–99.

Chapter 7: Impact of kraft lignin-based flocculants on the flocculation and sedimentation behaviour of kaolin suspensions

7.1 Abstract

Currently, kraft lignin is burned in the recovery cycle of the kraft pulping process; but it can be extracted and modified to produce value-added products. In this work, kraft lignin (KL) was polymerized with 2-[(methacryloyloxy) ethyl] trimethylammonium chloride (DMC) to produce cationic water soluble polymers. Five polymers of different molecular weights and charge densities were produced and their flocculation efficiency in kaolin suspensions was investigated. The adsorption, zeta potential and flocculation results confirmed that the polymer with the highest charge density and molecular weight (KLD5) was a more effective flocculant than other polymers. The structure and size of flocs formed via interaction of kaolin and KLD were determined by a focused beam reflectance measurement (FBRM). Furthermore, 8 and 32 mg/g of KLD5 addition to the kaolin suspension increased the chord length of particles from 53.12 to 65.3 μm, respectively. Sedimentation studies conducted under gravitational force (vertical scan analyzer) and centrifugal force (Lumisizer analytical centrifuge) revealed that KLD5 was more effective in flocculating the kaolin particles. The sediment compactness of KLDs decreased by increasing the settling velocity. For instance, at 32 mg/g dosage, the sediment compactness of KLD5 was found to be to 10.85 g/L with settling velocity of 173.40 mm/h. Under centrifugal forces, KLD5 generated the highest settling velocity (684 mm/h) and floc size (15.45 μm) at 32 mg/g of polymer concentration. The results showed that, the fractional dimension of KLD flocs, D_f, ranging from 1.82 to 1.35, indicates the formation of porous floc in interaction of KLD and kaolin.

7.2 Introduction

Industrial wastewater contains a wide range of toxic inorganic and organic matters (e.g., heavy metals, suspended particles, and aromatic molecules) imposing environmental pollutions (Pal et al., 2011; Fang et al., 2010). Flocculation processes have been used for treating wastewater for decades. Since most naturally occurring colloids are predominantly negatively charged, the

addition of cationic polymers is an effective means to isolate suspended particles from wastewater effluents (Ghimici et al., 2010; Petrak et al., 2015).

Synthetic organic polymers, such as cationic polyacrylamide (PAM) and poly diallyldimethylammonium chloride (PDADMAC), have been extensively applied as flocculants in wastewater of mineral processing and papermaking operations (Sun et al., 2015; Zhu et al., 2009; Yu et al., 2006; Yan et al., 2004; Solberg and Wagberg, 2003). These polymers reported to form larger and stronger flocs with acceptable settling performance, thus allowing their effective removal (Yang et al., 2016). Despite their wide range of applications, they are non-biodegradable, expensive and sometime cause health hazards (Pal et al., 2011; Yang et al., 2016).

Recently, considerable attention has been paid to producing environmentally friendly polymers due to their biodegradability and renewability (You et al., 2009). Natural polymers such as starch, chitosan, and cellulose, have been widely applied as flocculants in wastewater treatments (Tian and Xie, 2008). In addition, cationic polysaccharides, such as chitosan (Wang et al., , 2009), cellulose (Gao et al., 2016; Sirvio et al., 2011), and starch were produced and used as flocculants in different wastewater effluents (Li et al., 2015a; Yu et al., 2009; Wei et al., 2008; Pal et al., 2005). These polymers have a wide range of applications and are food source for human. Therefore, their usage as flocculants may not be very appealing. Despite its vast production, lignin has been an under-utilized product of the pulping industry. The first objective of this work was to produce cationic lignin polymers via polymerizing lignin and (2-methacryloyloxyethyl) trimethyl ammonium chloride (DMC) to be used as a flocculant for wastewater effluents.

When flocculants adsorb on particles, they change the physicochemical properties of the particles, which leads to their agglomeration following altered mechanisms (Yan et al, 2004; Yu et al, 2006; Li et al., 2006; Ghimici et al., 2010). Numerous investigations have demonstrated that flocs formed through bridging of particles can be settled readily (Gregory and Barany, 2011; Abraham et al., 2001; Rapp et al., 2015; Johnson et al., 2016, Du et al., 2010; Yukselen and Gregory, 2004), while flocs formed via charge neutralization and patching are more difficult to sediment (Gregory, 1988; Yu et al., 2006; Gregory and Barany, 2011; Wiśniewska et al., 2012). As it is unclear how lignin-based polymers would agglomerate particles, the second objective of this work was to investigate how the charge density and molecular weight of lignin-based

polymers impact the formation and settling of agglomerated kaolin flocs. In flocculation process, the settling behaviour of flocs can be related to its size and fractal dimension (D_f) (Li et al., 2015b). Previous reports stated that D_f played a crucial role in determining the density and porosity of the flocs (Vahedi and Gorczyca, 2012; Rong et al., 2013b; Spicer et al., 1998). Larger flocs reported to have less compact and more porous structures compared to the smaller ones (Dyer and Manning, 1999; Li et al., 2015b). Flocs with the D_f of 3 were considered compact, whereas flocs with a D_f close to 1 were reported to have loose, stringy, and voluminous structures (Adachi et al., 2012; Li et al., 2015c; Bowers et al., 2017). Also, porous aggregates have larger hydrodynamic radius than highly dense solid particles of the same mass. The third objective of this study was to determine the D_f of flocs formed via interacting cationic lignin polymers and relate it to the properties of cationic lignin polymers.

Furthermore, it was reported that the floc size, density, and porosity impact the settling performance of flocs (Kumar et al., 2010; Lapointe and Barbeau, 2016; Li et al., 2015c; Sun et al., 2015; Zhu et al, 2009; Bushell et al., 2002). The structure of the flocs may experience two possible consequences that impact their settling behaviour significantly: 1) the non-spherical shape of flocs, which may increase the drag when settled and 2) the porosity of flocs that increases permeability and thus reduces the drag force for settling. Therefore, knowledge of floc structure can play significant role in understanding the settling performance of flocs (Tang et al., 2002; Bushell et al., 2002; Chuah et al., 2015). Johnson et al. (1996) demonstrated that porosity and permeability significantly increase the settling velocity of flocs. Winterwerp and Kesteren (2004) concluded that flocs may be treated as sufficiently impermeable to neglect the effects of flow through the floc on settling velocity. The fourth objective of this work was to determine the fractal dimension of flocs and correlate them to flocs settling performance.

In this study, kraft lignin-based polymers were produced via free radical polymerization of DMC and lignin. The flocculation behaviour of the polymers (KLD) with different molecular weights and charge densities was investigated in a kaolin suspension for the first time. The main novelty of this work was the correlations developed among the properties of lignin-based polymers, their flocculants performance, floc properties, and settlement under different conditions using advanced tools.

7.3 Materials and Methods

7.3.1 Materials

Softwood kraft lignin was produced via LignoForce^{TM} technology of FPInnovations in Thunder Bay, ON (Kouisni et al., 2012). 2-[(methacryloyloxy) ethyl] trimethylammonium chloride (DMC) (80% in water), potassium persulfate ($K_2S_2O_8$) (analytical grades) and kaolin were obtained from Sigma-Aldrich company. Polydiallyldimethylammonium chloride (PDADMAC) with the molecular weight (M_w) of 100,000–200,000 g/mol was obtained from Sigma Aldrich Company and diluted to 0.005 M prior to use. Potassium polyvinyl sulfate (PVSK) with a M_w of 100,000–200,000 g/mol (97.7% esterified) was provided by Wako Pure Chem. Ltd. Japan. All chemicals were applied without further purification. Moreover, ethanol (95 vol. %) was received from Fisher Scientific company. Silicon oil and tetrafluoroethylene were received from formulation and used as standard chemicals for transmission and backscattering detectors of a vertical scan analyzer, respectively.

7.3.2 Lignin-DMC production and purification

Kraft lignin- DMC polymers were synthesized in 250 mL three-neck glass flasks under the reaction conditions illustrated in Table 7.1. After the reactions, the flasks were submerged in cold tap water for 20 min. Then, ethanol (80 vol. % in water) was mixed with the reaction media to precipitate the lignin-based polymers from the system (Wang et al., 2015). By adding ethanol to the reaction media, the solution reactions became suspensions. The suspension was centrifuged at 3500 rpm for 10 min in order to collect the precipitated copolymer (KL-DMC) and remove the homopolymer (PDMC) and unreacted monomers (DMC) present in the supernatant. After collection of the precipitates, they were mixed with ethanol (80 %v) for 5 min. Then, the mixtures were centrifuged again, and this process was repeated 3 times and the final product is considered lignin polymer, KLD. Subsequently, the precipitated KLD polymers were mixed with 200 mL of deionized water and the pH of the solution was adjusted to 7.0 ± 0.2 prior to use. After centrifugation, the solution containing the lignin-DMC polymer was dried at 105 °C, and the dried samples were kept for flocculation studies. This lignin-DMC polymer is denoted as KLD, while unmodified kraft lignin is denoted as KL in this work.

7.3.3 Solubility and charge density determination

To measure the solubility of the KLD products, 0.2 g of the polymers were added to 20 mL of deionized water by stirring at 100 rpm and 30 °C for 1 h in a water bath shaker (Innova 3100, Brunswick Scientific, Edison, NJ, USA). Then, the suspensions were centrifuged at 1000 rpm for 5 min. The supernatants were collected and used for analyzing the charge density and solubility of the polymer. The concentration of polymers in the supernatants was determined by drying the supernatants at 105 °C, and the solubility was determined based on the concentration of KLD in the supernatants and the initial concentration of polymers. The charge density of the polymers was measured by a particle charge detector, Mütek PCD 04 titrator (Herrsching, Germany) with a PVSK solution (0.0050 M) (Wang et al., 2015). The reported data in this experiment is the average of three repetitions.

7.3.4 Molecular weight analysis

About 5 mg sample of dried KLD polymers was dissolved in 10 mL of 5.0 wt. % acetic acid solution by stirring at 600 rpm for 48 h and 35°C, then the solutions were filtered with a 13 mm diameter nylon filters (pore size 0.2 μm). The filtered solutions were used for molecular weight analysis, which was carried out using a Malvern, GPCmax VE2001 Module + Viscotek system with viscometer and UV detectors. In this analysis, PolyAnalytic columns were used, and a 5.0 wt. % acetic acid was used as a solvent and eluent with the flow rate of 0.7 mL/min. The column temperature was set to 35 °C. Poly ethylene oxide was used as standard polymer for calibration of the system.

7.3.5 Elemental analysis

The elemental analysis of the samples was performed for KL and KLD polymers using an elemental analyzer, Elementar Vario EL Cube, by the combustion method (Jahan et al., 2012). The samples were first dried in an oven at 105 °C overnight to remove any moisture prior to analysis. Approximately, 2 mg of the dried samples were transferred into the carousel chamber of the elemental analyzer and combusted at 1200 °C to reduce the generated gasses for analyzing carbon, hydrogen, oxygen, and nitrogen contents of the samples.

7.3.6 Particle size analysis

The hydrodynamic diameter of kaolin particles and flocs of KLD/kaolin was analyzed using a MasterSizer 2000 particle size analyzer (Malvern Instruments). In this study, 1.0 g of clay suspension (20 g/L) was added to 50 mL of deionized water or 50 mL of KL or KLD solution so that KL or KLD dosage in the system remained at 8 and 32 mg/g dosage (based on kaolin). The system was stirred at 300 rpm and room temperature for 2 h. After stirring, the samples were analyzed for their particle size distribution. The measurement was conducted at the wavelength of 633 nm with red laser light, and the hydrodynamic diameter (d_h) of the particles was determined. The mean value d_h was determined as the average median value of three parallel measurements.

7.3.7 Adsorption studies

In this set of experiments, different amounts of KL or KLD were added to 50 mL of kaolin (clay) suspensions (0.4 g/L) to make 1 to 128 mg/g dosage of KL or KLD in clay suspensions for studying the adsorption of KL or KLD on clay particles. The suspensions were stirred at 300 rpm for 1 h at room temperature. Afterward, the suspensions were centrifuged for 15 min at 3500 rpm and then the concentrations of the KLD remained in the supernatants were determined by a UV/Vis spectrophotometer (Genesys 10S UV/vis, Thermo FisherScientific, USA) at the wavelength of 205 nm. The impact of pH was also studied on the adsorption of KLD on clay particles. The pH of the suspensions (ranging 2 to 12) was adjusted with 0.1 M NaOH solution or H_2SO_4 prior to adsorption experiments, and the steps indicated above were followed accordingly. Three repeats were carried out, and the average values were reported in the study.

7.3.8 Zeta potential analysis

The zeta potential of clay suspensions was characterized by a NanoBrook Zeta PALS (Brookhaven Instruments Corp, USA). In this study, 1 g of clay suspension (20 g/L) was added to 50 mL of deionized water and stirred at 300 rpm for 1 h and room temperature. Then, its zeta potential was measured in a 1.0 m M KCl aqueous solution. The pH of the clay suspensions was adjusted by using 0.1 M NaOH or H_2SO_4. All the measurements were carried out at room temperature with a constant electric field (8.4 V/cm). Three repeats were carried out for zeta potential measurement and the mean value was reported.

7.3.9 Flocculation analysis

In this experiment, the relative turbidity of the suspension was determined using a photometric dispersion analyzer (PDA 3000, Rank Brothers Ltd) connected to a dynamic drainage jar (DDJ) fitted with a 200-mesh screen (Wang et al., 2016). The variation in direct current (DC) voltage of the PDA instrument is an indicator of the average transmitted light intensity of the suspension passing through the PDA (Yu et al., 2010). In this study, 500 mL of distilled water was first added to the DDJ container and circulated from the DDJ to the PDA through a 3 mm plastic tube (Tygon, R-3603) until a steady flow rate of 20 mL/min was achieved. The flow rate was regulated by a peristaltic pump throughout the experiment. Then, 10 mL of a 20 g/L clay suspension was added into the DDJ (to make a 0.4 g/L clay concentration in DDJ) while stirring at 300 rpm. This caused a decrease from the initial base DC voltage (V_0) to a new DC voltage (Vi) in the PDA analyzer. After 100 s, KL and KLD were added to the DDJ to make a dosage between 1 and 128 mg/g KL or KLD based on clay. The increase in the DC voltage was represented as the DC voltage (V_f) of the final suspension. The effects of KLD dosage on the flocculation were studied. The relative turbidity of the clay suspensions was measured using equation 7.1 (Wang et al., 2009).

$$\text{Relative turbidity, } \tau_r = \frac{\tau_f}{\tau_i} = \frac{ln(\frac{V_0}{V_f})}{ln(\frac{V_0}{V_i})} \qquad (7.1)$$

where τ_f denoted the final suspension turbidity, and τ_i represented the initial suspension turbidity. All the experiments were performed in triplicates, and the mean values were reported in the study.

7.3.10 Flocculation analysis under dynamic conditions

The change in the size of kaolin and KLD/kaolin flocs was assessed in a real-time scenario using a focused beam reflectance measurement (FBRM, Mettler-Toledo E25). FBRM uses a focused beam laser light that scans across particles passing in front of the probe window to measure a chord length of the flocs. This distribution of the size depends on the shape, size, and concentration of the particles (Negro et al., 2006). The chord length distribution was acquired directly by using 90 log-channels over the range of 1 and 1000 µm using IC-FBRM software (Fatehi et al., 2016). Each particle's chord length is defined as a count and thus the counts of chord length in a specific channel can represent the number of particles with a similar chord

length in that particular channel. The counts of particles with different chord lengths were expressed as chord length distribution. In this set of experiments, 500 mL of distilled water was first added to the container. Then, 10 mL of a 20 g/L clay suspension was added (to make a 0.4 g/L clay concentration) while stirring at 300 rpm. The laser probe with a diameter of 25 mm was immersed in a suspension, the beam was rotated around the axis of the probe at a scan speed of 2 m/s with the scan diameter of 5 mm (Boxall et al., 2011) The focal point was set to -20 μm (as default), and the scan duration was set at 3 s (Boxall et al., 2011). This experiment was conducted for the suspensions containing KLD with the dosages of 8 mg/g and 32 mg/g based on dried weight of clay particles in the suspensions.

7.3.11 Gravitational sedimentation analysis

The flocculation and sedimentation performance of kaolin particles under static conditions in the absence or presence of KLD were assessed by a vertical scan analyzer, Turbiscan (Lab Expert, Formulaction). In this analysis, different dosages of KLD were added to the kaolin suspension. After stirring at 300 rpm for 2 min, 20 mL suspensions were added to the cylindrical glass cells for further analysis. Electro luminescent diode light at 880 nm scanned the cell from bottom to top at 40 μm height interval. The scanning process was conducted every 25s and the experiment lasted for 1 h (He et al., 2016). For each scan, a transmission detector received the light transmitted through the sample at 180° from the incident light, and a backscattering sensor received the light backscattered by the sample at 45° from the incident, the data was shown as transmission and backscattering data as a function of the height of sample (Mengual et al., 1999; Jarvis et al., 2005), which were used for evaluating the settling efficiency and calculating the sediment thickness and settling velocity.

Particles of different sizes produced by KLD would settle at different rates when flocculated. This settlement would clear the top part of the sample. The variations in transmission and backscattering data, collected from the top and bottom parts of the sample after settling for 1 h, were considered for evaluating the efficiency of KLD in flocculating kaolin suspensions.

The compactness of the sediment was determined as the ratio of the mass to volume for the settled flocs after 1 h of settling. In this set of experiments, samples were collected from the top part of the suspension before and after 1 h of treating with KLD, and dried in the oven at 105 °C overnight. The concentrations of clay in these samples were determined, which facilitated the

identification of settled mass after 1 h. In this analysis, the settling velocity of the flocs was determined as the rate of sediment thickness growth with respect to time (Waite et al., 2001).

The hydrodynamic diameter of the suspended particles in the system ($d_{h,s}$) was determined by the transmission data from top layer and the mean volume fraction of particles after settling for 1 h, obtained from Turbiscan software based on Lambert-Beer law (equations 7.2 and 7.3).

$$\mathrm{T}(l, r_i) = T_0 e^{-\frac{2r_i}{l}} \qquad (7.2)$$

$$l\left(d_{h,s}, \phi_s\right) = \frac{2d_{h,s}}{3\phi_s Q_s} \qquad (7.3)$$

where r_i is the internal radius of the measurement cell, l is photo mean free path, T_0 is the transmittance of continuous phase (i.e., water), and T is the transmittance of suspension (i.e., kaolin suspension) (Mengual et al., 1999; He et al., 2016). Therefore, the transmission data collected by the instrument directly depended on the mean hydrodynamic diameter of the suspended particles, $d_{h,s}$, and their volume fraction, ϕ_s. This study helped develop a relationship between the diameter of particles in the solutions and their volume fractions in the solution.

7.3.12 Centrifugal sedimentation analysis.

Sedimentation velocities of kaolin and KLD/kaolin flocs were measured by an analytical centrifugation analyzer, Lumisizer (LUM GmbH, Germany). This instrument determines the settling of flocs under different centrifugal forces by measuring near infra-red light transmission (880 nm) of the suspension as a function of time and position over the entire sample length, simultaneously (Erramreddy et al., 2017). In each measurement, 1 ml of a 0.4 g/L clay suspension was transferred into the cell of the instrument, centrifuged at different revolutions (200, 400, 800, 1600, and 3200 rpm) for 5 min, and the transmission data was collected after every 1s during this test (300 profiles). Measurements were performed at 25 °C and a light factor of 1. This experiment was conducted for the suspensions containing KLD/kaolin at the dosages of 8 mg/g and 32 mg/g based on dried weight of clay particles in the suspensions. Kaolin sample (0.4 g/L) was also used as a blank (without polymer). The relative centrifugal force (RCF) was calculated using equation 7.4, where r is the radius of centrifuge in mm.

$$RCF = \left(\frac{RPM}{1000}\right)^2 r \times 1.18 \qquad (7.4)$$

The transmission profiles of the samples were recorded as a function of the length of the cell and centrifugation time by the SEPView software. For each run at different RCF (6, 23, 94,375,1500 × g), the thickness of sedimentation layer in the cell was plotted as a function of time, the slope of which led to the sedimentation velocity (mm/h) of the particles at a RCF. By plotting the sedimentation velocity against RCF and extrapolating to one (1) RCF, which is equivalent to earth gravitation, an estimation of settling rate of KLD was identified.

Under the aforementioned experimental conditions, the size distribution of flocs was determined. The constant position analysis was used to determine volume-average particle diameters (Detloff et al., 2007). In each measurement, three positions (approximately 115.0 120.0, 125.0 mm) within the detection region (105-130 mm) were chosen to ensure that the results of the analysis were representative for all measurements.

7.3.13 Fractal dimension measurement

Fractal dimension (D_f), which describes the structural properties of flocs, could be used to determine the compactness of an aggregate, with porous aggregates having a low fractal dimension and more compact ones having a higher fractal dimension. The fractal dimension, D_f, of the flocs was measured by small-angle light scattering technology (SALLS) with Malvern Mastersizer 2000 and used to characterise compaction of flocs (Jarvis et al., 2005; Rong et al., 2013b). A detailed description of the determination of floc's D_f using SALLS is explained elsewhere (Jarvis et al., 2008; Waite et al., 2001; Tang et al., 2002). In this experiment, a beam of light was directed onto a sample containing the flocs and then the beam was scattered at different angles with respect to the incident direction. The intensities (I) of the light scattered at the angles of 0.01° and 40.6° are functions of the scattering vector (Q) (Waite et al., 2002; Rong et al., 2013a), which can be defined by following equation 7.5:

$$Q = \frac{4\pi n \sin(\theta/2)}{\lambda} \qquad (7.5)$$

where, n is the refractive of the fluid, θ is the scattered angle (from 0.01° to 40.6°), and λ is the wavelength of radiation (633 nm). Based on the Rayleigh-Gans-Debye (RGD) scattering theory, scattering vector and light intensity are related according to equation 7.6:

$$I \propto Q^{-D_f} \qquad (7.6)$$

In this equation, D_f is the fractal dimension of the flocs and has value between 1 and 3 in a three-dimensional space (Zhou et al., 2006; Jarvis et al., 2008).

7.4 Results and Discussion

3.1. Polymerization

The polymerization of kraft lignin and DMC was carried out following a free radicle polymerization mechanism. In the reaction mixture, potassium per sulfate generated two sulfite radical anions by thermal decomposition (scheme 7.1a). The sulfite radicals attacked the hydroxyl group (OH) of KL to form phenoxy radicles. These phenoxy radicals then react with double bonds of DMC to have them engaged in the polymerization reaction to produce KLD polymers (scheme 7.1b). On the other hand, sulfate radicals can initiate the homopolymerization of DMC to produce homopolymers (PDMC) as a by-product (scheme 7.1c).

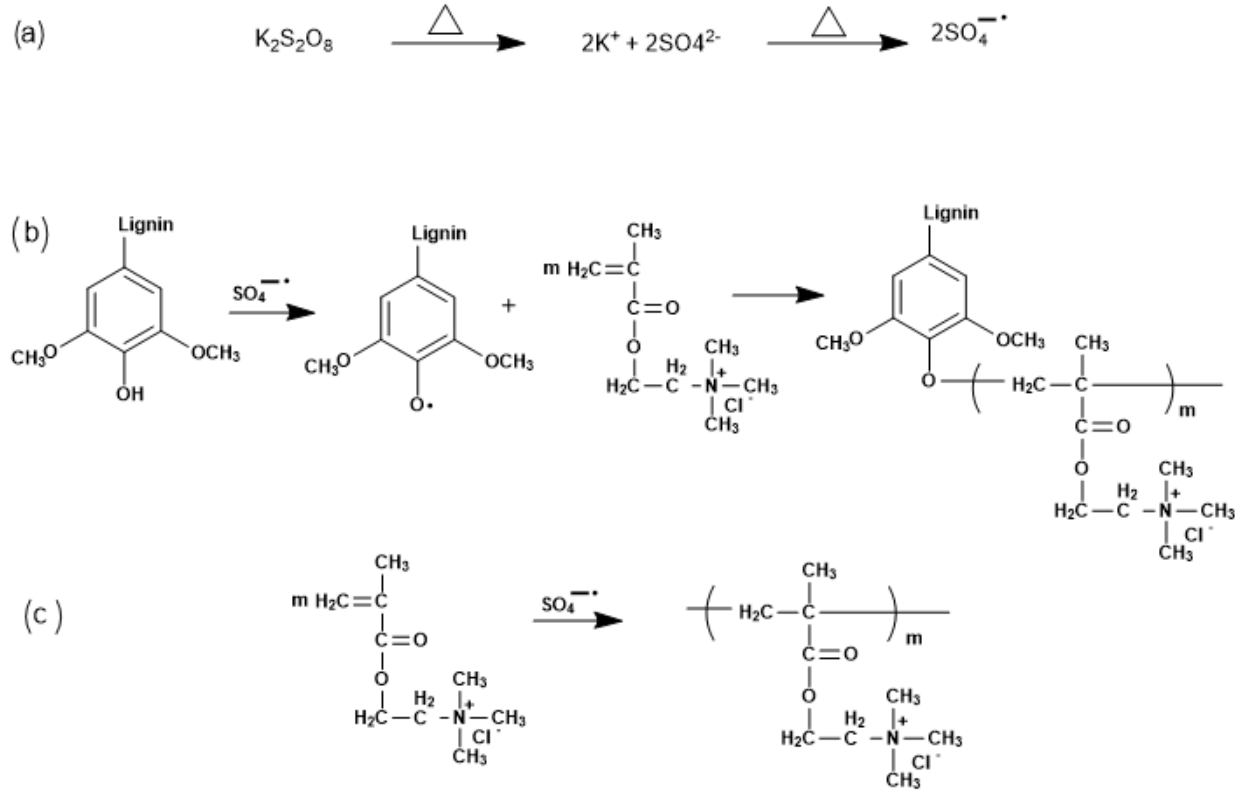

Scheme 7.1. Mechanism of the polymerization reaction of KL and DMC (a) thermal decomposition of potassium per sulfate, (b) polymers of KLD, and (c) homopolymers of PDMC.

7.4.1 Properties of KLD

The reaction conditions and properties of KLD polymers produced via free radical polymerization of KL and DMC are listed in Table 7.1. Under the experimental conditions studied, the polymers with varying charge densities and molecular weights were synthesized. It is evident that the nitrogen content, charge density, and molecular weight increased, confirming the grafting of DMC onto lignin backbone (Wang et al., 2013). The results also showed that varied DMC amount was responsible for different nitrogen contents, charge densities, and molecular weights of KLD polymer. In addition, the cationic charge densities of five KLDs were theoretically calculated from the nitrogen content, since quaternary ammonium group contained 1.0 meq charge density, theoretical charge densities were close to that of experimental value listed in Table 7.1.

Table 7.1. Reaction conditions and properties of KL and KLDs

Conditions	KL	KLD1	KLD2	KLD3	KLD4	KLD5
DMC, mol	-	0.009	0.009	0.014	0.019	0.024
KL, mol	-	0.027	0.016	0.011	0.011	0.022
pH	-	3	4	5	3	4
Temperature, °C	-	80	90	90	70	80
Time, h	-	4	5	4	5	3
Experimental charge density, meq/g	-0.2	0.74	1.52	2.5	2.93	3.66
Theoratical charge density, meq/g	0.021	0.70	1.47	2.41	2.86	3.60
Nitrogen, wt.%	0.03	0.98	2.05	3.40	3.97	5.05
Solubility, wt.%	5	39	40	42	56	66
M_w, g/mol	17,800	30,300	50,700	81,900	109,100	162,600
M_n, g/mol	5,100	22,700	35,400	56,200	70,600	96, 200
M_w/M_n	3.49	1.33	1.43	1.46	1.54	1.69

7.4.2 Adsorption of KLD on kaolin

Figure 7.1 shows the adsorption behaviour of KL or KLD on the surface of kaolin particles as a function of polymer dosage at pH 7. The adsorption increased as the charge density and molecular weight raised. This phenomenon may be attributed to electrostatic interaction between cationic KLD and negatively charged clay particles (Zhou et al., 2006; Sang and Xiao, 2008). Previous studies demonstrated that the adsorption of cationic polymers increased with increasing their charge density (Wickramasinghe et al., 2002; Zhou at al., 2008). Wang et al. (2016) articulated that an increase in the charge density of cationic xylan from 1.8 to 2.4 meq/g

enhanced the adsorption of cationic polymer from 3.1 to 4.6 mg/g onto kaolin particles at a 16 mg/L of polymer dosage. In another study, with increasing the concentration of cationic starch from 30 to 260 g/L in a clay suspension, the adsorption of cationic starch on the clay surface increased from 2 to 18 mg/g (Chen et al., 2007). It can be claimed that, KL had a limited adsorption on kaolin particles.

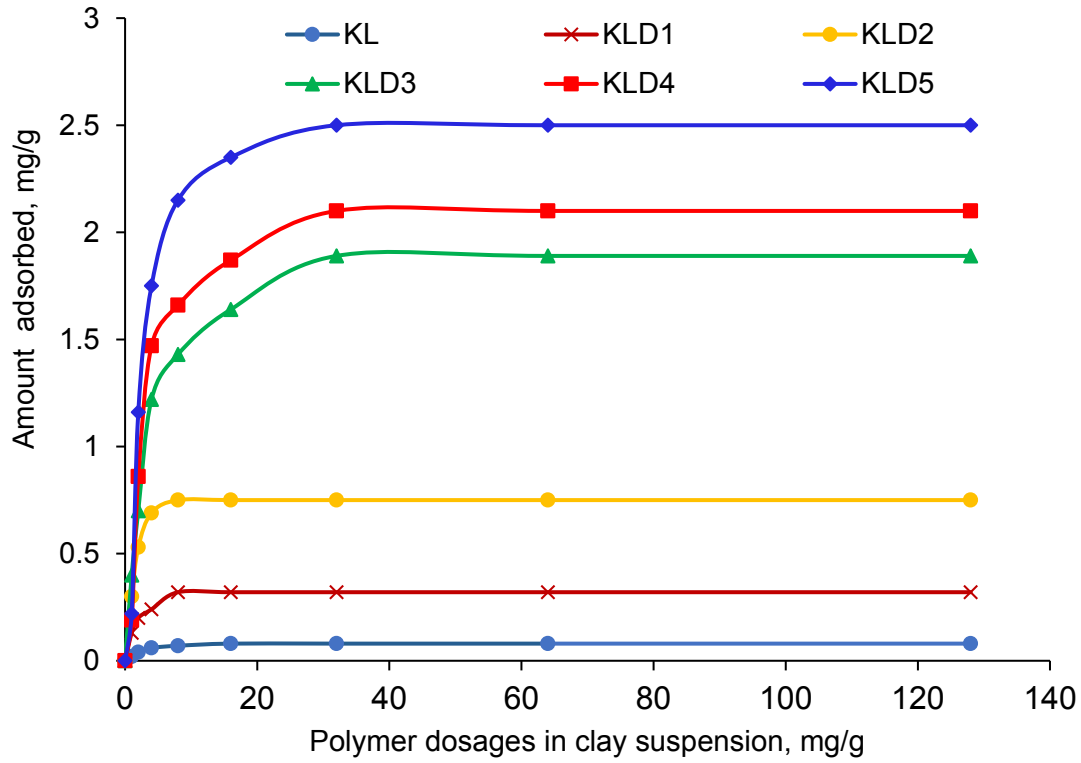

Figure 7.1. Adsorption of KL and KLD on kaolin particle as a function of polymer dosage, conducted under the conditions of pH 7, 25 °C, 1 h and 0.4 g/L clay concentration

7.4.3 Dynamic flocculation

Figure 7.2 shows the relative turbidity of kaolin suspensions as a function of their zeta potential. It is seen that, by increasing the dosage of KLD, the zeta potential became more positive, and the maximum zeta was obtained for KLD5. Also, the relative turbidity of the suspension reduced as the dosage increased, and the minimum relative turbidity was obtained for KLD5. Interestingly, the results confirmed that the charge density of KLD played an important role in altering the zeta

potential and relative turbidity of the suspension, and these changes are attributed to positive effect of charge density on the adsorption of KLDs on clay particles.

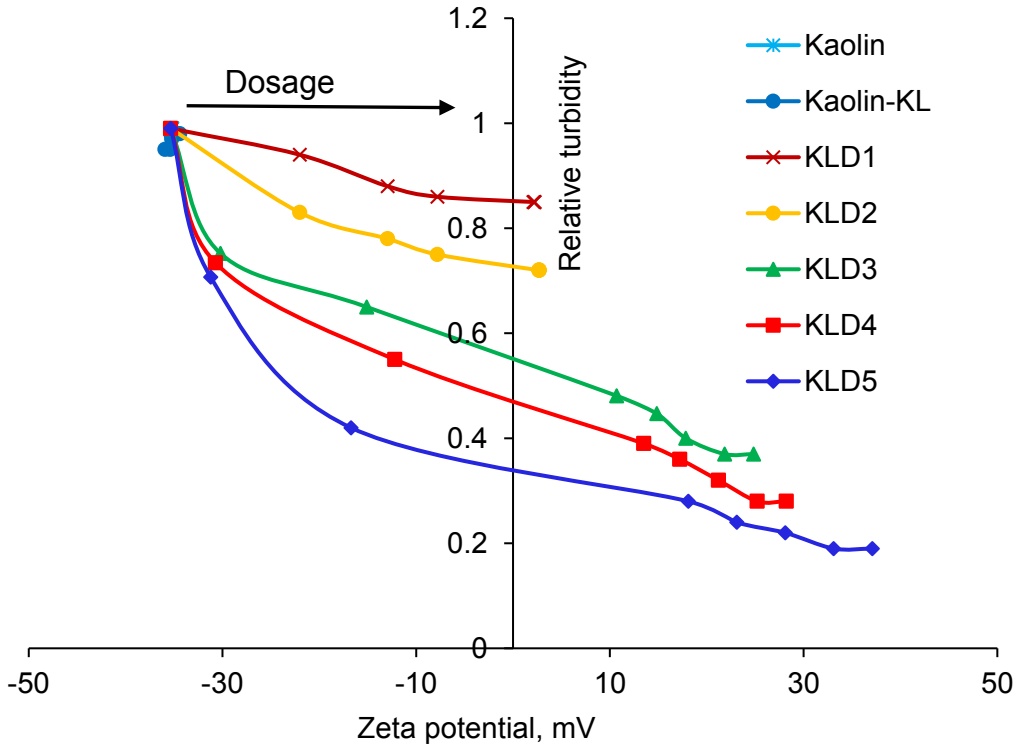

Figure 7.2. Effect of zeta potential on the relative turbidity of kaolin suspensions, conducted under the conditions of pH 7, 1h, 25 °C, and 0.4 g/L of kaolin concentration.

Based on the results obtained from the adsorption analysis (Figure 7.1), and the charge density of KLDs, it was possible to calculate the total charges introduced on the surface of kaolin particles after KLD adsorption. Figure 7.3 showed the influence of charges introduced to the particles via adsorbing KLD on the relative turbidity of the suspensions. As observed, KLD5 introduced more charges onto kaolin particles as compared to the other KLDs, and hence they reduced the relative turbidity more significantly (Figure 7.2). In addition, the last points on each curve represents the

relative turbidity of clay suspensions at the maximum adsorption amount (i.e., saturation adsorption) that was achieved in Figure 7.1. These points ("S" points in Figure 7.3) indicated that, by adding more KLDs to the suspensions, more of unadsorbed KLDs would remain after reaching the saturated level of adsorption. These results confirmed that the amount of the adsorbed KLD (and not the amount of unadsorbed KLD in suspensions) played a major role in the relative turbidity of clay suspension. Among the cationic polyacrylamides that Ariffin and coworkers (2005) studied in the flocculation of palm oil mill effluent, the flocculant with the molecular weight of $1.5x10^{-6}$ g/mol was the most effective one in turbidity removal.

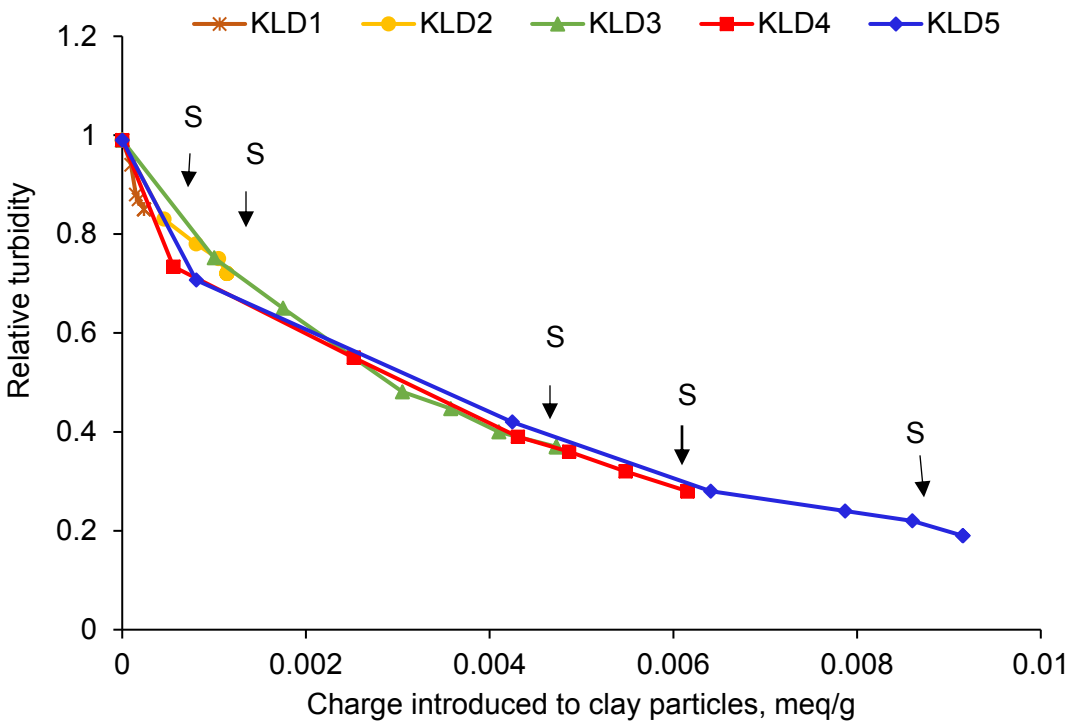

Figure 7.3. Effect of total charges introduced to particles on the relative turbidity of kaolin suspensions conducted under the conditions of pH 7, 1 h, 25 °C and 0.4 g/L of clay concentration.

7.4.4 Floc size measurement

The size distribution of flocculated kaolin particles was shown in Figure 7.4 for two different dosages of 8 and 32 mg/g KLD in clay suspension. The addition of KLD to the kaolin suspension widened the size distribution of particles in the suspension, while reducing their counts. This

phenomenon was observed by Miranada et al. (2008) in flocculation analysis of cationic polyacrylamides. These results were in agreement with the findings of Thapa et al. (2009), where high molecular weight and charge density polyacrylamide polymers were more effective than the low charged and low molecular weight ones in reducing the particle's counts in sludge flocculation process.

The results also confirmed that KLD5 widened the size distribution (and reduced the counts of flocs) more greatly than did other KLDs. The dosage of KLDs did not change the chord length of the flocs formed via treating with KLD1 and KLD2, but other KLDs increased the chord length at a higher dosage. In particular, the average chord length of KLD5 was 53 µm at 8 mg/g of dosage, while that was 65 µm at 32 mg/g. These results confirmed that higher molecular KLDs enhanced the flocculation efficiency and thus aggregation of the clay suspension (Gao et al., 2002; Wang et al., 2014).

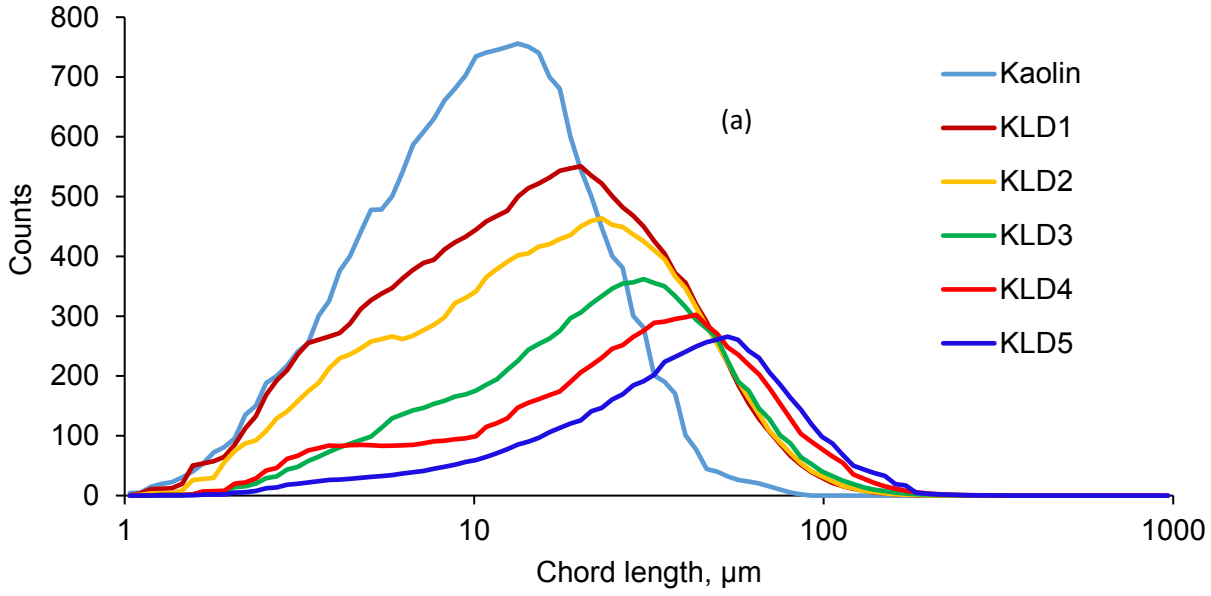

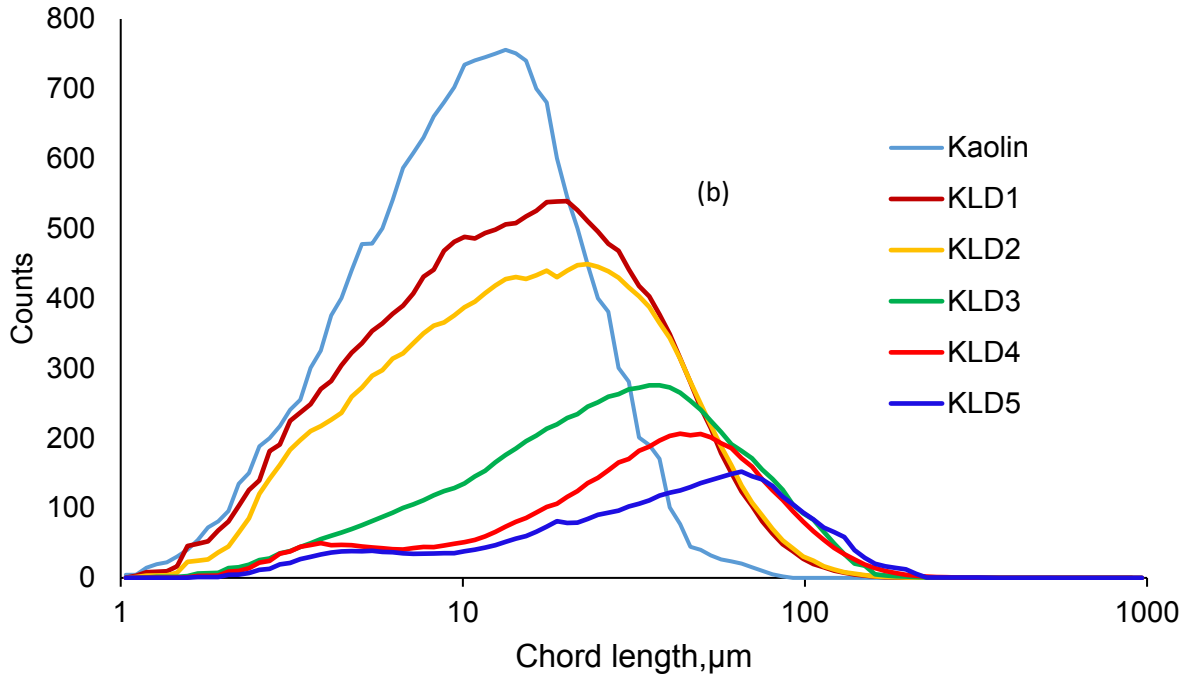

Figure 7.4. Chord length distribution of flocs formed at dosage of (a) 8 mg/g and (b) 32 mg/g conducted under the conditions of pH 7, 25 °C and 0.4 g/L of kaolin concentration.

7.4.5 Flocculation of kaolin under non-stirring conditions

The volume fraction of flocs in the suspension was plotted as a function of their hydrodynamic diameter (d_h) in Figure 7.5. As observed, the flocculation of kaolin particles by KLD increased the average particle size. In the absence of any polymer, the size of the kaolin particle was 4.7 µm. The higher molecular weight and charge density KLD5 achieved the maximum floc size. As shown in Figure 7.5, the floc size of KLD5 grew to 16.85 and 19.12 µm at 8 and 32 mg/g, respectively, after being treated with KLD at 8 and 32 mg/g of dosage. These results are in agreement with those reported in Figure 7.3. It was reported (Wickramasinghe et al., 2002) that increasing the polymer's charge density and molecular weight led to an increase in the floc size. In addition, these results indicated that increasing the KLDs dosage enhanced the floc growth, as well (Zhou and Franks, 2006).

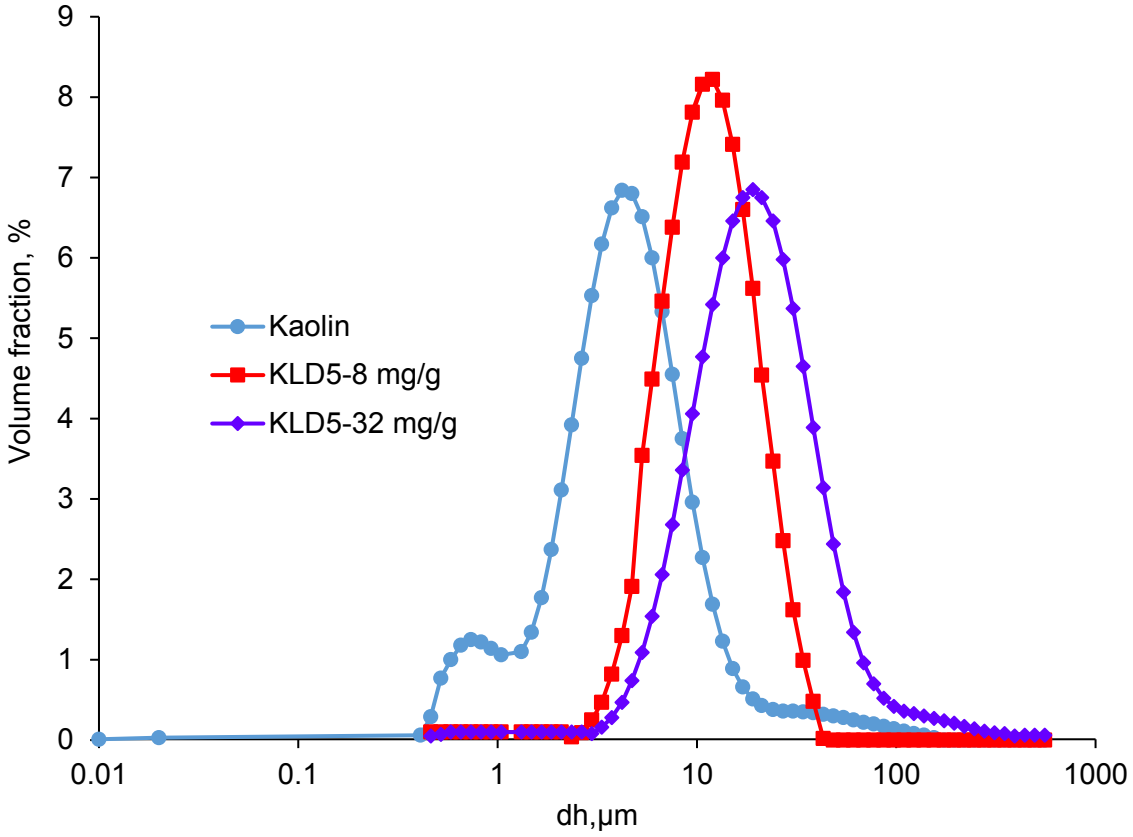

Figure 7.5. The floc size distribution of kaolin particles in the presence and absence of KLD at dosage of 8 and 32 mg/g, conducted under the conditions of pH 7, 25 °C and 0.4 g/L of kaolin concentration.

The impact of KLD on the transmission (%) of kaolin suspensions is shown in Figure 7.6. In the absence of KLD, the transmission of kaolin particles was the lowest (5.67 %) of all studied systems. After addition of KLD, the particles in the kaolin sample started to settle, which made a clear and transparent layer on top of the sample, and this increased the transmission of the samples. The increase in the transmission was more obvious for 32 mg/g dosage than 8 mg/g dosage (Figure 7.6). For example, the addition of KLD5 exhibited large sedimentation with fastest transmission increase to 35.20 and 62.91% at 8 and 32 mg/g of dosages, respectively. This improved settling behaviour of kaolin suspension may largely be attributed to the higher

adsorption of KLD5 onto clay particles as well as its higher charge density and molecular weight (Figure 7.1).

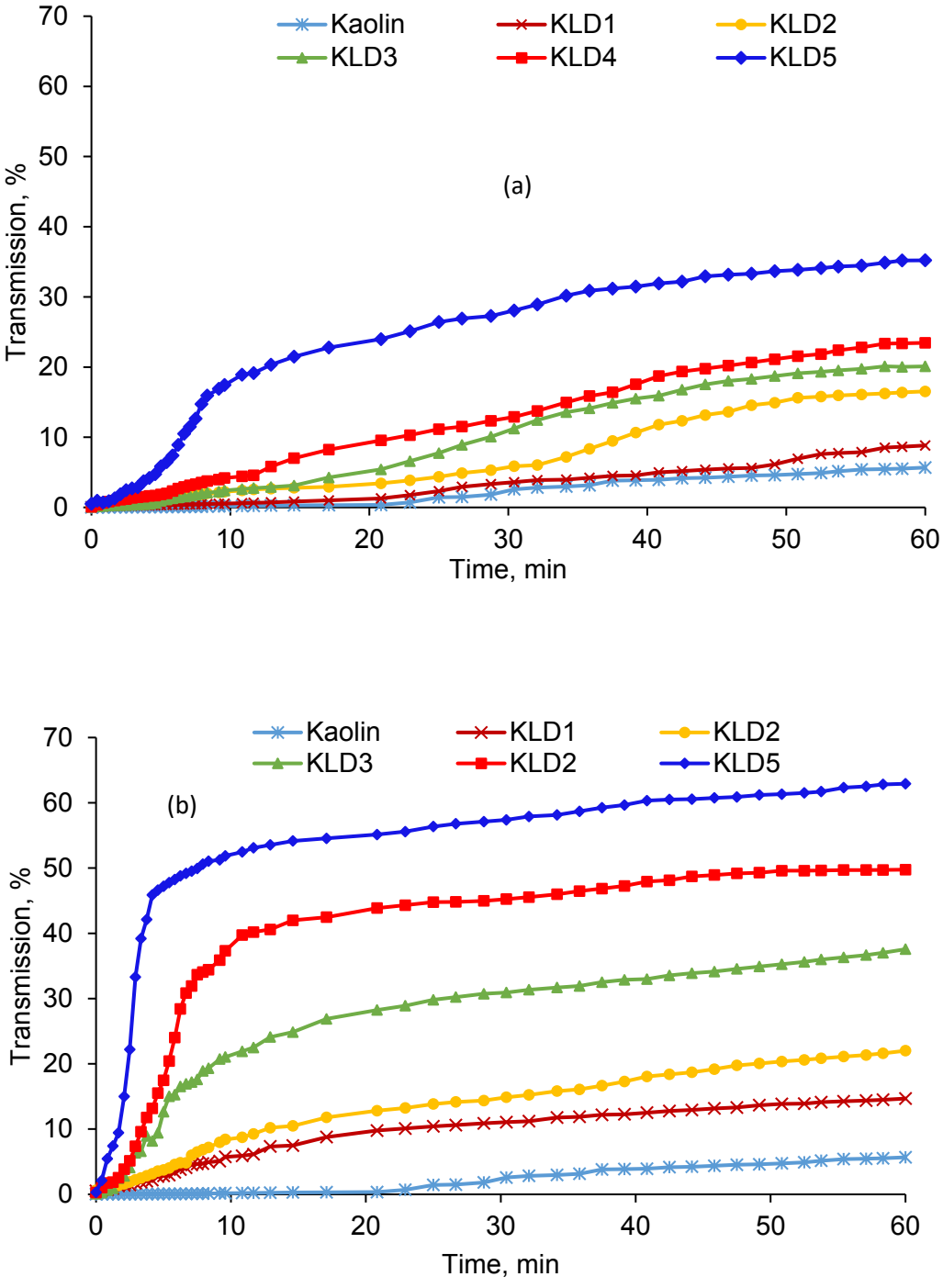

Figure 7.6. Transmission intensity of kaolin suspension (top layer) at the dosage of (a) 8 mg/g and (b) 32 mg/g, as a function of time, conducted under the conditions of 0.4 g/L clay at pH 7, 25 °C and 1h.

The settling velocity and the compactness of sediments after 1 h of settling in the absence and presence of KLD are listed in Table 7.2. The settling velocity is inversely related to the compactness of KLD. The smaller the settling velocity, the larger the compactness would be. Kaolin particles had the highest sediment compactness (42.76 g/L) and the lowest settling velocity (15.3 mm/h). At 8 mg/g of dosage, the sediment compactness decreased from 37.73 to 14.18 g/L; whereas, settling velocity increased from 17.2 to 130.7 mm/h for KLD1 to KLD5, respectively. A similar trend was observed for 32 mg/g dosage, but generally the compactness was smaller and settling velocity was faster. These results confirmed that the compactness of the settled flocs decreased with increasing the molecular weight of KLD. High molecular weight KLDs bridged the kaolin particles to form large porous flocs containing water that reduced its compactness. The formation of loose flocs via bridging mechanism is well documented in the flocculation of cement, kaolin, and hematite in the past (Gaudreault et. al., 2015; Negro et al., 2006; Zhu et al., 2009). The faster settling velocity of KLD5 (173.4 mm/h) confirmed that the flocs of higher molecular weight KLD were larger than lower molecular weight ones (Figures 4 and 5), and they had the fastest settling velocity (Zhu et al., 2009).

Table 7.2. Settling velocity and compactness of settled flocs after settling in 1 h of experiment

	Blank	**KLD1**		**KLD2**		**KLD3**		**KLD4**		**KLD5**	
Dosage (mg/g)		8	32	8	32	8	32	8	32	8	32
Sediment compactness (g/L)	42.76	37.73	35.01	33.99	30.78	26.19	20.59	18.15	13.93	14.18	10.85
Settling velocity (mm/h)	15.3	17.2	18.6	32.4	37.4	53.3	75.2	88.4	120.5	130.7	173.4

7.4.6 Size of suspended flocs

The hydrodynamic diameter of kaolin particles was determined in the absence and presence of KLD in Figure 7.7. The $d_{h,s}$ was approximately 0.19 μm for the suspended kaolin particles. For the samples treated with KLDs, the $d_{h,s}$ was insignificantly different from that of kaolin particles, indicating that the size of suspended particles did not remarkably change after treating with KLD, and the formed large flocs were probably settled. On the other hand, there was a slight

increase in the size of the suspended particles as the size of KLD increased in the system. These results are in agreement with those reported in Figure 7.5. As these larger flocs were loosely bounded with KLD, they had a relatively low compactness, which led to their suspension along with smaller flocs.

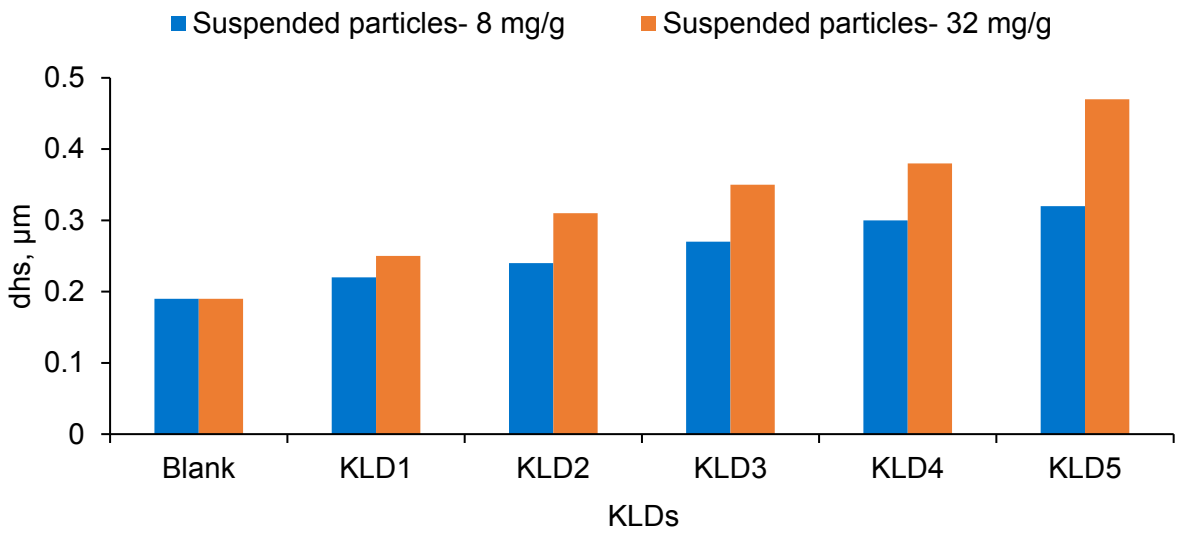

Figure 7.7. The size of suspended particles in the presence and absence of KLD conducted under the conditions of 0.4 g/L clay at pH 7, 25 °C and 1 h.

7.4.7 Sedimentation behavior under accelerated gravitation

The sedimentation velocities of KLDs at various RCFs are summarized in Figure 7.8 for two different dosages of 8 and 32 mg/g KLD in kaolin suspension. A typical linear regression behaviour has been found from kaolin particles as a function of RCF in Figure 8. This phenomenon was observed by Lerche (2002) in the stability analysis study of latex suspensions in the accelerated stability analysis. Generally, flocculants agglomerate particles and thus there is a change from a monodisperse to polydisperse system (Growney et al., 2015). As can be seen, the trend of sedimentation velocity was similar for all of the KLD at 8 mg/g and 32 mg/g dosages, but a more dramatic increase in sedimentation velocity was observed for the KLD5 than other KLDs with accelerating centrifugation. These results are in agreement with the results obtained in Table 7.2. The sedimentation velocity increased with increasing radial distance due

to the increase in centrifugal force (Detloff and Lerche, 2008). A study suggested that particles tend to move with varying orientation during centrifugal sedimentation (Chang and Liao, 2016). The higher settling rate of KLD induced flocs could be due to their orientation in parallel to the centrifugal direction at a high RCF (Lerche, 2002; Detloff and Lerche, 2008). Because of the polydispersity of the flocs, the flow resistance of KLD/kaolin particles was different from that of a spherical particle. Thus, the drag force experienced by the flocs was smaller and the settling velocity became faster when flocs were oriented parallel to the flow field. Similar phenomena were reported by Chang and Liao (2016) in measuring the sedimentation velocities of titanium oxide (TiO_2) nanoparticle under centrifugal forces. Thus, these results indicated that the KLD flocs in the suspension under centrifugal force did not settle uniformly. This study also confirmed that the rate of floc sedimentation in a kaolin suspension mainly depended on the particle size and density.

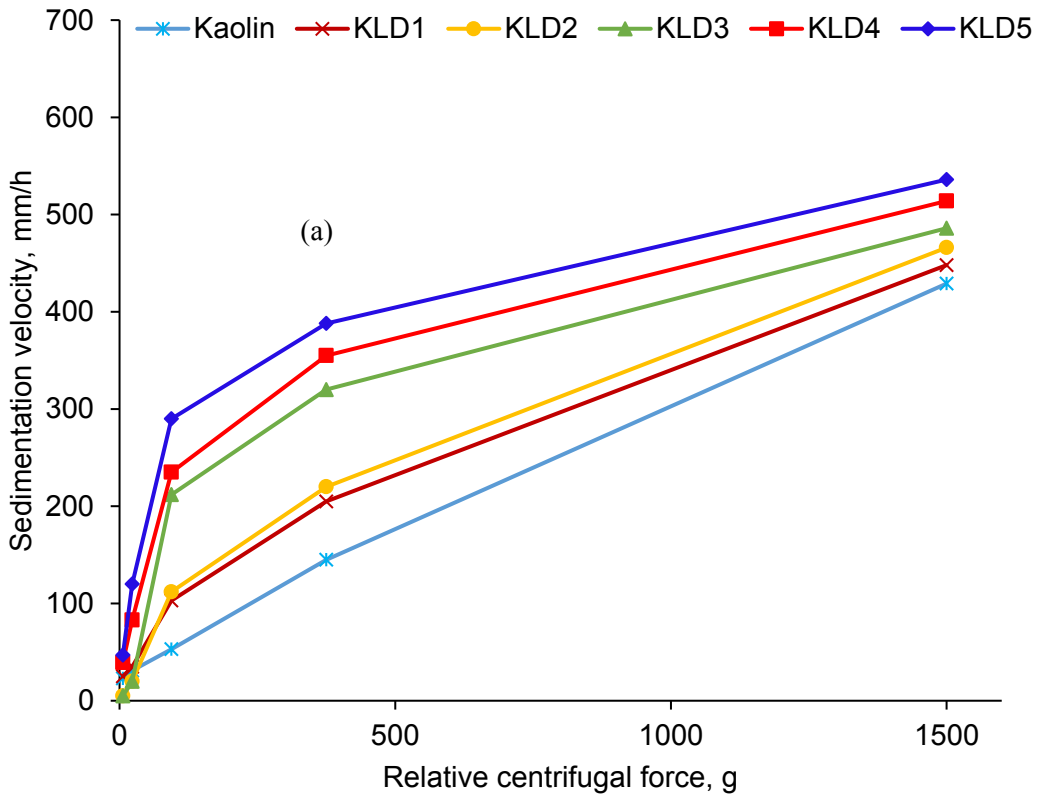

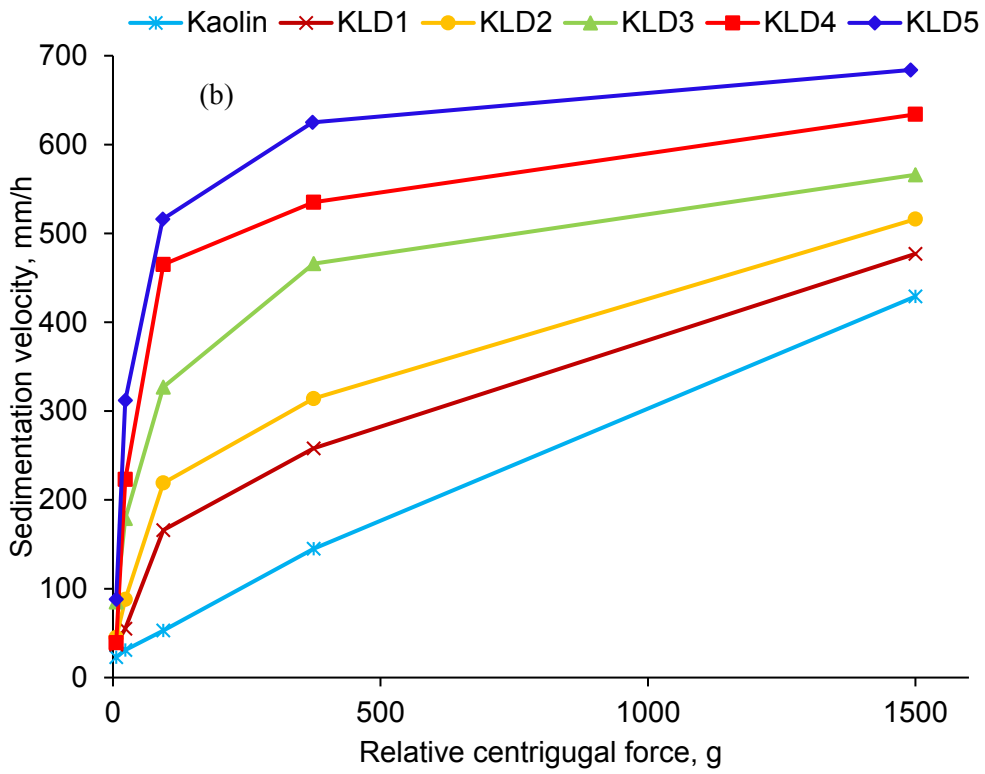

Figure 7.8. Sedimentation velocity of the KLD in kaolin suspension at the dosage of (a) 8 mg/g and (b) 32 mg/g as a function of RCF values conducted under the conditions of 0.4 g/L clay at 25 °C, pH 7 and 5 min.

The volume-weighted particle size distribution of the flocs was identified by analyzing the time evolution of the transmission at a fixed position and the results are shown in Figure 7.9. In the absence of KLD, kaolin particle size in stable dispersion was 4.7 µm. The addition of KLD led to the formation of larger particles that could settle faster, which are in good agreement with data reported in Figures 7.5 and 7.9. As observed, the particle size increased from KLD1 to KLD5 by increasing the centrifugal force. Claverie et al. (2013) reported that the particle size of silica dispersions increased with polymer concentration as well as increasing its molecular weight.

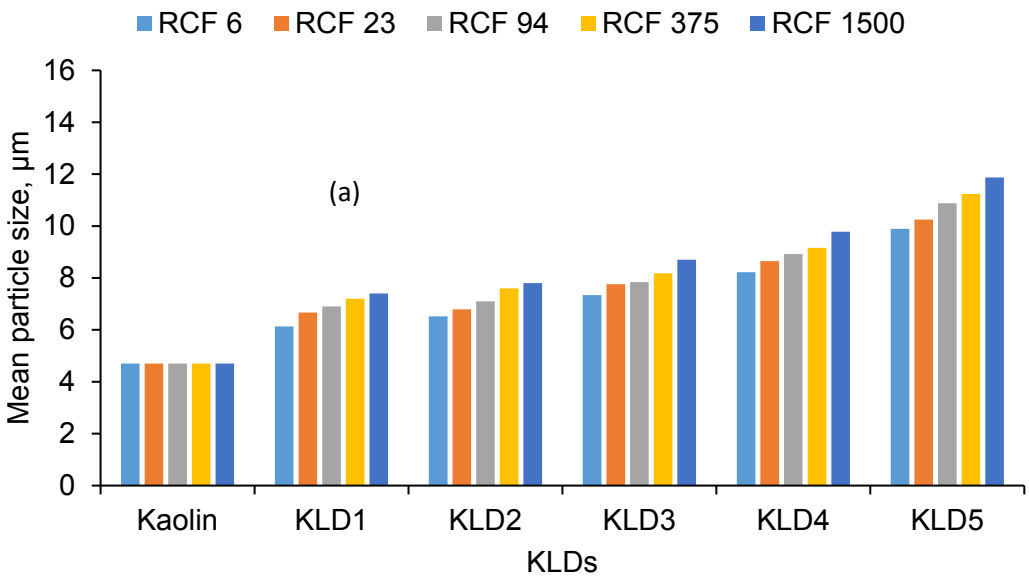

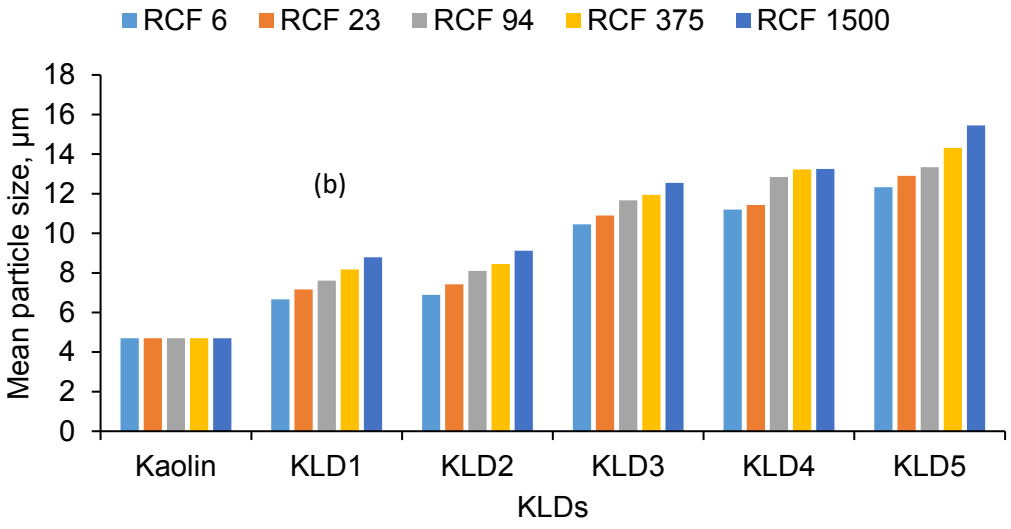

Figure 7.9. Particle size distributions obtained via centrifugation analysis in the presence or absence of KLDs at the dosage of (a) and 8 mg/g (b) 32 mg/g as a function of RCF values; under the conditions of 0.4 g/L clay at 25 °C, pH 7, and 5 min.

7.4.8 Fractal dimension of flocs

Figure 7.10 depicts the log–log plot of I against Q for the KLD/kaolin flocs. To demonstrate the structure of flocs, slopes of the curves in Figure 7.10 were calculated following equation 7.6, and the results of Df are listed in Table 7.3. The slopes of the curves for the kaolin and lower molecular weight KLDs were high and close, suggesting a more compact floc for these samples than for the higher molecular weight KLDs.

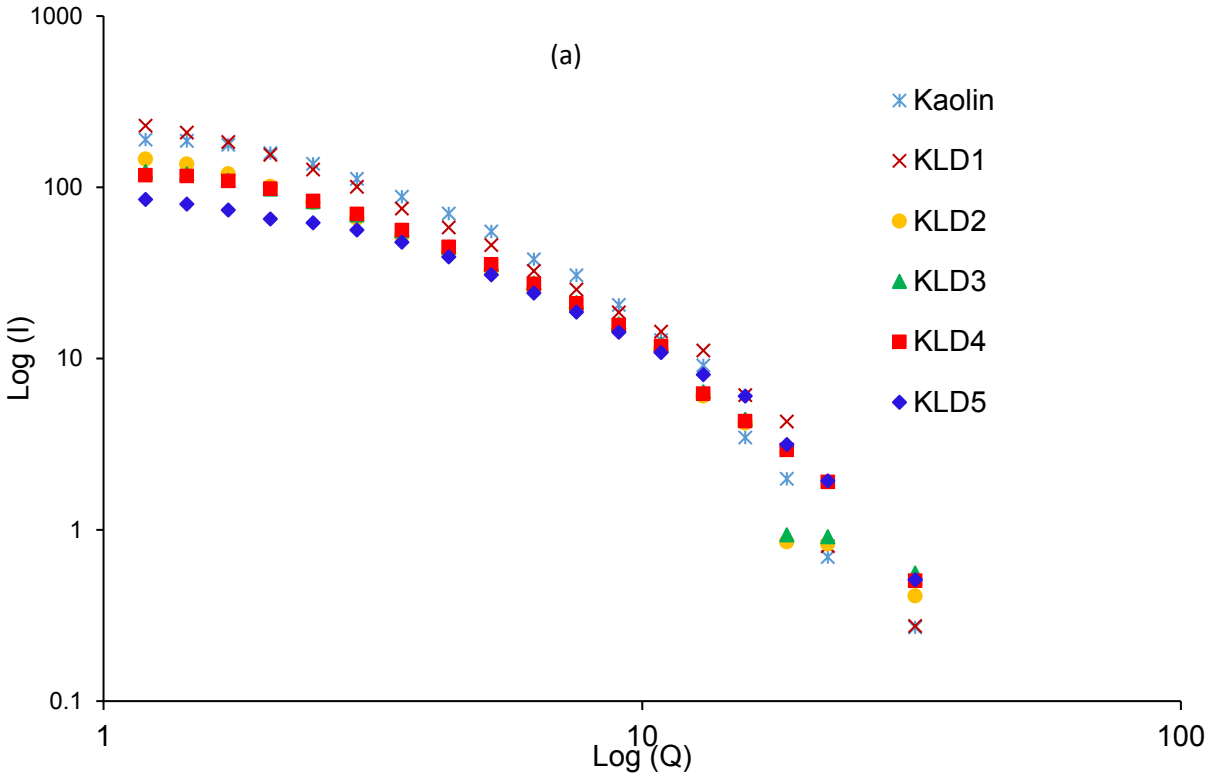

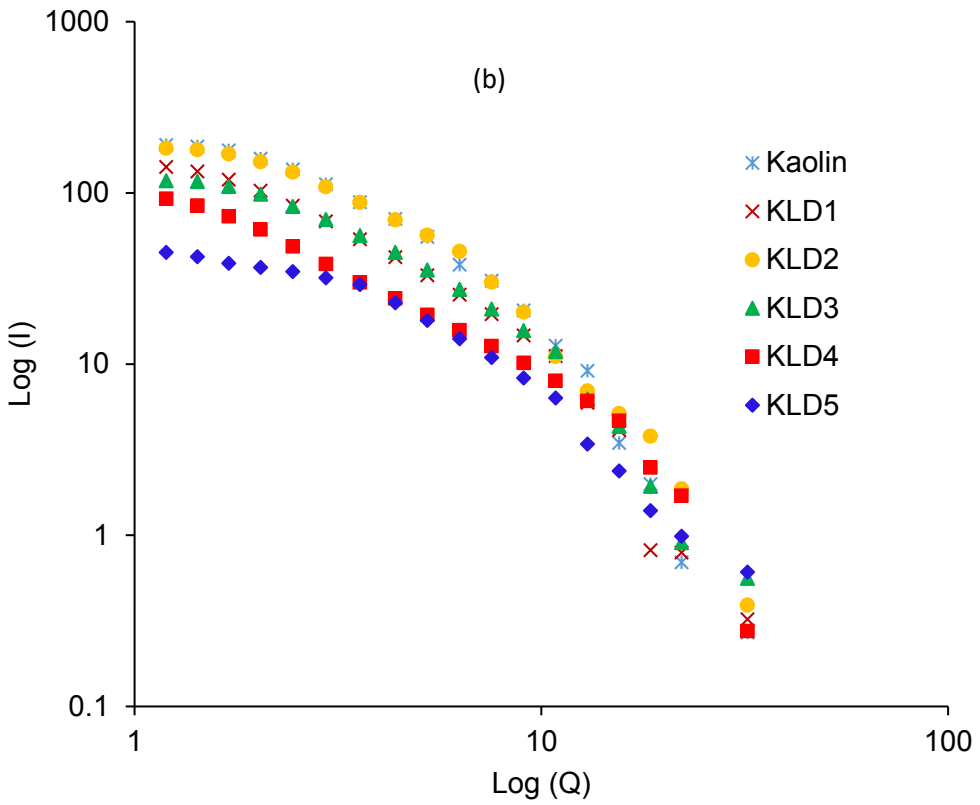

Figure 7. 10. The log–log plot of I as a function of Q at the KLD dosage: (a) 8.0 mg/g, (b) 32 mg/g.

For each KLD, a logarithmic equation was used to obtain the best fit to the experimental results (R^2) and D_f values. D_f obtained for kaolin was 1.91. The addition of KLDs showed a decrease in the D_f of flocs from 1.82 to 1.35, where the minimum R^2 obtained was 0.9 for these equations, which indicated that the equations fitted reasonably well into the experimental results (Yu et al., 2006; Li et al., 2015c). The D_f obtained were consistent with the values (1.3- 2.7) obtained in the literature for different materials (e.g., polystyrene latex, kaolin, aluminum oxide, quartz) under varied flocculants and flocculation conditions (Vahedi and Gorczyca, 2011). By considering the results in Figure 7.8 as well as in Tables 7.2 and 7.3, it can be concluded that the flocs with larger D_f and higher compactness had slower sedimentation velocity. Oppositely, flocs with a smaller D_f had looser structure and more sedimentation velocity (Das and Somasundaran, 2003; Das et al., 2009; Bushell et al., 2002).

Table 7.3. Equations fitting the logarithm relationship between scattered light, I, and scattering vector, Q, obtained from Figure 7.10.

Dosage	Sample	$I \sim Q$	D_f	R^2
8 mg/g	Kaolin	$I=722.34Q^{-1.919}$	1.919	0.903
	KLD1	$I=644.11Q^{-1.822}$	1.822	0.908
	KLD2	$I=406.36Q^{-1.775}$	1.775	0.919
	KLD3	$I=364.9Q^{-1.688}$	1.688	0.906
	KLD4	$I=318.48Q^{-1.559}$	1.559	0.931
	KLD5	$I=207.8Q^{-1.383}$	1.383	0.902
32 mg/g	KLD1	$I=424.08Q^{-1.809}$	1.809	0.913
	KLD2	$I=581.92Q^{-1.736}$	1.736	0.918
	KLD3	$I=344.08Q^{-1.637}$	1.637	0.919
	KLD4	$I=189.25Q^{-1.488}$	1.488	0.926
	KLD5	$I=109.48Q^{-1.351}$	1.351	0.918

7.5 Conclusions

The efficiency of KLD5 was higher than that of other KLDs in flocculating kaolin particles due to its higher adsorption as well as charge density and molecular weight. The relative turbidity of the suspension dropped more quickly and its zeta potential increased more dramatically with KLD5 than other KLD as it adsorbed more than other KLDs on kaolin particles. Generally, a more dramatic turbidity drop, larger particle size, lower compactness, smaller fractal dimension, and higher sedimentation velocity were obtained at a higher dosage of KLD and for larger KLD (than the smaller ones). By increasing KLD dosage, the adsorption of KLD increased and the maximum adsorption of 2.5 mg/g was achieved by KLD5 at 32 mg/g KLD concentration. By adding 32 mg/g of KLD, having the charge density of 3.66 meq/g and molecular weight of 162,600 g/mol, the minimum relative turbidity of 0.19 for kaolin suspensions was achieved. The destabilization of kaolin particles increased with KLD dosage. The sedimentation studies under gravitational force demonstrated that the compactness of KLD flocs decreased, while the settling velocity increased progressively with increasing concentration as well as increasing the

molecular weight. By increasing the centrifugal force, the size of the flocs and the settling velocity were increased regardless of the KAD properties. Also, the sedimentation velocities of KLD5 induced flocs were 536 mm/h and 684 mm/h, while the floc sizes increased to 11.87 μm and 15.45 μm at 8 and 32 mg/g of dosages, respectively. Addition of KLD resulted in change from monodisperse to polydisperse settling due to agglomeration/flocculation of kaolin particles by KLD. The fractal dimension, D_f, of the flocs ranged between 1.82 and 1.35. At a higher KLD concentration (32mg/g), the flocs formed by KLD5 were larger and had more porous structure (D_f of 1.35), while those formed by KLD1 were smaller and more compact (D_f of 1.80). Based on the relationship between the settling velocity and the floc size, as well as the flocs' fractal dimension, it is confirmed that floc porosity, in addition to floc size affected the settling behavior of the flocs.

7.6 References

Abraham, T., Kumpulainen, A., Xu, Z., Rutland, M., Claesson, P.M., Masliyah., J. 2001. Polyelectrolyte-mediated Interaction between Similarly Charged Surfaces: Role of Divalent Counter Ions in Tuning Surface Forces. Langmuir 17, 8321-8327.

Adachi, Y., Kobayashi, A., Kobayashi, 2012. M. Structure of Colloidal Flocs in relation to the Dynamic Properties of Unstable Suspension. Int. J. Polym. Sci., 1-14.

Ariffin, A., Shatat, R.S.A., Norulaini, A.R.N., Omar, A.K.M. 2005.Synthetic polyelectrolytes of varying charge densities but similar molar mass based on acrylamide and their applications on palm oil mill effluent treatment. Desalination, 173, 201-208.

Bowers, D.J., McKee, D., Jago, C.F., Nimmo-Smith, W.A.M.2017. The area-to-mass ratio and fractal dimension of marine flocs Estuarine. Coast. Shelf Sci., 189, 224-234.

Boxall, J. A., Koh, C. A., Sloan, E. D., Sum, A. K., Wu, D. T. 2011. Droplet Size Scaling of Water-in-oil Emulsions under Turbulent Flow. Langmuir, 28, 104-110.

Bushell, G. C., Yan, Y. D., Woodfield, D., Raper, J. U. D. Y. 2002. Amal R. On techniques for the measurement of the mass fractal dimension of aggregates. Adv. Colloid. Interfac., 95, 1-50

Chang, C.W., Liao, Y.C. 2016. Accelerated Sedimentation Velocity Assessment for Nanowires Stabilized in a Non-Newtonian Fluid. Langmuir, 32, 13620−13626.

Chen, Y., Liu, S., Wang, G. 2007. A kinetic investigation of cationic starch adsorption and flocculation in kaolin suspension. Chem. Eng. J., 133, 325–333.

Chuah, W. H., Zhang, W. L., Choi, H. J., Seo, Y. 2015. Magnetorheology of Core–Shell Structured Carbonyl Iron/Polystyrene Foam Microparticles Suspension with Enhanced Stability. Macromol., 48 (19), 7311-7319.

Claverie, A.L., Schwarz, S., Steinbach, C., Vargas, S.M.P., Genest, S. 2013. Combination of Natural and Thermosensitive Polymers in Flocculation of Fine Silica Dispersions. Int. J. Carbohyd. Chem., 8 pages, http://dx.doi.org/10.1155/2013/242684

Das, K. K., Somasundaran, P. 2003. Flocculation-dispersion Characteristics of Alumina using a Wide Molecular Weight range of Polyacrylic Acids. Colloid. Surface. A., 223, 17-25.

Das, K., Raha, S. 2009. Somasundaran P. Effect of Polyacrylic Acid Molecular Weight on the Floc Stability during Prolonged Settling. Colloid. Surface. A., 351, 1-8.

Detloff, T., Lerche, D. 2008. Centrifugal separation in tube and disc geometries: experiments and theoretical models. Acta Mech., 201, 83–94.

Detloff, T., Sobisch, T., Lerche, D. 2007. Particle size distribution by space or time dependent extinction profiles obtained by analytical centrifugation (concentrated systems). Powder Technol., 174, 50–55.

Du, J., Morris, G., Pushkarova, R. A., Smart, R. S. C. 2010. Effect of Surface Structure of Kaolinite on Aggregation, Settling rate, and Bed Density. Langmuir, 26, 13227-13235.

Dyer, K.R., Manning, A.J.1999. Observation of the size, settling velocity and effective density of flocs, and their fractal dimensions. J. Sea. Res., 41, 87–95.

Erramreddy, V.V., Tu, S., Ghosh, S. 2017. Rheological reversibility and long-term stability of repulsive and attractive nanoemulsion gels. RSC Adv., 7, 47818.

Fang, R., Cheng, X., Xu, X. 2010. Synthesis of lignin-base cationic flocculant and its application in removing anionic azo-dyes from simulated wastewater. Bioresour. Technol., 101, 7323−9.

Fatehi, P., Gao, W., Sun, Y. 2016. Dashtban M. Acidification of Prehydrolysis Liquor and Spent Liquor of Neutral Sulfite Semichemical Pulping Process. Bioresour. Technol., 218, 518-525.

Gao, B., Hahn, H. 2002. Hoffmann E. Evaluation of aluminum-silicate polymer composite as a coagulant for water treatment. Wat. Res., 36, 3573-3581.

Gao, Y., Li, Q., Shi, Y., Cha, R. 2016. Preparation and Application of Cationic Modified Cellulose Fibrils as a Papermaking Additive. Int. J. Poly. Sci., http://dx.doi.org/10.1155/2016/6978434

Gaudreault, R., Cesare, N.D., van de Ven, T.G.M., Weitz, D.A. 2015. Structure and Strength of Flocs of Precipitated Calcium Carbonate Induced by Various Polymers Used in Papermaking. Ind. Eng. Chem. Res., 54, 6234−6246.

Ghimici, L., Constantin, M., Fundueanu, G. 2010. Novel biodegradable flocculating agents based on pullulan. J. of Haza. Mat., 181, 351–358.

Gregory, J. 1988. Polymer Adsorption and Flocculation in Sheared Suspensions. Colloid. Surface., 131, 231-253.

Gregory, J., Barany, S. 2011. Adsorption and flocculation by polymers and polymer mixtures. Adv. Colloid. Interface Sci., 169, 1–12.

Growney, D.J. Fowler, P.W. Mykhaylyk, O.O., Fielding, L.A., Derry, M.J., Aragrag, N., Lamb, G.D., Armes, S.P. 2015. Determination of Effective Particle Density for Sterically Stabilized Carbon Black Particles: Effect of Diblock Copolymer Stabilizer Composition. Langmuir, 31, 8764−8773.

He, W., Zhang, Y. 2016. Fatehi P. Sulfomethylated Kraft Lignin as a Flocculant for Cationic Dye. Colloid. Surface. A., 503, 19-27.

Jahan, M.S., Liu, Z., Wang, H., Saeed, A., Ni, Y. 2012. Isolation and characterization of lignin from prehydrolysis liquor of kraft based dissolving pulp production. Cell. Chem. Technol., 46, 261–267.

Jarvis, P., Jefferson, B., Parsons, S. A. 2005. Breakage, Regrowth, and Fractal Nature of Natural Organic Matter Flocs. Environ. Sci. Technol., 39, 2307-2314.

Jarvis, P., Parsons, S. A., Henderson, R., Nixon, N., Jefferson, B. 2008. The Practical Application of Fractal Dimension in Water Treatment Practice–the Impact of Polymer Dosing. Sep. Sci. Technol., 43, 1785-1797.

Johnson, C.P., Li, X., Logan, B.E., 1996. Settling velocities of fractal aggregates. Environ. Sci. Technol., 30, 1911–1918.

Johnson, M., Peakall J. Fairweather M. Biggs S. Harbottle D. Hunter T. N. 2016. Characterization of Multiple Hindered Settling Regimes in Aggregated Mineral Suspensions. Ind. Eng. Chem. Res., 55, 9983-9993.

Kouisni L., Hindle, P. H., Maki, K., Paleologou, M. 2012. The lignoforcesystem ™: a new process for the production of high-quality lignin from black liquor. The Journal of Science & Technology for Forest Products and Processes, 2, 6–10.

Kumar, R.G., Strom, K.B., Kymani, A. 2010. Floc properties and settling velocity of San Jacinto estuary mud under variable shear and salinity conditions. Cont. Shelf. Res., 30, 2067–2081.

Lapointe, M., Bar beau, B. 2016. Characterization of ballasted flocs in water treatment using Microscopy. Water Res., 90, 119 -127.

Lerche, D. 2002. Dispersion Stability and Particle Characterization by Sedimentation Kinetics in a Centrifugal Field. J. Disp. Sci. Technol., 23(5), 699-709.

Li, T., Zhu, Z., Wang, D., Yao, C., Tang, H. 2006. Characterization of floc size, strength and structure under various coagulation mechanisms. Powder Tech., 168, 104–110.

Li, H., Cai, T., Yuan, B., Li, R., Yang, H., Li, A. 2015a. Flocculation of Both Kaolin and Hematite Suspensions Using the Starch-Based Flocculants and Their Floc Properties. Ind. Eng. Chem. Res., 54, 59−67.

Li, R., Gao, B., Sun, S., Wang, H., Liu, Y., Yue, Q., Wang, Y. 2015b. Coagulation behavior and floc structure characteristics of cationic lignin-based polymerpolyferric chloride dual-coagulants under different coagulation conditions. RSC Adv., 5, 100030–100038.

Li, R., Gao, B., Sun, S., Yue, Q., Li, M., Yang, X, Song, W., Jia, R. 2015c. Amine-Cross-Linked Lignin-Based Polymer: Modification, Characterization, and Flocculating Performance in Humic Acid Coagulation. ACS Sustainable Chem. Eng., 3, 3253−3261.

Mengual, O., Meunier, G., Cayré, I., Puech, K., Snabre, P. 1999. TURBISCAN MA 2000: Multiple Light Scattering Measurement for Concentrated Emulsion and Suspension Instability Analysis. Talanta., 50, 445-456.

Miranda, R., Blanco, A., Fuente, E., Negro, C. 2008. Separation of contaminants from deinking process water by dissolved air flotation: effect of flocculant charge density. Sep. Sci. Technol., 43, 3732–3754.

Negro, S., Sánchez, L.M., Fuente, E., Blanco, A., Tijero, J. 2006. Polyacrylamide induced flocculation of a cement suspension. Chem. Eng. Sci., 61, 2522 – 2532.

Pal, S., Ghorai, S., Dash, M.K, Ghosh, S., Udayabhanu, G. 2011. Flocculation properties of polyacrylamide grafted carboxymethyl guar gum (CMG-g-PAM) synthesised by conventional and microwave assisted method. J. Hazard. Mater., 115, 1580-1588.

Pal, S., Mal, D., Singh, R.P.N. 2005. Cationic starch: an effective flocculating agent. Carbohyd. Polym., 59, 417-423.

Petrak, D., Dietrich, S., Eckardt, G., Köhler, M. 2015. Two-dimensional Particle Shape Analysis from Chord Measurements to Increase Accuracy of Particle Shape Determination. Powder Technol., 3284, 25-31.

Rapp, M. V., Donaldson, S. H., Gebbie, M. A., Das, S., Kaufman, Y., Gizaw, Y., Israelachvili, J. N. 2015. Hydrophobic, Electrostatic, and Dynamic Polymer Forces at Silicone Surfaces Modified with Long-Chain Bolaform Surfactants. Small, 11, 2058-2068.

Rong, H., Gao, B., Dong, M., Zhao, Y., Sun, S., Yue, Q., Li, Q.2013a. Characterization of Size, Strength and Structure of Aluminum-polymer Dual-coagulant Flocs under Different pH and Hydraulic Conditions. J. Hazard. Mat., 252, 330-337.

Rong, H., Gao, B., Zhao, Y., Sun, S., Yang, Z., Wang, Y., Yue, Q., Li, Q. 2013b. Advanced lignin-acrylamide water treatment agent by pulp. J. Environ. Sci., 12, 2367-77.

Sang, Y., Xiao, H. 2008. Clay flocculation improved by cationic poly (vinyl alcohol)/anionic polymer dual-component system. J. Colloid. Interface Sci., 326, 420–425.

Sirvio, J., Honka, A., Liimatainen, H., Hormi, O. 2011. Synthesis of highly cationic water-soluble cellulose derivative and its potential as novel biopolymeric flocculation agent. Carbohyd. Polym., 86, 266-270.

Sobisch, T., Lerche, D. 2018. Separation behaviour of particles in biopolymer solutions in dependence on centrifugal acceleration: Investigation of slow structuring processes informulations. Colloids and Surf. A., 536, 74-81.

Solberg, D., Wagberg, L. 2003. Adsorption and flocculation behavior of cationic polyacrylamide and colloidal silica. Colloids Surf. A Physicochem. Eng. Asp. , 219, 161-172.

Spicer, P.T., Pratsinis, S.E., Raper, J., Amal, R., Bushell, G., Meesters, G. 1998. Effect of shear schedule on particle size, density, and structure during flocculation in stirred tanks. Powder Technol., 97, 26-34.

Sun, Y., Fan, W., Zheng, H., Zhang, Y., Li, F., Chen, W. 2015. Evaluation of Dewatering Performance and Fractal Characteristics of Alum Sludge, Published online, doi: 10.1371/journal.pone.0130683.

Tang, P., Greenwood, J., Raper, J. A. 2002. A Model to Describe the Settling Behavior of Fractal Aggregates. J. Colloid Intern. Sci., 247, 210-219.

Thapa, K.B., Qi, Y., Hoadley, A.F. 2009. Using FBRM to investigate the sewage sludge flocculation efficiency of cationic polyelectrolytes. Water Sci. Technol., 59, 583-93.

Tian, D., Xie, H.Q. 2008. Synthesis and Flocculation Characteristics of Konjac Glucomannan-g-Polyacrylamide. Polym. Bull., 61, 277–285.

Vahedi, A., Gorczyca, B. 2012. Predicting the Settling Velocity of Flocs Formed in Water Treatment Using Multiple Fractal Dimensions. Water Res., 46, 4188-4194.

Vahedi, A., Gorczyca, B. 2011. Application of Fractal Dimensions to Study the Structure of Flocs Formed in Lime Softening Process. Water Res., 45, 545-556.

Waite, T. D., Cleaver, J. K., Beattie, J. K. 2001. Aggregation Kinetics and Fractal Structure of γ-alumina Assemblages. J. Colloid. Interf. Sci., 241, 333-339.

Wang, S., Hou, Q., Kong, F., Fatehi, P. 2016. Production of cationic xylan–METAC copolymer as a flocculant for textile industry. Carbohyd. Polym., 124, 229-236.

Wang, S., Konduri, M.K.R., Hou, Q., Fatehi, P. 2016. Cationic xylan-METAC copolymer as a flocculant for clay suspensions. RSC Adv., 6(46), 1-34.

Wang, L., Zhang, Y., Li, G. 2014. Behavior of Polyamine Fixing Agents on Agglomeration of Dissolved and Colloidal Substances in Papermaking. BioResour., 9, 472-481.

Wang, J.P., Yuan, S.J., Wang, Y., Yu, H.Q. 2013. Synthesis, characterization and application of a novel starch based flocculant with high flocculation and dewatering properties. Water Res., 47, 2643-2648.

Wang J.P., Chen, Y.Z., Yuan, S.J., Sheng, G.P., Yu, H.Q. 2009. Synthesis and characterization of a novel cationic chitosan-based flocculant with a high water-solubility for pulp mill wastewater treatment. Water Res., 43, 5267-5275.

Wang, J.P., Chen, Y.Z., Ge, X.W., Yu, H.Q. 2007. Optimization of coagulation–flocculation process for a paper-recycling wastewater treatment using response surface methodology. Colloids Surf.A Physicochem. Eng. Asp., 302, 204-210.

Wang, S., Hou, Q., Kong, F., Fatehi, P. 2015. Production of cationic xylan–METAC copolymer as a flocculant for textile industry. Carbohyd. Polym., 124, 229-236.

Wei, Y., Cheng, F., Zheng, H. 2008. Synthesis and flocculating properties of cationic starch derivatives. Carbohyd. Polym., 74, 673–679.

Wickramasinghe, S., Wu, Y., Han, B. 2002. Enhanced microfiltration of yeast by flocculation. Desalination, 147, 25-30.

Winterwerp, J.C., Kesteren, V. K. W.G.M. 2004. Introduction to the Physics of Cohesive Sediment in the Marine Environment. Developments in Sedimentol- ogy series, 56. Elsevier, Amsterdam.

Wiśniewska, M., Chibowski, S., Urban, T. 2012. Investigation of the Stability of an Alumina Suspension in the Presence of Ionic Polyacrylamid. Thin Solid Films, 520, 6158-6164

Wu, R. M., Lee, D. J., Waite, T. D. 2002. Guan J. Multilevel Structure of Sludge Flocs. J. Colloid. Interf. Sci., 252, 383-392.

Yang, R., Li, H., Huang, M., Yang, H, Li, A. 2016. A review on chitosan-based flocculants and their applications in water treatment. Water Res., 95, 59-89.

Yan, Y.D., Glover, S.M., Jameson, G.J., Biggs, S. 2004. The flocculation efficiency of polydisperse polymer flocculants. Int. J. Miner. Process., 73, 161 – 175.

You, L., Lu, F., Li, D., Qiao, Z., Yin, Y. 2009. Preparation and flocculation properties of cationic starch/chitosan crosslinking-copolymer. J. Hazard. Mat., 172, 38–45.

Yu, J., Wang, D., Ge, X., Yan, M., Yang, M. 2006. Flocculation of kaolin particles by two typical polyelectrolytes: A comparative study on the kinetics and floc structures. Colloids Surf. A Physicochem. Eng. Asp., 290, 288–294.

Zhou, Y., Franks, G.V. 2006. Flocculation Mechanism Induced by Cationic Polymers Investigated by Light Scattering. Langmuir, 22, 6775-6786.

Zhou, Y., Gan, Y., Wanless, E.J., Jameson, G.J., Franks, G.V. 2008. Interaction Forces between Silica Surfaces in Aqueous Solutions of Cationic Polymeric Flocculants: Effect of Polymer Charge. Langmuir, 24, 10920–10928.

Zhu, Z., Li, T., Lu, J., Wang, D., Yao, C. 2009. Characterization of kaolin flocs formed by polyacrylamide as flocculation aids. Int. J. Miner. Pro., 9, 94–99.

Chapter 8: Stability of kaolin dispersion in the presence of lignin-acrylamide polymers

8.1 Abstract

Dispersion of kaolin in aqueous systems is important in many industries including ceramics, chemicals, pharmaceutical and paints. In this work, kraft lignin-acrylamide (KAM) polymers were produced via polymerizing kraft lignin and acrylamide (AM) monomer with different molar masses and charge densities, and they were used for stabilizing kaolin dispersion at varied pHs. The surface tension and contact angle studies demonstrated that KAM improved the surface hydrophilicity of kaolin mineral particles. Among KAM polymers (KAM-1, KAM-2 and KAM-3), KAM-3 with the highest molar mass (M_w) of 97,000 g/mol and charge density of -2.1 meq/g had the highest adsorption of 2.16 mg/g onto kaolin mineral particles. It was also found that KAM adsorption on kaolin mineral particles was pH dependent with KAM adsorption decreasing with increasing pH from 4 to 10. Generally, increasing ionic strength enhanced the adsorption of KAM on kaolin mineral particles. Salt reduced electrostatic repulsion between the anionic KAM polymers and the negatively charged kaolin mineral particles and facilitated the adsorption. Relationship between zeta potential and relative turbidity of kaolin dispersion was developed at different levels of KAM adsorption. KAM (especially KAM-3) increased the volume fraction of kaolin mineral particles in the dispersion. It also improved the stability of kaolin dispersion, and the impact was more noticeable at pH 10. Treating the dispersion with KAM was more effective than mechanical stirring in stabilizing kaolin mineral particles.

8.2 Introduction

The stabilization of aqueous kaolin dispersion is critical in the production of cosmetics, ceramics, paints, coating formulas and construction materials in order to obtain stable and homogenous colloidal systems (Brady et al., 1996). Dispersants have been widely used in the stabilization of kaolin mineral particles via inducing electrostatic/steric repulsion forces between particles (Yuan et al., 1998; Boisvert et al., 2001). As kaolin minerals carry slightly negative charges, anionic polymers are normally the most efficient dispersants for kaolin dispersion (Das and Somasundaran, 2001; Konduri and Fatehi, 2017).

The properties of dispersants play key roles in stabilization of dispersion systems. In the past, the utilization of carboxyl containing synthetic polymers, e.g., polyacrylamide (PAM), for stabilizing kaolin dispersion was reported (Agnes et al., 1981; Nabzar et al., 1987; Pefferkorn et al., 1987; Lee and Somasundaran, 1989; Morris et al., 2002; Nsib et al., 2006; Kim and Palomino, 2009; Aso et al., 2013; He and Fatehi, 2015; Konduri et al., 2015). However, synthetic polymers may be expensive and environmentally unfriendly. Recently, reports were made available on the modification of lignin, which is a natural polymer extracted from wood via mainly pulping processes, to produce semi-synthetic polymers with cationic and anionic charge densities (He and Fatehi, 2015; Couch et al., 2016; He et al., 2016, 2017; Konduri and Fatehi, 2017). The polymerization of lignin and acrylamide can lead to a polymer with more environmentally friendly features than PAM. As this polymer had a negative charge density, it would function as a dispersant for kaolin dispersion. In this regard, lignin-acrylamide polymers with different molar masses and/or charge densities can be produced. These polymers have different physical and chemical characteristics than synthetic polymers, which may impact their dispersion performance (Pefferkorn et al., 1987; Rong et al., 2013a, 2013b). The first objective of this work is to study the impact of lignin-acrylamide (KAM) polymer as a dispersant for kaolin dispersion.

The behavior of kaolin mineral particles in the dispersion is strongly affected by the chemistry of the dispersion, such as dispersion pH and salt concentration (Nsib et al., 2006; Chibowski et al., 2009). Variations in pH were also reported to alter the adsorption of polymers onto kaolin mineral particles (Atesok et al., 1988). Similarly, salt significantly affected the interaction of particles in dispersions, and thus the interaction and performance of dispersants in dispersion systems (Shirazi et al., 2003; Chibowski et al., 2009; Mishra et al., 2014). The second objective of this work is to investigate how pH and salt in kaolin dispersion impact the performance of lignin-acrylamide polymer as a dispersant.

The main novelty of this study is the investigation of the dispersion performance of kraft lignin-acrylamide polymer in kaolin dispersion at different pHs and salt concentrations. The correlations between KAM adsorption on kaolin mineral particles, and the changes induced by KAM on the zeta potential, relative turbidity, particle size and stability of kaolin minerals in dispersion are established for the first time.

8.3 Materials and Methods

8.3.1 Materials

Softwood kraft lignin (KL) was produced via LignoForce^{TM} technology of FPInnovations in Thunder Bay, ON (Kouisni et al., 2012). Acrylamide, AM (99.0 wt. %), potassium persulfate ($K_2S_2O_8$) (analytical grades), potassium hydroxide, para-hydroxybenzoic acid, hydrochloric acid (0.1 M), $NaNO_3$, NaOH, H_2SO_4 (98%), KCl, NaCl (all analytical grades) and kaolin were all obtained from Sigma-Aldrich company. Cellulose acetate dialysis membrane (molar mass cut off of 1,000 g/mol) was obtained from Spectrum Labs. Inc., USA. All chemicals were used without further purification. Ethanol (95 vol.%) was received from Fisher Scientific company. Potassium polyvinyl sulfate (PVSK) was provided by Wako Pure Chem. Ltd. Japan. Polydiallyldimethyl ammonium chloride (PDADMAC) with the molar mass of 100,000–200,000 g/mol was obtained from Sigma Aldrich company and diluted to 0.005 M prior to use.

8.3.2 Polymerization of lignin

The free radical polymerization of KL was carried out in a 250 mL three-neck round-bottom glass flask under the reaction conditions listed in Table 8.1. First, a required amount of KL was dissolved in 40 mL of deionized water while stirring at 300 rpm. Predetermined quantities of AM were added to the flask and stirred for 30 min. The pH of the solution was adjusted using 0.1 M sulfuric acid. The reaction solution was continuously purged with nitrogen to remove any residual oxygen at room temperature for 30 min. Subsequently, potassium persulfate was added as an initiator to the system and the reaction solution was purged for another 5 min. The polymerization was processed by placing the flask in a preheated water bath after adjusting the pH of the system. The reaction was allowed to proceed for the desired time intervals under a continuous nitrogen supply. These reaction conditions generated lignin-acrylamide polymers with a high molar mass, charge density and solubility in a previous study (Wang et al., 2016a).

After completion of reaction, the solution was cooled to room temperature by immersing the flask in tap water for 20 min. The kraft lignin-acrylamide polymer was precipitated by adjusting the solution pH to 1.5 using sulfuric acid. Then, the sample was centrifuged at 3500 rpm for 10 min using a Sorvall ST 16 laboratory centrifuge (Thermo Fisher) in order to separate the lignin polymers from homopolymers (polyacrylamide, PAM) and unreacted acrylamide monomers.

This precipitation/centrifugation process was repeated three times and then the lignin-acrylamide polymers were collected. Then, the precipitated lignin polymers were mixed with 200 mL of deionized water. After adjusting the pH of the solution to 7.0 using a 1M NaOH solution, the samples were dialyzed using the dialysis membrane for 48 h in order to remove impurities (e.g., inorganic salts and monomers) from the polymer solutions. The deionized water used for dialysis was changed every 12 h for 2 days. After dialysis, the solution containing lignin-acrylamide samples were dried at 105°C, and the dried samples were kept for further analysis. This lignin polymer is denoted as KAM, while unmodified kraft lignin is denoted as KL in this work. All experiments were repeated three times, and the average data and error bars are presented in this work.

Table 8.1. Reaction conditions and properties of KAM

Conditions	**KL**	**KAM-1**	**KAM-2**	**KAM-3**
Temperature, °C	-	90±0.02	60±0.03	80±0.02
Time, h	-	5±0.03	2±0.03	2±0.02
KL, mol	-	0.016±0.01	0.011±0.01	0.016±0.01
AM, mol	-	0.014±0.01	0.014±0.01	0.042±0.01
pH	-	4±0.2	2±0.2	5±0.22
Initiator, mmol	-	0.11±0.01	0.11±0.01	0.11±0.01
Anionic charge density, meq/g	0.21±0.03	0.82±0.03	1.37±0.05	2.1±0.02
COOH content, mmol/g	0.14±0.01	0.63±0.02	1.1±0.03	1.78±0.04
Solubility, g/L	0.5±0.04	4.5±0.1	4.5±0.1	4.7±0.09
M_w, g/mol	17, 890±11.54	24, 590±10.34	50215±11.76	96992±10.23
M_n, g/mol	5150±5.77	23129±9.77	28741±8.55	69716±10.35
Nitrogen, wt.%	0.03±0.01	1.57±0.03	3.8±0.05	6.2±0.05

8.3.3 Specific surface area analysis of kaolin

The specific surface area of kaolin was determined by using Quantachrome surface area analyzer, a Nova 2200e instrument, USA. In this experiment, the samples were initially dried in an oven at 105 °C overnight, and approximately 0.05 g of sample was pretreated for 4 h at 250

°C prior to analysis. The specific surface area of the samples was then determined according to Brunauer-Emmett-Teller (BET) method via adsorption-desorption isotherms using nitrogen gas at -180°C in the relative pressure range of 0.01 and 0.99 (Oveissi and Fatehi, 2014).

8.3.4 Chemical analysis of kaolin

The chemical composition of kaolin was determined using scanning electron microscopy (SEM), Hitachi Su-70, with energy dispersive X-ray spectroscopy (EDX) (Senoussi et al., 2016). In this set of experiments, 0.2 g of kaolin was dispersed in 20 mL of acetone under ultrasonic vibrations for 5 min and allowed to air dry for 24 h. After drying, the sample was coated with carbon using Edward Auto 306 system (Edward International Corp, UK) under vacuum (3×10^{-5} mbar) for 10 min prior to SEM analysis.

X ray diffractometry (XRD) analysis was carried out to determine the compositions of the samples and their distribution using spinning stage PANalytical X'pert-PRO diffractometer (XRD), PW1050–3710 with a Cu Kα (λ = 1.5405 Å) radiation source (Senoussi et al., 2016). A 0.5 g of kaolin samples were air dried and transferred onto the spinner of XRD. The XRD scan of kaolin was performed in a continuous mode from 6 to 97° with a 0.026° step size and a scan speed of 0.164 (°/Sec) for total scan time of 9 min. The chemical compositions were identified by analyzing the positions of the peaks using the X'pert High Score software package supplied with the instrument (Mcintosh et al., 2015). The loss on ignition (LOI) of kaolin was determined via following TAPPI T413 method by incinerating the kaolin at 900 °C for 8 h (Santisteban et al., 2004). All experiments were repeated three times and the average values were reported.

8.3.5 Solubility and charge density determinations

To measure the solubility of the KAM products, 0.2 g of KAM was added to 20 mL of deionized water by stirring at 100 rpm and 30 °C for 1 h in a water bath shaker (Innova 3100, Brunswick Scientific, Edison, NJ, USA). Then, the dispersions were centrifuged at 1000 rpm for 5 min. The supernatants were collected and used for analyzing the charge density and solubility of the polymers. The concentration of the polymers in the supernatants was determined by drying the supernatants at 105 °C, and the solubility was determined based on the concentration of the polymers in the supernatants and the initial amount of the polymer (0.2 g). The charge density of the polymers was measured by a particle charge detector, Mütek PCD 04 titrator (Herrsching, Germany) with a PDADMAC solution (0.0050 M) following the method established earlier

(Wang et al., 2016a, 2016b). Three repeats were carried out, and the average values were reported.

The surface charge density analysis of the particles was performed via following a back-titration method with a Mutek, PCD 04, particle charge detector (Germany). Approximately, 0.2 g of kaolin was suspended in 50 mL of PDADMAC (0.005M) solution and the dispersion was incubated at 30 °C for 1 h and 150 rpm. After the incubation, the samples were filtered using Whatman#1 filter membranes and the filtrates were titrated against PVSK (0.0055 M) solution. Similarly, the titration analysis was conducted for the control sample (i.e., PDADMAC solution with no kaolin addition), and the difference was considered for quantifying the surface charge density of kaolin mineral particles.

8.3.6 Carboxylate group analysis

The carboxylate groups of KL and KAM were measured using an automatic potentiometric titrator, 785 Titrino. In this analysis, 0.06 g of lignin samples were placed in a 250 mL beaker and then 1 mL of potassium hydroxide (0.8 M) was added. Afterward, 0.02 g of para-hydroxybenzoic acid were added as internal standard to the solution and subsequently 100 mL of deionized water were added. The solution was stirred for 30 min to ensure proper mixing. In addition, control samples were prepared by mixing 0.02 g of para-hydroxybenzoic acid, 1 mL of 0.8 M potassium hydroxide solution and 100 mL of deionized water in beakers. After completion, the prepared solutions were titrated with a 0.1 M HCl standard solution. In the titration experiment, the last three endpoints appeared in sequence of pH drop of the sample solutions were noted as V_1', V_2' and V_3', respectively. The corresponding three endpoints in the titration curve of blank sample were specified as V_1, V_2 and V_3, respectively. The carboxylate contents of samples were calculated according to Equation (8.1):

$$\text{Carboxylate group } \left(\frac{mmol}{g}\right) = \frac{C_{HCl}\left[\left(V_3' - V_2'\right) - \left(V_3 - V_2\right)\right]}{m} \qquad (8.1)$$

where C_{HCl} is the concentration of HCl solution (0.1 mmol/L) as titrant, and m is the mass (g) of the sample. V_2 and V_3 are the volumes (mL) of HCl solution used for the two endpoints in the

blank titration. V'_2 and V'_3 are the volumes (mL) of HCl solution, used for the two endpoints in sample titration, respectively. The reported data in this chapter is the average of three repetitions.

8.3.7 Molar mass analysis

About 5 mg sample of dried KAM polymer was dissolved in 10 mL of 5.0 wt.% acetic acid solution by stirring at 600 rpm for 48 h and 35 °C, and then the solution was filtered with a 13 mm diameter nylon filter (pore size 0.2 μm). The filtered solutions were used for the molar mass analysis, which was carried out using a gel permeation chromatography (GPC) (Viscotek GPCmax, Malvern, UK) with viscometer and UV detectors. PolyAnalytic, A206 and A203 columns were set at operating temperature of 35 °C. 0.1M of $NaNO_3$ solution was used as solvent and eluent with the flow rate of 0.7 mL/min. Polyethylene oxide was used as standard for calibrating the GPC instrument. All experiments were repeated three times and the average values were reported.

8.3.8 Elemental analysis

The elemental analysis was performed for KL and KAM polymers using an elemental analyzer, Elementar Vario EL Cube, following the combustion method (Jahan et al., 2012). The samples were first dried in an oven at 105 °C overnight to remove any moisture prior to analysis. Approximately, 2 mg of dried samples were transferred into the carousel chamber of the elemental analyzer and combusted at 1200 °C to reduce the generated gasses to analyze carbon, hydrogen, oxygen and nitrogen contents of the samples. The report values in this chapter are the average of three repetitions.

8.3.9 Hydrodynamic diameter assessment of KL and KAM in aqueous solutions

The hydrodynamic diameter (Hy) of the KL and KAM polymers was measured using a static light scattering analyzer (BI-200SM Brookhaven Instruments Corp., USA). The light source was a power solid state laser with a maximum power of 35 mW and a wavelength of 637 nm. The scattering angle was set at 90°. In this set of experiments, 0.5 g/L of KL and KAM polymer samples were prepared in 0.01 M NaCl solution and stirred for 30 min at pH 4, 7, and 10. The samples were kept at room temperature for 24 h to reach equilibrium (Kong et al., 2015). In another set of experiments, 0.5 g/L of KAM polymer samples at different salt concentrations

(0.1-1M NaCl) were prepared and stirred for 30 min at pH 7. The pH of the solution was adjusted using 0.1 M sulfuric acid. Each test was performed for 2 min. Subsequently, 20 mL of the sample solutions were filtered with a 0.22 μm disposable syringe filters and kept in glass bottles. The hydrodynamic diameter of the samples was analyzed by the light scattering instrument. All measurements were carried out in triplicate.

8.3.10 Contact angle and surface tension determination

KL and KAM polymers were coated on glass slides using a spin coater. In this set of experiments, KAM solution (16 mg/g based on kaolin) was added to deionized water (25 mL) and stirred for 1 h at 300 rpm and 30°C. The pH of the solution was adjusted to 4, 7 and 10 using 0.1 M NaOH or 0.1 M H_2SO_4. 2 mL of KL and KAM solutions were dropped on the glass slide located in the chamber of a spin coater (Model WS-650, Laurell Technologies Corp., USA), while rotating at 200 rpm. This rotation was continued for 30 sec, then increased to 250 rpm and continued for another 30 sec. In this process, the system was continuously purged with N_2 gas at 60 psi (Ponnusamy et al., 2012). Once the KAM coated slides were dried at room temperature, drops (5 μL) of water were placed at different locations of the KAM coated glass slide and the contact angles of the droplets and the surface were identified after 20 sec using an optical tensiometer (Theta Lite, Biolin scientific, Finland) at 25 °C. The contact angle of each droplet was determined as a mean value of measurements on 3 different spots on the glass slides.
The surface tension of KAM solutions was measured using an Attention Surface tensiometer (Biolin, model # Sigma 700) via the du Nouy ring method. In this set of experiments, 20 mL of previously made KAM solution at a 10 g/L concentration was transferred to glass containers for surface tension determination. This test was performed by placing the ring in the liquor and then pulling the ring upward through the surface of the liquid slowly. The distance between the immersed ring and liquid surface was maintained to ensure a clean break of the meniscus on the immersed platinum–iridium ring. The radius of the ring was given by the manufacturer as 9.545 mm and the radius of the cross-section of wire was 0.185 mm. The platinum loop was cleaned with ethanol and deionized water between each test. The surface tension of KAM solutions was measured, and each measurement was replicated 10 times to ascertain the reproducibility of the results. All the measurements were carried out at 25 °C and pH 4, 7 and 10. The reported data in this chapter is the average of three repetitions.

8.3.11 Hydrodynamic size determination of kaolin

The size distribution of kaolin at varying pH (4, 7, and 10) was analyzed using a particle size analyzer, MasterSizer 3000 (Malvern Instruments). In this study, 1.0 g of clay dispersion (20 g/L) was added to 50 mL of deionized water or 50 mL of KAM solution containing the polymers at the dosage of 16 mg/g (based on clay) and stirred at 300 rpm and room temperature for 1 h. After stirring, the particle size distribution of the samples was analyzed. The pH of the suspensions was adjusted with 0.1 M NaOH solution or H_2SO_4. The range of hydrodynamic diameter distributions of minerals and flocs in kaolin and kaolin/KAM dispersions was assessed using this machine, and the results were considered for correlating the particle size distribution and volume fractions of minerals and flocs in the section 8.3.14. The reported data in this chapter is the average of three repetitions.

8.3.12 Adsorption studies

The adsorption of KL or KAM on kaolin at varying pHs (4, 7 and 10) and dosages (2 – 128 mg/g based on kaolin) was studied. In this set of experiments, varied dosages (2 to128 mg/g on kaolin) of KL or KAM were added to the kaolin dispersion (0.4 g/L) at a desired pH and stirred at 300 rpm and 25°C for 1 h. The pH of the kaolin dispersion was adjusted to 4, 7 and 10 using 0.1 M NaOH or 0.1 M H_2SO_4. After adsorption process, the samples were centrifuged for 15 min at 3500 rpm and then the concentrations of KAM remaining in the supernatants were determined by UV/Vis spectrophotometer (Genesys 10S UV–vis, Thermo FisherScientific, USA) at a wavelength of 205 nm. To determine the salt impact, the optimal dosage of 16 mg/g (based on kaolin) of KL or KAM was maintained in the kaolin dispersion (0.4 g/L) at different salt concentrations (0.1-1 M NaCl), and the aforementioned analysis was repeated. All the experiments were performed in triplicates and the average values were reported in the study.

8.3.13 Zeta potential analysis

The zeta potential of kaolin was determined using a NanoBrook Zeta PALS (Brookhaven Instruments Corp, USA). In this study, different dosages (2 to 128 mg/g based on kaolin) of KL or KAM polymers were prepared in 50 mL of kaolin dispersion (0.4 g/L) at pH 4, 7 and 10 and stirred at 300 rpm and 25°C for 1 h. After mixing, their zeta potential was measured in a 1.0 mM KCl aqueous solution. All the measurements were carried out at room temperature with a

constant electric field (8.4 V/cm). The experiments were carried out three times and the average values were reported in this study.

8.3.14 Dispersion analysis under dynamic conditions

Dispersant performance of KAM in kaolin dispersions was assessed using a photometric dispersion analyzer (PDA 3000, Rank Brothers Ltd) that was connected to a dynamic drainage jar (DDJ) with a 70 mm mesh screen (Fatehi et al., 2013). In this set of experiments, 490 mL of distilled water was first added into the DDJ container and circulated from the DDJ to the PDA through a 3 mm plastic tube until a steady flow rate of 20 mL/min was achieved. The flow rate was regulated by a peristaltic pump throughout the experiment. Then, 10 mL of a 20 g/L kaolin dispersion was added into DDJ (to make a 0.4 g/L kaolin concentration) at varying shearing rates (between 50 and 500 rpm). In another set of experiments, the optimal dosage of 16 mg/g (based on kaolin) of KL or KAM was maintained in the DDJ at varying shear rates of 50 to 500 rpm. This caused a decrease in the initial base DC voltage (V_0) to a new DC voltage (V_i). After 100 s, varying dosages of KL or KAM (2 to 128 mg/g of kaolin) were added into DDJ containing 500 mL of the kaolin dispersion (0.4 g/L) at 300 rpm. The increase in DC voltage was represented as the DC voltage (V_f) of the final dispersion. All of the tests were carried out at three different pH of 4, 7 and 10 of kaolin dispersion, which was controlled by adding 0.1 M NaOH or 0.1 M H_2SO_4. The reported data in this chapter is the average of three repetitions.

The relative turbidity of the kaolin dispersion was measured using equation 8.2 (Wang et al., 2009):

$$\text{Relative turbidity, } \tau_r = \frac{\tau_f}{\tau_i} = \frac{ln(\frac{V0}{Vf})}{ln(\frac{V0}{Vi})} \qquad (8.2)$$

where τ_f is denoted as the final dispersion turbidity, and τ_i is denoted as initial dispersion turbidity.

8.3.15 Dispersion analysis under static conditions

The stability of the kaolin dispersion in the presence and absence of KAM was investigated using a vertical scan analyzer, Turbiscan Lab Expert, Formulaction, France. This method has been used for studying the stability of waste and mineral dispersion (Vie et al., 2007; Jamrozik et al., 2014; He et al., 2016). In one set of experiments, kaolin dispersions (0.4 g/L) with altered pH

of 4, 7 and 10 were prepared in the presence (dosages of 2 to 128 mg/g based on kaolin) or absence of KAM. Then, 20 mL of the dispersion was transferred to the cylindrical tube of the instrument and subjected to analysis for 1 h. The dispersions were vertically scanned at 880 nm wavelength every 2 sec at 30 ºC and the results were analyzed using Turbisoft 2.1 software. In this equipment, two synchronous optical sensors receive light that is transmitted through and light that is backscattered by the sample. One sensor is placed at an angle of 180° relative to the incident light beam and measures the transmitted light intensity and the other is placed at an angle of 45° to the light source to measure the backscattered light intensity. The backscattering signals generated by the sample were compared with that of the standard silicon oil, which was used for calibrating the instrument (Mengual et al., 1999).

The backscattering (BS) intensity of incident light is measured by determining the mean free path of photons ($l*$) through the medium (Breitung et al., 2011). The backscattering data can be obtained for concentrated dispersions as a function of photo transport mean free path, I* (Breitung et al., 2011) in equation 8.3:

$$BS = \frac{1}{\sqrt{I^*}} \qquad (8.3)$$

In addition, the photo transport mean free path, I*, can be obtained via following equation 8.4.

$$I^*(d, \theta) = \frac{2d}{3\theta\,(1-g)Q_s} \qquad (8.4)$$

where d is the particle mean diameter, θ is the particle volume fraction, g and Qs are the scattering efficiency factors, which depend on the particle diameter (d), wave length of light (λ), refractive index of suspended kaolin minerals particles (n_p) and the refractive index of continuous phase (n_f). In this work, the computation was based on the refractive indices of kaolin mineral particles (1.54) and water (1.33) in the sample (He et al., 2016).

According to Eqs. 8.3 and 8.4, the intensity of backscattering light depends on the particle mean diameter, d, and their volume fraction, θ (Celia et al., 2009). Information about the diameter of kaolin minerals can facilitate the determination of the volume fraction of the particles. The hydrodynamic size distribution of kaolin (ranging 0.06 and 18.7 μm) was measured as stated in

section 8.3.11 and the hydrodynamic size distribution of kaolin/KAM dispersion was in the range of 0.08 and 29.7 μm. These ranges were considered for identifying the volume fraction of the minerals using equation 8.4 in the dispersion analysis. The reported data in this chapter is the average of three repetitions.

8.4 Results and Discussion

8.4.1 Characterization of kaolin minerals

Table 8.2 lists the properties of kaolin. The average particle size and specific surface area of kaolin were 4.7 μm and 55.65 m^2/g, respectively. The surface charge density of kaolin was – 5.5 μeq/g, and this charge is attributed to the presence of oxide anions on their surface (Loginov et al., 2008). The chemical analysis of kaolin (Table 8.2) revealed the significant presence of Al_2O_3 (34.92 wt.%) and SiO_2 (49.12 wt.%), as well as the loss of ignition was 13.6 wt.%. Furthermore, the loss of ignition for kaolin was 13.6 wt.%. XRD showed that kaolin contains kaolinite (85 wt.%) as a major mineral constituent along with small amount of dickite (6 wt.%), narcite (2 wt.%), quartz (4 wt.%) and hematite (2 wt.%).

Table 8.2. Chemical compositions of kaolin

Oxides	**Al_2O_3**	**SiO_2**	**Na_2O**	**K_2O**	**TiO_2**	**Fe_2O_3**	**LOI***
Wt.%	34.92±0.03	49.12±0.02	0.49±0.01	0.68±0.01	0.60±0.01	0.71±0.01	13.6±0.01

8.4.2 Polymerization of KAM

The polymerization of kraft lignin and AM was carried out following a free radical polymerization mechanism. In this reaction, potassium per sulfate acts as an initiator in an aqueous solution. As illustrated in scheme 8.1a, potassium per sulfate initially produce sulfate radicles in the reaction medium, which converts lignin to phenoxy radicals and the radicals serve as a reaction site on the lignin backbone for the polymerization. These free radical sites then react with AM monomers to form KAM polymers (scheme 8.1b). Also, sulfate radicals can initiate the homopolymerization of AM, resulting in polyacrylamide (PAM) as a by-product (scheme 8.1c).

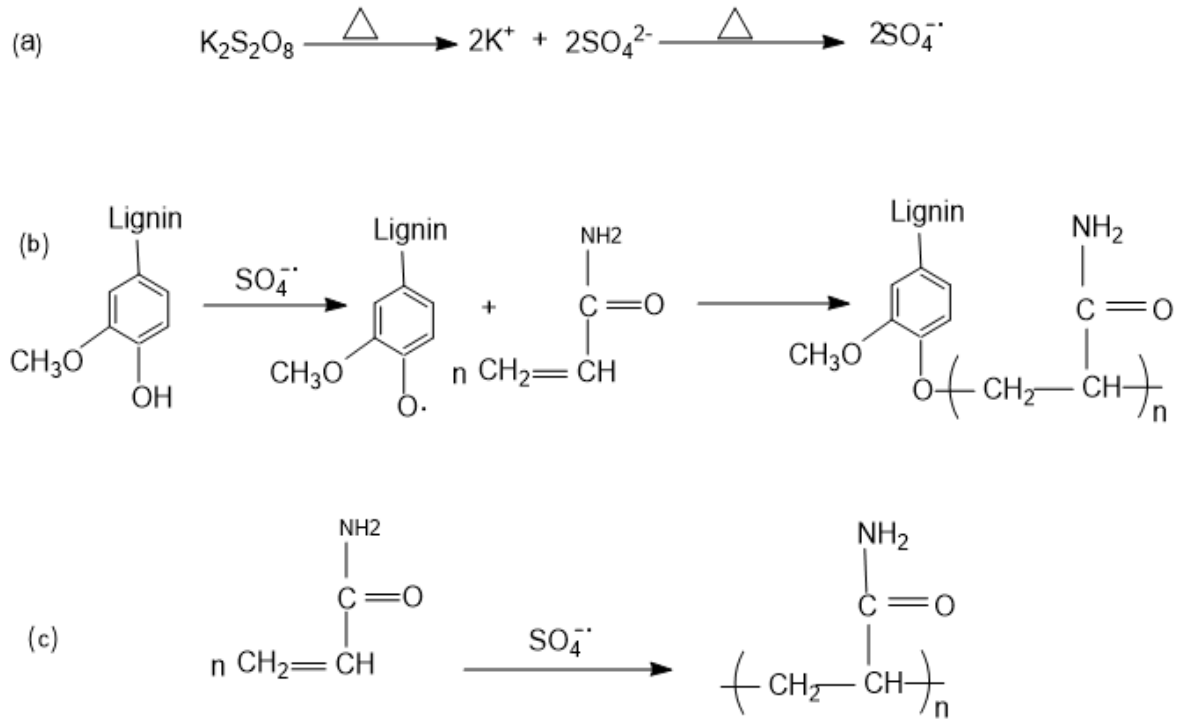

Scheme 8.1. Copolymerization of kraft lignin and acrylamide.

8.4.3 Properties of KAM

The KL and AM was synthetized to produce KAM with different molar masses but a similar solubility (Table 8.1). The increase in the nitrogen content confirmed the grafting of AM onto the lignin backbone, which was well aligned with the change in the molar mass of KAM-1, KAM-2 and KAM-3. An increment in the molar mass average (M_w) was observed for KAM-1 (M_w of 24, 590 g/mol), KAM-2 (M_w of 50, 215 g/mol) and KAM-3 (M_w of 96, 992 g/mol). A similar trend was observed for number average molar mass (M_n) in Table 8.1. The solubility of unmodified KL was found to be 0.5 g/L, whereas KAM-1, KAM-2 and KAM-3 were approximately 4.5 g/L soluble in water. It is also seen that the anionic charge densities and carboxylate groups on the KAM backbone increased with increasing its molar mass.

Also, KAM-3, which was produced under the reaction conditions of 80°C, 2 h, 0.016 mol of KL, 0.042 mol of AM and pH 5, had the highest molar mass and nitrogen content among all (Table 8.1). It is seen that the temperature of 80°C was more effective than other temperatures in generating KAM with a high molar mass and charge density. Apparently, a more acidic reaction

environment and longer reaction time (5 h) hampered the progress of the polymerization reaction and generated a polymer with a smaller molecular mass and charge density (Naguib, 2002; Fang et al., 2009).

8.4.4 Contact angle and surface tension

The variations in the contact angle (°) and surface tension (mN/m) of water on the slides coated with KL/KAM are listed in Table 8.3. The contact angle of water droplet on the glass slide was 21°. As observed, water droplet created a larger contact angle with the slide coated with KL, suggesting the hydrophobic nature of lignin polymer. After coating the slides with KAM, the slide's surface became more hydrophilic, and a smaller contact angle was observed for the water droplet on the surface. It can be seen that, KAM significantly reduced the surface tension of water (72.75 mN/m). This result can be correlated well with the contact angle results, suggesting an increase in wettability of the surface when KAM was used.

By increasing the charge density of KAM, the contact angle and surface tension of the KAM coated slides were reduced, implying that KAM-3 made the surface of glass slide more hydrophilic than did other KAMs. The wettability of KAM could be significantly influenced by the interactions of water molecules with hydrophilic group originated from -$CONH_2$, -COO, -OH groups of KAM (Carmes et al., 2011; Yang et al., 2007) at the slide surface. The attraction force developed between water molecules and KAM became more significant than between water molecules themselves due to the presence of hydrophilic functional groups of KAM. As a result, water molecules started to spread on the glass slides coated with KAM. It is also seen that the surface tension and contact angle was lower at a higher pH for all samples.

Table 8.3. Contact angle and surface tension results

	pH 4		**pH 7**		**pH 10**	
Polymer	Contact angle (°)	Surface tension (mN/m)	Contact angle (°)	Surface tension (mN/m)	Contact angle (°)	Surface tension (mN/m)
KL	32.15±0.03	65.6±0.07	30.51±0.09	59.35±0.5	28.33±0.02	57.1±0.05
KAM-1	21.43±0.09	63.29±0.07	20.46±0.06	58.23±0.07	19.34±0.03	56.2±0.05
KAM-2	19.34±0.05	62.74±0.09	15.34±0.06	56.35±0.06	14.66±0.05	52.13±0.01
KAM-3	15.71±0.08	62.13±0.06	14.46±0.08	55.1±0.05	13.7±0.1	51.6±0.1

8.4.5 Adsorption analysis

Figure 8.1 shows the adsorption of KAM on kaolin as a function of KAM dosage at pH 4, 7 and 10. As can be seen, KAM adsorption increased to saturation as the dosages of KAM was enhanced. It is implied that the higher molar mass of KAM-3 formed a large number of hydrogen bonds between kaolin minerals and polymer chains, which enhanced its adsorption on kaolin mineral particles as compared to KAM-1 and KAM-2.

At pH 4, KAM-3 (2.16 mg/g), KAM-2 (1.92 mg/g) and KAM-1 (1.82 mg/g) achieved the maximum adsorption at 16 mg/g of polymer dosage (based on kaolin). At a pH higher than kaolin minerals' isoelectric point (i.e. pH of 2.2) (Besra et al., 2002), the surface charge density of kaolin minerals reported to be negative due to the deprotonation of its aluminol groups (Pefferkorn et al., 1987). On the other hand, KAM polymer has more protonated carboxylate group (-COOH) than deprotonated (-COO) at pH 4 (pK of 4.7). Hence, its driving force for adsorption on kaolin minerals is predominated by hydrogen bonding and not by electrostatic charge interaction at pH 4 (Pefferkorn, 1999; Mpofu et al., 2005). The results shown in Figure 8.1 are in agreement with the findings of other researchers (Chibowski and Knipa, 2000; Wisniewska, 2010). In one study, the adsorption of polyvinyl pyrrolidone on kaolin was decreased by 14.0 wt.% with an increase in the pH from 2 to 10 (Bhatti et al., 2012).
Table 8.4 lists the hydrodynamic diameter (Hy) of KAM at different pHs. It is seen that Hy of KAM was generally smaller at lower pH values. At a low pH, KAM polymer carries less ionized functional groups, thus weak repulsive forces created within KAM segments triggering the polymer chains to coil (Das et al., 2013). In one study, the hydrodynamic diameter of anionic polyacrylamide in alumina dispersion reported to be increased from 19.5 to 25.1 nm with the pH increase from 3 to 9 (Wisniewska and Urban, 2015a). Hence, the smaller size of KAM at pH 4 (Table 8.4) enhanced its adsorption as the smaller KAM occupied less specific surface area and thus more of these polymers could adsorb on the surface (Chibowski et al., 2009). This trend is consistent with the finding of Wisniewska et al. (2015b) stating that the adsorption of anionic PAM on the alumina surface decreased with the pH increase from 3 to 9. Ma and Bruckard (2010) also reported that starch adsorption on kaolin mineral particles was pH dependent in that its adsorption decreased with increasing pH from 7 to 10.5.

Table 8.4. Hydrodynamic diameter (nm) of KL and KAM in 0.01 M NaCl solution

Polymer	pH 4	pH 7	pH 10
KL	8±0.10	9.5±0.11	10.5±0.05
KAM-1	33.5±0.11	49.7±0.10	58.2±0.10
KAM-2	37.63±0.11	59.3±0.11	68.9±0.05
KAM-3	40.69±0.09	73.12±0.10	85.3±11

At pH >4, the carboxylate group of KAM would be deprotonated, which improves its hydrogen bonding capability (Farrokhpay et al., 2004; Mekhamer et al., 2009). However, the higher charges of KAM would induce higher repulsion between the adsorbed KAM and approaching KAM from the medium for adsorption on the kaolin minerals' surface.

At pH > 10, KAM polymer is fully ionized due to the deprotonation of carboxylate and phenolate groups. The anionic charges on the KAM causes the polymer chain to be more stretched due to intramolecular electrostatic repulsion leading to an extended Hy (Table 8.4). Also, strong repulsion force is developed between adsorbed KAM on the surface and approaching KAM from the medium to the surface. Therefore, the larger Hy and stronger repulsion force were probably the reason for the lower adsorption of KAM at pH greater than 4. In addition, hydroxyl ions in the dispersion may also compete with KAM to adsorb on kaolin mineral particles at a high pH. Therefore, the larger hydrodynamic size, stronger repulsion force and competition with hydroxyl ions were probably the primary factors for the lower adsorption of KAM under alkaline pH on kaolin mineral particles (Figure 8.1).

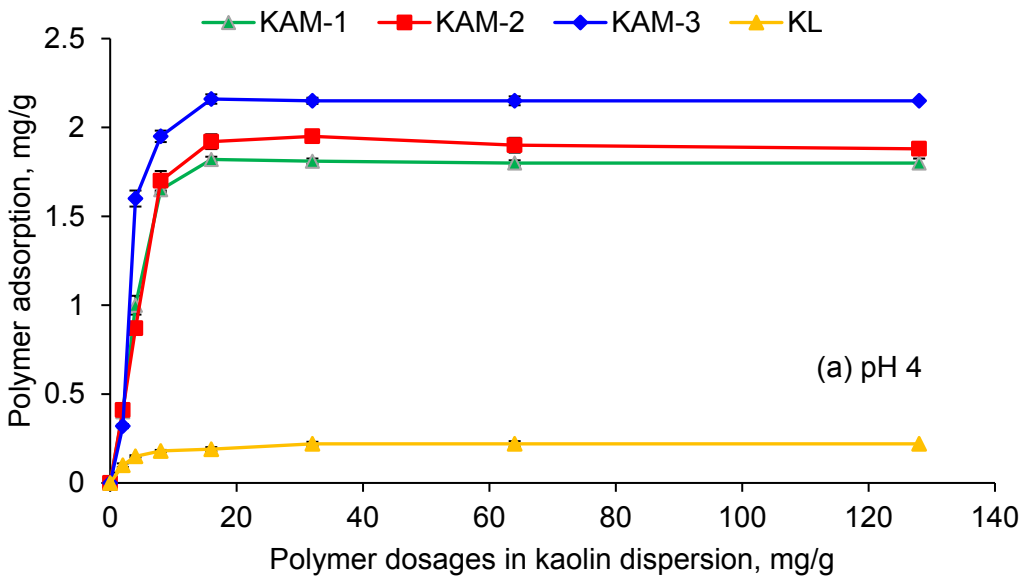
KAM-1
KAM-2
KAM-3
KL
Polymer adsorption, mg/g
Polymer dosages in kaolin dispersion, mg/g
(a) pH 4
0
0.5
1
1.5
2
2.5
0
20
40
60
80
100
120
140

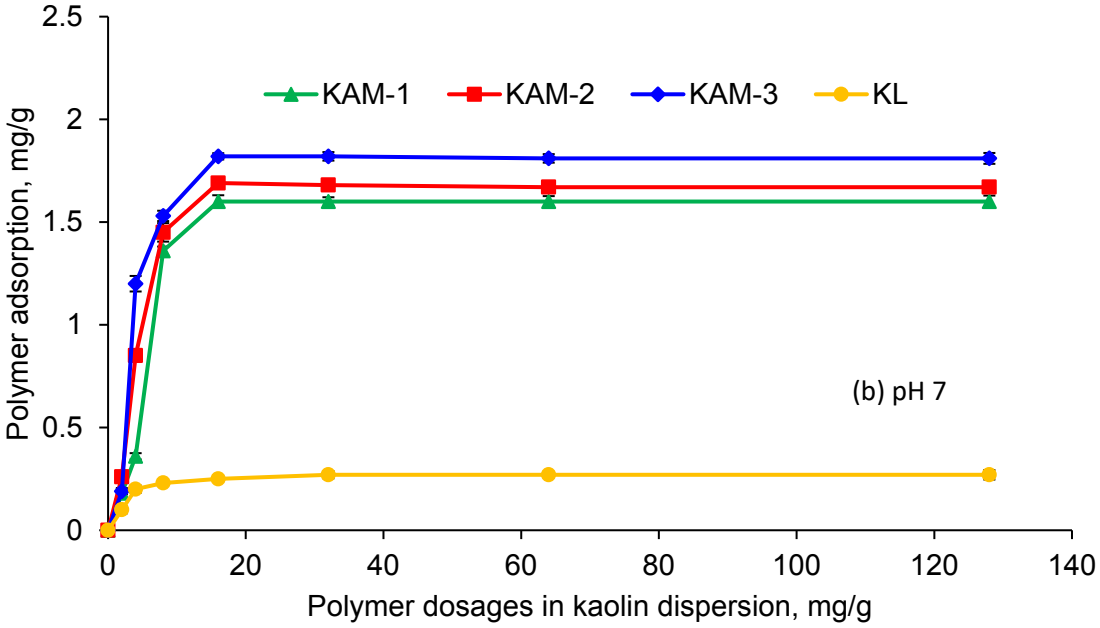
KAM-1
KAM-2
KAM-3
KL
Polymer adsorption, mg/g
Polymer dosages in kaolin dispersion, mg/g
(b) pH 7
0
0.5
1
1.5
2
2.5
0
20
40
60
80
100
120
140

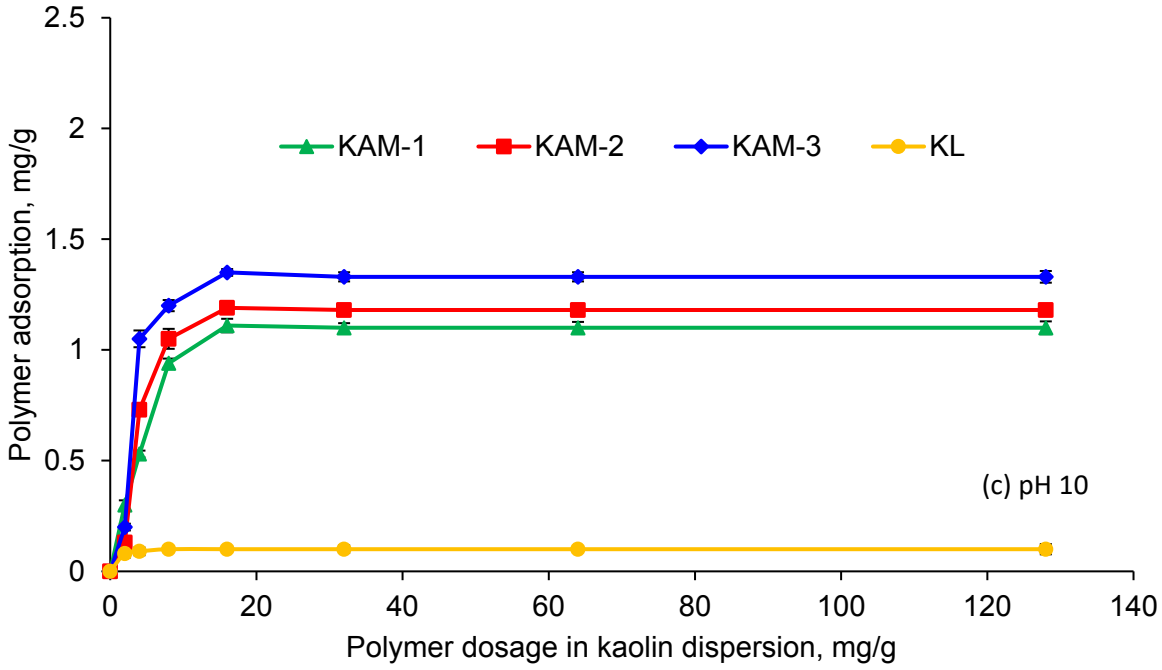

Figure 8.1. Adsorption of KL/KAM on the surface of kaolin as a function of KAM dosage; under the conditions of 0.4 g/L kaolin, 25°C and 1 h.

In order to gain a greater insight into the relationship between adsorption and the size of KAM, the hydrodynamic diameter of the KAM was determined as a function of salt concentration at pH 7 in Figure 8.2. It is observed that the higher NaCl concentration led to the smaller hydrodynamic diameter, which is in agreement with previous results (Mishra et al., 2014). The decrease in the hydrodynamic diameter is most likely attributed to the reduction in the repulsion force between the anionic charged groups within the KAM structure due to counterion screening induced by salts (Yoshikawa and Lewis, 2008). In the past, NaCl reduced the electrostatic repulsion between the $–COO^-$ groups of PAM and induced PAM with a collapsed coil shape structure (Chen et al., 2012). In another research (Yoshikawa and Lewis, 2008), the hydrodynamic diameter of polyacrylic acid was decreased from 4 to 2.7 nm with salinating the solution. Among the three KAM polymers, the extent of hydrodynamic size reduction for KAM-3 (228 to 34 nm) found to be the greatest as compared to other KAM. These findings revealed that with increasing ionic strength, the higher molar mass polymers had a more compact coiled conformation and less electrostatic intersegment repulsion. Thus, the salt concentration had

possibly more pronounced impact in reducing the hydrodynamic size of this polymer segment (KAM-3).

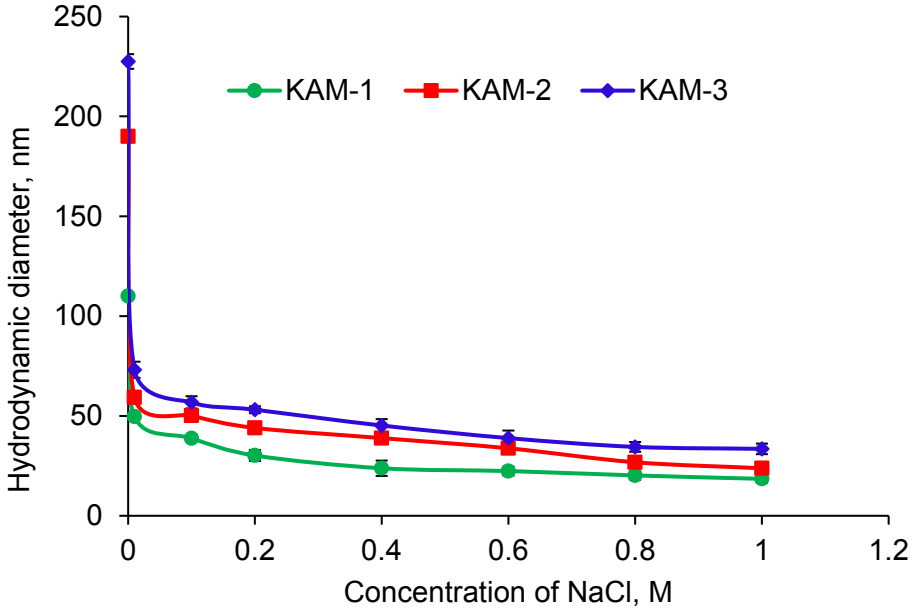

Figure 8.2. Effect of NaCl concentration (0.1-1M) on the Hy of KAM, conducted under the conditions at pH 7, 25 °C in aqueous solution.

Adsorption of KL and KAM on kaolin at different ionic strengths was assessed in Figure 8.3. As observed, the adsorption capacity of KAM increased with increasing NaCl concentration and decreasing pH. These results are in agreement with the findings in the literature (Morris et al, 2002; Ali and Mahmud, 2015). NaCl could screen the repulsive forces between charges on KAM segments and reduce the Hy of KAM (Table 8.2 and Figure 8.2). This implies that at a high salt concentration, KAM polymer becomes more compact, and thus requires smaller specific surface area to be adsorbed on the particle's surface. In addition, NaCl can screen the repulsive forces developed between the adsorbed KAM and approaching KAM segments facilitating the adsorption of KAM on the particles via developing hydrogen bonds. Morris et al. (2002) also observed that the adsorption of anionic polyacrylamide onto talc increased at high ionic strength or low pH. In another research, the adsorption capacity of PAM on sepiolite was enhanced from 151.5 to 188.7 mg/g with increasing NaCl concentration from 0.001 to 0.1M (Tekin et al., 2006).

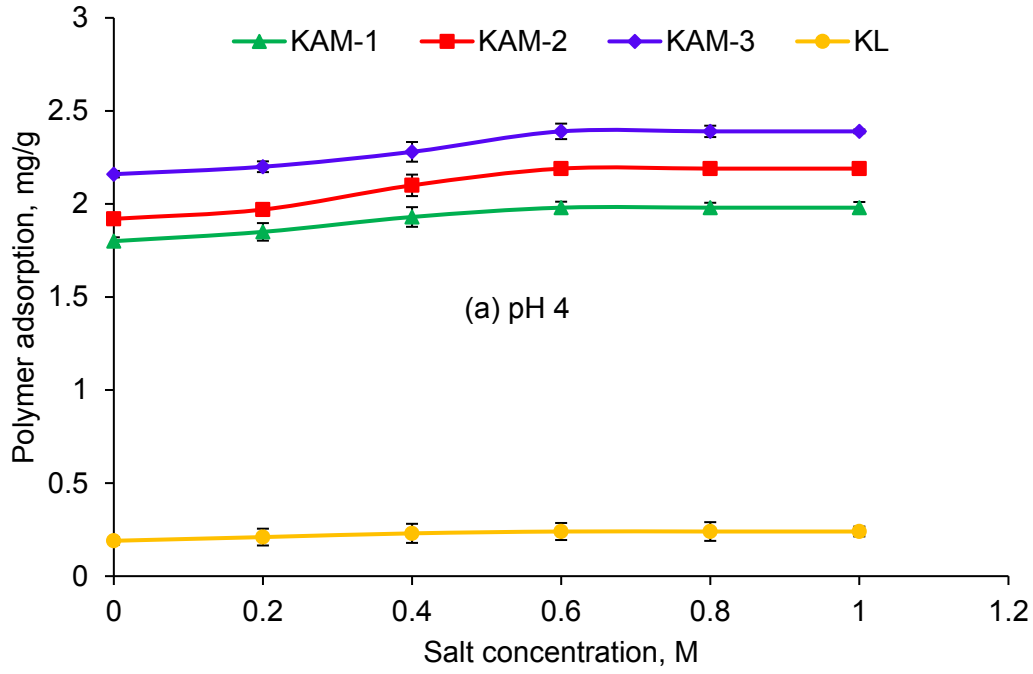
KAM-1
KAM-2
KAM-3
KL
Polymer adsorption, mg/g
(a) pH 4
Salt concentration, M
0
0.5
1
1.5
2
2.5
3
0
0.2
0.4
0.6
0.8
1
1.2

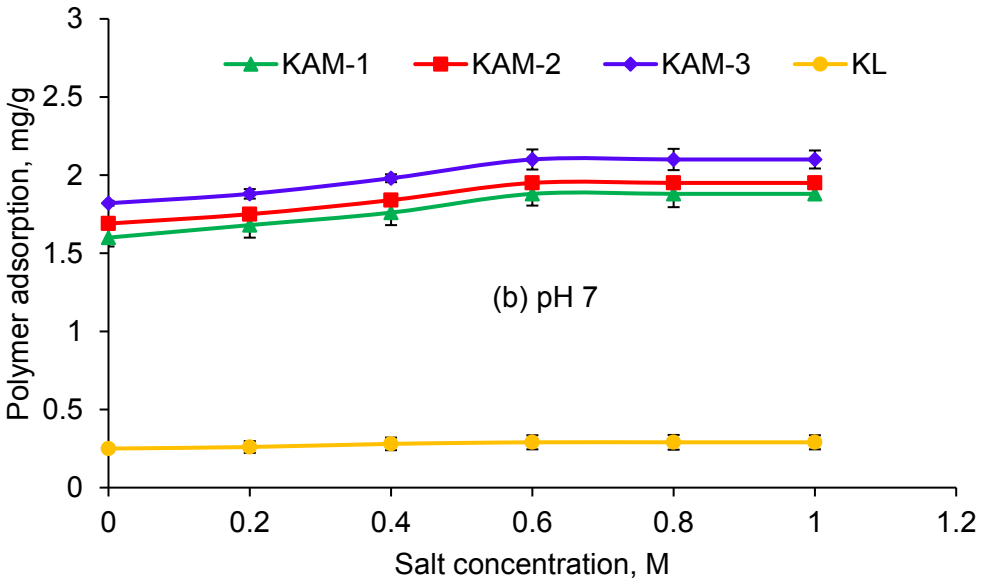
KAM-1
KAM-2
KAM-3
KL
Polymer adsorption, mg/g
(b) pH 7
Salt concentration, M
0
0.5
1
1.5
2
2.5
3
0
0.2
0.4
0.6
0.8
1
1.2

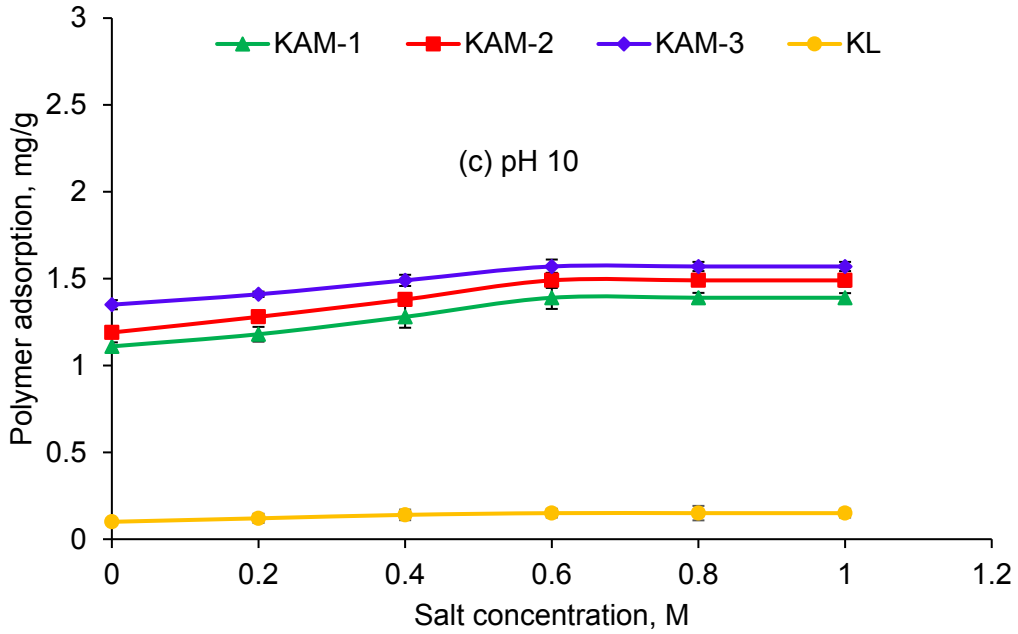

Figure 8.3. Effect of NaCl concentration on the adsorption of KL/KAM on kaolin, conducted under the conditions of 16 mg/g of dosage, 0.4 g/L kaolinite, 25 °C and 1 h.

8.4.6 Zeta potential analysis

Figure 8.4 shows the zeta potential of kaolin mineral particles at pH 4, 7 and 10 as a function of the adsorbed KAM. It is observable that the zeta potential of the kaolin dispersion was negative over the entire pH range after KAM adsorption. Moreover, an increase in the adsorption reduced the zeta potential of the dispersion regardless of their pH. This reduction is attributed to adsorption of KAM on kaolin mineral particles (Figure 8.1), which increased the overall negative charges of the double layer of kaolin mineral particles (Mpofu et al., 2003).

The results also suggest that the zeta potential of the kaolin dispersion was reduced more significantly as the adsorption of KAM increased. Due to its higher charge density, KAM-3 was more effective in the zeta potential change at any adsorption level and pH (Figure 8.4). KL did not affect the zeta potential of kaolin dispersion at any pH, and thus not shown in the figure. The last points on each curve (point “S” in Figure 8.4) represents the zeta potential of kaolin mineral particles at the maximum adsorption amount (i.e., saturation adsorption in Figure 8.1). For these points, the adsorption amount on kaolin was similar, but the unadsorbed KAM were still

available in the dispersion for adsorption (Figure 8.1). These results provide evidence that the presence of unadsorbed KAM in the kaolin dispersion was inconsequential for affecting the zeta potential of the kaolin dispersion.

Generally, the zeta potential of kaolin dispersion dropped less via KAM adsorption at pH 4 than other pH because carboxylate groups of KAM polymers were protonated at this pH. At pH 10, the phenolate groups of lignin in KAM was deprotonated in addition to carboxylate groups, which would induce extra negative charge on the surface of kaolin mineral particles upon adsorption, and this results in a more negative zeta potential change. In one research (Cerrutti et al., 2012) on the stabilization of alumina dispersion using carboxymethyl lignin, the zeta potential of the dispersion was reduced from 20 to -60 mV at the polymer dosage of 0.2 wt.% and pH 10.

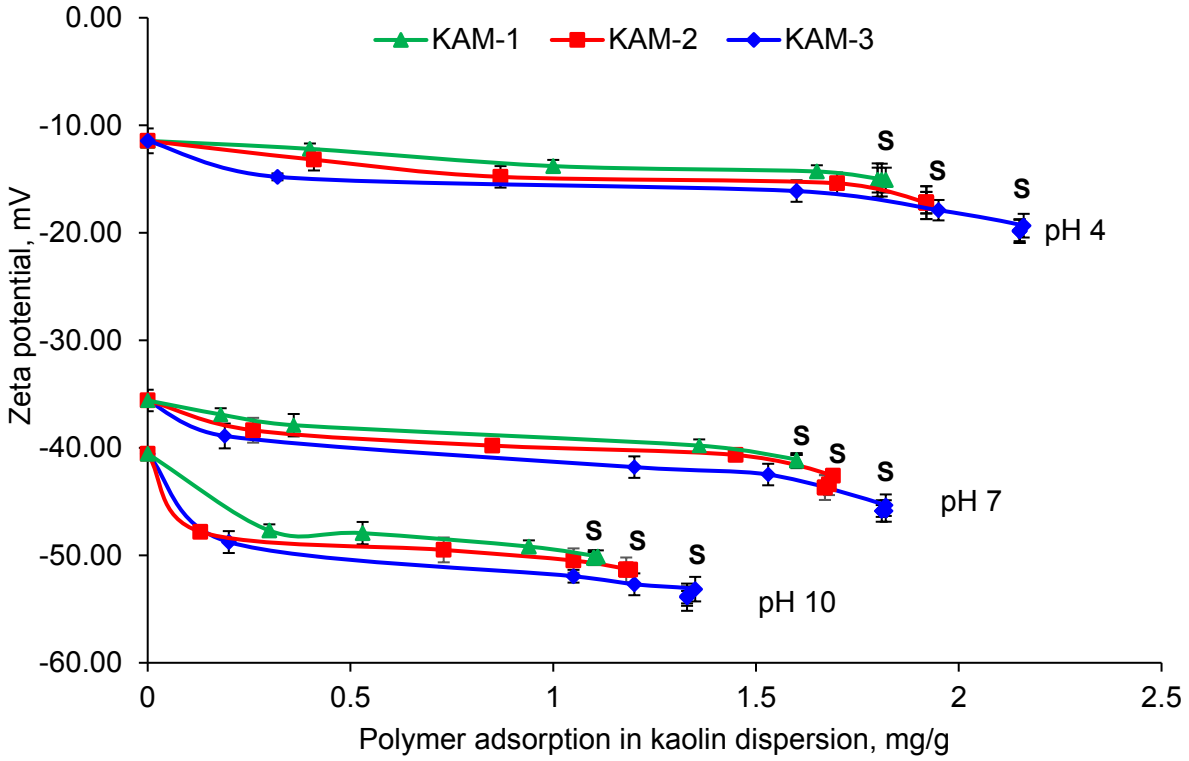

Figure 8.4. Effect of adsorbed amount of KAM on the zeta potential of kaolin (conducted under the conditions of 0.4 g/L kaolin, 25°C and 1 h).

8.4.7 Dispersion under dynamic conditions

The effect of KAM dosage on the relative turbidity of kaolin dispersion at pH 4, 7 and 10 is shown in Figure 8.5. KL did not change the relative turbidity of the dispersion at any pH (not shown). The results showed that KAM-3 increased the relative turbidity of the kaolin dispersion the most at any pH studied, which is related to 1) its higher adsorption on kaolin mineral particles (Figure 8.1) and 2) the higher zeta potential of particles (Figure 8.4). As explained earlier, the carboxylate and phenolate groups of KAM are dissociated under alkaline conditions, and thus they repel each other more significantly. Upon adsorption, as they had a larger Hy and more repulsion intensity, they were probably able to repel particles to a farther distance and larger extent. In addition, the variation in the relative turbidity at different pHs is in harmony with the surface tension and contact angle results in Table 8.3. KAM-3 reduced the surface tension of water and improved the hydrophilicity of kaolin mineral particles the most (improving its interaction with water). Therefore, the modified kaolin minerals with KAM-3 had more tendency to interact with other modified kaolin mineral particles, which promoted their repulsion (i.e., increase in relative turbidity).

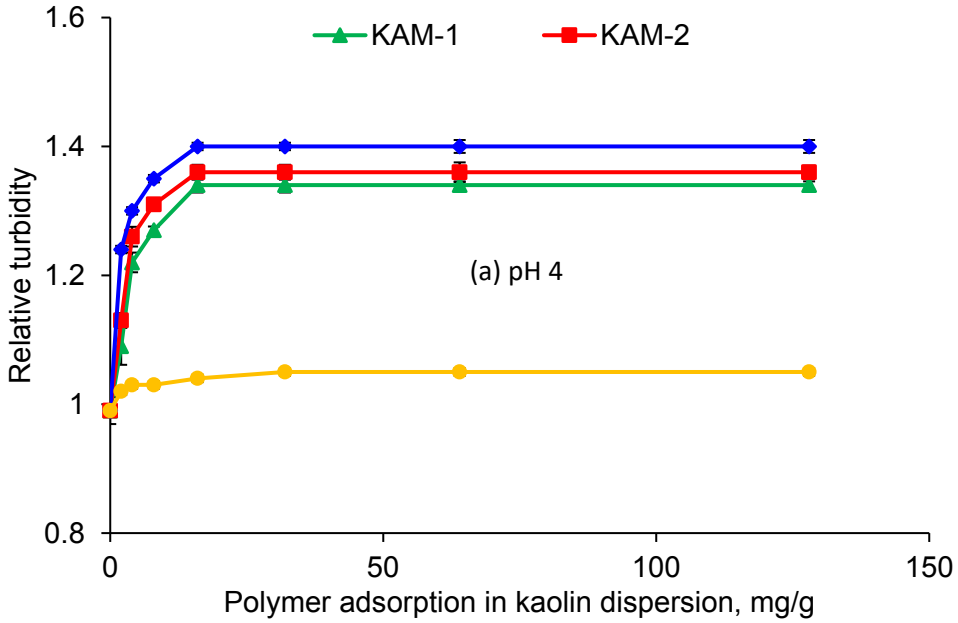

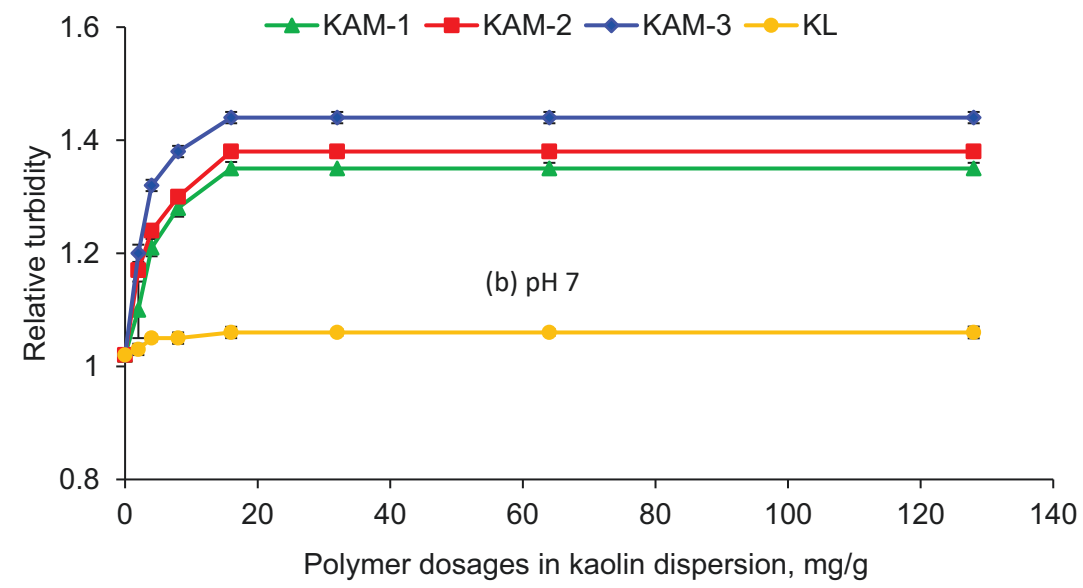

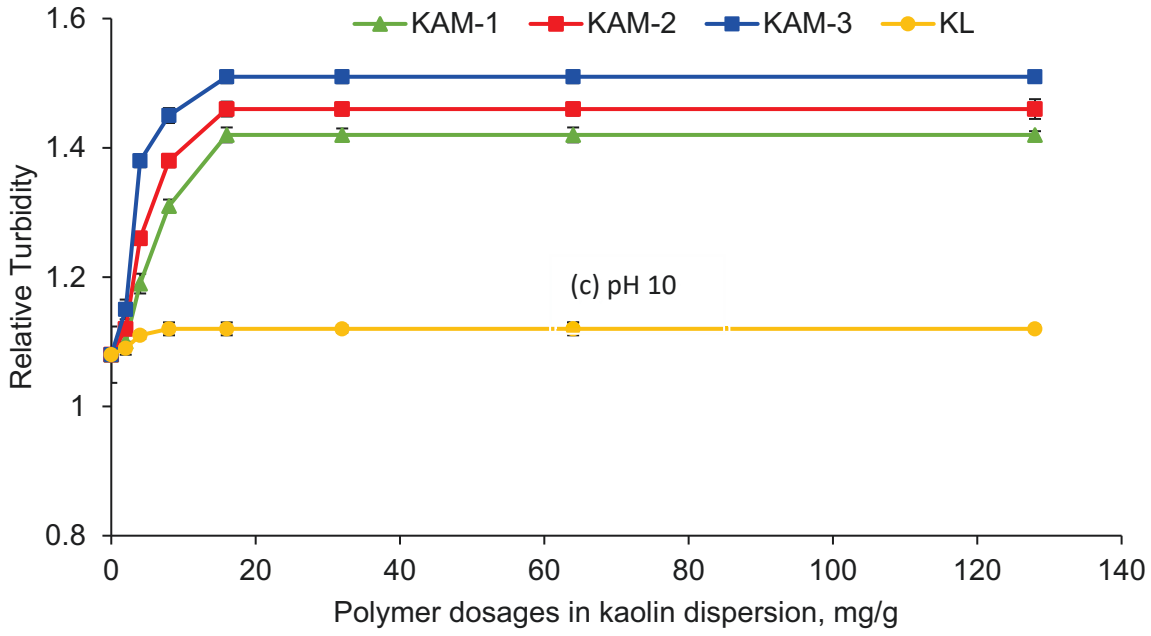

Figure 8.5. Effect of KAM dosage on the relative turbidity of kaolin dispersion, conducted under the conditions of 0.4 g/L kaolin, 25 °C and 1 h.

A better comprehension of the interaction mechanism between kaolin mineral particles and KAM under varied pHs can be revealed by assessing the correlation between the zeta potential and the relative turbidity of the kaolin dispersion (Wang et al., 2016b). To determine the stabilization mechanism of KAM in kaolin dispersion, the relative turbidity of kaolin dispersion was plotted against their zeta potential in Figure 8.6. A similar relative turbidity could be obtained at different zeta potentials; hence the zeta potential was not the only indicator of the changes in relative turbidity and stability of the dispersion. The last points (point "S" in Figure 8.6) on each curve exhibited the relative turbidity of kaolin dispersion corresponding to the maximum adsorption and minimum zeta potential (as indicated in Figures 8.1 and 8.4). When KAM adsorption reached plateau, the zeta potential and relative turbidity of kaolin dispersion attained constant values, indicating that the unadsorbed KAM did not contribute to relative turbidity of the dispersion.

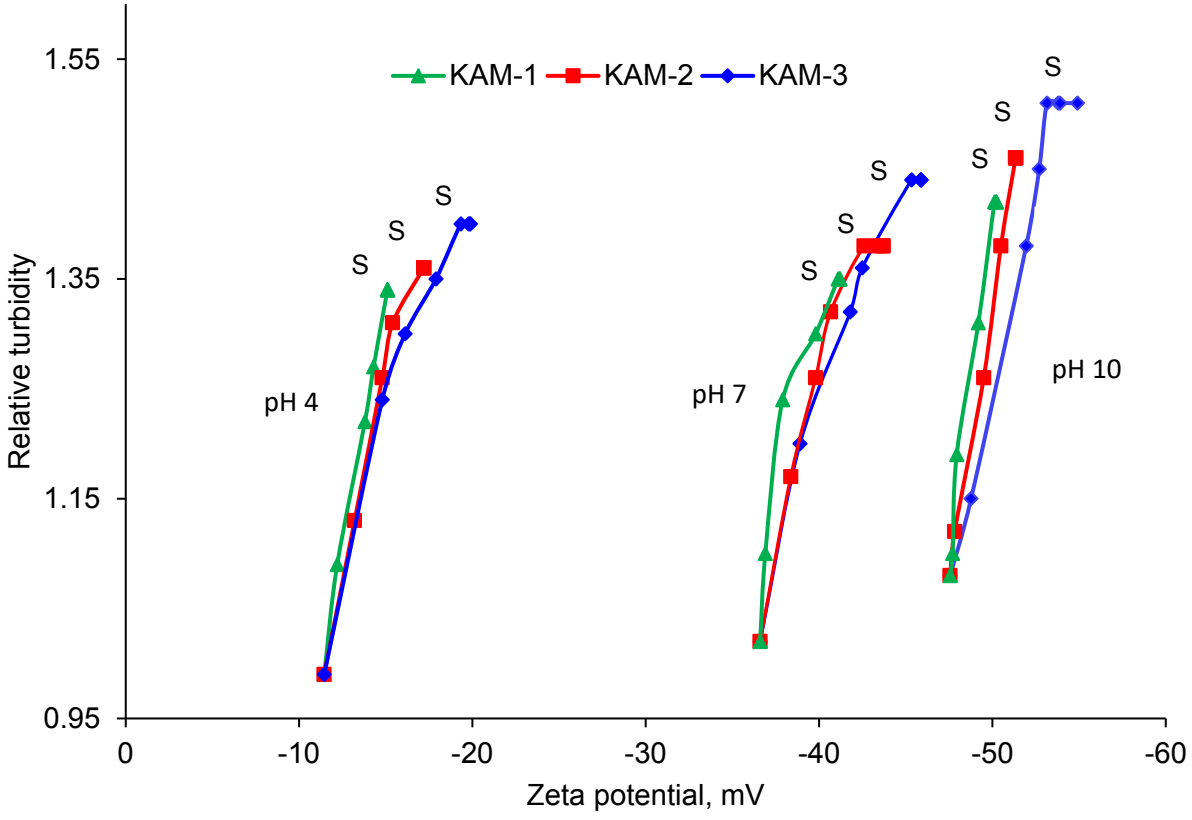

Figure 8.6. Effect of zeta potential on the relative turbidity of kaolin (conducted under the conditions of 0.4 g/L kaolin, 25 °C and 1 h).

8.4.8 Dispersion under static conditions

As KAM-3 was more effective than other KAM, the dispersion study under static conditions was conducted only using this polymer. The impact of KAM-3 dosage on the backscattering intensity of kaolin dispersion at different pH was shown in Figure 8.7. In the absence of KAM-3, the backscattering intensity of kaolin mineral particles was lower at pH 4 (5.5%) than pH 7 (26.5%) and 10 (29.3%), which is due to the settlement of particles as a results of weak electrostatic repulsion force between the kaolin mineral particles at a low pH (corresponding to a low zeta potential in Figure 8.4). In the presence of KAM-3, the kaolin dispersion showed an increase in backscattering intensity with dosages, and the increase was more pronounced at pH 10 than other pHs. As discussed above, the adsorption of KAM-3 reduced the zeta potential of the dispersion (i.e., elevated electrostatic repulsion force between particles) and surface tension of water more greatly at pH 10 than other pHs, which stabilized the dispersion at pH 10 more greatly. Similar behaviors were observed in another study when backscattering of chromium (III) oxide particles reached to a maximum level (55%) at pH 9 in the presence of polyacrylamide (Wisniewska et al., 2016).

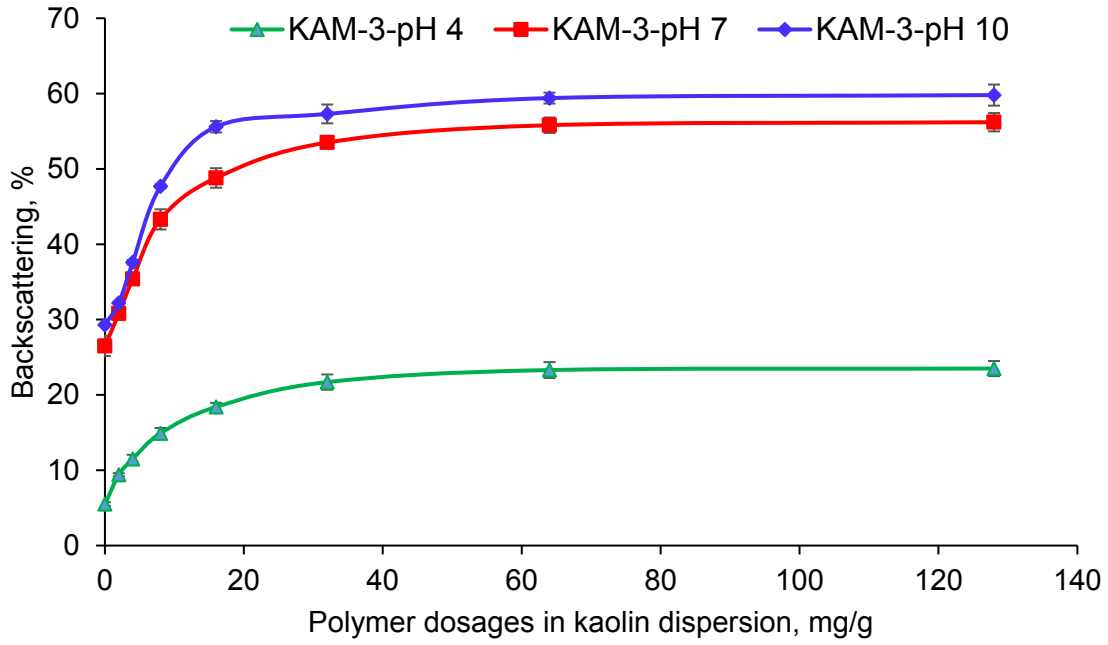

Figure 8.7. Backscattering intensity of kaolin dispersion as a function of KAM dosage, which was conducted under the conditions of 0.4 g/L kaolinite at 25 °C and 1h.

Figure 8.8 presents the size of the particles and their volume fraction in the dispersion at varying pH (4, 7 and 10) and 16 mg/g KAM dosage (based on kaolin). In the absence of KAM, the particles settled with negligible volume fraction in the dispersion at pH 4. The volume fraction of particles in the range of 0.1 to 8 µm increased in the kaolin dispersion at pH 7 and 10, which is attributed to the stronger electrostatic repulsion between the particles (larger negative zeta potential in Figure 8.4) that stabilized the particles, as explained earlier. The KL addition slightly increased the volume fraction as compared to kaolin at any pH. With increasing KAM's molar mass, the volume fraction of particles increased in the dispersion. The particles with the size of 4 µm had the highest volume fraction in the kaolin dispersion. This phenomenon showed that the particles that could remain suspended in the dispersion were probably those in the size range of 0.1 and 7 µm. Those with larger sizes than 7 µm were most likely settled, regardless of the KAM molar mass and pH of the dispersion.

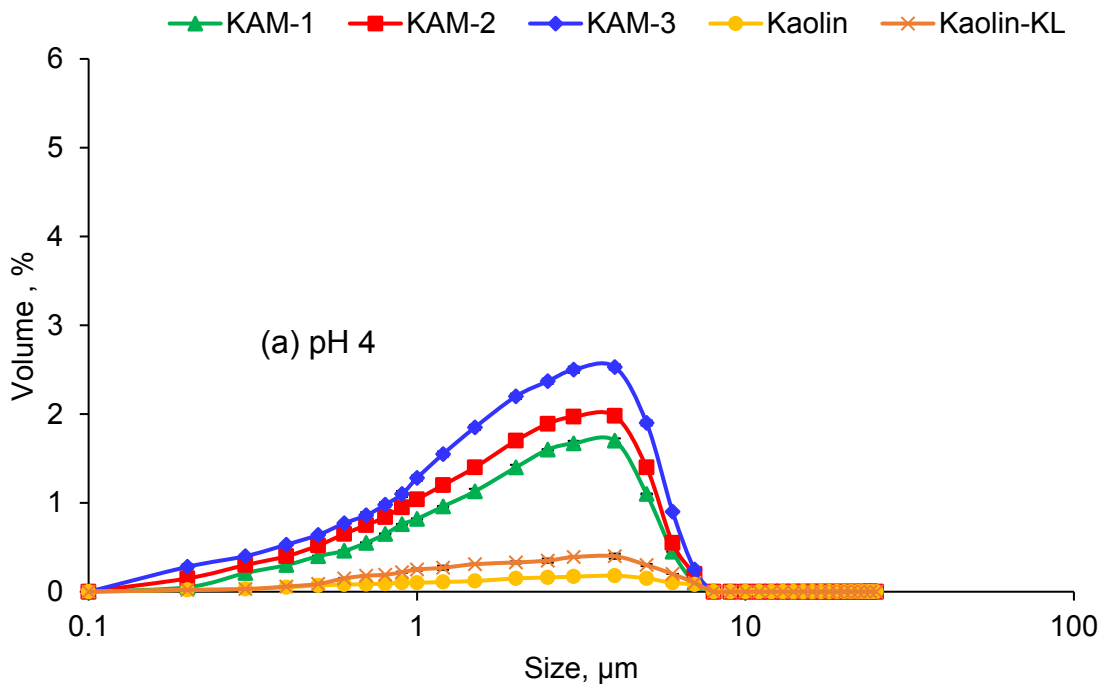

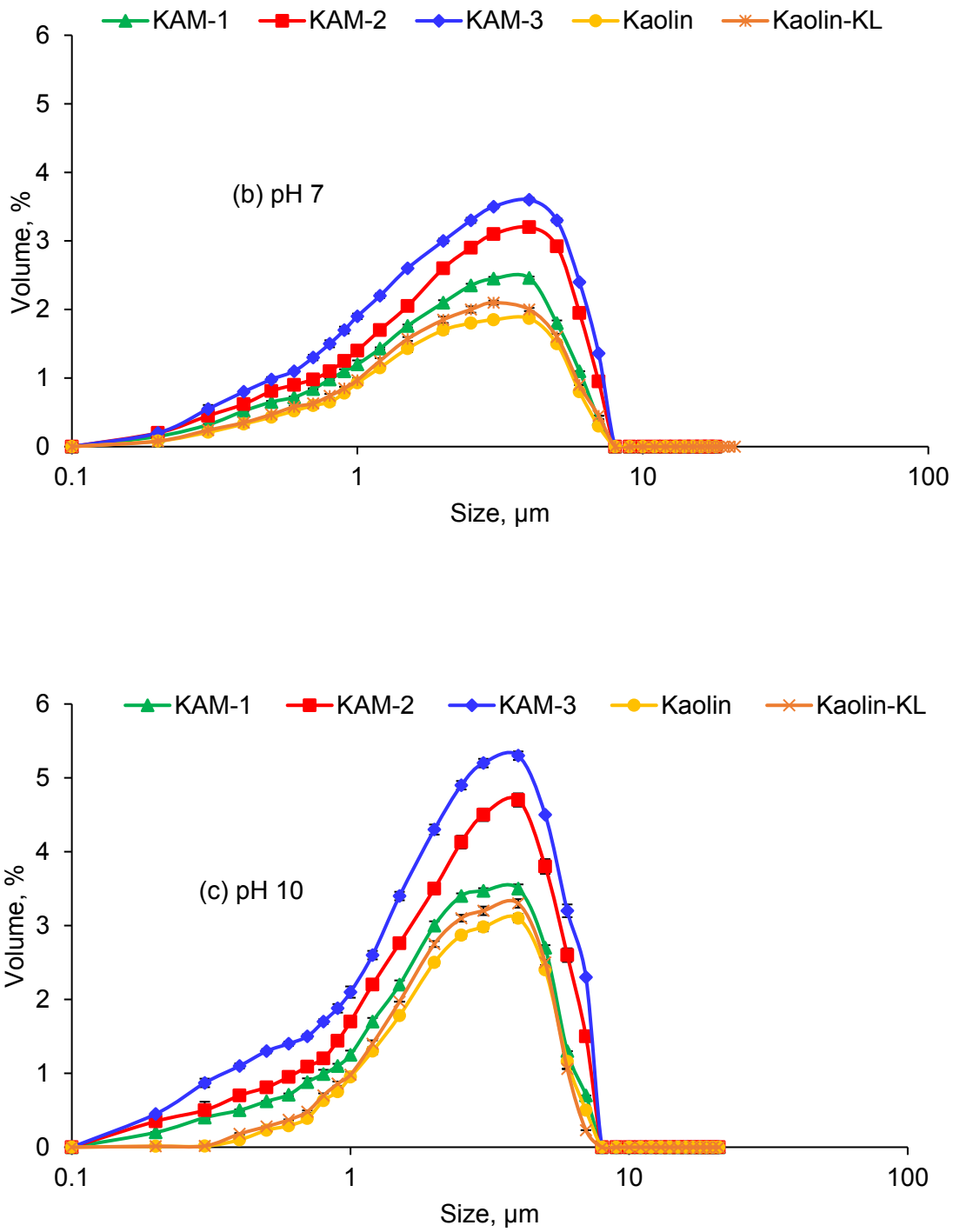

Figure 8.8. Size of particles in the presence or absence of KAM, conducted under the conditions of 16 mg/g of KAM dosage, 0.4 g/L kaolin at 25 °C and 1 h.

8.4.9 Effect of shear on kaolin dispersion

The effect of shear rates on the relative turbidity of the KAM-3 and kaolin dispersion was investigated in Figure 8.9. It is apparent that the share rate affected the efficiency of KAM-3 at a higher pH more effectively. As can be seen, there is an optimum shear rate for better dispersion performance (300 rpm). At a lower shear rate (<300 rpm), the dispersion tended to depend on the shear rate (Nsib et al., 2006). Upon addition of KAM, the relative turbidity of kaolin dispersion was increased to 1.40, but it was 1.15 in the absence of KAM at 300 rpm. KL insignificantly affected the relative turbidity of kaolin dispersion. This observation indicates that KAM-3 played a critical role in stabilizing the kaolin dispersion at any shear rates, and its impact was greater than that of shear rate alone.

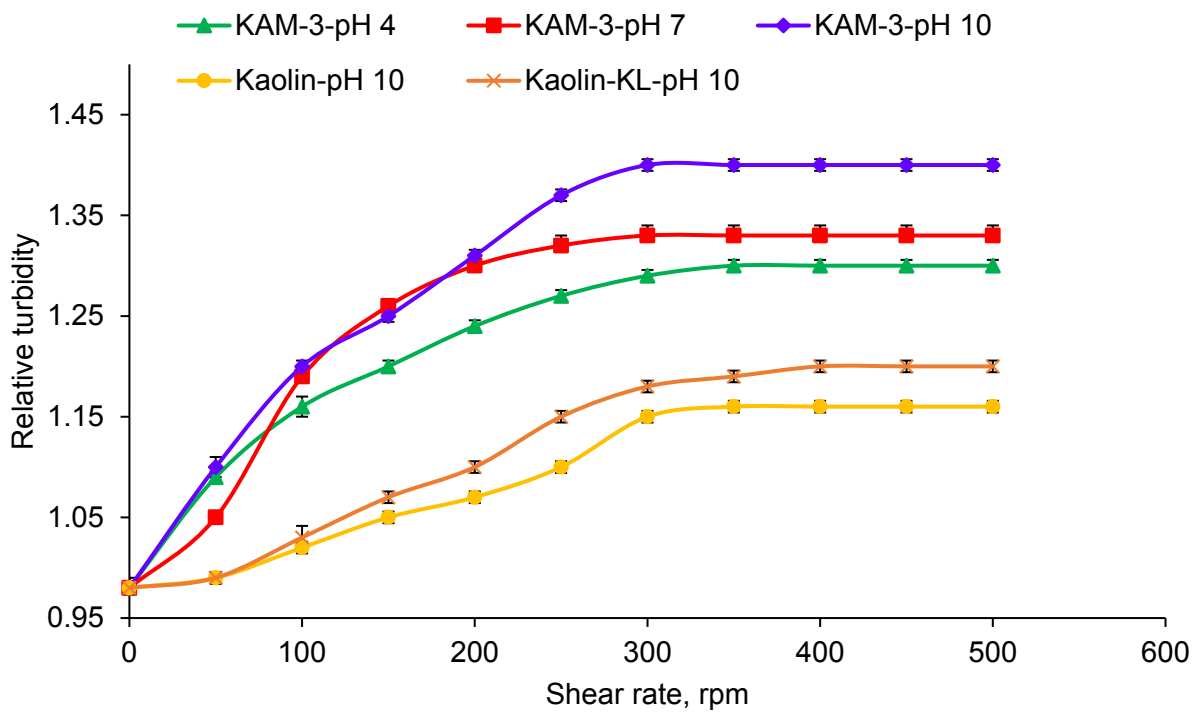

Figure 8.9. Effect of shear rate on the relative turbidity of kaolin dispersion in the presence of KAM at varied pH; under the conditions of 16 mg/g of dosage, 0.4 g/L kaolin at 25 °C and 1 h.

8.5 Conclusions

KAM proved to be an efficient dispersant in a wide pH range, and its efficiency was better under alkaline environment. The stability of kaolin dispersion with KAM was also confirmed by the increases in the backscattering light intensity and volume fraction of kaolin mineral particles in the suspended state. In addition, KAM addition (i.e., a chemical treatment) was more effective than the shear rate (i.e., a mechanical treatment) in improving the stability of kaolin dispersion. Overall, KAM-3 with higher charge density and molar mass was more effective than other KAM in improving the stability of kaolin dispersion.

8.6 References

Agnes, F., Hollander, A. F., Somasundaran, P., Gryte, C.C. 1981. Adsorption characteristics of polyacrylamide and sulfonate-containing polyacrylamide copolymers on sodium kaolinite. J. Appl. Polym. Sci., 26, 2123- 2138.

Ali, M., Mahmud, H.B. 2015. The effects of concentration and salinity on polymer adsorption isotherm at sandstone rock surface. Mater. Sci. Eng. doi:10.1088/1757-899X/78/1/012038.

Aso, T., Koda, K., Kubo, S., Yamada, T., Nakajima, I., Uraki, Y. 2013. Preparation of novel lignin-based cement dispersants from isolated lignins. J. Wood Chem. Technol., 33, 286-298

Atesok, G., Somasundaran, P., Morgan, L.J. 1988. Charge effects in the adsorption of polyacrylamides on sodium kaolinite and its flocculation. Powder Technol., 54, 77 – 83.

Besra, L., Sengupta, D.K., Roy, S.K., Ay, P. 2002. Polymer adsorption: its correlation with chemistry, production, properties, biodegradability, and performance. J. Biomater. Appl., 25,176.

Bhatti, Q. A., Baloch, M.K., Schwarz, S., Petzold, G. 2012. Impact of various parameters over the adsorption of polyvinylpyrrolidone onto kaolin. J. Dispersion Sci. Technol., 33, 1739–1745.

Boisvert, J.P., Persello, J., Castaing. J.C., Cabane, B. 2001. Dispersion of alumina coated TiO_2 particles by adsorption of sodium polyacrylate. Colloids and Surf. A., 178, 187-198.

Brady, P.V., Cygan, R.T., Nagy, K.L. 1996. Molecular controls on kaolinite surface charge. J. Colloid Interface Sci., 183, 356-364.

Breitung-Faes, S., Kwade, A. 2011. Production of transparent suspensions by real grinding of fused corundum. Powder Technol., 212, 383–389.

Carmes, T.R., Aldeek, F., Balan, L., Corbel, S., Schneider, R. 2011. Aqueous dispersions of core/shell CdSe/CdS quantum dots as nanofluids for Electrowetting. Colloids Surf. A. 377, 269–277

Chen, P., Yao, L., Liu, Y., Luo, J., Zhou, G., Jiang, B. 2012. Experimental and theoretical study of dilute polyacrylamide solutions: effect of salt concentration. J. Mol. Model., 18, 3153-3160.

Chibowski, S., Knipa, M. 2000. Studies of the influence of polyelectrolyte adsorption on some properties of the electrical double layer of ZrO_2- electrolyte solution interface. J. Dispersion Sci. Technol., 21, 761-783.

Chibowski, S., Grządka, E., Patkowski., J. 2009. Influence of a type of electrolyte and its ionic strength on the adsorption and the structure of adsorbed polymer layer in the system: polyacrylic acid/SiO_2. Croat. Chem. Acta., 82, 623–631

Celia, C., Trapasso, E., Cosco, D., Paolino, D., Fresta, M. 2009. Turbiscan lab expert analysis of the stability of ethosomes and ultradeformable liposomes containing a bilayer fluidizing agent. Colloids Surf. A., 72, 155–160.

Cerrutti, B.M., De-souza, C.S., Castellan, A., Ruggiero, R., Frollini, E. 2012. Carboxymethyl lignin as stabilizing agent in aqueous ceramic suspensions. Ind. Crops Prod., 36, 108–115.

Couch, R., Price, J.T., Fatehi, P. 2016. Production of flocculant from thermomechanical pulping lignin via nitric acid treatment. ACS Sustain. Chem. Eng., 4(4), 1954-1962.

Das, K.K., Somasundaran, P. 2001. Ultra-low dosage flocculation of alumina using polyacrylic acid. Colloids Surf A., 182, 25–33.

Das, R., Ghorai, S., Pal, S. 2013. Flocculation characteristics of polyacrylamide grafted hydroxypropyl methyl cellulose: An efficient biodegradable flocculant. Chem. Eng. J., 229, 144-152.

Fang, R., Cheng, S.U., Fu, J., Zheng, Z. B. 2009. Research on the Graft Copolymerization of EH-lignin with acrylamide. Nat. Sci., 1, 17-22.

Farrokhpay, S., Morris, G., Fornasiero, D. P. 2004. Self role of polymeric dispersant functional groups in the dispersion behavior of titania pigment particles. Prog. Colloid. Polym. Sci., 128, 216–220.

Fatehi, P., Shen, J., Hamdan, F. C., Ni. Y. 2013. Improving the adsorption of lignocelluloses of prehydrolysis liquor on precipitated calcium carbonate. Carbohyd. Polym., 92, 2103-2110.

He, W., Fatehi. P. 2015. Preparation of sulfomethylated softwood kraft lignin as a dispersant for cement admixture. RSC Adv., 5, 47031–47039.

He, W., Zhang, Y., Fatehi, P. 2016. Sulfomethylated kraft lignin as a flocculant for cationic dye. Colloid Surf. A., 503, 19-27.

He, W., Gao, W., Fatehi, P. 2017. Oxidation of kraft lignin with hydrogen peroxide and its application as a dispersant for kaolin suspensions. ACS Sustain. Chem. Eng., 5(11), 10597-10605.

Jahan, M. S., Liu, Z., Wang, H., Saeed, A., Ni, Y. 2012. Isolation and characterization of lignin from prehydrolysis liquor of kraft based dissolving pulp production. Cell. Chem. Technol., 46, 261–267.

Jamrozik, A., Gonet, A., Fijal, J., Terpilowski, K., Czekaj, L. 2014. Analysis of waste mud Stability. AGH drilling, oil, gas. http://dx.doi.org/10.7494/drill.2014.31.1.25.

Kim, S., Palomino, A. M. 2009. Polyacrylamide-treated kaolin: A fabric study. Appl. Clay Sci., 45, 270–279.

Konduri, M.K., Kong, F., Fatehi, P. 2015. Production of carboxymethylated lignin and its application as a dispersant. Eur. Polym. J., 70, 371–383.

Konduri, M.K., Fatehi, P. 2017. Dispersion of kaolin particles with carboxymethylated xylan. Appl. Clay Sci., 137, 183-191.

Kong, F., Wang, S., Price, J. T., Konduri, M.K.R., Fatehi, P. 2015. Water soluble kraft lignin acrylic acid copolymer: synthesis and characterization. Green Chem., 17, 4355-4366.

Kouisni, L., Hindle, P.H., Maki, K., Paleologou, M. 2012. The lignoforcesystem ™: a new process for the production of high-quality lignin from black liquor. The Journal of Science & Technology for Forest Products and Processes, 2, 6–10.

Lee. L. T., Somasundaran, P. 1989. Adsorption of Polyacrylamide on Oxide Minerals. Langmuir, 5, 854-860

Loginov, M., Larue, O., Lebvoka, N., Vorobeiv, E. 2008. Fluidity of highly concentrated kaolin suspensions: Influence of particle concentration and presence of dispersant. Colloid Surf. A., 325, 64-71.

Ma, X., Bruckard, W.J., 2010. The effect of pH and ionic strength on starch–kaolinite interactions. Int. J. Miner. Process., 94, 111–114.

Mcintosh, A., Lawther, S.E.M., Kwasny, J., Soutsos, M.N., Cleland, D., Nanukuttan, S. 2015. Selection and characterization of geological materials for use as geopolymer precursors. Adv. Appl. Ceram., 114, 378–385.

Mekhamer, W.K., Andis, N. A., Shabanat, M. l. 2009. Kinetic study on the sedimentation behavior of Na- and Ca-kaolinite suspension in the presence of polyethyleneimine. J King Saud Univ (Science), 21, 125–132.

Mengual, O., Menuier, G., Cayre, I., Puech, K., Sanbre, P. 1999. Characterization of instability of concentrated dispersions by a new optical analyzer: the Turbiscan MA 1000. Colloids Surf. A., 152, 111–123.

Mishra, S., Bera, A., Mandal. A. 2014. Effect of polymer adsorption on permeability reduction in enhanced oil recovery. J. Pet. Sci. http://dx.doi.org/10.1155/2014/395857

Morris, G. E., Fornasiero D., Ralston, J. 2002. Polymer depressants at the talc–water interface: adsorption isotherm, microflotation and electrokinetic studies. Int. J. Miner. Process., 67, 211–227.

Mpofu, P., Mensah, J. A., Ralston, J. 2003. Investigation of the effect of polymer structure type on flocculation, rheology and dewatering behavior of kaolinite dispersions. Intl. J. Miner. Process., 71, 247– 268.

Mpofu, P., Addai, J. M., Ralston, J. 2005. Interfacial chemistry, particle interactions and improved dewatering behavior of smectite clay dispersions. Intl. J. Miner. Process., 75, 155– 171.

Nabzar, L., Pefferkorn, E., Varoqui, R. 1987. Stability of polymer- clay suspensions. The polyacrylamide- sodium kaolinite system. Colloids Surf. A., 30, 345-353.

Naguib, H.F. 2002. Chemically Induced Graft Copolymerization of Itaconic Acid onto Sisal Fibers. J. Polym. Res., 9(3), 207-211.

Nsib, F., Ayed, N., Chevalier, Y. 2006. Dispersion of hematite suspensions with sodium polymethacrylate dispersants in alkaline medium. Colloid Surf. A., 286, 17–26.

Oveissi, F., Fatehi, P. 2014. Isolating lignin from spent liquor of thermomechanical pulping process via adsorption. Env. Tech., 35, 2597-2603.

Pefferkorn, E., Nabzar, L., Varoqui, R. 1987. Polyacrylamide Na-kaolinite interactions – effect of electrolyte concentration on polymer adsorption. Colloid Polym. Sci., 265, 889-896.

Pefferkorn, E. 1999. Polyacrylamide at Solid/Liquid Interfaces. J. Colloid. Interf. Sci., 216, 197–220.

Ponnusamy, T., Lawson, L.B., Lucy, C., Freytag, L.C., Blake, D.A., Ayyala, R.S., John, V.T. 2012. In vitro degradation and release characteristics of spin coated thin films of PLGA with a “breath figure” morphology. Biomatter., 2, 77–86.

Rong, H., Baoyu Gao, B., Dong, M., Zhao, Y., Sun, S., Wang, Y., Yue, Q. Li, Q. 2013a. Characterization of size, strength and structure of aluminum-polymer dual-coagulant flocs under different pH and hydraulic conditions. J. Hazard. Mater. 252, 330– 337.

Rong, H., Gao, B., Zhao, Y., Sun, S., Yang, Z., Wang, Y., Yue, Q., Li, Q. 2013b. Advanced lignin-acrylamide water treatment agent by pulp and paper industrial sludge: Synthesis, properties and application. J. Env. Sci., 25, 2367–2377.

Santisteban, J. I., Mediavilla, R., Lopez-Pamo, E., Dabrio, C. J., Zapata, M. B. R., García, M. J. G., Castano, S., Martínez-Alfaro, P. E. 2004. Loss on ignition: a qualitative or quantitative method for organic matter and carbonate mineral content in sediments? J. Paleolimnol., 32 (3), 287-299.

Senoussi, H., Osmani, H., Courtois, C., Bourahli, M.H. 2016. Minerological and chemical charcaterization of DD3 kaolin from the east of Algeria. J. Span. Ceram. Glass Soc., 55, 121–126.

Shirazi, M., Van de Ven, T.G.M., Garnier, G. 2003. Adsorption of modified starches on pulp fibers. Langmuir, 19, 10835-10842.

Tekin, N., Dincer, A., Demirbas, O., Alkan, M. 2006. Adsorption of cationic polyacrylamide onto sepiolite. J. Hazard. Mater., 134, 211–219.

Vie, R., N. Asemia, N., Quintin, J.C., Toured, E., Faultier, M. 2007. Study of suspension settling: A approach to determine suspension classification and particle interactions. Colloid Surf. A, 298, 192.

Wang, L.J., Wang, J. P., Zhang, S. J., Chen, Y. Z., Yuan, S. J., Sheng, G. P., Yu, H. Q. 2009. A water-soluble cationic flocculant synthesized by dispersion polymerization in aqueous salts solution. Sep. Purif. Technol., 67, 331-335.

Wang, S., Sun, Y., Kong, F., Yang, G., Fatehi, P. 2016a. Preparation and characterization of lignin-acrylamide copolymer as a paper strength additive. BioResour., 11, 1765-1783.

Wang, S., Konduri, M.K.R., Hou, Q., Fatehi, P. 2016b. Cationic xylan–METAC copolymer as a flocculant for clay suspensions. RSC Adv., 6, 40258.

Wisniewska, M. 2010. Temperature effect on adsorption properties of silica-polyacrylic acid interface. J. Therm. Anal. Calorim., 101, 753-760.

Wisniewska, M., S., Urban, T. 2015a. Impact of anionic and cationic polyacrylamide on the stability of aqueous alumina suspension—comparison of adsorption mechanism. Colloid Polym. Sci., 293, 1171–1179.

Wisniewska, M., Chibowski, S., Urban., T. 2015b. Modification of the alumina surface properties by adsorbed anionic polyacrylamide—Impact of polymer hydrolysis. J. Ind. and Eng. Chem., 21, 925–931.

Wisniewska, M., Chibowski, S. Urban, T. 2016. Synthetic polyacrylamide as a potential flocculent to remove commercial chromium (III) oxide from aqueous suspension. Intl. J. Environ. Sci. Technol., 13, 679–690.

Yang, F., Niu, Q., Lan, Q., Sun, D. 2007. Effect of dispersion pH on the formation and stability of Pickering emulsions stabilized by layered double hydroxides particles. J. Coll. Inter. Sci., 306, 285–295.

Yoshikawa, J., Lewis, L. J. 2008. Comb polymer architecture, ionic strength, and particle size effects on the $BaTIO_3$ suspension stability. J. Am. Ceram. Soc. doi:10.1111/j.1551-2916.2008.02647.x

Yuan, J., Garforth, W.L., Preutt, R.J. 1998. Influence of dispersants on the solubility of calcined kaolin. Appl. Clay Sci., 13, 137-147.

Chapter 9: Self-assembly of kraft lignin-acrylamide polymers

9.1 Abstract

Lignin has long been obtained as a by-product of the pulping industry but has rather low added-value applications. The production of lignin polymers has shown pathways to produce water soluble products to be used as flocculants and dispersants. However, these lignin-based polymers may interact with each other and form large flocs that could reduce their efficiency in interacting with other colloidal particles. This study aims at evaluating the self-assembly of kraft lignin-acrylamide polymers in aqueous environments under different salt concentrations. The present study revealed a significant self-assembly of lignin polymers with time in the presence or absence of salt. The sedimentation studies showed that the higher molecular weight lignin polymer had a higher tendency for aggregation. Quartz crystal microbalance with dissipation (QCM-D) was used for studying the self-assembly behavior of lignin polymers with different molecular weights. These results suggested that lignin polymer with the higher molecular weight of 96, 992 g/mol had a higher tendency to self-assemble by forming a loose and thick layer as compared to that with a lower molecular weight. Also, salt disrupted the self-assembly of lignin polymers greatly.

9.2 Introduction

In the past few decades, self-assembly of particles has been focus of research (James et al., 2014). The potential of polymers to self-organize in solutions at specific conditions is a very attractive phenomenon, which can be exploited to produce a wide range of nano- and mesoscopic structures with different chemical compositions, shapes and functionalities (Lehn, 1995; Whitesides and Grzyboski, 2002; Hartgerink et al., 2001). These self-assembled particles can have applications in many fields, such as chemical separations, biomedical, catalysis, drug delivery, and sensors (Zhang, 2012; James et al., 2014).

Industrial nanoparticles, especially those made of metal, semiconductors, and synthetic compounds constitute a tiny portion but significant pollution source that can pose adverse environmental hazard (Buzea et al., 2007). Thus, increased attention has been paid to the

development of self-assembled nanoparticles obtained from natural renewable resources due to their inherent biodegradability and biocompatibility. Among these systems, the use of natural polysaccharides in developing nanoparticles has significantly increased (Zhang et al., 2011; Aumelas et al., 2007; Leonard et al., 2003). In one study, the aqueous self-assembly of the cellulose modified with chlorosulfuric acid was investigated using transmission electron microscopy (TEM) and dynamic laser scattering (DLS), and the results showed that the modified cellulose was capable of forming polymeric micelles in water with an average particle diameter ranging from 20 to 67 nm (Cheng et al., 2008). In another study, cellulose was catatonically modified with (2-hydroxypropyl trimethylammonium chloride (HPTAC) and self-organized into cationic micelles in distilled water with the average hydrodynamic radius of 320 - 430 nm (Song et al., 2011). In another investigation by Zhang and coworkers (2007) self-assembled nanoparticles based on oleoyl-chitosan with a mean diameter of 255.3 nm were produced. Although self-assembly would reduce the effectiveness and functionality of some polymers in solutions (Qian et al., 2014), the concept of self-assembly would be used to eliminate polymers from some systems (Salentinig and Schubert, 2017).

Today, starch, chitosan, and cellulose are heavily used for other purposes worldwide, and their usage in producing new chemicals may not be an excellent option in future. Interestingly, other under-utilized chemicals, such as lignin, can be used for this purpose. Lignin is a natural polymer that currently has a very limited industrial use and available in a large quantity (Pouteauet al., 2003; Zakzeski et al., 2010). The production of environmentally friendly lignin-based nanoparticles has been reported recently (Frangville et al., 2012; Gilca et al., 2015; Lievonen et al., 2016; Wurm and Weiss, 2014; Yiamsawas et al., 2014; Salentinig and Schubert, 2017). Lignin itself has tendency for agglomeration in solvents (Xiong et al., 2017). Frangville et al. (2012) reported the formation of nanoparticles by acidifying ethylene glycol solution containing lignin. In another work, the addition of water to acetylated wheat alkali lignin dissolved in tetrahydrofuran (THF) resulted in the formation of solid nano sized colloidal spheres (Qian et al., 2014). The formation of sulfate lignin colloids was also exploited by Jiang et al. (2013) to produce lignin nanoparticles used for reinforcing natural rubber composites. However, it is not clear how modified semi natural large lignin polymers can participate in a self-assembly process. In the past, the production of semi natural kraft lignin polymers via polymerizing kraft lignin, as acrylamide, was reported (Wang et al., 2016). It was stated that the product can be used as

strength additives in papermaking, as well as flocculants and dispersants in the chemical industry (Rong et al., 2013; Wang et al., 2016; Fang et al., 2009). Despite promising performance, its self-aggregation may generate nano-particles that have limited functionality. The first objective of this work was to study the self-assembly behavior of kraft lignin- acrylamide polymer in aqueous solutions.

The mechanism of self-assembly of various polymeric materials have been studied in colloidal systems (Beysens and Narayanan, 1999; Tomilov et al., 2013; Cates and Tailleur, 2013; Furukawa and Tanaka, 2010). Charged polymers contain various functional groups such as carboxylic acid, hydroxyl groups, and amine. These groups can also interact with each other as a result of steric, electrostatic forces, van der Waals forces, hydrogen bonding, and π-π interactions to agglomerate in clusters (Palberg, 1997; James et al., 2014; Wang et al., 2016). In aqueous solutions, polymers may lose their functionality upon self-assembly as they form large clusters. Another objective of this work was to identify the mechanism of self-assembly of lignin-acrylamide polymers in solutions.

The molecular weight and charge density of the polymers and the concentration of ionic species present in solutions influence the self-assembly of the polymers in aqueous solutions (Macakova et al., 2007). For example, Fan and co-workers (2010) investigated a series of water-soluble triblock polymers of poly (ethylene oxide), and reported that the number of micelle aggregates increased with polymer's molecular weight. The presence of salt can also affect self-assembly of polymers (Ozbas et al., 2004). For instance, Caplan et al. (2000) showed that self-assembly of oligopeptide was remarkably influenced by the ionic strength of the solution. Another objective of this study was to investigate how the molecular weight of lignin-acrylamide polymers affects its aggregation behavior in various degrees of salinity.

In our previous chapter, we reported the production of kraft lignin – acrylamide (KAM) polymers (Hasan and Fatehi, 2018.). In this study, the self-assembly of KAM polymers in aqueous solutions was investigated in the presence or absence of salt and the colloidal stability of the system containing KAM was analyzed by a vertical scan analyzer. Also, Quartz crystal microbalance with dissipation (QCM-D) was employed to investigate the adsorption characteristics and self-assembly of KAM polymers.

9.3 Materials and Methods

9.3.1 Materials

Softwood kraft lignin was produced via LignoForce^{TM} technology of FPInnovations in Thunder Bay, ON (Kouisni et al., 2012). Acrylamide (99.0 %), potassium persulfate ($K_2S_2O_8$) (analytical grades NaOH, H_2SO_4 98%) and NaCl (all analytical grades) were all obtained from Sigma-Aldrich company. Cellulose acetate dialysis membrane (molar mass cut off of 1,000 g/mol) was obtained from Spectrum Labs. Inc., USA. All chemicals were applied without further purification. Ethanol (95 vol. %) was received from Fisher Scientific company. Polydiallyldimethyl ammonium chloride (PDADMAC) with the molar mass of 100,000–200,000 g/mol was obtained from Sigma Aldrich Company and diluted to 0.005 M prior to use.

9.3.2 Polymerization of lignin

The free radical polymerization of KL was carried out in a 250 mL three-neck round-bottom glass flask under the reaction conditions listed in Table 9.1. First, a required amount of KL was dissolved in 40 mL of deionized water while stirring at 300 rpm. Predetermined quantities of AM were added to the flask and stirred for 30 min. The pH of the solution was adjusted using 0.1 M sulfuric acid. The reaction solution was continuously purged with nitrogen to remove any residual oxygen at room temperature for 30 min. Subsequently, potassium persulfate was added as an initiator to the system and the reaction solution was purged for another 5 min. The polymerization was processed by placing the flask in a preheated water bath after adjusting the pH of the system. The reaction was allowed to proceed for the desired time intervals under a continuous nitrogen supply. After the completion of the reaction, the solution was cooled to room temperature by immersing the flask in tap water for 20 min. The kraft lignin-acrylamide polymer was precipitated by adjusting the solution pH to 1.5 using sulfuric acid. Then, the sample was centrifuged at 3500 rpm for 10 min using a Sorvall ST 16 laboratory centrifuge (Thermo Fisher) in order to separate lignin-acrylamide polymers from homopolymers (polyacrylamide, PAM) and unreacted acrylamide monomers. This precipitation/centrifugation process was repeated three times, and the lignin-acrylamide polymers were then collected. The precipitated lignin-acrylamide polymers were mixed with 200 mL of deionized water. After adjusting the pH of the solution to 7.0 using a 1M NaOH solution, the sample was dialyzed using the dialysis membrane for 48 h in order to remove impurities (e.g. inorganic salts and monomers)

from the polymer solution. The deionized water used for dialysis was changed every 12 h for 2 days. After dialysis, the solution containing lignin-acrylamide (lignin-AM) polymer was dried at 105 °C, and the dried sample was kept for further analysis. The procedure stated above was repeated under different conditions stated in Table 9.1 to form lignin polymers with different properties. This lignin-acrylamide polymer is denoted as KAM, while unmodified kraft lignin is denoted as KL in this work.

9.3.3 Solubility and charge density determination

To measure the solubility of the KAM, 0.2 g of the lignin polymers was added to 20 mL of deionized water by stirring at 100 rpm and 30 °C for 1 h in a water bath shaker (Innova 3100, Brunswick Scientific, Edison, NJ, USA). Then, the samples were centrifuged at 1000 rpm for 5 min. The supernatants were collected and used for analyzing the charge density and solubility of the polymers. The concentration of the polymers in the supernatants was determined by drying the supernatants at 105 °C, and its solubility was determined based on the concentration of the polymers in the supernatants and the initial amount of the polymer (0.2 g). The charge density of the polymers was measured by a particle charge detector, Mütek PCD 04 titrator (Herrsching, Germany) with a PDADMAC solution (0.0050 M) as stated previously (Wang et al., 2015). Three repeats were carried out, and the average values were reported.

9.3.4 Molecular weight analysis

About 5 mg sample of dried KAM polymers were dissolved in 10 mL of 5.0 wt.% acetic acid solution by stirring at 600 rpm for 48 h and 35 °C, and the solution was then filtered with a 13 mm diameter nylon filter (pore size 0.2 μm). The filtered solutions were used for molecular weight analysis, which was carried out using GPC, ViscotekGPCmax, Malvern, UK, with viscometer and UV detectors. PolyAnalytic, A206 and A203 columns were used, and a 0.1 M of $NaNO_3$ solution was used as solvent and eluent with the flow rate of 0.7 mL/min. The column temperature was set to 35 °C. Poly ethylene oxide was used as standard in GPC analysis.

9.3.5 Elemental analysis

The elemental analysis was performed for KL and KAM polymers using an elemental analyzer, Elementar Vario EL Cube, following the combustion method (Jahan et al., 2012). The samples were first dried in an oven at 105 °C overnight to remove any moisture prior to analysis. Approximately, 2 mg of dried samples were transferred into the carousel chamber of the elemental analyzer and combusted at 1200 °C to reduce the generated gasses to analyze carbon, hydrogen, oxygen and nitrogen contents of the samples.

9.3.6 Zeta potential analysis

The zeta potential analysis of kaolin particles was determined using a NanoBrook Zeta PALS (Brookhaven Instruments Corp, USA). In this study, 0.5 g/L of KAM polymers were prepared in the absence and presence of NaCl (0.2 M) and stirred at 300 rpm and 25 °C for 30 min at pH 7. After mixing, their zeta potential measurements were carried out at room temperature at a constant electric field (8.4 V/cm). The experiments were carried out three times and the average values were reported in this study.

9.3.7 Hydrodynamic diameter

The hydrodynamic radius of KAM polymers was measured using a static light scattering analyzer (BI-200SM Brookhaven Instruments Corp., USA). The light source was a power solid state laser with a maximum power of 35 mW and a wavelength of 637 nm. The scattering angle was set at 90°. In this set of experiments, 0.5 g/L of KAM polymers were prepared in the absence and presence (0.2 M) of NaCl and stirred for 30 min at pH 7. The samples were kept at room temperature for 24 h to reach equilibrium (Kong et al, 2015). Subsequently, 20 mL of the polymer solutions were filtered with a 0.22 μm disposable syringe filters and kept in glass bottles. The samples were gently shaken prior to measurement. The self-assembly of KAM particles in aqueous solutions was analyzed at desired time intervals. The measurements were conducted in triplicate. The pH of the solution was adjusted using 0.1 M sulfuric acid.

9.3.8 Sedimentation analysis

The sedimentation of KAM aqueous solution was assessed using a vertical scan analyzer, Turbiscan Lab Expert, Formulaction, France. This method has been applied for studying the stability of waste and mineral dispersions (Jamrozik et al., 2014, Vie et al., 2007). In this analysis, two synchronous optical sensors receive the light transmitted through and the light that is backscattered by the sample. One sensor is placed at an angle of 180° relative to the incident light beam and measures the transmitted light, while the other is placed at an angle of 45° to the light source to measure backscattering intensity. The backscattering signals generated by the sample were compared with the standard silicon oil, which was used for calibrating the instrument (Mengual et al., 1999). In this experiment, KAM solutions (0.5 g/L) were sonicated in an ultrasound bath (25 kHz) for 15 min at 25 °C, and then transferred to a 20 mL cylindrical tube to analyze for 12 min. The samples were vertically scanned at 880 nm wavelength every 2 sec at 30 ºC and the results were measured using Turbisoft 2.1 software.

Based on the data collected, the destabilization kinetics of the samples was determined using Turbisoft 2.1 software, which provides evidence for settling of particles in the sample cells. Equation 9.1 presents the formula for determining the destabilization index of KAM in the samples:

$$\text{Destablization index} = \sum_i \frac{\sum_h |scan_i(h) - scan_{i-1}(h)|}{H} \qquad (9.1)$$

where $scan_i(h)$ and $scan_{i-1}(h)$ are the transmission signals for two consecutive time intervals at a given height and H is the total height of the sample. The sediment thickness at the bottom of the cells was obtained based on the backscattering data received from the precipitated layer at the bottom of the cells.

9.3.9 QCM-D measurements

The self-assembly of lignin polymers was assessed by a Quartz crystalline microbalance with dissipation (QCM)-D. The principle of this instrument was comprehensively discussed elsewhere (Rodahl et al., 1995; Alagha et al., 2013). The quartz crystal resonator with a fundamental resonant frequency of 5 MHz was mounted in a fluid cell with one side exposed to the solution.

The cell was mounted on a Peltier element, which provided an accurate temperature control (±0.02 °C). Experiments were run at 23 °C and pH 7. The changes in frequency and dissipation were measured simultaneously at the resonance frequency of 5MHz and at the overtones of 5, 15, 25, 35, 45, 55, and 75 MHz. To analyze the self-assembly of KAM, the gold QCM sensors were coated with KAM solutions (0.05g/L) using a spin coater for 2 min at 1000 rpm and then gently dried with nitrogen gas. The adsorption of KAM on the sensors coated with the same KAM polymers was studied at 23 °C with a flow rate of 0.1 ml/min for 15 min. Afterword, the sensor layers were rinsed with excess of Milli-Q water for 20 min. In another set of experiments, the above-mentioned analysis was repeated in the presence of 0.2 M NaCl solution.
In a QCM-D system, the dissipation of sensors's energy, D, which results from the adsorption of a viscous or loose layer, was also measured (Long et al., 2013). This dissipation energy is given by Equation 9.2:

$$D = \frac{E_d}{2\pi E_s} \qquad (9.2)$$

where E_d is the energy dissipated during one oscillation and Es is the energy stored in the oscillating system. The voltage applied to the QCM is suspended and the decay of the amplitude of the crystal is measured as a function of time. In case of very rigid polymer, no change in dissipation will be observed as a function of adsorption. However, for an adsorbed viscoelastic layer, the energy dissipated through the adsorbed layer will increase with time. Therefore, by observing the change in dissipation (D), a qualitative measure of the relative stiffness or conformation of an adsorbed layer may be determined. Based on Voight model, provided by Q-tools software in the QCM-D instrument, it is possible to determine the viscous and shear modulus components of the adsorbed layer (Alagha et al., 2013). Voight model was used for determining the adsorption of KAM. The frequency and dissipation energy loss were considered in the modeling analysis, while the adsorbed layer was assumed to be uniform in both thickness and density. In this work, third overtone (15 MHz) was used to interpret the adsorption results due to its stable response (Saarinen et al., 2009).

9.4 Results and Discussion

9.4.1 Properties of KAM

The KL and AM were synthetized to produce KAM with different molecular weights (Table 9.1). The increase in the nitrogen content confirmed the grafting of AM onto the lignin backbone, which was well aligned with the change in the molecular weight of KAM1and KAM2. The solubility of unmodified KL was found to be 0.05 g/L; whereas, KAM1and KAM2 were approximately 4.5 g/L soluble in water. It is also seen that the anionic charge densities of the KAM backbone increased with increasing its molecular weight.

Table 9.1. Reaction conditions and properties of KAMs

Conditions	KL	KAM1	KAM2
Temperature, °C	-	90	80
Time, h	-	5	2
KL, mol	-	0.016	0.016
AM, mol	-	0.014	0.042
pH	-	4	5
Initiator, mmol	-	0.11	0.11
Anionic charge density, meq/g	0.21	0.82	2.10
Solubility, g/L	0.05	4.5	4.7
M_w, g/mol	17, 890	24, 590	96,992
M_n, g/mol	5,150	23,129	69,716
Nitrogen, %	0.03	1.57	6.2

9.4.2 Hydrodynamic diameter of KAM

The change in the hydrodynamic diameter of KAM polymer in the presence or absence of salt in aqueous solution is shown in Figure 9.1 as a function of time at pH 7. As observed, the hydrodynamic diameter of KAM increased gradually with time, regardless of salt. This time dependence evolution of the hydrodynamic diameter revealed that individual polymers agglomerated in the aqueous solution and generated larger clusters, regardless of salt. The

clusters of KAM2 were larger (240 to 386 nm) than those of KAM1 (120 to 249 nm). The larger polymers may be engaged in hydrogen bonding more greatly than the smaller ones due to their more carboxylate and hydroxyl groups. Therefore, polymers with the high molecular weight (e.g., KAM2) has generally higher tendency to aggregate, leading to the formation of large clusters.

Salts are known to screen charges of electrolytes, reduce their interactions and self-assembly of the charged polymers. The hydrodynamic size of KAM1 and KAM2 polymers were smaller in the presence of salt than its absence (Figure 9.1b). This smaller hydrodynamic size for KAM1 and KAM2 is generally attributed to their reduced interactions. Another reason for the decrease in the hydrodynamic diameter of KAM can be the reduction in the repulsion force between the anionic charged groups within the KAM structures due to counterion screening (Yoshikawa and Lewis, 2008). Previously, NaCl in aan queous solution reduced the electrostatic repulsion between the $–COO^-$ groups of PAM and generated the PAM with a collapsed coil structure (Chen et al., 2012; Mishra et al, 2014). By elapsing time, KAM2 seemed to have more growth in the hydrodynamic size as compared to KAM1. This noticeable increase in hydrodynamic size is ascribed to its higher molecular weight and thus higher affinity for agglomeration.

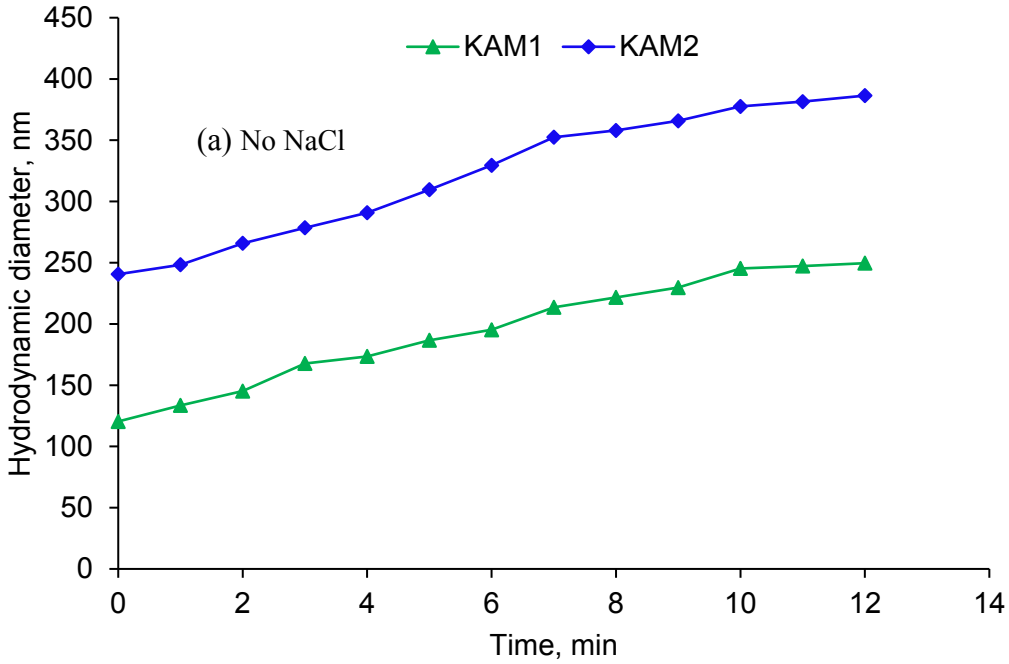

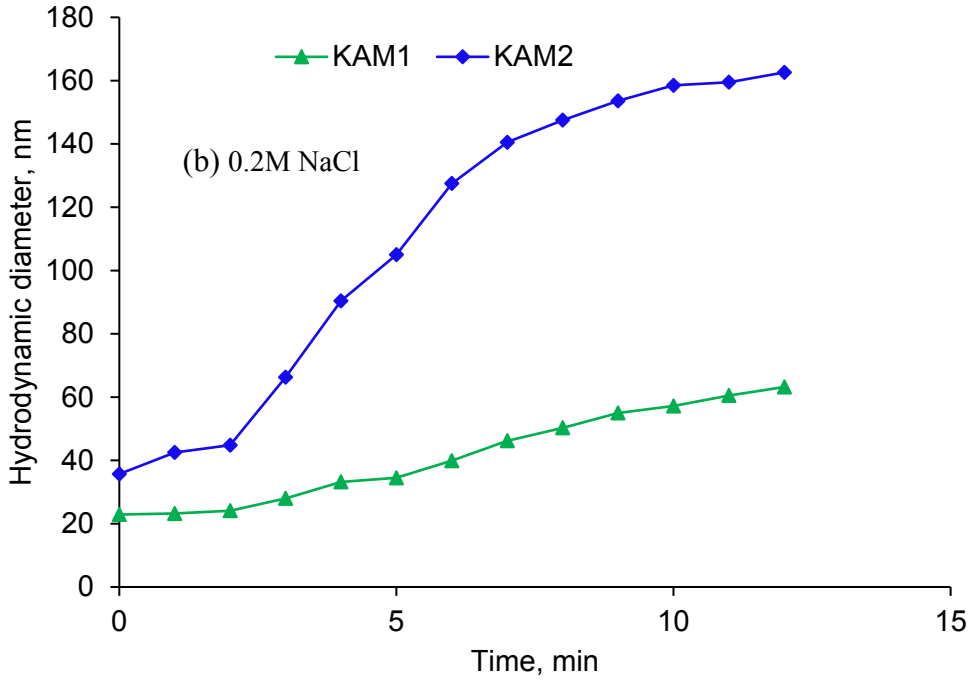

Figure 9.1. Effect of time on the hydrodynamic diameter of KAM at (a) no salt, (b) 0.2M NaCl; conducted under the conditions at pH 7, 25 °C in aqueous solution.

9.4.3 Sedimentation analysis

Figure 9.2 shows the destabilization index of KAM as a function of time. It is observable that the destablization index of the samples increased more significantly for KAM2 and the change was more dramatic in the presence of salt. Figure 9.3 shows the thickness of the precipitated KAM agglomerates as a function of time. Clearly, the particles generated a thicker sediment in the presence of salt. Considering the Hy of the particles and their sedimentation (Figures 9.1 and 9.3), it can be understood that the self-assembly of KAM was more intense in the absence of salt, but the formed clusters were stable in the solution. In the presence of salt, although smaller flocs were formed, they precipitated from the system remarkably. The carboxylate ($–COO^-$) groups on the backbone of KAM polymer increased the overall negative charge density of KAM (Table 9.1); inducing more repulsion between the large KAM polymers and their clusters and thus hampered the sedimentation of the particles. This is in agreement with the higher negative zeta potential value of KAM solution in the absence of salt (Table 9.3).

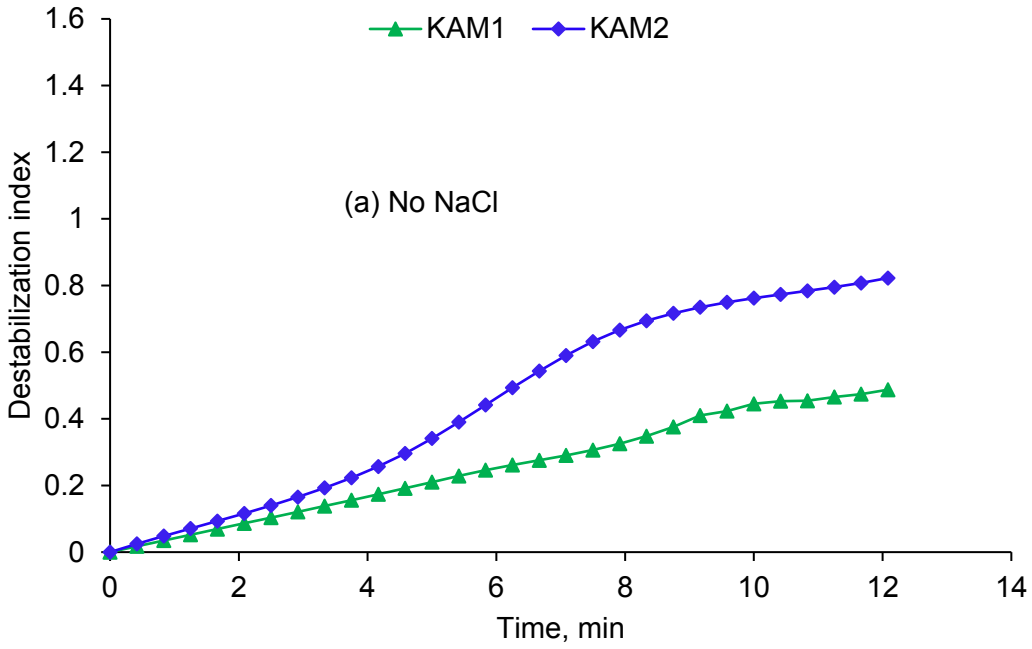

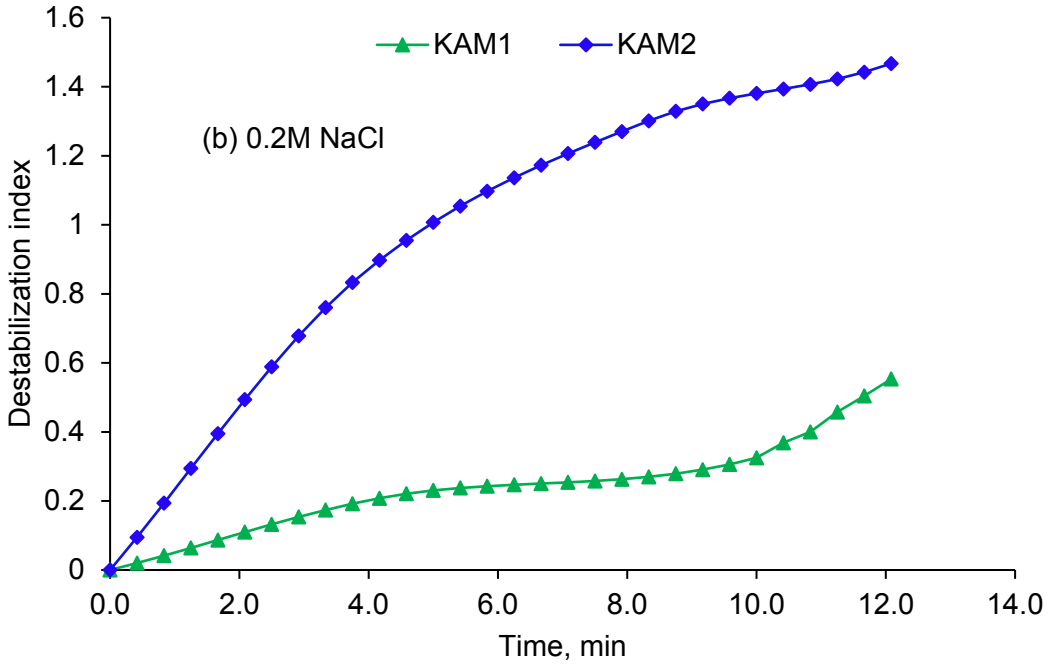

Figure 9.2. Destabilization of KAM polymers as function of time in the (a) absence and b) presence of 0.2M NaCl salt at pH 7 and 25 °C.

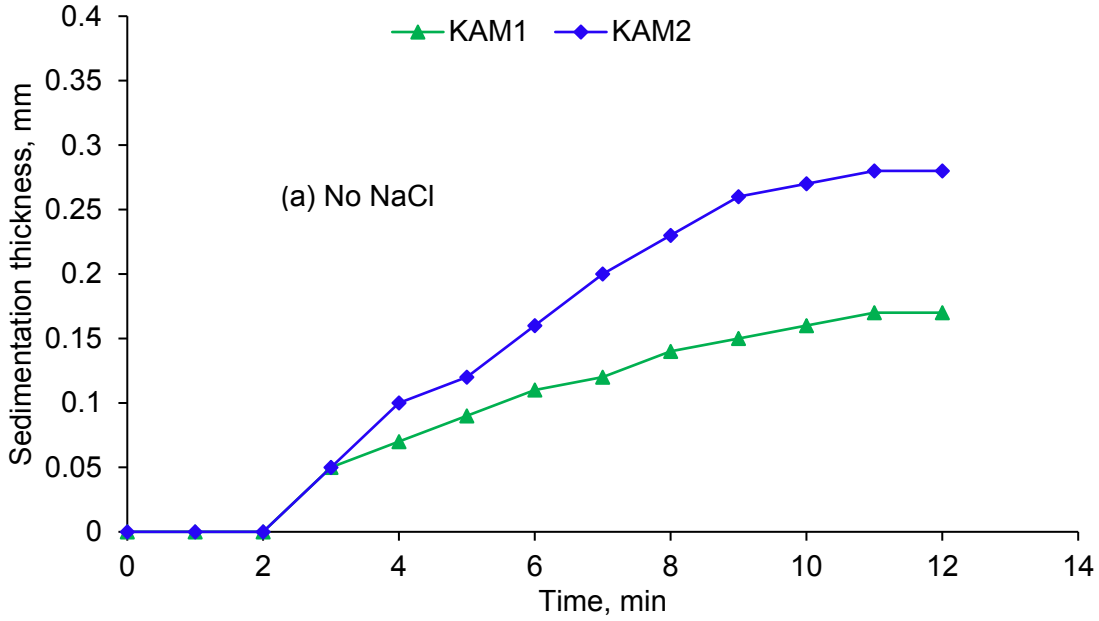

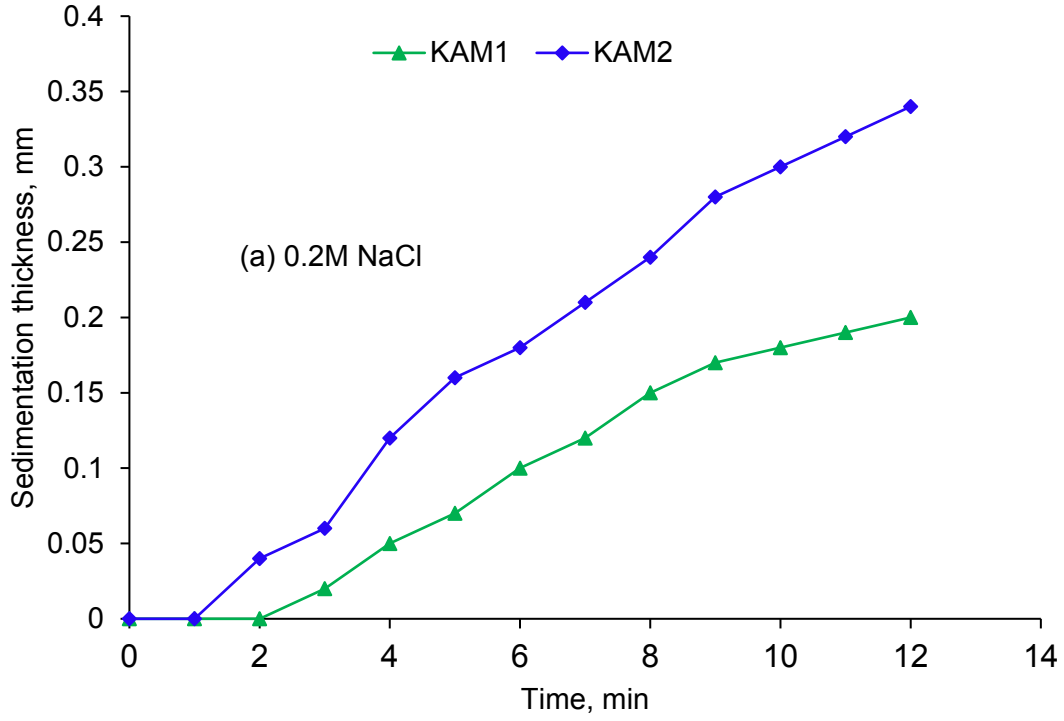

Figure 9.3. Effect of time on the settling of KAM in the presence of (a) no salt and (b) 0.2M NaCl salt; conducted under the conditions of pH 7, 25 °C in aqueous solution.

9.4.4 Adsorption kinetics

The adsorption behavior of KAM polymers on the coated QCM sensor is shown as a function of time in the absence and presence of salt (0.2 M NaCl concentration) in Figure 9.4. The decrease in the frequency reflects the adsorption of KAM, and the increase in the dissipation reveals the increase in the viscoelasticity of the adsorbed KAM layer. Slightly higher values of dissipation and lower frequency were obtained for KAM2 (6.5, -18.8 MHz) than for KAM1 (6.0, -29.5 MHz), which indicates more adsorption mass and creation of a soft and more viscoelastic film for KAM2. As KAM2 had more charged groups and molecular weight, it interacted more dramatically with the adsorbed KAM2 (Salmi et al., 2009). The higher adsorbed mass and thickness of KAM2 (80 mg/m^2, 30 nm) than those of KAM1 (65 mg/m^2, 18 nm) supported the stronger interaction and self-assembly of KAM, and the relative results can be found in Figure 9.1 (Merta et al., 2004; Long et al., 2013).

Generally, the dissipation and frequency were smaller for KAM2 (3.6, -8.3 MHz) and KAM1 (2.18, -7.19 MHz) in the presence of salt than its absence (Figure 9.4). These results indicated that the interaction of KAM was hampered in the presence of salt. This was accompanied by the decrease in the adsorption and thickness for KAM2 (45 mg/m^2, 21 nm) and KAM1 (23 mg/m^2, 10 nm) in the presence of salt (Table 9.2). Although the adsorption of KAMs was lower in the presence of salt, the interaction of KAM was sufficiently high for self- assembly of KAM, as evidenced in Figures 9.1 and 9.4. As the viscoelastic properties of KAM2 were higher than KAM1 in the absence and presence of salt, it can be concluded that KAM2 generated a looser structure upon self-assembling (Morris et al, 2002; Ali and Mahmud, 2015). In the presence of salt, more coiled conformation could be generated due to the reduced repulsion between the charged polymer segments. Therefore, more KAM molecules can fit onto the surface, causing the change in frequency and dissipation to increase.

After the adsorption reached a saturation plateau, rinsing with water resulted in a desorption, that is the removal of adsorbed mass and reduction in dissipation. This desorption was attributed to the weak binding of KAM particles in the presence of strong electrostatic repulsion between the negatively charged KAM polymer and the negatively charged KAM polymers coated surface (Alagha et al., 2013). A sudden spike in the dissipation was associated with a strong drop in frequency; implying an increase in mass adsorption at the experimental time of 25 min (Figure 9.4a). This increase was due to the replacement and adsorption of water on KAM adsorbed layer. In other words, rinsing of the system with water led to desorption of a part of adsorbed KAM, and swelling of the remaining adsorbed KAM. This behavior was observed in a study on the adsorption of SiO_2-nanoparticles on Hexamethyldisiloxane (HMDSO) oxygen plasma and related to capillary force increase as rinsing with water induced the growth of capillary force (Torun et al., 2014). On the other hand, the KAM in the presence of salt exhibited a much smooth layer with a linear increase in dissipation with no transitional sharp dissipation signal; indicating a drop in the capillary growth and contact force between the particles (Torun et al., 2014).

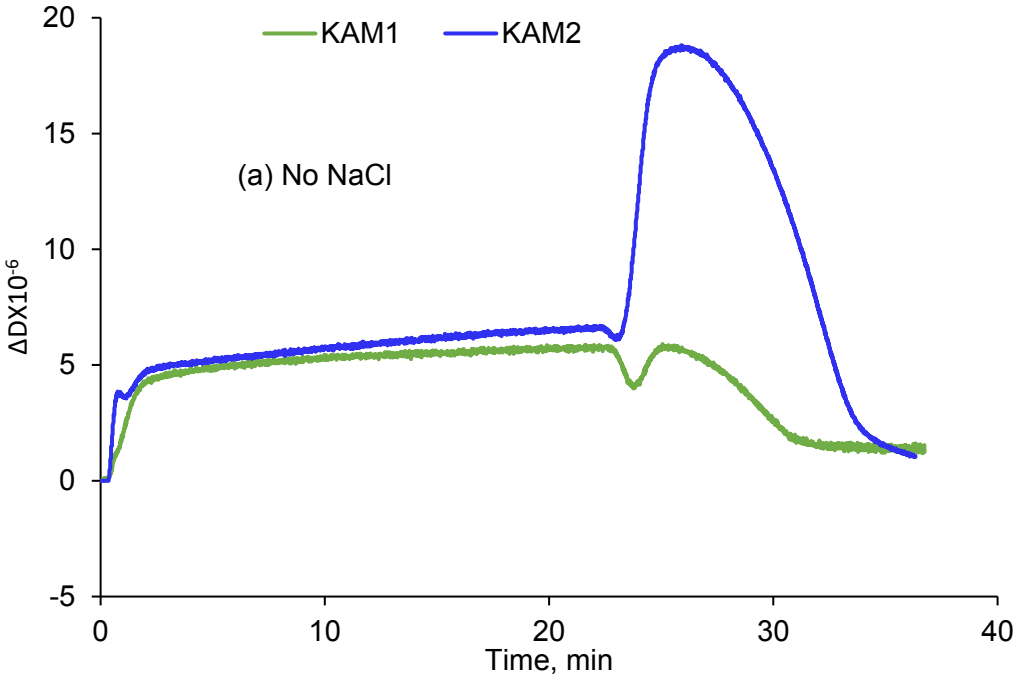
KAM1
KAM2
(a) No NaCl
ΔDX10-6
20
15
10
5
0
-5
0
10
20
30
40
Time, min

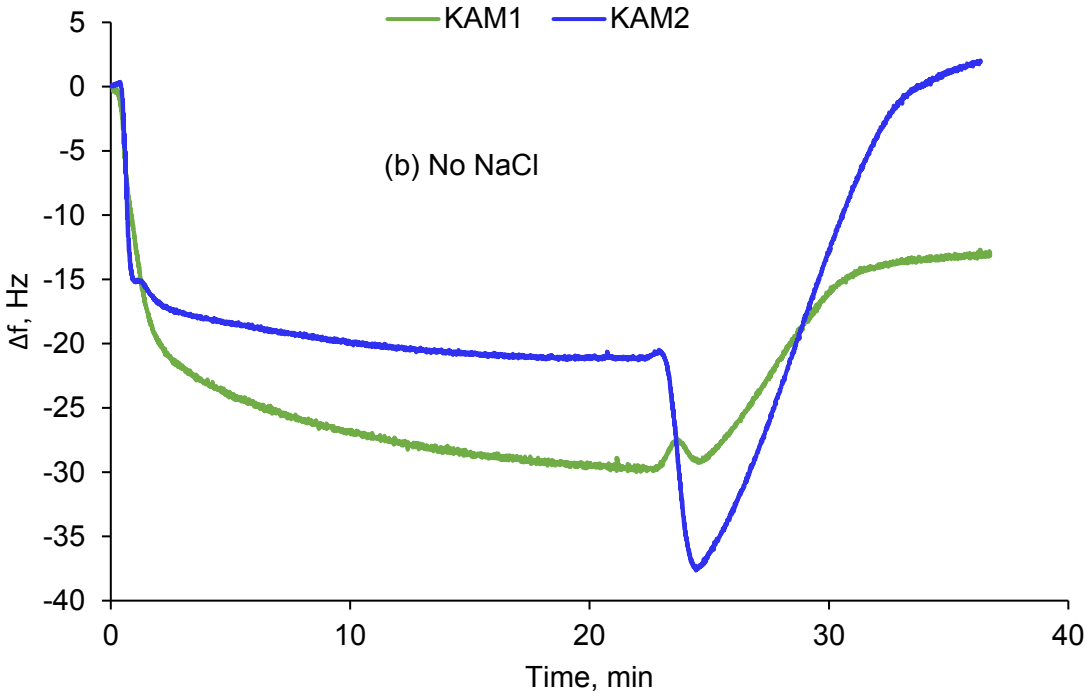
KAM1
KAM2
(b) No NaCl
Δf, Hz
5
0
-5
-10
-15
-20
-25
-30
-35
-40
0
10
20
30
40
Time, min

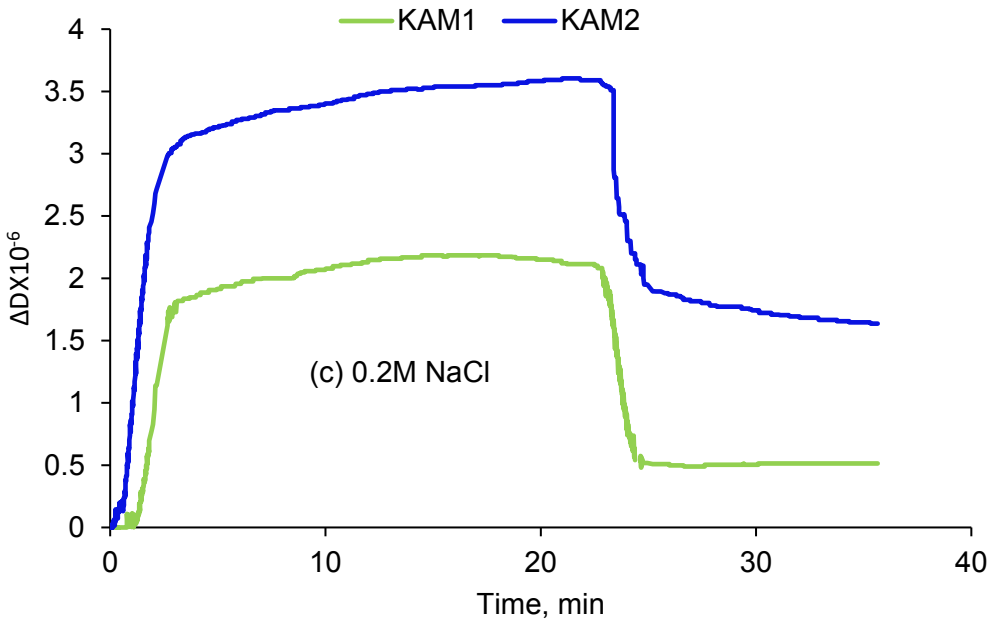

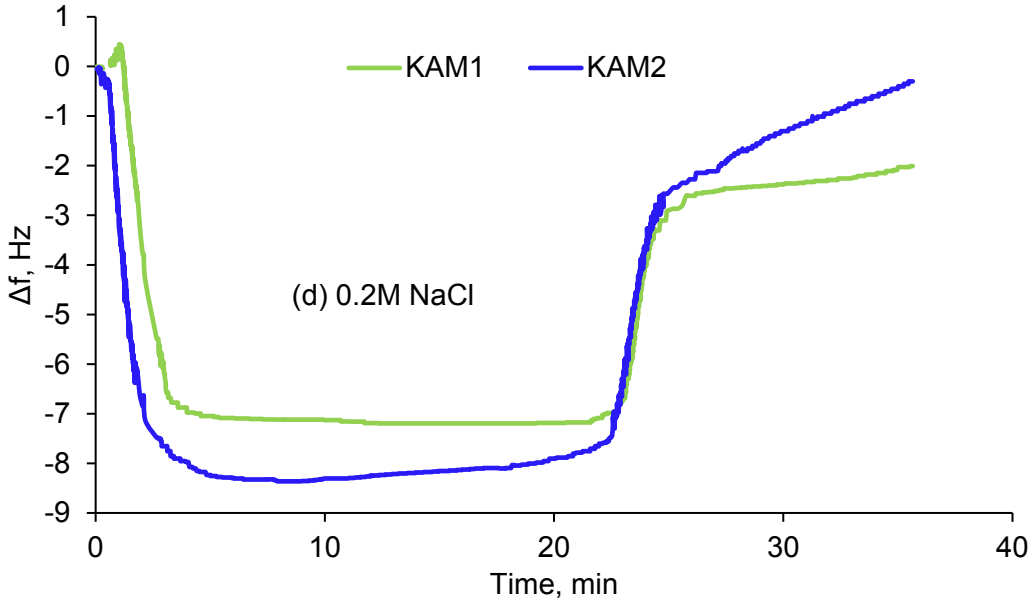

Figure 9.4. Frequency and dissipation of KAM as function of time in aqueous solution with (a, b) no NaCl, (b, c) 0.2 M NaCl; using Voigt model under the conditions of f0 =5 MHz, overtone 15 MHz.

Table 9.2. Parameters used for evaluation of KAM adsorption

	NaCl concentration (M)	Mass, mg/m^2	Thickness, nm
KAM1	0	65	18
	0.2	23	10
KAM2	0	80	30
	0.2	45	21

Table 9.3. The zeta potential of KAM polymers in solutions

Polymer	NaCl concentration (mol/L)	Zeta potential (mV)
KAM1	0	-12
	0.2	-4
KAM2	0	-20
	0.2	-16

9.5 Conclusions

The self-assembly of kraft lignin-acrylamide polymers aqueous solutions was studied in this work. It was demonstrated that the self-assembly of the polymer was enhanced with time. The larger KAM2 was aggregated more effectively than the smaller KAM1, both in the absence (240-386 nm) and presence of salt (35-165 nm). The sediment of KAM was more intense in the presence of salt than its absence due to charge screening effect of salt. In addition, the clusters made of KAM2 had faster settling and generated thicker sediment either in the presence or absence of salt. The Voigt model was applied to explore the viscoelastic properties of KAM polymer layer adsorbed on the coated KAM surface. It was discovered that KAM2 generated more viscoelastic layer than did KAM1, which implied that KAM2 generated more loose and porous structure. Therefore, the self-assembly of KAM2 was more intense than KAM1 in the presence and absence of salt, and the clusters of KAM2 had more loose and porous structures. Despite lower tendency for aggregation, salt facilitated the settlement of the formed aggregates.

9.6 References

Alagha, L., Wang, S., Yan, L., Xu, Z., Masliyah, J. 2013. Probing adsorption of polyacrylamide-based polymers on anisotropic basal planes of kaolinite using quartz crystal microbalance. Langmuir, 29, 3989−3998.

Ali, M., Mahmud, H.B. 2015. The effects of Concentration and Salinity on Polymer Adsorption Isotherm at Sandstone Rock Surface. Mater. Sci. Eng., doi: 10.1088/1757-899X/78/1/012038.

Aumelas, A., Serrero, A., Durand, A., Dellacherie, E. Leonard, M. 2007. Nanoparticles of hydrophobically modified dextrans as potential drug carrier systems. Colloids Surf. B Biointerfaces, 59(1), 74-80.

Beysens, D., Narayanan, T. 1999. Wetting-induced aggregation of colloids. J. Stat. Phys., 95:997–1008.

Buzea, C., Pachecob, I.I., Robbiec, K. 2007. Nanomaterials and nanoparticles: Sources and toxicity. Biointerphases, 2 (4), 17-71.

Caplan, M. R., Moore, P. N., Zhang, S. G., Kamm, R. D., Lauffenburger, D. A. 2000. Self-Assembly of a â-Sheet Protein Governed by Relief of Electrostatic Repulsion Relative to van der Waals Attraction. Biomacromol., 1, 627-631.

Cates, M.E., Tailleur, J. 2013. When are active Brownian particles and run-and-tumble particles equivalent? Consequences formotility-induced phase separation. EPL Europhys. Lett., 101, 20010

Chen, P., Yao, L., Liu, Y., Luo, J., Zhou, G., Jiang, B. 2012. Experimental and theoretical study of dilute polyacrylamide solutions: effect of salt concentration. J. Mol. Model., 18, 3153-3160.

Cheng, F., Wei, Y. P., Hou, G., Sun, S. F. 2008. Amphiphilic cellulose: Surface activity and aqueous self-assembly into nano-sized polymeric micelles. React. Funct.

Polym. 68(5), 981-989.

Fan, L., Degen, M., Grupido, N., Bendle, S., Pennartz, P. 2010. Effects of molecular weight, temperature and salt on the self-assembly of triblock copolymer solutions. Mat. Sci. Eng. A, 528, 127–136.

Fang, R., ChenG, X.S., Fu, J., Zheng, Z.B. 2009. Research on the Graft Copolymerization of EH-lignin with acrylamide. Natural Sci., 1, 17-22.

Frangville, C., Rutkeviccius, M., Richter, A. P., Velev, O. D., Stoyanov, S. D., Paunov, V. N. 2012. Fabrication of environmentally biodegradable lignin nanoparticles. ChemPhysChem, 13, 4235− 4243.

Furukawa, A., Tanaka, H. 2010. Key role of hydrodynamic interactions in colloidal gelation. Phys. Rev. Lett., 104, 245702.

Gilca, I. A., Popa, V. I., Crestini, C. 2015. Obtaining lignin nanoparticles by sonication. Ultrason. Sonochem., 23, 369−375.

Hasan, A., Fatehi, P. 2018. Stability of kaolinite dispersion in the presence of lignin-acrylamide polymer. Appl. Clay Sci. 1578, 72-82.

Hartgerink, J.D., Beniash, E, Stupp, S.I. 2001. Self-assembly and mineralization of peptideamphiphile nanofibers. Science, 294, 1684–1688. (doi:10.1126/science.1063187).

Jiang, C., He, H., Jiang, H., Ma, L., Jia, D. M. 2013. Nano-lignin filled natural rubber composites: Preparation and characterization. eXPRESS Polym. Lett., 7(5), 480-493.

Lehn, J.M. 1995. Supramolecular chemistry: concepts and perspectives. Weinheim, Germany: Wiley- VCH.

James W. Swan, J, † Jonathan, L. B., Liu, Y., Eric, M. 2014. Directed colloidal self-assembly in toggled magnetic fields. Furst Soft Matter, 10, 1102.

Jamrozik, A., Gonet, A., Fijal, J., Terpilowski, K., Czekaj, L.2014. Analysis of waste mud Stability. AGH drilling, oil, gas., http://dx.doi.org/10.7494/drill.2014.31.1.25.

Jahan, M. S., Liu, Z., Wang, H., Saeed, A., Ni, Y. 2012. Isolation and characterization of lignin from prehydrolysis liquor of kraft based dissolving pulp production, Cell. Chem. Technol., 46, 261–267.

Kouisni, L., Hindle, P.H., Maki, K., Paleologou, M. 2012. The lignoforcesystem ™: a new process for the production of high-quality lignin from black liquor. The Journal of Science & Technology for Forest Products and Processes, 2, 6–10.

Kong, F., Wang, S., Price, J. T., Konduri, M.K.R., Fatehi, P. 2015. Water soluble kraft lignin acrylic acid copolymer: synthesis and characterization. Green Chem., 17, 4355-4366

Leonard, M., Rouzes, C., Durand, A. Dellacherie, E. 2003. Influence of polymeric surfactants on the properties of drug-loaded PLA nanospheres. Colloids and Surfaces B-Biointerfaces, 32(2), 125-135.

Lievonen, M., Valle-Delgado, J. J., Mattinen, M. L., Hult, E.L., Lintinen, K., Kostiainen, M. A., Panned, A., Szilvay, G. R., Setala, H., Osterberg, M. A. 2016. Simple process for lignin nanoparticle preparation. Green Chem., 18, 1416−1422.

Long, Y., Wang, T., Liu, L., Liu, G., Zhang, G. 2013. Ion Specificity at a Low Salt Concentration in Water−Methanol Mixtures Exemplified by a Growth of Polyelectrolyte Multilayer. Langmuir, 29, 3645−3653.

Makarova, L., Blomberg, E. 2007. Clauson, P.M. Effect of Adsorbed Layer Surface Roughness on the QCM-D Response: Focus on Trapped Water. Langmuir, *23,* 12436-12444.

Merta, J., Tammelin, T., Stenius, P. 2004. Adsorption of complexes formed by cationic starch and anionic surfactants on quartz studied by QCM-D. Colloids Surf. A Physicochem. Eng. Asp., 250, 103–114.

Mishra, S., Bera, A., Mandal. A. 2014. Effect of Polymer Adsorption on Permeability Reduction in Enhanced Oil Recovery. J. Pet. Sci., 1-9.

Mengual, O., Menuier, G., Cayre, I., Puech, K., Sanbre, P. 1999. Characterization of instability

of concentrated dispersions by a new optical analyzer: the Turbiscan MA 1000. Colloids Surf. A., 152, 111–123.

Morris G. E., Fornasiero D., Ralston, J. 2002. Polymer depressants at the talc–water interface: adsorption isotherm, microflotation and electrokinetic studies. Int. J. Miner. Process, 67, 211–227.

Ozbas, B., Kretsinger, J., Raja gopal, K., Schneider, J.P., Pochan, D.J. 2004. Salt-Triggered Peptide Folding and Consequent Self-Assembly into Hydrogels with Tunable Modulus. Macromol., 37, 7331-7337.

Palberg, T. 1997. Colloidal crystallization dynamics. Curr. Opin. Colloid Interf. Sci., 2, 607–614.

Pouteau, C., Dole, P., Cathala, B., Averous, L., Boquillon, N. 2003. Antioxidant properties of lignin in polypropylene, Polym. Degrad. Stab., 81(1), 9-18.

Qian, Y., Deng, Y., Qiu, X., Li, H., Yang, D. 2014. Formation of uniform colloidal spheres from lignin, a renewable resource recovered from pulping spent liquor. Green Chem., 16, 2156.

Rodahl, M., Hook, F., Krozer, A., Brzezinski, P., and Kasemo, B. 1995. Quartz crystal microbalance setup for frequency and *Q*-factor measurements in gaseous and liquid environments. Rev. Sci. Instrum., 66, 3924–3930. http://dx.doi.org/10.1063/1.1145396.

Rong, H., Gao, B., Zhao, Y., Sun, S., Yang, Z., Wang, Y., Yue, Q., Li, Q. 2013b. Advanced lignin-acrylamide water treatment agent by pulp. J. Environ. Sci., 12, 2367-77.

Salmi, J., Nypelo, T., Österberg, M., Laine, J. 2009. Layer structures formed by silica nanoparticles and cellulose nanofibrils with cationic polyacrylamide (c-pam) on cellulose surface and their influence on interactions. Bioresour., 4(2), 602-625.

Saarinen, T., Osterberg, M., Laine, J. 2009. Properties of Cationic Polyelectrolyte Layers Adsorbed on Silica and Cellulose Surfaces Studied by QCM-D—Effect of Polyelectrolyte Charge Density and Molecular Weight. J. Disp. Sci. Technol., 30:969–979.

Salentinig, S., Schubert, M. 2017.Softwood Lignin Self-Assembly for Nanomaterial Design. Biomacromol., 18, 2649−2653.

Song, Y., Zhang, L., Gan, W., Zhou, J., Zhang, L. 2011. Self-assembled micelles based on hydrophobically modified quaternized cellulose for drug delivery. Colloids and Surf.B, 83, 313–320.

Tomilov, A., Videcoq, A., Cerbelaud, M., Piechowiak, M.A, Chartier, T., Ala-Nissila, T., Bochicchio, D., Ferrando, R. 2013. Aggregation in colloidal suspensions: Evaluation of the role of hydrodynamic interactions by means of numerical simulations. J. Phys. Chem. B., 117:14509–14517

Torun, B., Kunze, C., Zhang, C., Kuhne, T.D., Grundmeier, G. 2014. Study of water adsorption and capillary bridge formation for SiO2 nanoparticle layers by means of a combined in situ FT-IR reflection spectroscopy and QCM-D set-up. Phys.Chem.Chem.Phys., 16, 7377.

Vie, R., N. Azema, N., Quantin, J.C., Touraud, E., Fouletier, M. 2007. Study of suspension settling: A approach to determine suspension classification and particle interactions. Colloids Surf. A, 298, 192.

Wang, S., Sun, Y., Kong, F., Yang, G., and Fatehi, P. 2016. Preparation and characterization of lignin-acrylamide copolymer as a paper strength additive. Bioresour., 11(1), 1765-1783.

Wang, W., Xu, Y., Backes, S., Li, A., Micciulla, S., Kayitmazer, A., Li, L., Guo, X., Klitzing, R.V. 2016. Construction of Compact Polyelectrolyte Multilayers Inspired by Marine Mussel: Effects of Salt Concentration and pH As Observed by QCM-D and AFM. Langmuir, 32, 3365−3374.

Wang, S., Hou, Q., Kong, F., Fatehi, P. 2015. Production of cationic xylan–METAC copolymer as a flocculant for textile industry. Carbohyd. Polym., 124, 229-236.

Whitesides, G.M., Grzyboski, B. 2002. Self-assembly at all scales. Science 295, 2418–2421. (doi:10.1126/science.1070821).

Wurm, F. R., Weiss, C. K. 2014. Nanoparticles from renewable polymers. Front. Chem., 2, 1−13.

Xiong, F., Hana, Y., Wanga, S., Lia, G., Qina, T., Chena, Y., Chua, F. 2017. Preparation and formation mechanism of size-controlled ligninnanospheres by self-assembly. Ind. Crop. Prod., 100, 146–152.

Yiamsawas, D., Baier, G., Thines, E., Landfester, K., Wurm, F. R. 2014. Biodegradable lignin nanocontainers. RSC Adv., 4, 11661− 11663.

Yoshikawa, J., Lewis, L. J. 2008. Comb Polymer Architecture, Ionic Strength, and Particle Size Effects on the BaTiO3 Suspension Stability. J. Am. Ceram. Soc., doi:10.1111/j.1551-2916.2008.02647.x

Zakzeski, J., Bruijnincx, P.C.A., Jongerius, A.L., Weckhuysen, B.M. 2010. The catalytic valorization of lignin for the production of renewable. Chem. Rev., 110 (6), 3552– 3599.

Zhang, K., Jiang, M., Chen, D. 2012. Self-assembly of particles—The regulatory role of particle flexibility. Pro. Polym. Sci., 37, 445– 486.

Zhang, L. M., Lu, H. W., Wang, C., Chen, R. F. 2011. Preparation and properties of new micellar drug carriers based on hydrophobically modified amylopectin. Carbohyd. Polym., 83(4), 1499-1506.

Zhang, J., Chen, X. G., Li, Y. Y., Liu, C. S. 2007. Self-assembled nanoparticles based on hydrophobically modified chitosan as carriers for doxorubicin. Nanomed-Nanotechnol., 3, 258-265.

Chapter 10: Conclusions and recommendations for future work

10.1 Conclusions

The graft copolymer was synthesized by graft copolymerization of kraft lignin, acrylamide (AM) and (2-methacryloyloxyethyl) trimethyl ammonium chloride (DMC). The properties of the copolymers were characterized by means of NMR, FTIR, elemental, charge density, and molecular weight analyses as well as TGA. The effects of the reaction conditions on the graft copolymerization were investigated via considering one factor at a time approach. The copolymers with the optimal reaction conditions were produced at an initiator dosage of 0.11 mmol, 2 h of reaction, pH 4.0, 80 °C, and AM/DMC/KL molar ratio of 0.028 /0.024/0.011. The charge density and solubility of the resulting copolymer (KAD) were 1.76 meq/g and 50 wt. %, respectively, with a solubility in 10 g/L solution.

The factors influencing the charge density and solubility of KAD copolymers, such as monomer concentration, reaction temperature, time, and pH were systematically investigated using the orthogonal experiment design (i.e., multifactor at a time). The optimal reaction conditions for KAD copolymer production were 0.011 mol of KL, 0.014 mol of AM, 0.024 mol of DMC, pH 3, 3 h, and 80 °C, which are slightly different from the conditions obtained via considering one-factor-at-a- time approach. Under optimized conditions, the copolymer had a charge density of 2.13 meq/g and solubility of 56% in a 10 g/L aqueous solution.

The KAD copolymers with different charge densities and similar molecular weights were synthesized via copolymerizing kraft lignin, AM and DMC, under different conditions. It was observed that the charge density of KAD significantly affected the performance of KAD in the flocculation of kaolin and bentonite suspensions in that the higher charged copolymer flocculated the clay suspensions more effectively. It was revealed that the higher charged KAD adsorbed more than the lower charged one, influencing the flocculation efficiency. KAD1 with a higher charge density showed a higher adsorption on kaolin (2.58 mg/g) and bentonite particles (1.83 mg/g) at 4 mg/g of dosage. The use of higher charge density KAD resulted in higher optimum removal rates, larger flocs, in general clearer supernatants (after polymer treatment). This study

showed that by adding 4 mg/g of higher molecular KAD1, having the charge density of 2.13 meq/g and molecular weight of 185,900 g/mol, the maximum relative turbidity of 0.53 and 0.2 was achieved for kaolin and bentonite suspensions, respectively.

The KAD copolymers with different molecular weights, but with similar charge densities, were produced and their effectiveness as flocculants for clay suspensions was investigated. It was noticed that the KAD with a higher molecular weight had a higher adsorption on clay particles than the one with smaller molecular weight due to its bridging capacity that generated larger and bulkier flocs. The higher molecular KAD reached the higher adsorption of 1.4 and 1.08 mg/g at very low dosage of 8 mg/g on kaolin and bentonite, respectively. The flocculation properties of kaolin and bentonite suspensions depended on the KAD dosage and pH, and also varied with the adsorbed amount of KAD on kaolin and bentonite suspensions. The growth, breakage, and re-growth of the flocs generated from the kaolin and bentonite suspensions were assessed for two different KADs. This study showed that higher molecular weight KAD was able to produce stronger flocs with better recovery factors (i.e., the regrowth after breakage) in the kaolin suspension than bentonite suspension due to polymer bridging and electrostatic patch effects.

Kraft lignin was polymerized with DMC to produce kraft lignin-DMC (KLD). The effects of molecular weight and charge density of KLDs on their adsorption and flocculation performance were evaluated. The flocculation of kaolin particles was promoted by higher molecular weight lignin polymer. Generally, the low molecular weight ones acted as flocculants via mainly charge neutralization, while those with higher molecular weights acted as flocculants via bridging mechanism. Also, the higher molecular weight polymers generated larger flocs with a higher settling rates; while the low molecular weight ones induced flocs with more compact structure. Moreover, the separation behavior in centrifugal field of initially monodisperse kaolin in aqueous solutions was investigated and compared with the results generated by the vertical size analyzer for all of the KLDs. The addition of KLD resulted in change from monodisperse to polydisperse settling due to agglomeration/flocculation. The results showed that the measured KLD sedimentation velocities via the analytical centrifugation were different from the highly dense spherical particles predicted by the Stokes' law.

The polymerization of kraft lignin and acrylamide (AM) was conducted to produce kraft lignin-acrylamide (KAM) polymers with different molecular weights and charge densities. The results

showed that the KAM's dosage, molar mass, and charge density had great impacts on the stabilization of clay particles at different pHs. The presence of NaCl salts had a significant effect on polymer adsorption and stability of clay suspension. Increasing the salt concentration enhanced the adsorption. The pH increase reduced the adsorption level but increased the relative turbidity of clay suspension. The surface tension and contact angle studies demonstrated that the wettability of KAM polymer increased by increasing the pH of the solution. Kinetic studies also confirmed the effect of both charge density and molecular weight of KAM on kaolin dispersions. KAM was found to be more effective in stabilizing kaolin dispersions than just a shear rate increase.

Dynamic light scattering method was employed to monitor the self-assembly of kraft lignin-acrylamide (KAM) in solutions to understand the kinetics of growth, aggregation, and surface interactions of fine particles. The KAM with a larger molecular weight had more tendency for self-aggregation, which led to a larger self-assembly of KAM process. A larger hydrodynamic size of 240-386 nm was observed for the higher molecular weight KAM in the absence of salt, while in the presence of salt its hydrodynamic size reduced to 35-165 nm. In addition, KAM particles showed greater settling behavior in the presence or absence of salt. Moreover, quartz crystal microbalance with dissipation (QCM-D) was employed to monitor the self-assembly behavior of the adsorbed KAM onto the solid surface coated with KAM. The investigation of the KAM film formation using QCM-D supported the stronger interaction and self-assembly with higher molecular weight KAM. The viscoelastic properties of KAM found to be higher for KAM with larger size in the absence and presence of salt.

It was discovered that kraft lignin can be successfully modified via copolymerization of cationic and nonionic monomers in aqouous systems to produce flocculants and dispersants for wastewater treatment. This study proved that the molecular weight and charge density of lignin-based polymers has great impacts on their flocculation performance. This study also confirmed that the flocculant characteristics greatly affect the properties of induced flocs and their settling performance. Moreover, this study demonstrated that the effectiveness of the lignin-based polymers as dispersants and flocculants as well as their self assembly behavior, was greatly influenced by their solution characteristics.

10.2 Future work

The structure of lignin polymers should be discovered in detail. The impact of reaction parameters on the structure of the lignin polymers should also be investigated. The present work has focused mainly on the flocculation of kaolin and bentonite suspensions via using lignin polymers. The changes in the molecular weight and charge density of cationic lignin polymers and their influence on the clay suspension's stability were also investigated. To gain further knowledge, the flocculation kinetic and floc's characteristics in different mineral suspensions should be studied. Correlations between the characteristics of lignin polymers and their performance should be studied more comprehensively and for lignin polymers generated with different charged monomers. Furthermore, the filtration and sedimentation efficiencies of flocculation and dispersion systems containing lignin polymers should be evaluated in detail.

Chapter 11: Appendix

11.1 Optimized production of kraft lignin-p (DMC) via Taguchi method

Run	Temp, °C	Time, h	DMC, mol	pH	KL, mol	Charge, meq/g	Solubility, wt.%
1	90	3	0.0193	2	0.0277	2.45	56
2	80	3	0.0241	4	0.0111	3.19	67
3	70	2	0.0144	4	0.0277	-0.84	30
4	60	2	0.0096	2	0.0111	-0.36	42
5	60	3	0.0144	3	0.0166	-0.66	48
6	70	3	0.0096	5	0.0222	-0.98	22
7	70	5	0.0193	3	0.0111	2.93	56
8	70	4	0.0241	2	0.0166	2.83	44
9	90	2	0.0241	3	0.0222	2.58	38
10	60	4	0.0193	4	0.0222	1.25	30
11	90	5	0.0096	4	0.0166	1.52	40
12	90	4	0.0144	5	0.0111	2.5	42
13	80	5	0.0144	2	0.0222	2.46	28
14	80	2	0.0193	5	0.0166	2.51	41
15	80	4	0.0096	3	0.0277	0.74	30
16	60	5	0.0241	5	0.0277	-0.93	40
Optimum	80	3	0.0243	4	0.0222	3.66	66

A. 1. The Taguchi orthogonal parameters and levels (L^{16}) and the responses.

A. 2. ANOVA analysis for charge density and solubility of cationic KLD

Factor	Sum of squares		Mean Square		F-Value	
	Charge density, meq/g	Solubility, wt.%	Charge density, meq/g	Solubility, wt.%	Charge density, meq/g	Solubility, wt.%
Model	34.12	1895.75	3.79	157.98	5.28	10.37
Temperature, °C	1.64	16.19	0.58	5.40	0.19	0.018
Time, h	2876.5	73.69	4.1	24.56	35.29	1.61
DMC, mol	12.1	408.69	1.49	136.23	5.57	8.95
pH	12.57	153.69	0.86	419.90	0.23	3.36
KL, mol	4.44	1259.70	1.50	15.23	2.02	27.57

Standard deviation		Coefficient of variation,%		R^2		Predicted R^2		Adjusted R^2	
Charge density, meq/g	Solubility, wt.%	Charge density, meq/g	Solubility, wt.%	Charge density, meq/g	Solubility, wt.%	Charge density, meq/g	Solubility, wt.%	Charge density, meq/g	Solubility, wt.%
0.85	3.90	62.47	9.93	0.887	0.9754	0.71	0.3304	0.2199	0.8872

A. 3. Model coefficients estimated by regression analysis.

Term	Charge density, meq/g				Solubility, wt.%			
	Coefficient Estimate	Standard Error	95% Cl Low	95% Cl High	Coefficient Estimate	Standard Error	95% Cl Low	95% Cl High
Intercept	1.35625	0.2124032	0.8365182	1.8759818	39.3125	0.9756141	36.207658	42.417342
A[1]	-1.59375	0.3678931	-2.493951	-0.693548	-1.3125	1.6898132	-6.690244	4.0652446
A[2]	-0.29875	0.3678931	-1.198951	0.6014519	2.4375	1.6898132	-2.940244	7.8152446
A[3]	0.86875	0.3678931	-0.031451	1.7689519	-2.8125	1.6898132	-8.190244	2.5652446
B[1]	-1.18625	0.3678931	-2.086451	-0.286048	-5.8125	1.6898132	-11.19024	-0.434755

B[2]	-0.41875	0.3678931	-1.318951	0.4814519	-2.3125	1.6898132	-7.690244	3.0652446
B[3]	1.04875	0.3678931	0.1485481	1.9489519	0.1875	1.6898132	-5.190244	5.5652446
D[1]	0.65125	0.3678931	-0.248951	1.5514519	-3.3125	1.6898132	-8.690244	2.0652446
D[2]	0.19125	0.3678931	-0.708951	1.0914519	3.6875	1.6898132	-1.690244	9.0652446
D[3]	0.65125	0.3678931	-0.928951	0.8714519	2.4375	1.6898132	-2.940244	7.8152446
E[1]	0.19125	0.3989911	-0.714379	1.2382126	12.4375	1.6898132	7.0597554	17.815245
E[2]	-0.02875	0.4074723	-0.698238	1.2958594	4.1875	1.6898132	-1.190244	9.5652446
E[3]	-0.02875	0.4159536	-0.682097	1.3535063	-9.8125	1.6898132	-15.19024	-4.434755

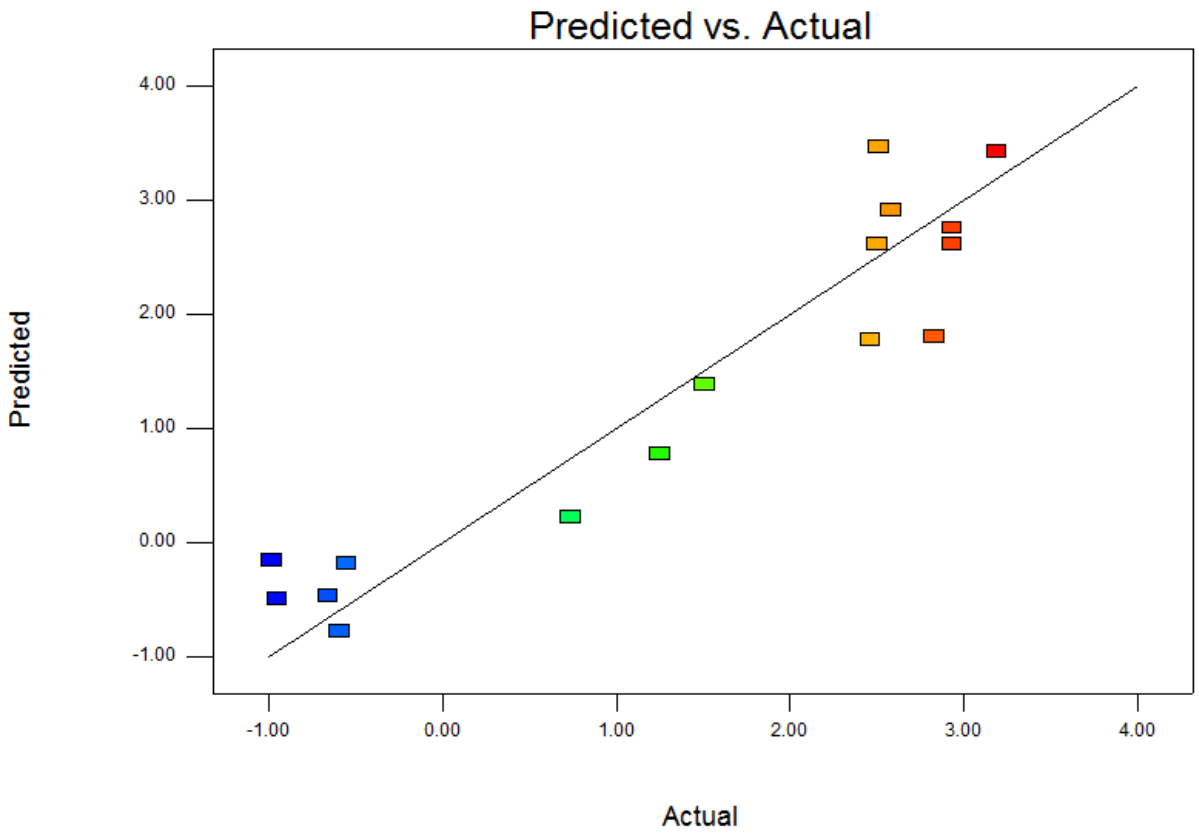

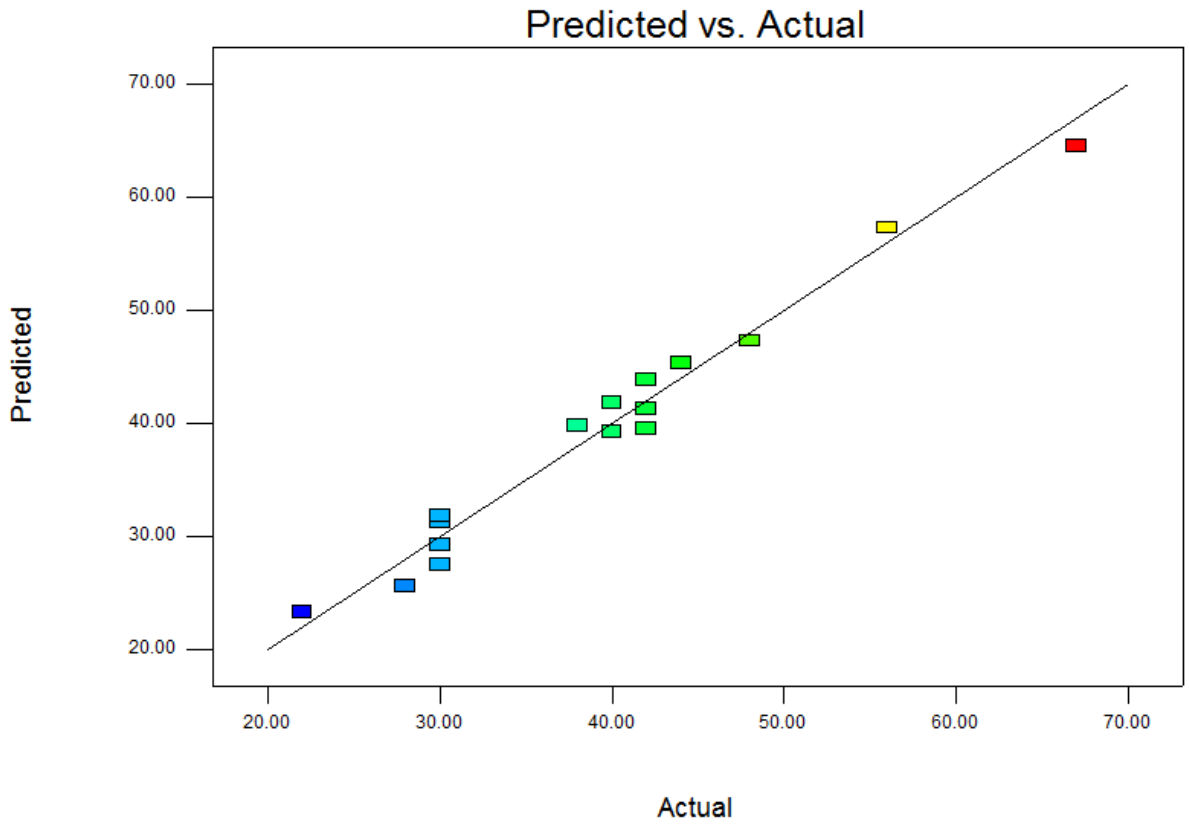

A. 1. Relationship between the predicted values and experimental values for (a) charge density and (b) solubility based on Taguchi orthogonal design.

11.2 Optimized production of kraft lignin-p (AM) via Taguchi method

A. 4. The Taguchi orthogonal parameters and levels (L^{16}) and the responses.

RUN	Temp, °C	Time, h	pH	AM, mol	KL, mol	Solubility, g/L	N %
1	60	4	4	0.042	0.022	8.8	2.63
2	70	5	3	0.042	0.011	5.5	4.85
3	60	2	2	0.014	0.011	4.5	3.8
4	90	5	4	0.014	0.016	4.5	1.57
5	90	3	2	0.042	0.027	5.3	2.24
6	80	5	2	0.028	0.022	4.7	2.16
7	80	4	3	0.014	0.027	6.9	1.18
8	90	4	5	0.028	0.011	7.5	2.9
9	70	4	2	0.056	0.016	9.3	4.72
10	60	5	5	0.056	0.027	5.5	2.52
11	60	3	3	0.028	0.016	5.6	1.73
12	70	3	5	0.014	0.022	5.5	1.2
13	90	2	3	0.056	0.022	3.4	3.56
14	70	2	4	0.028	0.027	6.6	1.44
15	80	3	4	0.056	0.011	6.9	4.6
16	80	2	5	0.028	0.016	3.9	4.3
Optimum	80	2	5	0.042	0.016	4.7	6.2

A. 5. ANOVA analysis for nitrogen content and solubility of KAM

Factor	Sum of squares		Mean Square		F-Value	
	Solubility, g/L	N %	Solubility, g/L	N %	Solubility, g/L	N %
Model	38.095	33.79	3.176	2.82	11.67	18.37
Temperature, °C	6.335	2.43	2.11	0.81	7.77	5.22
Time, h	28.765	4.44	9.58	1.48	35.29	9.57
AM, mol	14.65	15.09	0.48	5.03	1.8	32.49
pH	1.53	11.83	0.51	3.94	1.88	25.48
KL, mol	4.49	9.7	1.5	5.23	0.12	7.57

Standard deviation		Coefficient of variation, %		R^2		Predicted R^2		Adjusted R^2	
Solubility, g/L	N %	Solubility, g/L	N %	Solubility, g/L	N %	Solubility, g/L	N %	Solubility, g/L	N %
0.521	0.39	8.95	13.28	0.97	0.9854	0.97	0.9804	0.8999	0.9372

A. 6. Model coefficients estimated by regression analysis.

Term	Solubility, g/L				N %			
	Coefficient Estimate	Standard Error	95% Cl Low	95% Cl High	Coefficient Estimate	Standard Error	95% Cl Low	95% Cl High
Intercept	5.85	0.13	5.4.1031	6.296863	2.9625	0.0983669	2.6494524	3.2755476
A[1]	0.275	0.23	-0.4432576	0.9325769	-0.2925	0.1703764	-0.8347143	0.2497143
A[2]	0.9	0.23	0.1817423	1.682577	0.09	0.1703764	-0.4522143	0.6322143
A[3]	-0.525	0.23	-1.232577	0.935769	0.5975	0.1703764	0.0552857	1.1397143
B[1]	-1.025	0.23	-1.7432577	-0.374231	0.7875	0.1703764	0.2452857	1.3297143
B[2]	-0.5	0.23	-1.282577	0.225769	-0.52	0.1703764	-1.0622143	0.0222143
B[3]	0.23	0.23	1.517423	3.082577	-0.4375	0.1703764	-0.9797143	0.1047143
D[1]	-0.475	0.23	-1.132577	0.2325769	-0.6925	0.1703764	-1.2347143	-0.1502857

D[2]	0.275	0.23	-0.4325769	0.9325769	-1.2125	0.1703764	-1.7547143	-0.6702857
D[3]	0.25	0.23	-0.4825769	0.9825769	1.0175	0.1703764	0.4752857	1.5597143
E[1]	0.125	0.23	- 0.5325769	0.8325769	0.7425	0.1703764	0.2002857	1.2847143
E[2]	-0.475	0.23	-1.132577	0.2325769	0.925	0.1703764	0.3827857	1.4672143
E[3]	0.375	0.23	-0.325769	1.032577	-0.55	0.1703764	-1.0922143	-0.0077857

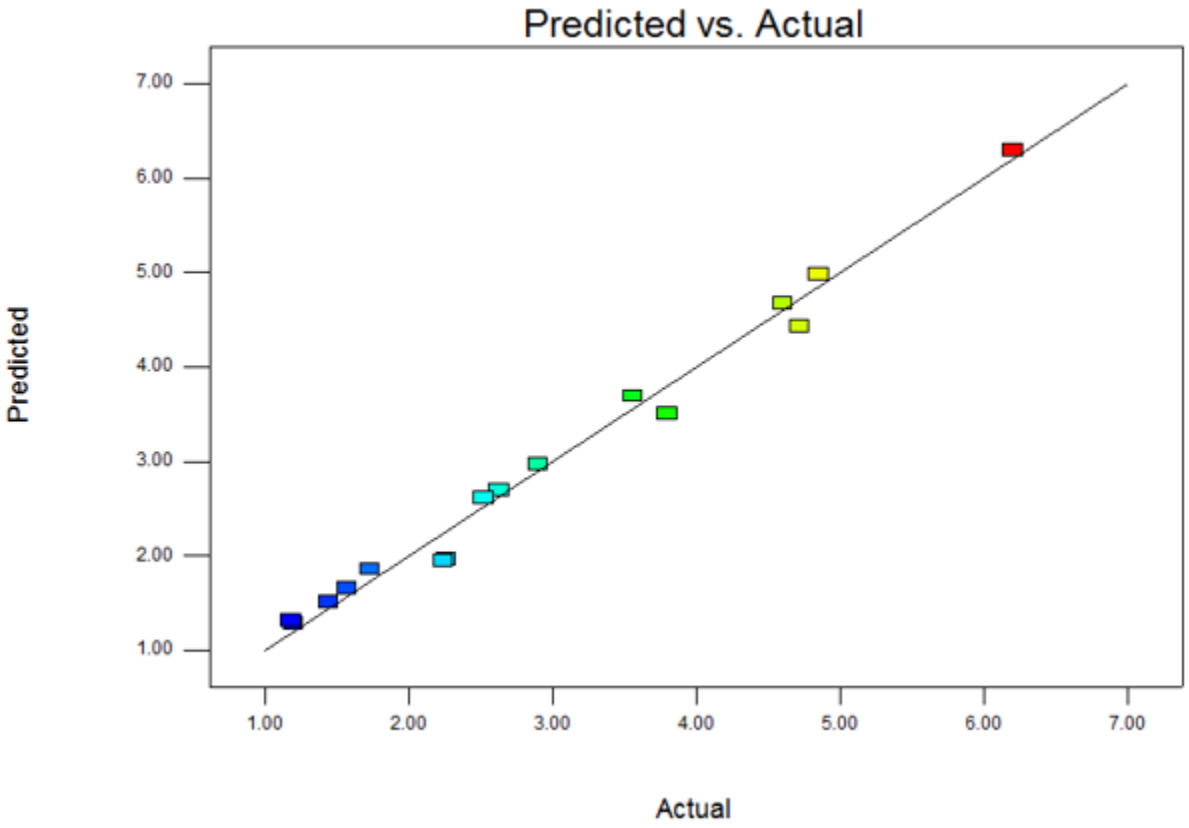

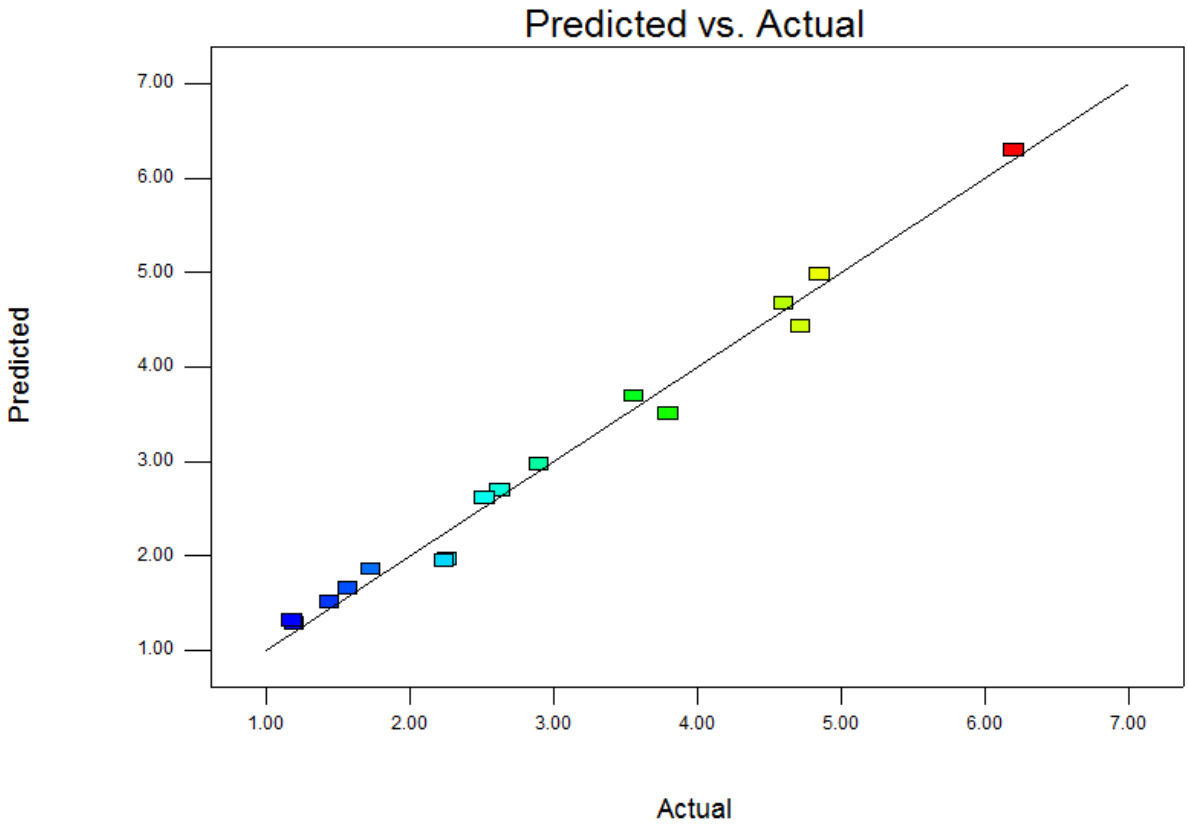

A. 2. Relationship between the predicted values and experimental values for (a) solubility and (b) nitrogen based on Taguchi orthogonal design.